SAR IMAGING OF SHIP WAKES IN THE GULF OF ALASKA

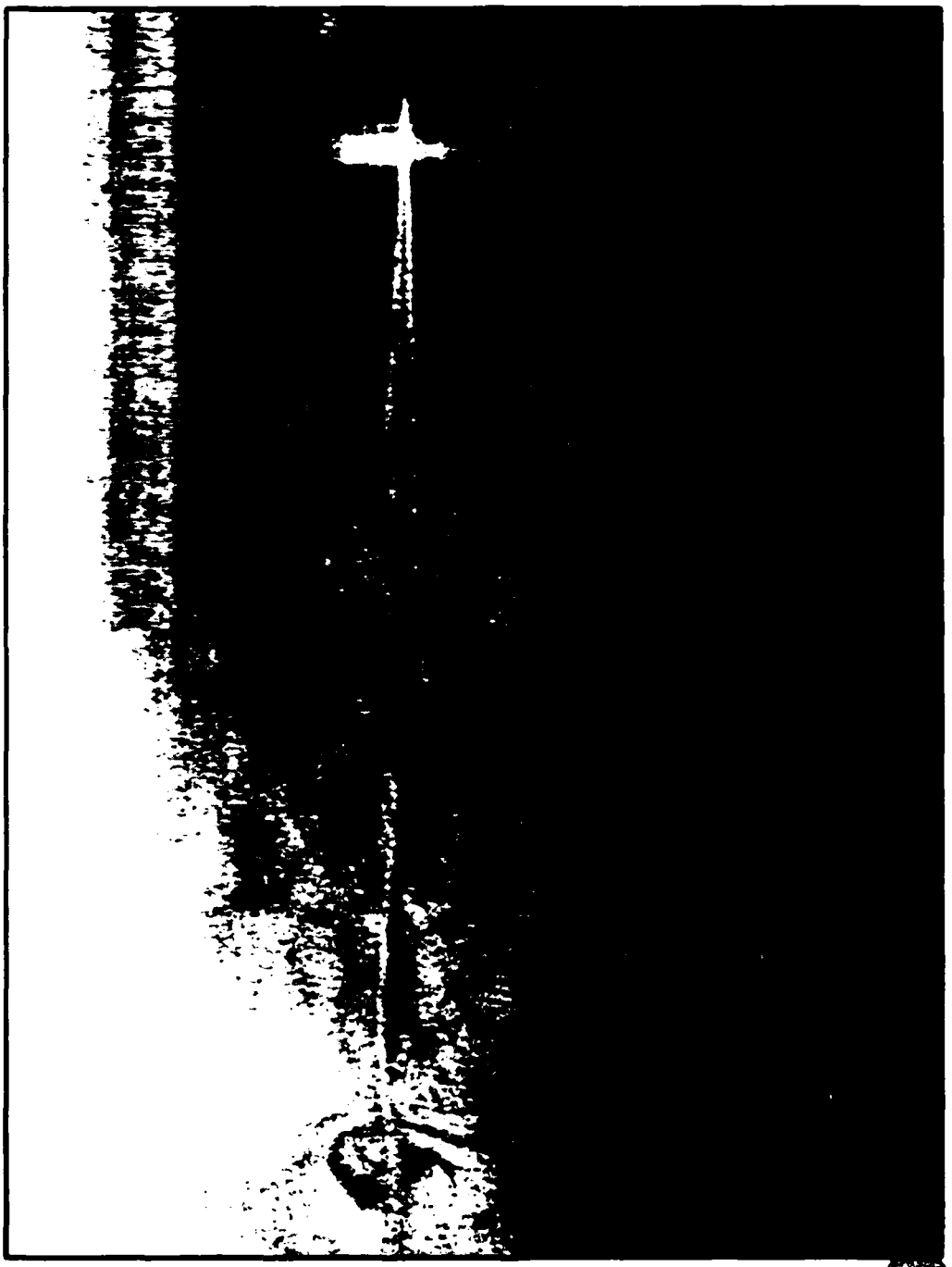

SECURITY CLASSIFICATION OF THIS PAGE (When Data Entered)

REPORT DOCUMENTATION PAGE

READ INSTRUCTIONS BEFORE COMPLETING FORM

1. REPORT NUMBER	2. GOVT ACCESSION NO. A186 554 / 3. RECIPIENT'S CATALOG NUMBER
4. TITLE (and Subtitle) SAR Imaging of Ship Wakes in the Gulf of Alaska	5. TYPE OF REPORT & PERIOD COVERED Final Report 1984 - 1987
	6. PERFORMING ORG. REPORT NUMBER
7. AUTHOR(s) O. H. Shemdin	8. CONTRACT OR GRANT NUMBER(s) 1. N00014-84-WRM-2212 2. N00014-85-C-0221
9. PERFORMING ORGANIZATION NAME AND ADDRESS 1. Jet Propulsion Laboratory, Pasadena, CA 2. Ocean Research & Engineering, La Canada, CA	10. PROGRAM ELEMENT, PROJECT, TASK AREA & WORK UNIT NUMBERS 0803 - Dynamic Oceanography 1709 - Radar Detection
11. CONTROLLING OFFICE NAME AND ADDRESS Office of Naval Research 800 N. Quincy Street Arlington, VA 22217	12. REPORT DATE February, 1987
	13. NUMBER OF PAGES 87
14. MONITORING AGENCY NAME & ADDRESS(if different from Controlling Office)	15. SECURITY CLASS. (of this report) Unclassified
	15a. DECLASSIFICATION/DOWNGRADING SCHEDULE

16. DISTRIBUTION STATEMENT (of this Report)

Approved for Publication Release; Distribution Unlimited

17. DISTRIBUTION STATEMENT (of the abstract entered in Block 20, if different from Report)

18. SUPPLEMENTARY NOTES

19. KEY WORDS (Continue on reverse side if necessary and identify by block number)

Synthetic Aperture Radar, Ship Wakes, Surface Waves, Radar Backscatter.

20. ABSTRACT (Continue on reverse side if necessary and identify by block number)

The Gulf of Alaska SAR experiment was conducted during 9-14 March 1984 to investigate SAR imaging of narrow-V wakes in a deep mixed-layer environment so that surface manifestations of ship-generated internal waves could be made small. Five SAR flights were executed over large ships of opportunity in deep water where the mixed layer depth exceeded 100 m in all cases. SAR images were obtained in Sea States 1-4. Range and azimuthally traveling ships were imaged. The incidence angles of azimuthally traveling ships ranged from 24 to 53 degrees.

DD FORM 1 JAN 73 1473 EDITION OF 1 NOV 65 IS OBSOLETE
S/N 0102-LF-014-6601

Unclassified
SECURITY CLASSIFICATION OF THIS PAGE (When Data Entered)

The following specific conclusions are derived:

1. The half-angles associated with narrow-V wakes are consistent with first-order Bragg surface wave theory described by Case et al. (1984).

2. The decay rate along the bright arms of the narrow-V wake is consistent with a combined viscous and radiation decay of short surface waves with first-order Bragg wave lengths.

3. Narrow-V wakes are observed in Sea States 1-3 at incidence angles less than or equal to 44 degrees. The limitation is due to the noise threshold of the SAR system used.

4. The longest narrow-V wakes bright-arm observed is 12.0 km (31 degree incidence angle) in Sea State 1, 3.9 km (44 degree incidence angle) in Sea State 2 and 4.3 km (24 degree incidence angle) in Sea State 3. In Sea State 4 no narrow-V wakes could be observed.

5. The turbulent wake (dark band between bright arms) is observed in Sea States 1-3 at incidence angles less than 53 degrees. The limitation is due to the noise threshold in the SAR system used.

6. The longest turbulent wake length observed is 41 km (37 degree incidence angle) in Sea State 1, 4.5 km (35 degree incidence angle) in Sea State 2 and 5.5 km (24 degree incidence angle) in Sea State 3. No turbulent wake is observed in Sea State 4.

7. Continued follow-on effort is recommended to formulate and test models for predicting lengths of narrow-V and turbulent wakes. More specifically, the following tasks require additional effort: (a) establish decay rates of surface waves in Sea States greater than 1, (b) verify the clutter levels in Sea States 1-4, (c) determine the interaction of surface waves with current in the turbulent wake region, and (d) incorporate the influence of sea state on degradation of SAR resolution in producing reduced signals in the bright arms.

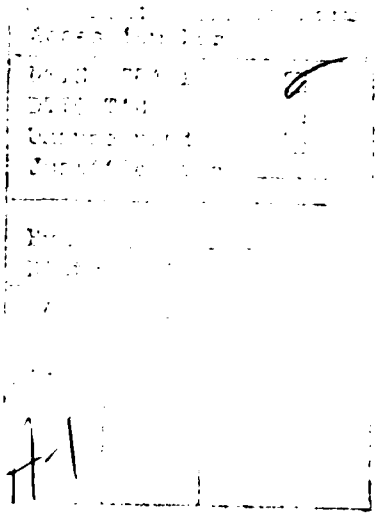

SAR IMAGING OF SHIP WAKES IN THE GULF OF ALASKA

FINAL REPORT

PREPARED BY
OMAR H. SHEMDIN
Ocean Research and Engineering
749 Foothill Blvd.
La Canada, CA 91011

For

OFFICE OF CHIEF OF NAVAL OPERATIONS
CRYSTAL CITY, VIRGINIA

(Technical Monitor: Richard Lauer)

JULY 1987

ACKNOWLEDGEMENT

The success of the Gulf of Alaska SAR experiment is credited to participation by a number of organizations. Initial planning was based on ship traffic reports provided by Ocean Routes, Inc., and environmental information provided by C.Sinex of APL. Logistical support in planning and coordination was given by Lt. J. Reed of the office of the Chief of Naval Operations. The U.S. Navy Fleet P-3 provided ship locations and the local environment. The NASA CV-990 aircraft was operated by Ames Research Center. The participation was arranged through J. Reller; G. Grant acted as Mission Director. The JPL in-flight SAR measurements were managed by T.W. Thompson. Digital SAR Processing was executed by D. Held and N. Donovan. Initial analysis of ship wakes was conducted by S.V. Hsiao. S. Borchardt of Dynamic Technology, Inc. provided the analysis of ship-generated internal waves. D. Hayt of Ocean Research and Engineering made a substantial contribution to the analysis towards the later half of the project. Program guidance and financial support was provided by Dr. Ed Harper of the Office of the Chief of Naval Operations.

EXECUTIVE SUMMARY

The Gulf of Alaska SAR experiment was conducted during 9-14 March 1984 to investigate SAR imaging of narrow-V wakes in a deep mixed-layer environment so that surface manifestations of ship-generated internal waves could be made small. Five SAR flights were executed over large ships of opportunity in deep water where the mixed layer depth exceeded 100 m in all cases. SAR images were obtained in Sea States 1-4. Range and azimuthally traveling ships were imaged. The incidence angles of azimuthally traveling ships ranged from 24 to 53 degrees. The following results are reported:

1. The half angles associated with narrow-V wakes are consistent with first order Bragg surface wave theory described by Case et al. (1984).

2. The decay rate along the bright arms of the narrow-V wake is consistent with a combined viscous and radiation decay of short surface waves with first order Bragg wave lengths.

3. Narrow-V wakes are observed in Sea States 1-3 at incidence angles less than 45 degrees. The limitation is due to the noise threshold of the SAR system used.

4. The longest narrow-V wakes bright-arm observed is 12.0 km (31 degree incidence angle) in Sea State 1, 3.9 km (44 degree incidence angle) in Sea State 2 and 4.3 km (24 degree incidence angle) in Sea State 3. In Sea State 4 no narrow-V wake is observed.

5. The turbulent wake (dark band between the bright arms) is observed in Sea States 1-3 at incidence angles less than 53 degrees. The limitation is due to the noise threshold in the SAR system used.

6. The longest turbulent wake length observed is 41 km (37 degree incidence angle) in Sea State 1, 4.5 km (35 degree incidence angle) in Sea State 2 and 5.5 km (24 degree incidence angle) in Sea State 3. No turbulent wake is observed in Sea State 4.

7. Continued effort is desirable to verify the model developed for predicting lengths of narrow-V wakes. More specifically, additional effort is needed to: (a) incorporate the decay rate of surface waves in sea states greater than 1, (b) verify the clutter levels in Sea States 1-4, (c) determine interaction of surface waves with current in turbulent wake region, and (d) incorporate the influence of sea state on degradation of SAR resolution in producing reduced signals in the bright arms.

TABLE OF CONTENTS

PAGE

Acknowledgement ii

Executive Summary iii

List of Figures vi

List of Tables x

I. Introduction 1

II. Experimental Strategy and Measurements 8

III. Data Analysis 26

IV. Experimental Results and Modeling 50

V. Summary and Conclusions 84

References 86

Appendix A. B-V Profiles for 1984 Gulf of Alaska Survey

Appendix B. CV-990 Aircraft Data and Optical Images from the Gulf of Alaska Experiment

Appendix C. Model for Determining Lengths of Bright Arms in Narrow V-Wakes

FIGURES

Figure 1. SAR and Ship Wake Geometries. 3

Figure 2. North Pacific and Gulf of Alaska Map Showing Valdez-San Francisco Se. Lane and Monthly Averaged Mixed-Layer Depth Contours for March. 10

Figure 3. Test Areas Selected. Test Area-1 Provides Abundance of Ships of Opportunity in a Deep Mixed-Layer Environment. In Test Area-2 Extensive In-Situ Measurements were Acquired During the Test Period. 11

Figure 4. Aircraft SAR Geometry. 18

Figure 5. Nominal SAR Flight Tracks Over Ships. 19

Figure 6. Daily Schedule for Deployment of P-3 and CV-990 Aircraft. .22

Figure 7. Synoptic Weather Chart for the Gulf of Alaska Provided by the National Weather Service on 13 March 1984. 25

Figure 8. Locations of P-3 AXBT Drops and Locations of Historical Profiles Examined. 27

Figure 9. AXBT Temperature Profiles Obtained on 11 March 1984. 28

Figure 10. Historical Depth-Salinity Profiles at Locations Shown in Figure 8 Obtained During February and March of Prior Years .29

Figure 11. Temperature Profile From Drop No. 15 and Salinity Profile Obtained From Model Fit to Historical Data at Station 56° 17' N, 143° 42' W. 30

Figure 12. B-V Profile Determined for Station 56° 17' N, 143° 42' W During Month of March. This Station is in Proximity of Bay Ridge When Imaged by SAR on 13 March 1984. 31

Figure 13. Salinity Model Profile Compared to In-Situ Measurements Acquired in Test Area - II. 33

Figure 14. SAR Flight Pattern Over Bay Ridge on 13 March 1984, Sea State 1. Time Ticks Every One Minute, Anchorage Local Time. . . .36

Figure 15. SAR Image of Bay Ridge on 13 March 1984 in Sea State 1. Ship is Traveling in the Same Direction as Aircraft and Located in SAR Image at 31° Incidence Angle. 37

Figure 16. Same as Figure 15 except that Ship is Traveling in Opposite Direction to Aircraft and is Located in SAR Image at 32° Incidence Angle. 38

Figure 17. Same as Figure 14 Except Ship is Located in SAR Image at 53° Incidence Angle. The Ship is Traveling in the Opposite Direction to Aircraft. 39

Figure 18. Same as Figure 14 Except Ship is Traveling in Range Direction. 41

Figure 19. SAR Flight Pattern Over San Sinena II on 11 March 1984, Sea State 2. Time Tics Every One Min., Anchorage Local Time 42

Figure 20. SAR Image of San Sinena-II on 11 March 1984, Sea State 2. Ship is Traveling in the Same Direction as Aircraft and Located in SAR Image at 44° Incidence Angle. 43

Figure 21. SAR Flight Pattern Over Unidentified Ship, Sea State 3. Time Ticks Every One Minute, Anchorage Local Time. 45

Figure 22. SAR Image of Unidentified Ship on 14 March 1984 in Sea State 3. Ship is Traveling in Same Direction as Aircraft and is located in SAR Image at 46° Incidence Angle. 46

Figure 23. Same as Figure 22, Except Ship is Traveling in Opposite Direction to Aircraft and is Located in SAR Image at 43° Incidence Angle. 47

Figure 24. SAR Image of San Sinena II on 15 March 1984, Sea State 3. Ship is Traveling in the Same Direction as Aircraft and is Located in SAR Image at 24° Incidence Angle. 48

Figure 25. Narrow-V Wake Half Angle vs. Radar Incidence Angle. The Solid Lines are Based on First and Second Order Bragg Theory for a Ship Speed 7.7 m/s ± .25 m/s (The Solid Lines Error Bands are Based on Ship Speed Uncertainty). The Error Bands of Measurements are Based on Seperate Measurement Attempts. Only One Measurement from the Georgia Straits Experiment was Available, at Ship Speed 7.7 m/s. 51

Figure 26. Coordinate Transformation of Ship Wake in Figure 15 from Polar to Cartesian Coordinates. The Distance between the Two Parallel Bright Arms of the Wake Gives the Ship Wake Angle, 2θ. The Top View has 11m Resolution Along the Wake Axis. The Bottom View has 143m Resolution Along the Wake Axis. 53

Figure 27. Bay Ridge on 13 March 1984, Sea State 1. 55

Figure 28. Raster of Cross-Wake Cuts for the Bay Ridge Displaced 143m Apart. The Bottom Cut is Located 143m Aft of the Bay Ridge. The Top Cut is Located 5,291m Aft of the Ship. The Bay Ridge Image is Shown in Figure 15.

Figure 29. Cross-Wake Cuts for Bay Ridge, shown in Figure 15. Locations

of Cuts are Noted in Insert. 57

Figure 30. Cross-Wake Cuts for San Sinena II, shown in Figure 20, Sea State 2. Arrows Locate Positions of the Bright Arms for Each Cut. Locations of Cuts are Shown in Insert. 59

Figure 31. Cross-Wake Cuts for San Sinena II, Shown in Figure 24, Sea State 3. Arrows Locate Positions of Bright Arms for Each Cut. Locations of Cuts are Shown in Insert. 60

Figure 32. Cross-Wake Cuts for Arco Sag River, Sea State 4. Arrows Locate Positions of Bright Arms. Locations of Cuts are Shown in Insert. 61

Figure 33. Cross-Wake Cuts at 858 m Aft of Ships. Arrows Locate Positions of Bright Arms in Sea States 1 and 2. 63

Figure 34. San Sinena II (Empty) on 11 March 1984, Sea State 2. 64

Figure 35. San Sinena II (Laden) on 15 March 1984, Sea State 3, Stern View. 65

Figure 36. San Sinena II (Laden) on 15 March 1984, Sea State 3, Side View. 66

Figure 37. San Sinena II (Laden) on 15 March 1984, Sea State 3, Side View (Cont'd). 67

Figure 38. Brightness Amplitude Decay Along Bright Arm with Distance Aft of Ship (Bay Ridge, $\phi = 31°$, Sea State 1). 69

Figure 39. Radar Cross Section σ_o, L-Band, HH, vs. Wind Speed and Incidence Angle. 71

Figure 40. Narrow-V Wake Length vs. Incidence Angle for Sea States 1-4. Solid Lines are Best Fits to the Data Points. 74

Figure 41. Narrow-V Wake Length vs. Sea State for Incidence Angles 30-55 Degrees. Solid and Dashed Lines Are Expected Fits to Data. . . .75

Figure 42. Comparison between Predicted and Measured Wake Lengths. 77

Figure 43. B-V Profile Used by Dynamic Technology (See Figure 12) to Compute Ship-Generated Internal Wave Modulations. 79

Figure 44. Dispersion Curves for Gulf of Alaska Stratified Layer in the Proximity of Bay Ridge on 13 March 1984. 80

Figure 45. (a) Surface Velocities and (b) Surface Strains Computed by Dynamic Technology for Bay Ridge on 13 March 1984. 81

Figure 46. Simulated Radar Modulation Induced by Ship-Generated Internal Waves that Would Correspond to Bay Ridge on 13 March 1984. 83

TABLES

Table 1. Vessel Traffic To/From Valdez, Alaska (November, 1983) . . 12

Table 2. Vessel Details Enroute To/From Valdez, Alaska (November 1983 , Measurements are in Meters) 13

Table 3. NASA/JPL Aircraft L-Band SAR Parameters 16

Table 4. NASA/JPL Aircraft SAR Digital Processing Parameters. 17

Table 5. Site Location, Ship-Related Information and Environmental Observations Reported by the P-3 Aircraft. 23

Table 6. Summary of Ships Encountered and Observations Obtained with Each Aircraft. 24

Table 7. Summary of Turbulent Wake Lengths Measured for All the Ships Encountered in the Gulf of Alaska. 78

I. INTRODUCTION

A variety of ocean surface features have been imaged by the SEASAT synthetic aperture radar (SAR). A compilation of representative images can be found in Fu and Holt (1982). The SEASAT-SAR operated at 1.275 GHz frequency and 23 deg incidence angle. The Bragg resonant waves correspond to short gravity waves that are approximately 30 cm in length. Hence, the features observed with the SEASAT-SAR are modulations of short gravity waves induced by ambient processes naturally present in the ocean, or induced by ships. The observed features suggest that surface waves, internal waves, boundary currents, warm and cold rings, bathymetric features, atmospheric turbulence imprints and ship wakes can be observed under certain environmental conditions.

Progress has been achieved toward understanding how and why SAR images ocean surface features. Among the better understood processes are those associated with surface waves. Less understood, but now more vigorously pursued, are the SAR processes associated with internal waves, ship wakes and current boundaries.

SAR imaging of ship wakes is investigated systematically in this report. Narrow V-wakes (inclusive angles ranging from 6 to 20 deg) have been reported (Hammand et al., 1984) based on analysis of SEASAT-SAR and aircraft SAR images. The classical Kelvin Wake (39 deg inclusive angle) has been observed in SAR images under certain conditions (highly visible in range travelling ships).

Initial analysis of narrow V-wakes emphasized ship-generated internal waves as the generating mechanism. Here, internal waves, which are associated with small phase speeds, compared to surface waves, propagate outward from the axis of ship motion. The surface strain induced by internal waves modulate the short surface waves which in turn cause a modulated radar backscatter. The

wake angle, being proportional to the ratio of internal wave phase velocity to ship speed, is smaller than that of a traditional Kelvin wake. This seemingly logical explanation has many difficulties which defy present understanding of the physics associated with straining of short surface waves by internal waves. The predicted radar backscatter modulations derived from the internal wave modulations in a deep mixed layer region (mixed layer depth greater than 100 m) are one to two orders of magnitude smaller than the observed modulations across the narrow-V wake arms. These, and other discrepancies constituted the need for the additional investigation, described here, to determine the genesis of the narrow V-wakes.

Another possible explanation of the narrow-V wakes is the backscatter from short surface waves that are generated by the ship's hull, as a result of a highly turbulent boundary layer that is interacting with the ocean surface. This mechanism is hypothesized by Case et al (1984) to be composed of scattering centers of short waves generated along the ship's hull. A possible analysis of such a mechanism is given by Witting and Vaglio-Laurin (1985). The waves generated in each scattering center propagate outward along radial lines at their group velocities. Hence, radar may detect such short waves at any number of look angles relative to the ship's axis. The angle in the V-wake is determined, to a large extent, by the ratio of the short waves group velocity to the ship's speed. A more precise determination of the narrow V-angle requires definition of the radar look angle relative to the ship axis, as shown in Figure 1. Using the above hypothesis, the wake half-angles on the starboard, θ_s, and port, θ_p, sides differ and are given by

$$\sin \theta_s = \left(\frac{C_g}{U}\right) \cos (\psi + \theta_s) \quad , \tag{1}$$

and

$$\sin \theta_p = \left(\frac{C_g}{U}\right) \cos (\psi - \theta_p) \quad , \tag{2}$$

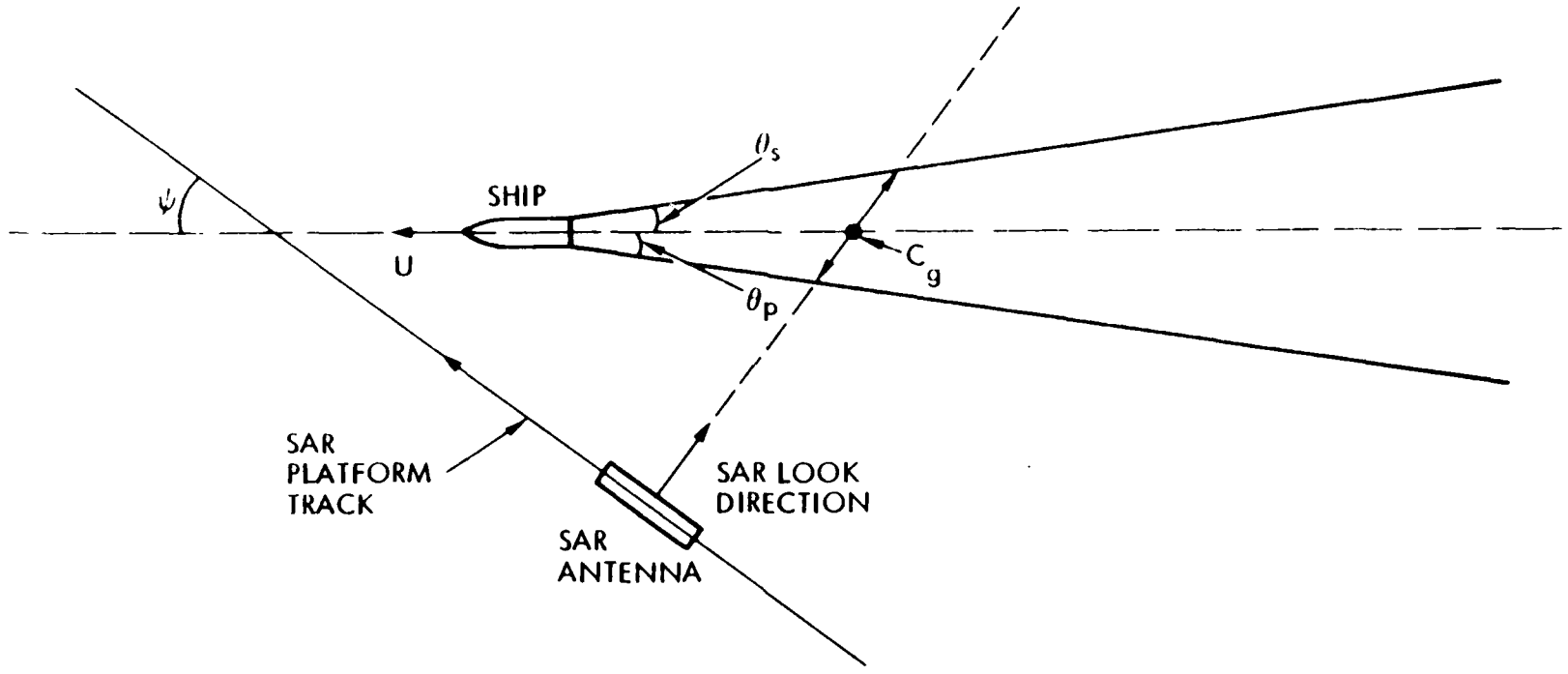

Figure 1. SAR and Ship Wake Geometries.

where C_g is the group velocity of short waves, U is ship speed and γ is the angle between the SAR platform track and ship axis. For short surface waves the group velocity is given by

$$C_g = \frac{1}{2}\left\{\frac{g}{2\pi}\lambda_s\right\}^{1/2} = 0.62\,\lambda_s^{1/2} \quad , \tag{3}$$

where g is gravitational acceleration and λ_s is wave length of short surface waves.

Radar backscatter from the sea surface is known to be dominated by specular backscatter at incidence angles less than 20 deg and by Bragg backscatter at incidence angles in the range of 20 to 70 deg (Valenzuela, 1978). At larger incidence angles wave sheltering plays an important role. Such a relatively simplified description of backscatter has been recently questioned by Kwoh and Lake (1983) who suggest, based on laboratory studies, that specular and wedge type backscatter mechanisms may be significant at incidence angles greater than 20 deg, especially for wavelengths of order 3.0 cm and shorter (X-Band and higher radar frequencies).

The Bragg backscatter to "first order" is given by (superscript refers to order)

$$\lambda_s^{(1)} = \frac{\lambda_r}{2 \sin \theta} \quad , \tag{4}$$

where λ_r is radar wave length and θ is radar incidence angle. The recent results from the Georgia Strait experiment (see Hammond et al, 1984) indicate that "higher order" Bragg backscattering may be significant. At "second order" the surface waves are twice as long as those given in Equation (4), i.e.,

$$\lambda_s^{(2)} = \frac{\lambda_r}{\sin \theta} \quad , \tag{5}$$

and the group velocity greater by $\sqrt{2}$ compared to that given in Equation (3).

In the Georgia Straits experiment (Gasparovic et al., 1986), the energy level of short waves corresponding to "first-order" Bragg were measured by in-situ slope sensors and found to be small. On the other hand, the energy level at "second-order" Bragg was found to be above the noise level. The wake half-angles observed in the SAR images were compared with those calculated [by using Equations (1) - (5)] for the SAR geometry of the experiment (ψ = 0, ϕ = 25 deg) and ship speed (7.0 m/s).

It is noted that Equations (1) and (2) are equal for ψ = 0 (azimuthly travelling ship). Both predict zero for Θ_s and Θ_p at ψ = 90 deg (range travelling ship). Hence, no narrow-V wake is predicted if the ship is travelling in the range direction (consistent with SEASAT observations). However, for such a geometry the classical Kelvin Wake (19.5 degree half-angle) has been observed in moderately active environmental conditions (moderate winds and sea states). The mechanism responsible for imaging wakes under such conditions is perceived to be different from that associated with narrow-V wakes at small ψ values. Here, the imaging mechanism is perceived to be a "Bragg Carpet" like surface that is modulated by classical Kelvin-type waves, yielding imaged wake geometries that are similar to the classical Kelvin wake (19.5 degree half-angle).

An important consideration derived from SEASAT-SAR images is that the geometries of narrow V-wakes are dependent on near surface environmental conditions. More specifically, the wind speed appears to play an important role in whether one, two, or no arms of the narrow V-wake are observed. The "turbulent wake", also referred to as the "stern wake", appears not to be as strongly dependent on wind speed. The turbulent wake appears, in most ship wake images, either as a dark band because the short wind-generated surface waves are destroyed by the current gradient in the wake, or as a bright band because the roughened surface in the

turbulent wake is high compared to the surrounding ocean.

Hull-generated short waves, considered to be responsible for imaging narrow-V wakes, appear in competition with the ambient short waves (Bragg Carpet) generated by the wind. Hence, successful imaging of narrow-V wakes requires that ship-generated short waves rise above the ambient short wave environment. This condition is dependent on ship size and operating conditions, and on wind speed.

A required environmental consideration (related to the generation of narrow-V wakes) is ocean stratification, as specified by the Brunt- Vaisala frequency N-values

$$N = [\frac{g}{\rho} \frac{\partial \rho}{\partial Z} - \frac{g^2}{C^2}]^{\frac{1}{2}} , \qquad (6)$$

where ρ is density, g is gravitational acceleration and C is speed of sound in water. The period of internal waves, T is given by

$$T = 2\pi/N . \qquad (7)$$

The B-V values, in cycles per hour (CPH), are computed from

$$B\text{-}V = \frac{N}{2\pi} \times 3600 . \qquad (8)$$

Evidences of ship-generated and ambient internal waves have been observed in SEASAT-SAR images in regions of shallow water stratification (see Liu et al., 1984). Narrow wakes, on the other hand, have been observed in deep and shallow waters regardless of stratification. A definitive assessment of the responsible mechanisms for SAR imaging of narrow-V wakes requires simultaneous in-situ measurements underlying the SAR images. Such in-situ measurements had not been available to supplement the SEASAT-SAR images. This situation was

amended to some extent in the Georgia Straits experiment, where B-V profiles were measured at the sites of the ship wakes being imaged. The stratification in Knight Inlet was found to be significantly higher than that in Dabob Bay. The Knight Inlet B-V values and mixed layer depths admit the possibility of non-trivial generation of ship-induced internal waves.

The Georgia Straits experiment appears to have produced useful data. However, the data set does not provide definitive information that is needed to distinguish between narrow-V wakes generated by ship-induced waves (of Bragg lengths), or by surface waves modulated by ship-generated internal waves. This ambiguity can be better resolved if the ship wake is imaged in a deep mixed-layer, or totally unstratified, ocean environment.

In summary, while progress has been made to reduce the level of speculation on the mechanisms responsible for SAR imaging of ship wakes, further work is required to provide more definitive answers on the relative importance of the surface versus subsurface mechanisms responsible for generating narrow-V wakes.

The objectives of the Gulf of Alaska SAR Experiment are:

1. Obtain images of ship wakes in a deep mixed - layer ocean environment.
2. Investigate dependence of ship wake signatures on wind speed (sea state), SAR geometry, ship track relative to SAR flight direction, decay rates of short waves, SAR noise and ambient backscatter (clutter).

II. EXPERIMENTAL STRATEGY AND MEASUREMENT

A. Site - Selection

The considerations that determined the selection of Gulf of Alaska as a site for SAR imaging of ship wakes are:

(a) Existence of a stable and deep mixed layer (in excess of 100m) during the winter months.

(b) Frequent ships of opportunity traveling along the sea lane from Los Angeles/San Francisco, California to Valdez, Alaska.

In a deep mixed layer the keels of large ships, such as super-tankers, remain well above the mixed layer depth. The internal waves generated by a ship's hull remain small in amplitude. Hence, their induced strain on the ocean surface is expected to be small (calculations are discussed in Chapter IV). In such a setting, ship-generated surface waves play a dominant role in determining the magnitude of radar backscatter in the narrow-V wake bright arms. The detectability of a narrow-V wake is dependent on radar clutter which is in turn dependent on sea state (e.g. wind speed and swell). In the open ocean it is desirable to investigate surface waves generated by large ships so that radar backscatter intensity in the wake arms can remain large compared to ambient backscatter. The oil tanker traffic along the Valdez-San Francisco sea lane offers a desirable opportunity to investigate wakes of such large ships.

Another consideration for the selection of the Gulf of Alaska site is the availability of facilities for deployment of aircraft. Here, both Seattle, Washington and Anchorage, Alaska provided satisfactory sites.

In summary, the requirements considered primary for achieving the objectives of the Gulf of Alaska experiment are:

(a) Presence of a deep mixed layer (depths in excess of 100m) over

a large area of interest.

(b) High probability of encounter with ships of opportunity.

(c) Possibility of achieving a varied range of sea states over the aircraft operating range.

The test area selected is in the north-east Pacific Ocean. The median mixed-layer depths for this area are given by Stark and Sinex (1983), shown in Figure 2 for the month of March. This figure indicates that the mixed layer depths exceed 100m over a large area of the north-east Pacific Ocean. The sub-area selected for ship encounters is shown in Figure 3. It is bounded by the 100m mixed-layer depth contour to the south, the west coast of continental U.S. and Canada to the east and longitude 160°W to the west. Within this sub-area, two specific test areas are selected:

(a) 200km swath bounding the Valdez-San Francisco/Los Angeles sea lane, denoted by Test Area I.

(b) The area in proximity of Latitude 50°N, Longitude $155^{o}W$, denoted by Test Area II. The latter was selected because of availability of research vessels during March 1984, to provide relevant in-situ measurements.

The frequency of vessel traffic along the San Francisco-Valdez sea lane is shown in Table 1 for a typical month, November 1983. From 29 October to 1 December 1983, 24 major vessels filed plans in San Francisco to steam to, or arrive from, Valdez. The characteristics of these vessels are shown in Table 2. The ship lengths are in the range 191-291m, the drafts are in the range 11-17m, and the beams are in the range 29-42m. The smallest vessel displaced 34,474 DWT and the largest displaced 121,000 DWT.

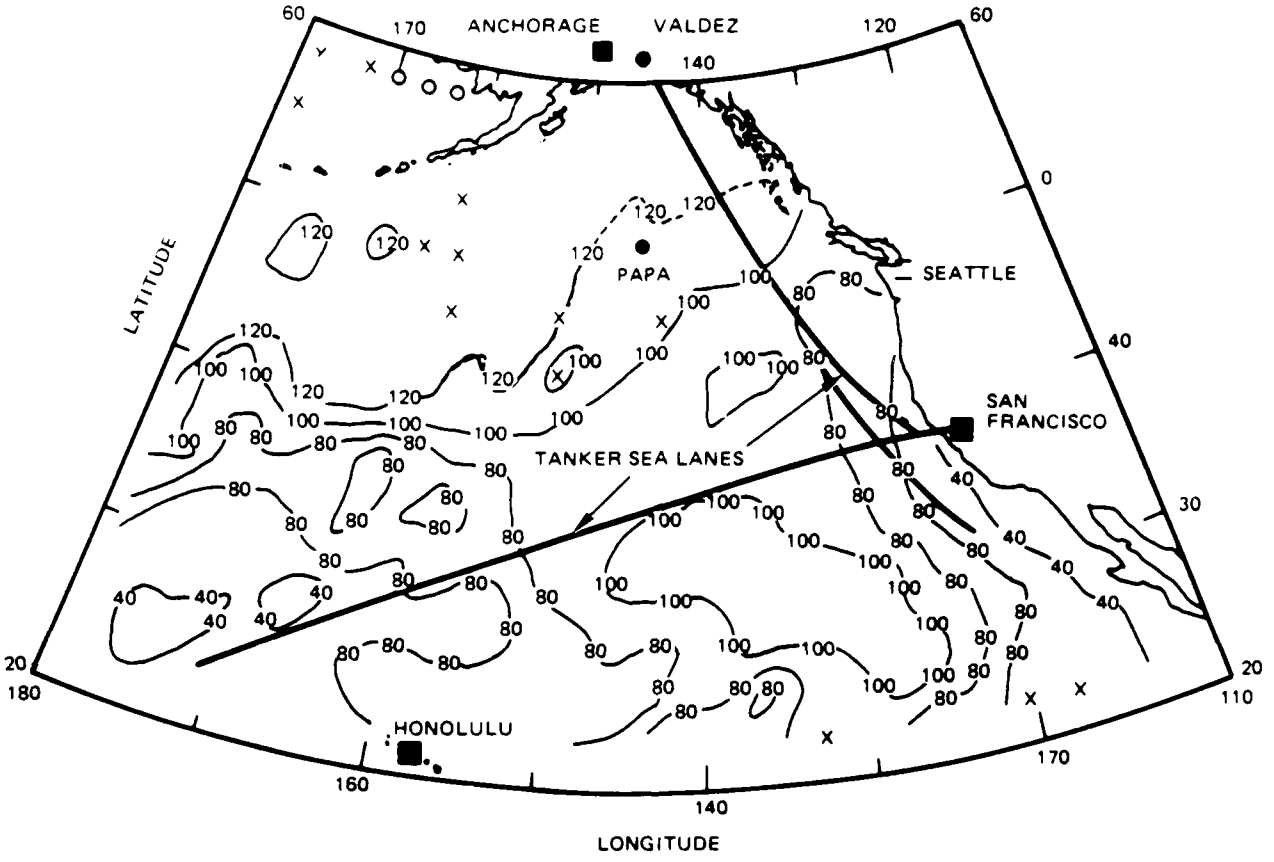

X INDICATES FEWER THAN 10 PROFILES IN GRID CELL

■ AIRPORTS

Figure 2. North Pacific and Gulf of Alaska Map Showing Valdez-San Francisco Sea Lane and Monthly Averaged Mixed-Layer Depth Contours for March.

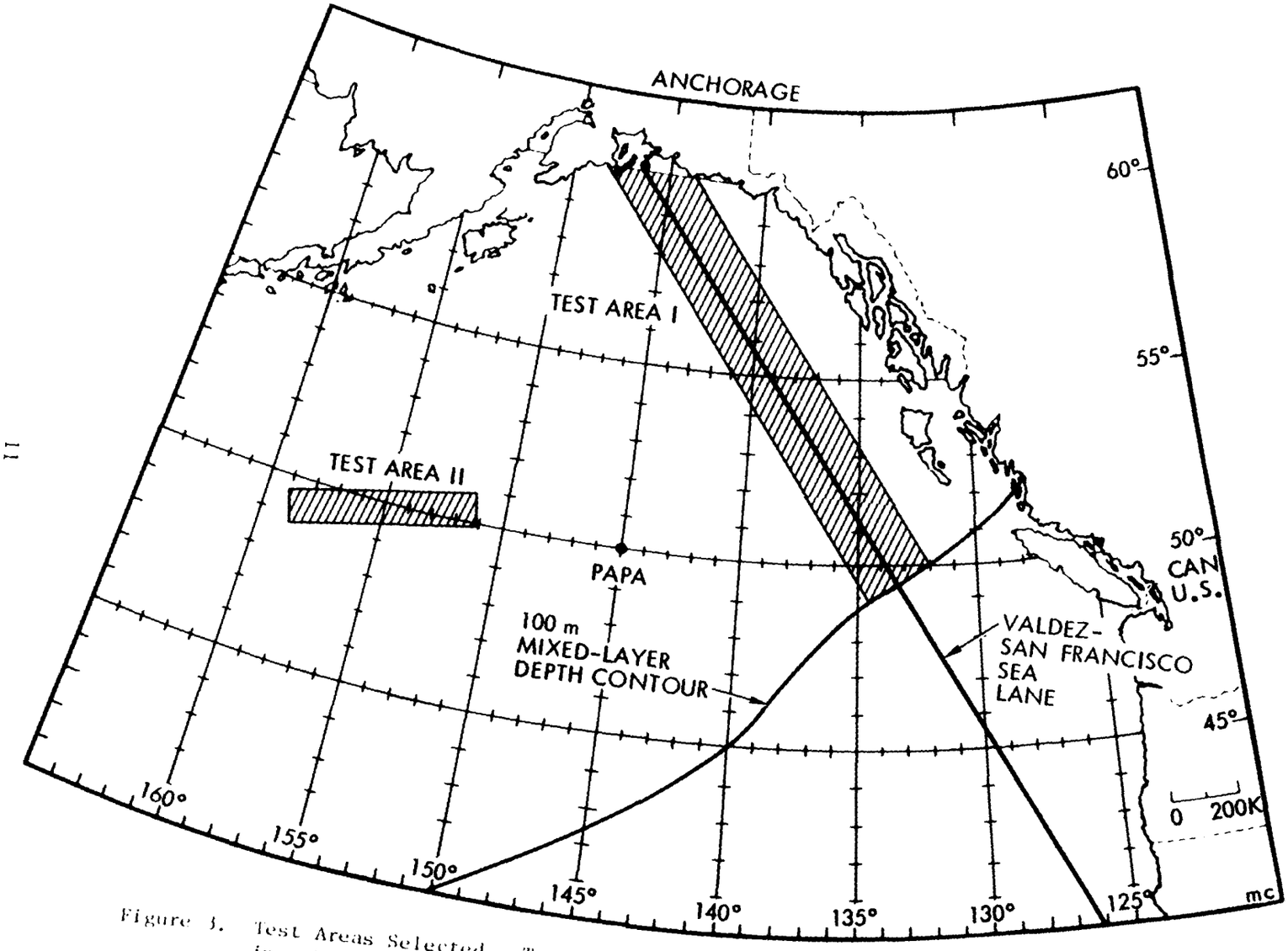

Figure 3. Test Areas Selected. Test Area-1 Provides Abundance of Ships of Opportunity in a Deep Mixed-Layer Environment. In Test Area-2 Extensive In-Situ Measurements were Acquired During the Test Period.

Table 1. Vessel Traffic To/From Valdez, Alaska (November, 1983).

	Vessel Name	Approximate Time Departure to Valdez	Approximate Time of Arrival from Valdez
1.	ARCO SAG River	29 Oct-0245L	
2.	Chevron Oregon		30 Oct-0615L
3.	Exxon New Orleans	30 Oct-1355L	
4.	Chevron Louisiana		31 Oct-1215L
5.	Chevron Oregon	31 Oct-1755L	
6.	ARCO Juneau	04 Nov-1645L	
7.	Chevron California	08 Nov-0425L	
8.	Exxon Philadelphia		08 Nov-1500L
9.	Chevron Washington	08 Nov-2200L	
10.	Exxon Philadelphia	10 Nov-0825L	
11.	Exxon New Orleans		11 Nov-0910L
12.	Chevron Colorado		11 Nov-2030L
13.	Exxon New Orleans	12 Nov-2335L	
14.	Prince Willaim Sound	13 Nov-0020L	
15.	Overseas Juneau	14 Nov-1420L	
16.	Manhatten	15 Nov-1300L	
17.	Exxon Philadelphia		21 Nov-0900L
18.	Exxon Philadelphia	23 Nov-2130L	
19.	Exxon New Orleans		24 Nov-0135L
20.	Exxon New Orleans	25 Nov-2155L	
21.	Chevron Mississippi		27 Nov-1535L
22.	Chevron Mississippi	29 Nov-1940L	
23.	Chevron Washington		30 Nov-1200L
24.	Overseas Juneau	01 Dec-0240L	

Table 2. Vessel Details Enroute To/From Valdez, Alaska, (November, 1983). (All Measurements are in Meters)

Vessel Name	Length	Breadth	Draft	Freeboard	DWT
ARCO Sag River	240	32	13	4	70917
ARCO Juneau	259	42	16	5	120319
Chevron California	240	32	13	4	70213
Chevron Colorado	191	29	11	4	34474
Chevron Louisiana	191	29	11	4	39515
Chevron Mississippi	240	32	13	4	70213
Chevron Oregon	191	29	11	4	40119
Chevron Washington	191	29	11	4	39561
Exxon New Orleans	233	35	13	4	67847
Exxon Philadelphia	233	38	13	4	75649
Manhatten	291	40	16	5	120000
Overseas Juneau	259	42	16	5	120476
Prince William Sound	252	42	17	5	121000

The third consideration for choosing the test area is wind speed. To assess this concern, sea level pressure patterns were examined over the North Pacific to determine the frequency of high, moderate and low wind speeds over the region. Two prevailing pressure patterns were identified. The first is a high pressure cell over the Gulf of Alaska that produces low to moderate wind speeds over both of the test sites shown in Figure 3. The second pattern is a low pressure cell over the Gulf of Alaska that produces high wind speeds over both test sites.

The wind speed statistics from Ocean Station PAPA (50°N, 155°W) are noted below:

Wind Speed (m/s)	% Occurrence
0 - 2	2
2 - 3.5	4
3.5 - 5.5	10
5.5 - 8.5	20
8.5 - 11	17
11 - 14	20
14 - 17	14
17 - 20.5	9
20.5 - 24	2
>24	

The most frequent wind speeds at this fixed position are in the range of 5.5 to 14 m/s.

B. Measurements

1. Synthetic Aperature Radar

The Jet Propulsion Laboratory (JPL) L-Band SAR system was used as the primary system for imaging ship wakes. The SAR system was deployed aboard NASA CV-990 aircraft (both SAR and aircraft were destroyed in a fire 18 months after the Gulf of Alaska experiment). The characteristics of the JPL radar are given in Tables 3 and 4. The radar had a center frequency of 1.225 GHz, which corresponds to 25cm in radar wave length. The antenna beam width was 18 degrees. The nominal SAR resolution for four looks was 11m x 11m in range and azimuth directions, respectively. The angles of incidence ranged from 0 - 60 deg. Both horizontal and vertical polarizations could be achieved. The SAR slant range/ground geometries are depicted in Figure 4, for both quad-and dual polarizations. The quad polarization provided 10.0km swath widths, while dual polarization provided 18.0km swath widths. The HH polarization (horizontal transmit/horizontal receive) was adopted as the primary mode for data acquisition and processing. The results in this report are based on these HH images. The JPL - SAR system had been subjected to extensive calibration tests over a well known site in Death Valley, California. The pixel intensities in the SAR image were compared with corresponding σ_o values and found to match within ± 1.0 db in relative magnitude and within ±2.5 db in absolute magnitudes. In the Gulf of Alaska experiment, the variation in pixel intensity (dynamic range) was considered adequate for defining radar backscatter variability over a ship wake.

The flight pattern selected over ships is shown schematically in Figure 5. Initial plans included ship crossings at 45 degrees with respect to the direction of the ship track (see Figure 19). After the first flight this pattern was found not to be achievable. Consequently, a horse race-track

Table 3. NASA/JPL Aircraft L-Band SAR Parameters.

Parameters	Value
Frequency	1225 MHz
Wavelength	24.6 cm
Pulse length	4.9 μs
Bandwidth	19.3 MHz
Peak radiated power	4 kW
Transmitted polarizations	Horizontal and Vertical interlaced
Received polarizations	HH, HV, VV, VH
Antenna azimuth beamwidth	5 deg (Summer-85, microstrip II)
	18 deg (baggage door, see note)
	7 deg (Fall-84, microstrip I)
Antenna range beamwidth	75 deg (all antennas)
Antenna beam center gain	18 dB (Summer-85, microstrip II)
	12 dB (baggage door, see note)
	16 dB (Fall-84, microstrip I)
Nominal altitude	6.0 to 12.0 km
Nominal velocity	200 to 250 m/s
Pulse repetition frequency	1.5 (aircraft velocity in knots)
Look angle range	0-60 deg
Optical sweep time	55 μs
Optical sweep film width	25 mm

Note: The baggage door antenna was used during the Gulf of Alaska Experiment.

Table 4. NASA/JPL Aircraft SAR Digital Processing Parameters.

Parameters	Value
DIGITAL IMAGES	
Raw data quantization	6 bits
Azimuth pixel spacing/resolution	11 m/13 m
Number of azimuth pixels	1024
Number of looks	4
Slant range pixel spacing/resolution	7.5 m/7.9m
Ground range pixel spacing	15 m at 30 deg, 10 m at 50 deg
Ground range resolution	16 m at 30 deg, 10 m at 50 deg
Number of range pixels	927

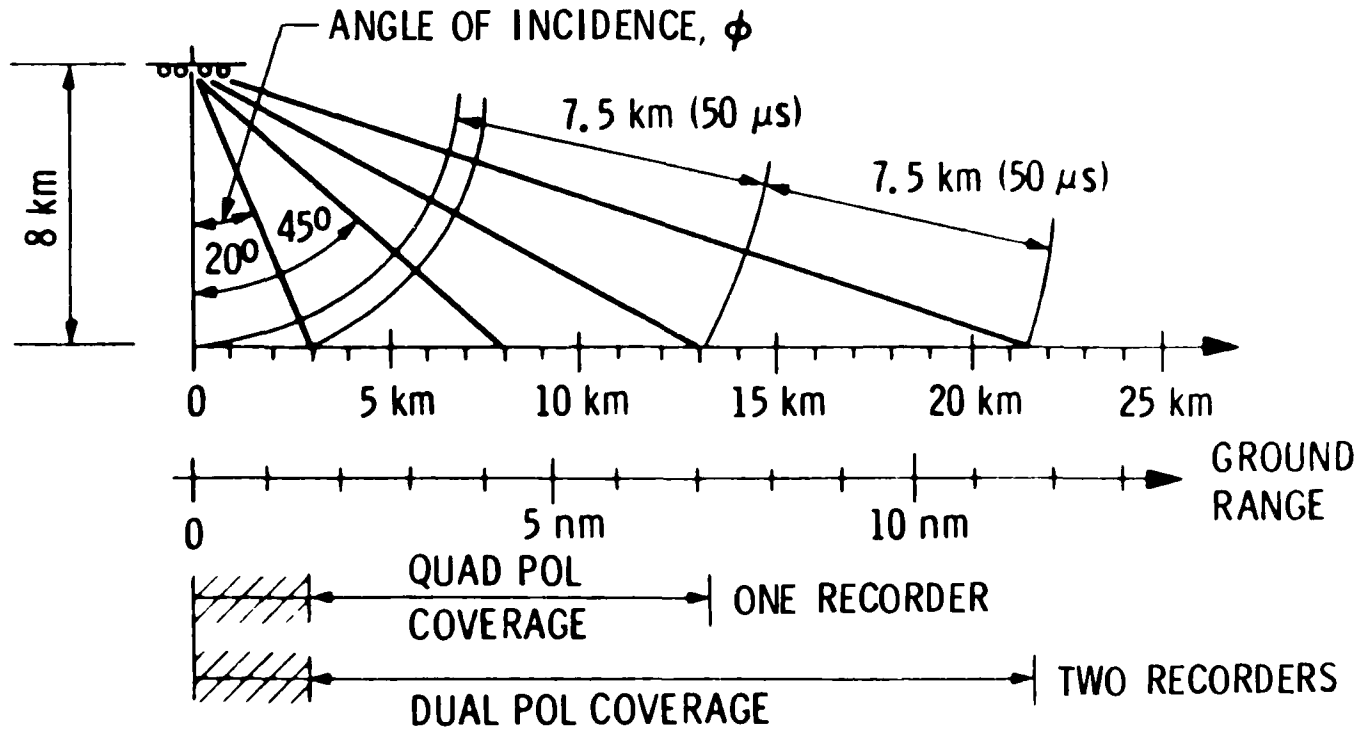

Figure 4. Aircraft SAR Geometry.

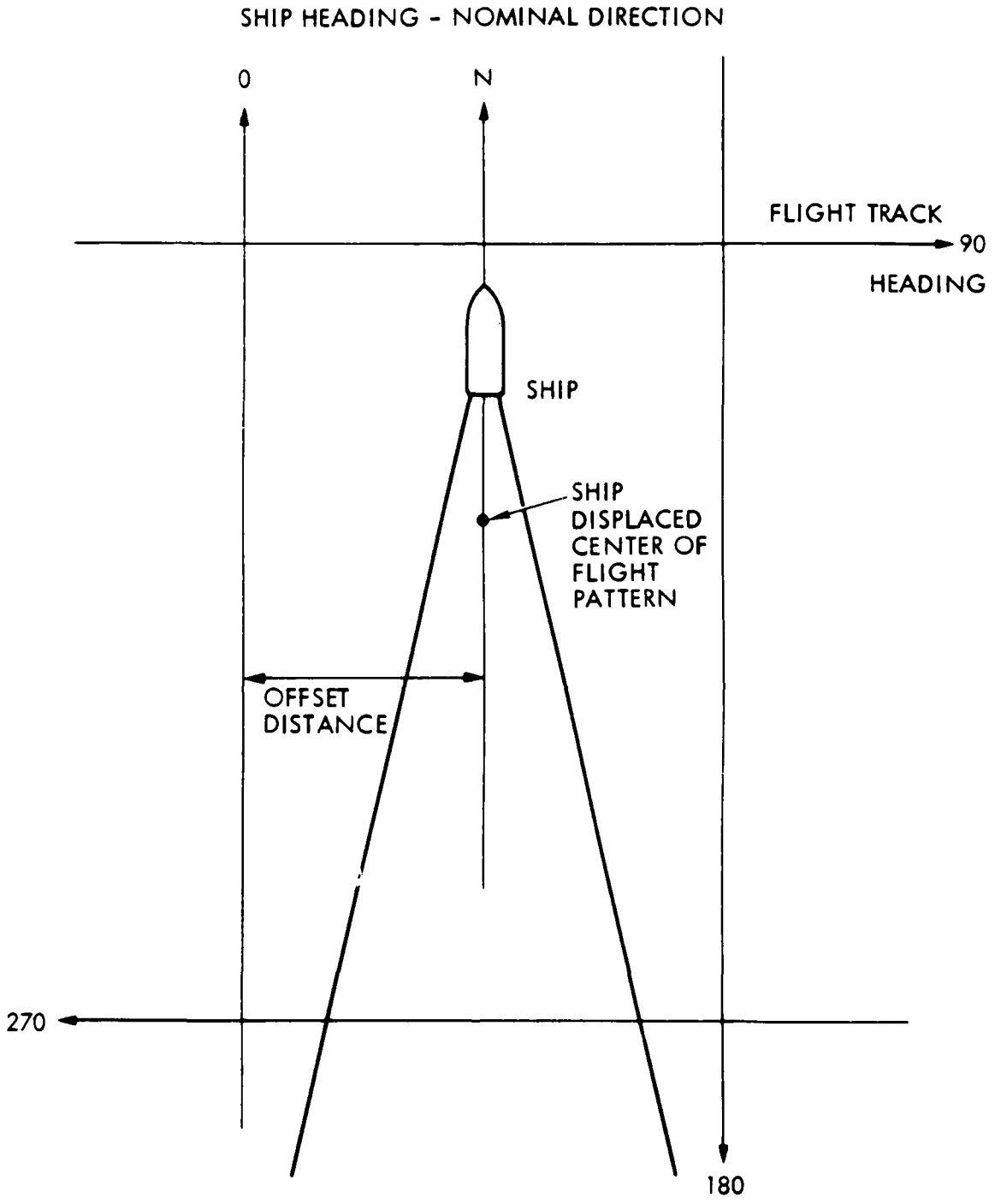

Figure 5. Nominal SAR Flight Tracks Over Ships.

pattern was adopted for the remaining flights (see Figure 14). This provided images of ships traveling only in pure range (ψ = 90) or pure azimuth (ψ = 0) directions. The offset of the ship axis was varied relative to aircraft nadir (ψ = 0). The data sets provide azimuthally traveling ships (ψ = 0) in the range of incidence angles, θ, 26 - 56 degrees.

2. Environmental Measurements and In-Situ Observations

Environmental measurements and in-situ observations were obtained using a U.S. Navy Fleet P-3 aircraft. The aircraft operated out of Elmendorff, Alaska in coordination with the NASA: CV-990 aircraft to support the objectives of this experiment. The tasks performed by the P-3 aircraft are indicated below:

(a) Conduct a search and localization of candidate ships of opportunity that were known to be in transit in Area I.

(b) Select a ship with a prominent wake; identify and report its coordinates and time of encounter to the coordination center in Elmendorff.

(c) Drop AXBT's in the proximity of selected ship locations and record data for later analysis.

(d) Provide estimates of wind speed and direction, air temperature and wave height.

(e) Obtain still and moving pictures of the ship and its wake to 20km aft of the ship.

(f) Remain in the ship proximity to guide the CV-990 aircraft to the target area.

(g) Depart the target area when the CV-990 begins its high altitude pattern over the ship.

A daily flight schedule for deployment of the P-3 and CV-990 aircraft is shown in Figure 6. Because of limited CV-990 flights available to support the

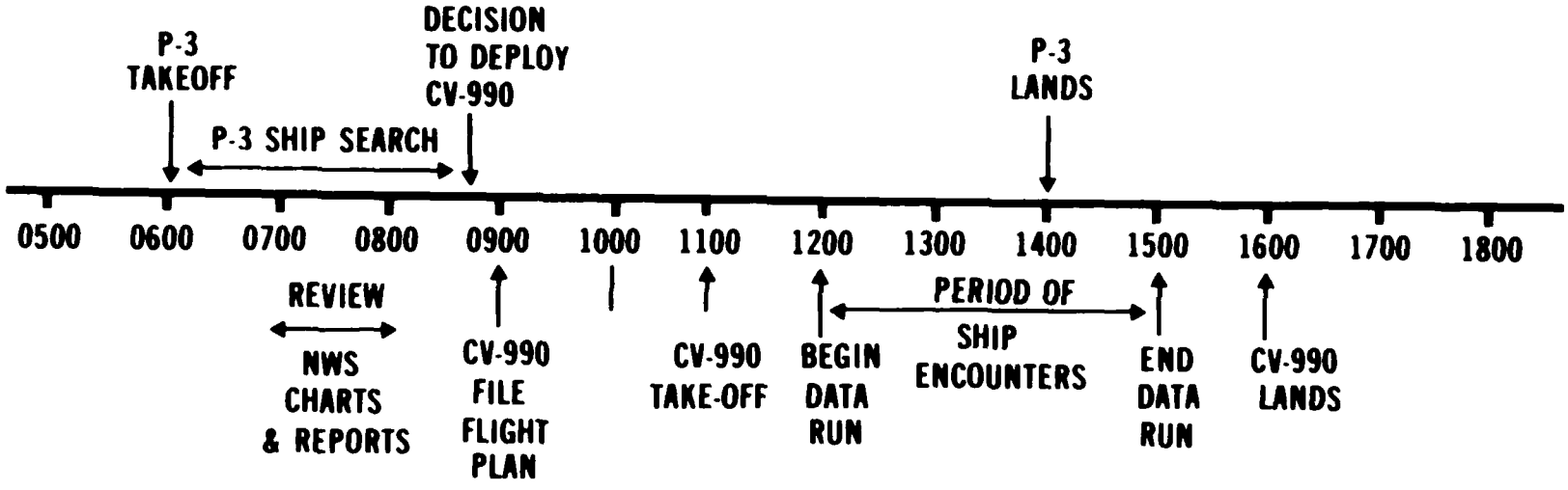

Figure 6. Daily Schedule for Deployment of P-3 and CV-990 Aircraft.

Gulf of Alaska experiment, the aircraft was deployed only after: (a) a substantial wake had been located by the P-3 and (b) desirable environmental conditions could be reported for the area. A summary of the observations reported by the P-3 is given in Table 5.

The CV-990 executed 5 missions in support of the Gulf of Alaska experiment. The mission flown on 14 March 1984 was over Test Area II. Path finding by the P-3 aircraft was not requested for the latter mission. Here, the CV-990 was able to locate a vessel at 49° 46.6'N and 155° 57.2'W. The vessel was cruising at 7.5 m/s speed with heading 087. A summary of data related to all ships encountered, and the observations obtained with each aircraft, are noted in Table 6. The ability to obtain SAR images in sea states 1-4 during this period is reflected in the synoptic weather chart shown in Figure 7. The meteorological "high" prevailing over the Gulf of Alaska allowed SAR imaging of ship wakes in Sea State 1, on 13 March 1984. Then, gradually as the meteorological "low" moved eastward from west of the Gulf of Alaska, sea state began to increase. SAR flights were scheduled systematically to capture the increasing winds. The key to the success of this effort was the availability of many targets of opportunity in different parts of the ocean.

Table 5. Site Location, Ship-Related Information and Environmental Observations Reported by the P-3 Aircraft.

Encounter Date	9 March	11 March	13 March	15 March
Designation	ARCO SAG RIVER	SAN SINENA II (Empty)	BAY RIDGE	SAN SINENA II (Laden)
LAT	54° 11.3'N	55° 25'N	57° 31.8'N	53° 29'N
LON	139° 47.4'W	141° 46'W	142° 56'W	139° 44'N
Speed (m/s)	9.0	7.5	7.5	7.5
Heading (°T)	330	305	145	140
Length (m)	246.0	246.9	334.9	246.9
Beam (m)	32.0	32.1	43.7	32.1
Draft (m)	13.2	13.3	21.4	13.3
Weight $(\frac{DWT^1}{GT^2})$	$\frac{70,917}{35,646}$	$\frac{71,589}{35,633}$	$\frac{205,000}{103,812}$	$\frac{71,589}{35,633}$
Wind Speed (m/s)	17.0	5.0	2.5	7.0-10.0
Wind Direction (°T)	125	100	110	150
Sea Surface Temp (°C)	---	7.0	---	6.0
Sea State	4	2	1	3
Wave Height (m)	2.5	1.5	1.0	3.0
Length of Wake (m) (Visiual Observation)	---	2,000	7,500	2,000

1. Dead weight tonnes

2. Gross weight tonnes

Table 6. Summary of Ships Encountered and Observations Obtained with Each Aircraft.

DATE	9 MARCH	11 MARCH	13 MARCH	14 MARCH	15 MARCH
LOCATION	AREA I	AREA I	AREA I	AREA II	AREA I
ENVIRONMENT					
SEA STATE	4	2	1	3	3
WIND SPEED (KNOTS)	33	10	5	15	15
WIND DIRECTION (°T)	125	100	110	135	150
WAVE HEIGHT (m)	2.5	1.5	1.0 (CALM)	2.0	3.0
SHIP					
DESIGNATION	ARCO SAG RIVER	SAN SINENA II	BAY RIDGE	–	SAN SINENA II
SPEED (KNOTS)	18	15	15	15	15
COURSE (°T)	330	305	145	087	140
DWT (GT)	70,917 (35,646)	71,589 (35,633)	205,000 (103,812)	–	71,589 (35,633)
LENGTH (m)	246	250	335	–	250
CV-990					
SAR IMAGES	X	X	X	X	X
PHOTOS	–	–	X	X	–
P-3					
PATH FINDING	X	X	X	–	X
WEATHER	X	X	X	–	X
AXBT	X	X	–	–	X
PHOTOS	X	X	–	–	X

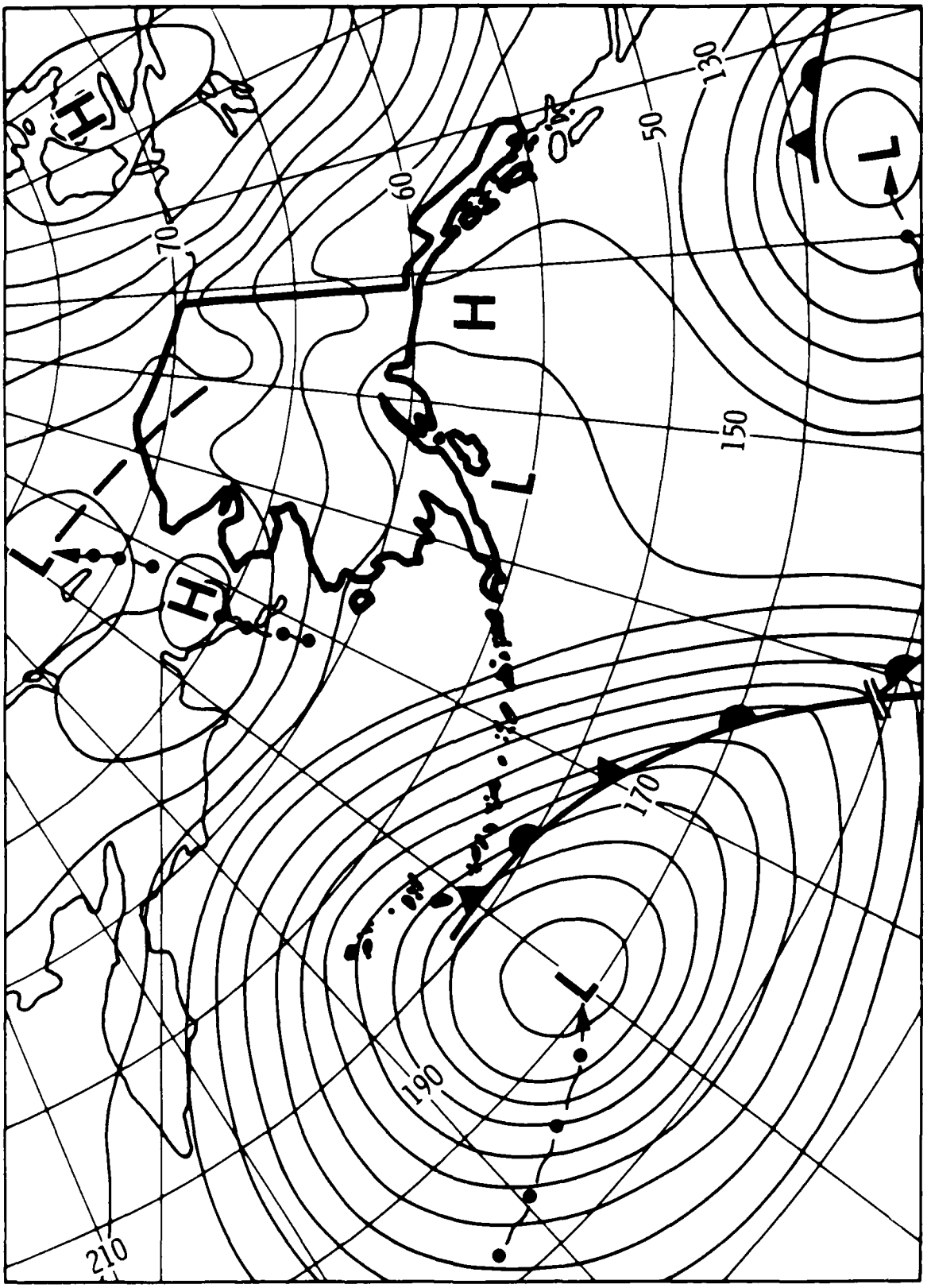

Figure 7. Synoptic Weather Chart for the Gulf of Alaska Provided by the National Weather Service on 13 March 1984.

III. DATA ANALYSIS

A. Determination of Mixed Layer Depth and B-V Profiles

Three AXBT's were dropped by the U.S. Navy Fleet P-3 in support of the Gulf of Alaska experiment; all three were dropped on 11 March 1984. The drop locations are shown in Figure 8 (see Sinex, 1984, Appendix A). The temperature profiles are shown in Figure 9. The locations of ship encounters by the CV-990 are also shown in Figure 8. The following correspondence is noted:

- Drop No. 14 location is in proximity of Arco Sag River encounter on 9 March 1984, and San Sinena II encounter on 11 March 1984.
- Drop No. 15 location is in proximity of Bay Ridge encounter on 13 March 1984.
- Drop No. 16 location is in proximity of San Sinena II encounter on 15 March 1984.

The three drops and derived B-V profiles are relevant to all the ships encountered in Test Area I, as noted in Table 5.

Because salinity is required in the determination of the total density distribution, the AXBT's by themselves are insufficient for determining the B-V profiles. Aircraft-deployed salinity measurements could not be obtained during the Gulf of Alaska experiment. Hence, a model of the salinity profile was determined for the area of interest, based on historical salinity profiles obtained in February and March months of previous years. The locations of six such historical profiles are shown in Figure 8. Ten historical salinity profiles are shown in Figure 10. A model based on these profiles is shown in Figure 11. Also, shown in Figure 11 is the temperature profile from AXBT Drop No. 15. The B-V profile, obtained by using the salinity and temperature profiles in Figure 11, is shown in Figure 12.

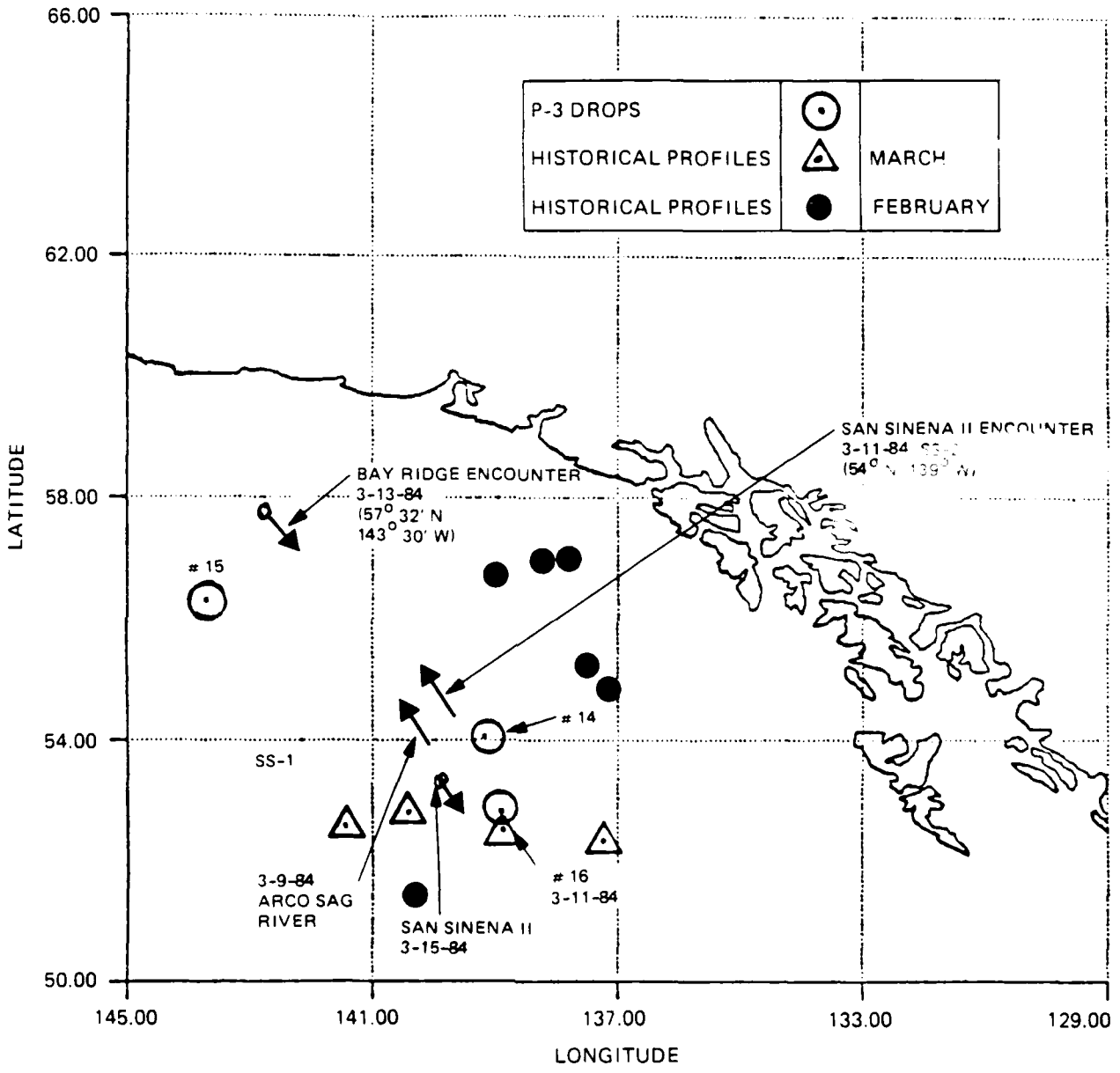

Figure 8. Locations of P-3 AXBT Drops and Locations of Historical Profiles Examined.

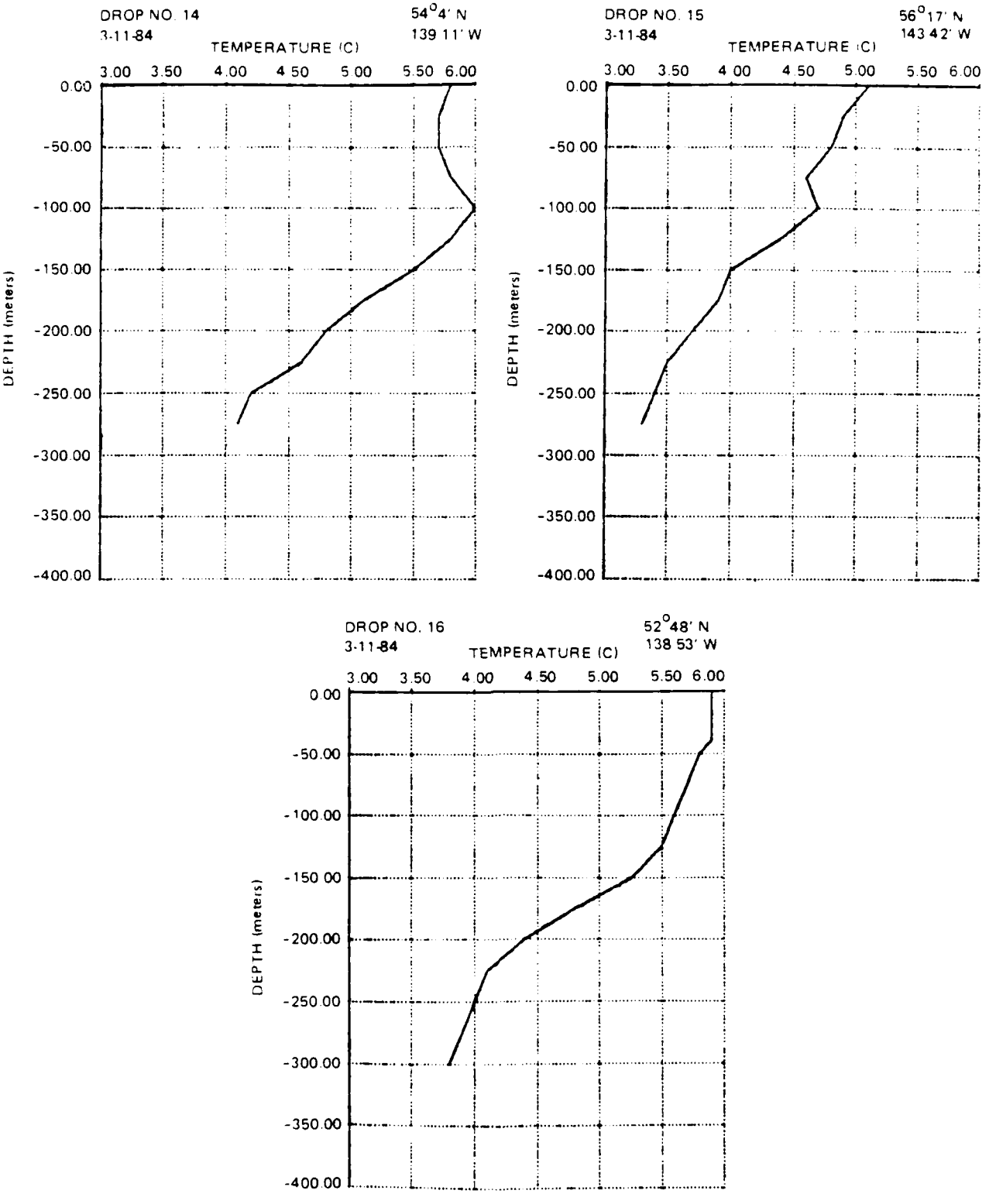

Figure 9. AXBT Temperature Profiles Obtained on 11 March 1984.

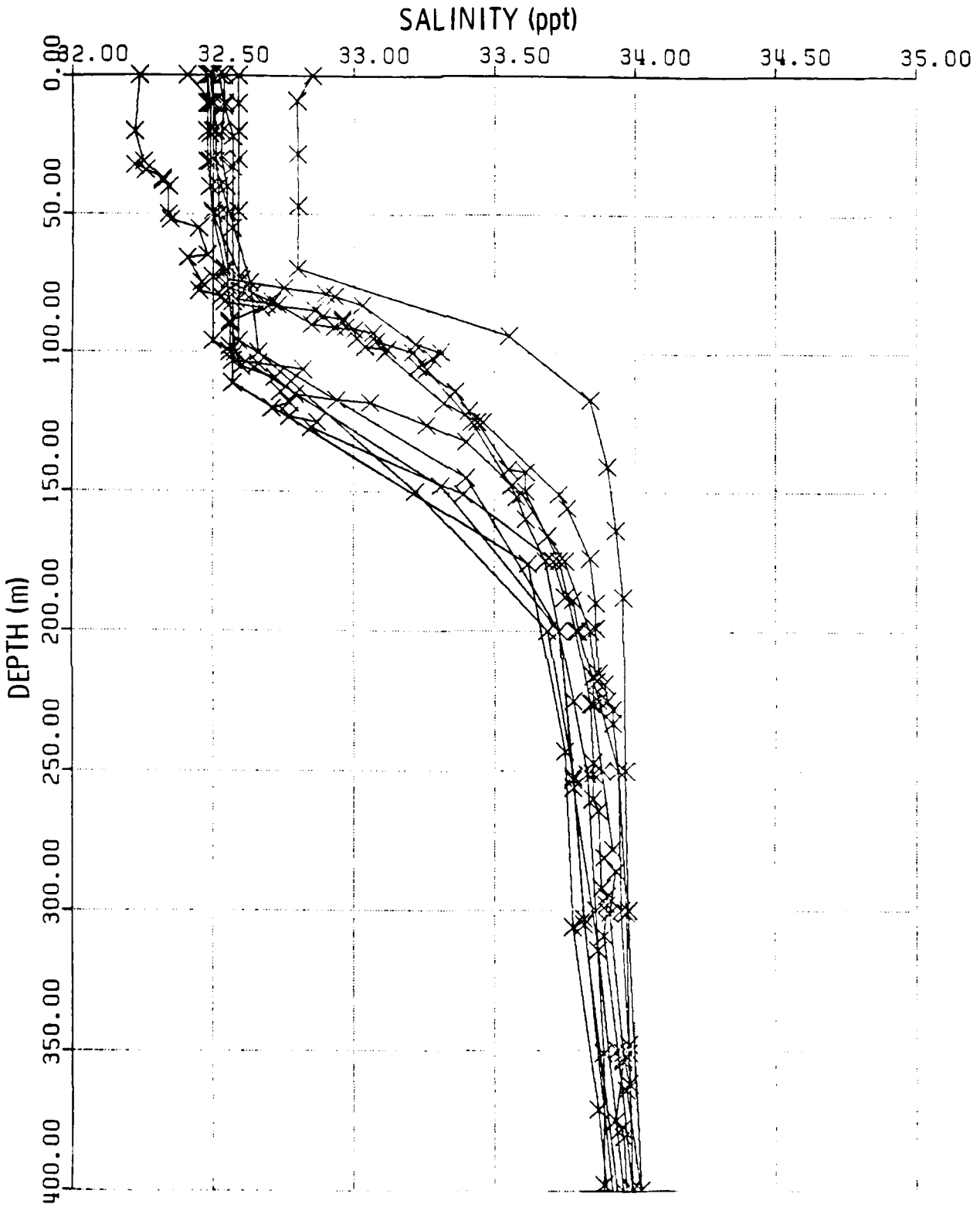

Figure 10. Historical Depth-Salinity Profiles at Locations Shown in Figure 8 Obtained During February and March.

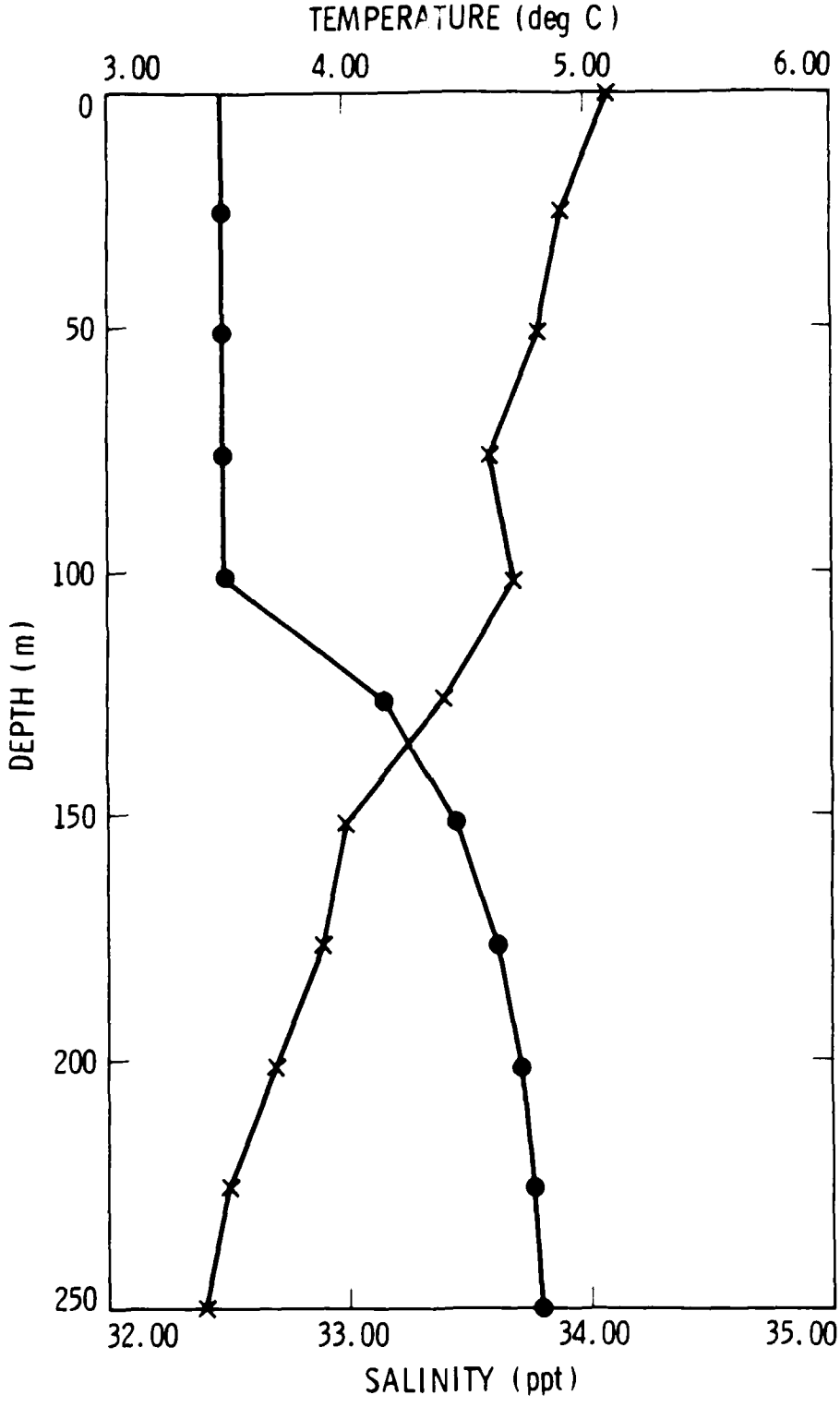

Figure 11. Temperature Profile From Drop No. 15 and Salinity Profile Obtained From Model Fit to Historical Data at Station 56° 17' N, 143° 42' W.

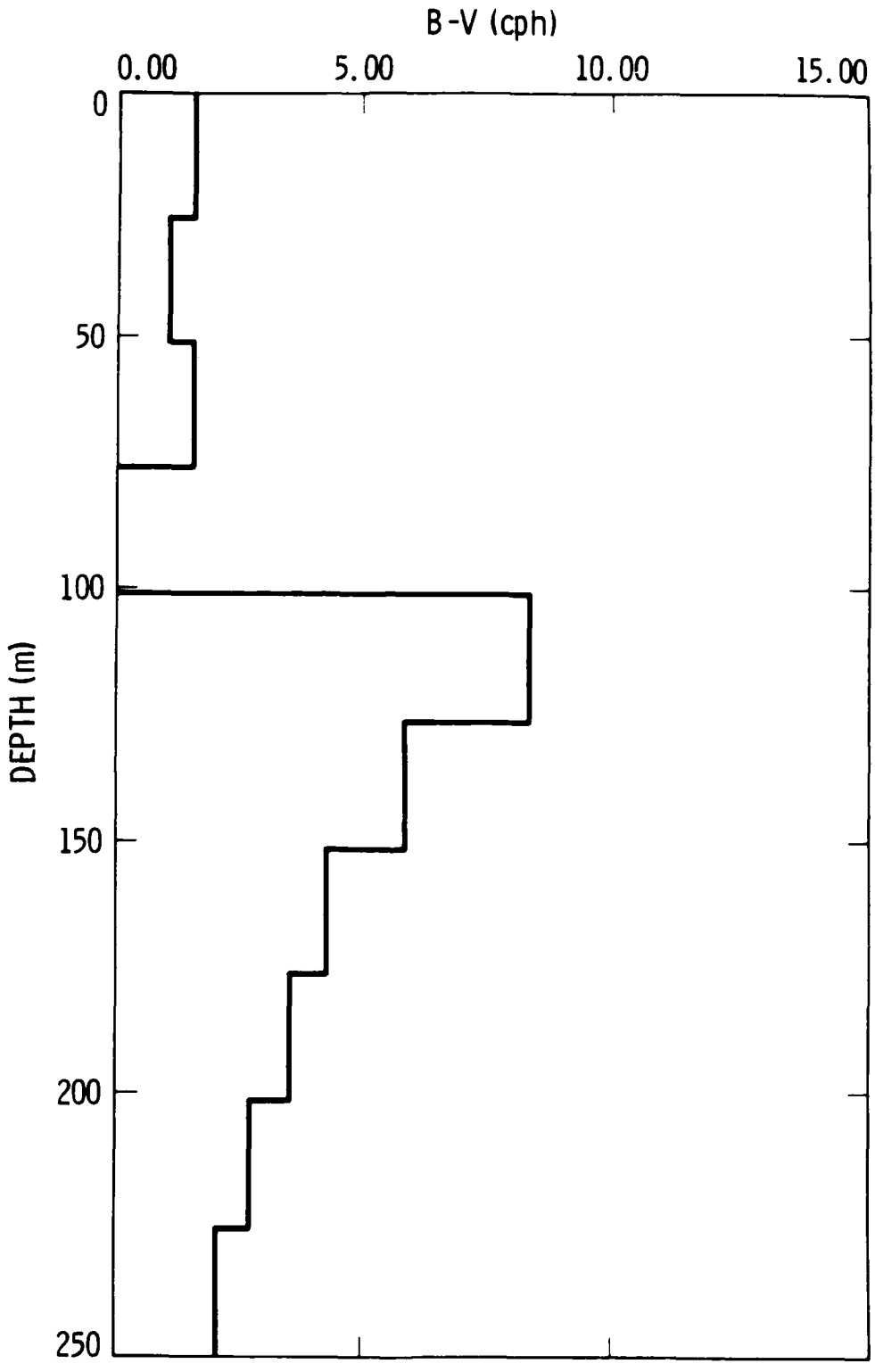

Figure 12. B-V Profile Determined for Station 56° 17' N, 14° 42' W During Month of March. This Station is in Proximity of Bay Ridge When Imaged by SAR on 13 March 1984.

A comparison of the salinity profile shown in Figure 11 with a measured in-situ profile could not be achieved in Test Area I (see Figure 2) because of lack of in-situ salinity measurements. Such a comparison was achieved in Test Area II, where in-situ salinity profiles were obtained. The latter comparison is shown in Figure 13. It demonstrates close agreement between the model, derived from historical salinity profiles, and the measured salinity profiles. The shape of the salinity profile below the mixed layer depth is approximately constant in the Gulf of Alaska, as can be inferred from Figure 10. The model salinity distribution, below the mixed layer, is specified below:

Distance Below Halocline Top (m)	Salinity (ppt)
0	32.5
25	33.16
50	33.45
75	33.62
100	33.72
125	33.77
150	33.80
175	33.82
200	33.85
225	33.87
250	33.90

The procedure followed in matching the salinity and temperature profiles is described in detail by Sinex (1984, Appendix A). Briefly, the mixed layer depth is determined by comparing the temperature profile from AXBT drops to historical profiles of salinity and temperature in the same area. Given the mixed layer depth, the salinity profile is fixed such that it is a constant above the mixed layer depth, and the salinity distribution, noted above, is specified below the mixed layer depth. The temperature distribution measured with the AXBT drop is then used with the model salinity profile to determine the B-V profile.

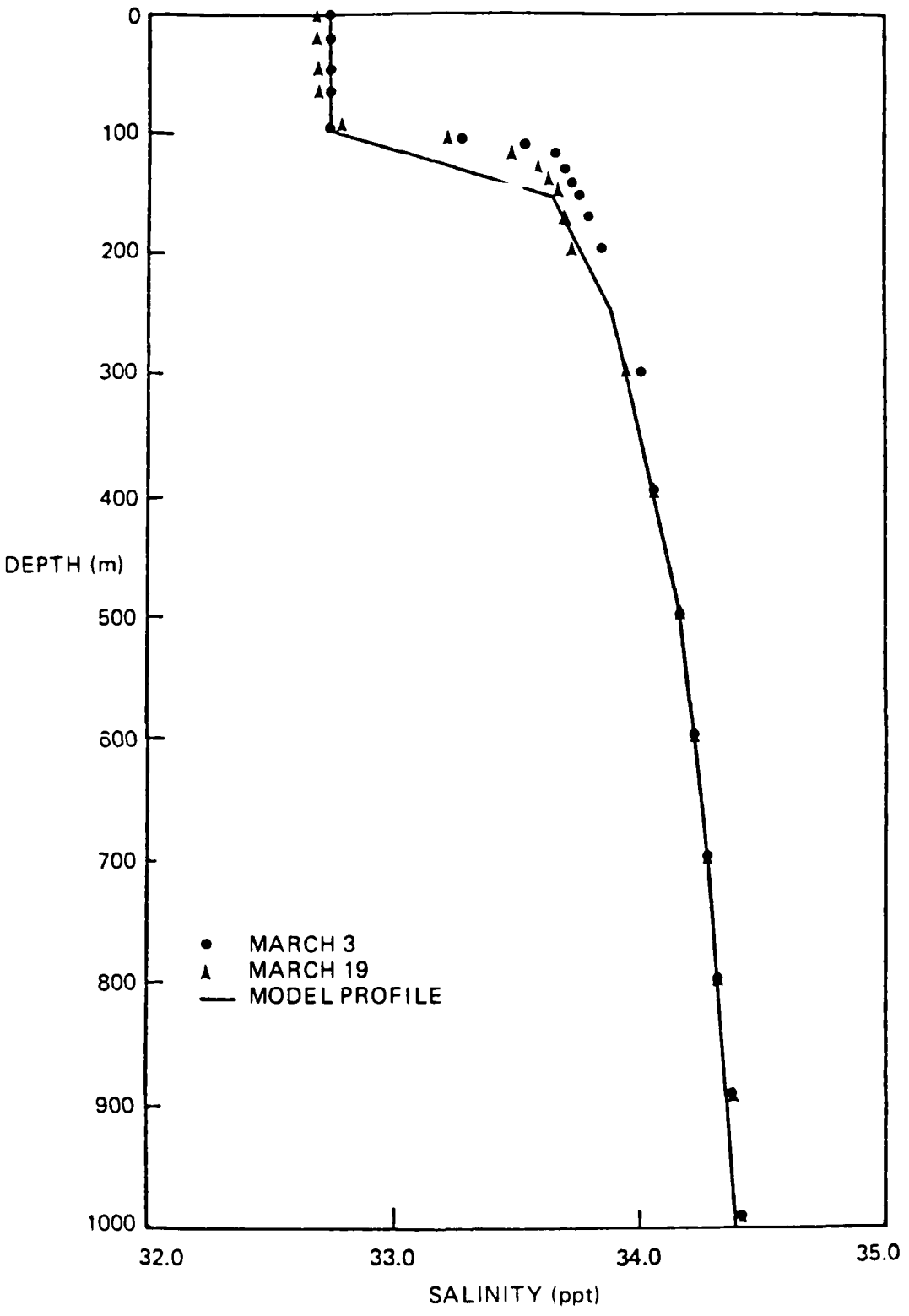

Figure 13. Salinity Model Profile Compared to In-Situ Measurements Acquired in Test Area - II.

The B-V profile shown in Figure 12 is similar in shape to three other profiles determined for Test Area I. It is also similar in shape to those determined for Test Area II. In the mixed layer a constant salinity of 32.5 ppt was assumed. Below the mixed layer the salinity was assumed to increase by 1.5 ppt down to a depth of 500m.

The B-V profile shown in Figure 12 (Drop No. 15) is also similar to the historical B-V profiles determined for Test Area I (see Sinex, 1984). The peak B-V values are typically 10 cph at the mixed layer depth and immediately below. Within the mixed layer depth, weak temperature gradients produce B-V values in the range 1-2 cph. Comparing these estimates to histroical records of salinity and temperature profiles, it is concluded that actual stratification levels within the mixed layer do not generate a B-V value in excess of 2 cph.

In summary, the mixed layer depths and maximum B-V values expected in the proximity of the ships encounterd are tabulated below:

Date	9 March	11 March	13 March	14 March	15 March
Ship Designation	Arco Sag River	San Sinena II	Bay Ridge	-	San Sinema II
Mixed Layer Depth (m)	100	100	100	100	125
Peak B-V Value in Halocline (cph)	8.3	8.3	8.3	6.8	8.3
Peak B-V Value in Mixed Layer (cph)	1.2	1.2	1.6	1.5	1.9

B. CV-990 Aircraft Data and SAR Processing

As already outlined in Table 6, five SAR missions were executed in support of the Gulf of Alaska experiment. Here, details of the flight operations and supporting aircraft data are presented to facilitate scientific analysis of

the ship wake data. Also, sample SAR images from each of the missions are presented. Detailed analysis of the SAR images and the results derived are presented in Chapter (IV).

1. SAR Flight over "Bay Ridge": Sea State - 1

The flight pattern over the oil super-tanker "Bay Ridge", on 13 March 1984, is shown in Figure 14. The flight track and detailed aircraft data is given in Appendix B. A "horse race-track" pattern was flown parallel to the ship axis. The ship heading was 145° T. Cross passes were flown to obtain images of the ship traveling in the range direction.

A SAR image of the "Bay Ridge" is shown in Figure 15. The ship is traveling in the same direction as aircraft, at an incidence angle, θ, equal to 31°. This image shows the arms of the narrow-V wake to be 7.5-12km long. The turbulent wake is found to be at least 13.0km long. Detailed analysis of the cross section increases across the arms are given in Chapter IV. Another image of the "Bay Ridge" is shown in Figure 16. Here, the ship is traveling in the opposite direction to aircraft at an incidence angle of 32°. In the image the narrow-V wake arms disappear into background clutter at approximately 4.0km aft of the ship. Also, one arm of the 19° Kelvin wake is visible. The turbulent wake is discerned as a dark strip through the ambient backscatter to 9.0km aft of the ship. It is important to note that the image in Figure 16 was obtained prior to that in Figure 15. In the latter, the ship had moved out of the clutter region (presumably associated with a region of higher wind speed) into a calm sea area. Both Figures 15 and 16 demonstrate the importance of background clutter in determining the radar cross-section rise across the bright arms of the narrow-V wake.

In contrast to the above two images, the "Bay Ridge" is imaged in Figure 17 at an incidence angle of 53°. Here, the ship is traveling in the opposite

Figure 14. SAR Flight Pattern Over Bay Ridge on 13 March 1984, Sea State 1. Time Ticks Every One Minute, Anchorage Local Time.

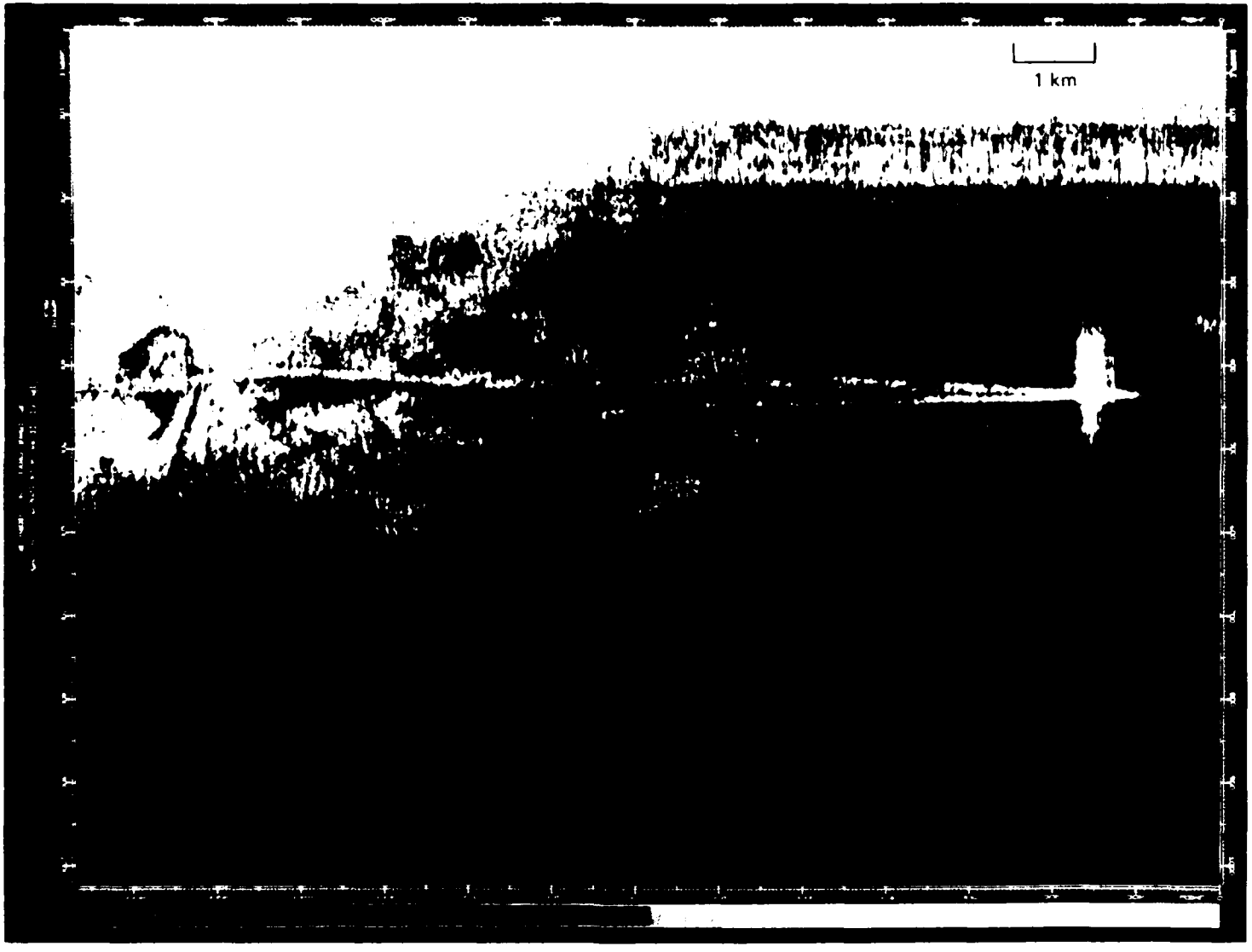

Figure 5.1 SAR Image of Bay Ridge on 13 March 1986 in Sea State 1. Ship is Traveling in the Same Direction as Aircraft and Located in SAR Image at 45° Incidence Angle.

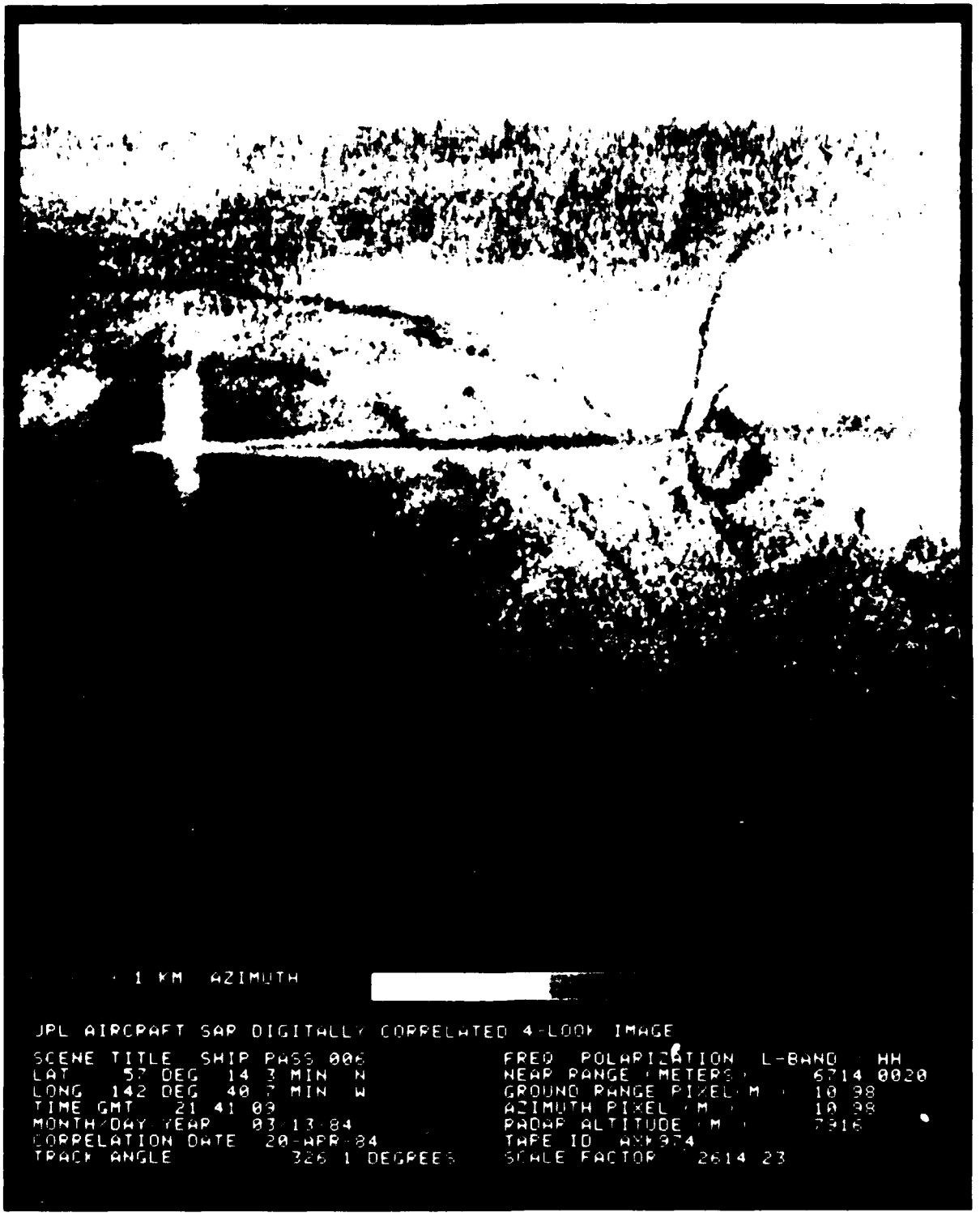

Figure 16. Same as Figure 14 Except that Ship is Traveling in Opposite Direction to Aircraft and is Located in SAR Image at 32° Incidence Angle.

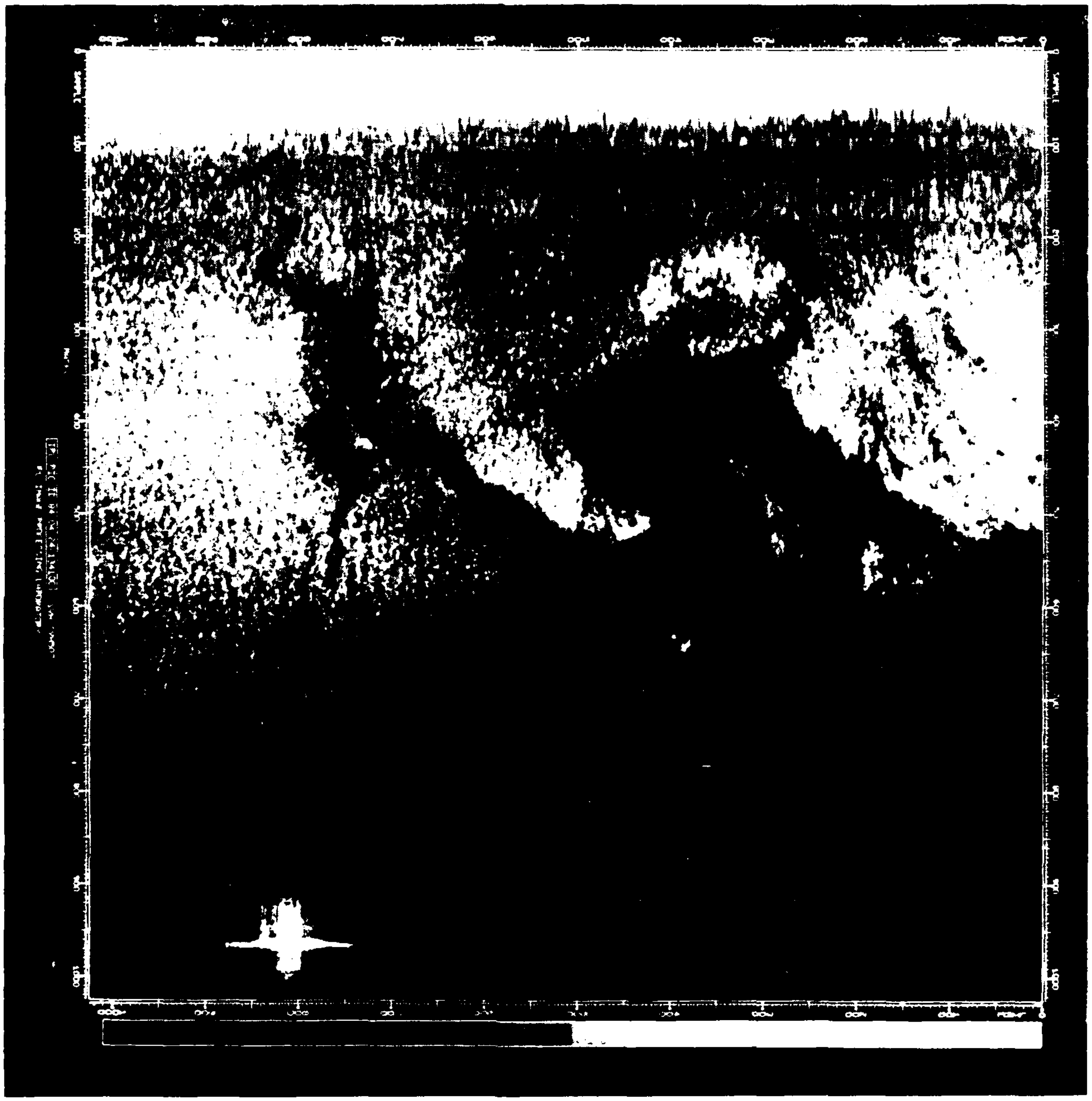

directions to aircraft. The ship itself is clearly visible, but the bright arms are not. A dark strip, compared to background, can be discerned in the turbulent wake region to a distance of 6.0km aft of the ship.

The "Bay Ridge" is shown in Figure 18 traveling in the range direction towards the aircraft. The ship's position in the image is at nadir. The turbulent wake appears as a dark band to 6.0km aft of the ship. The narrow V-wake arms are not strikingly visible as when the ship is traveling in the azimuth direction. The narrow V-wake arm on the ship starboard side is more visible than that on the port side. The wind is blowing from the port direction at 35° from the ship heading. The 19° Kelvin wake is also visible in Figure 18.

2. SAR Flight over "San Sinena II" in Sea State 2

The flight pattern over the ship "San Sinena II" on 11 March 1984 is shown in Figure 19. The mission flight track and detailed aircraft data are given in Appendix B. The complex flight track is indicative of the difficulty experienced in executing the six-sided flight pattern over a moving target (15 knots speed, 305°T heading). Such a pattern is easily executed over a fixed target (e.g. tower). The six-sided pattern was planned to image ships traveling at various azimuthal angles with respect to the radar look angle. The difficulty encountered on 11 March 1984 in locating the ship position mandated the simpler "horse race-track" pattern, shown in Figures 14 and 21. Consequently, no SAR images of ship wakes at 45^{o}, with respect to aircraft direction, were obtained in the Gulf of Alaska experiment.

A SAR image of "San Sinena II", in Sea State 2, is shown in Figure 20, with the ship traveling in the same direction as aircraft. The ship is at 44 deg incidence angle. The narrow-V wake bright arms and the dark turbulent wake

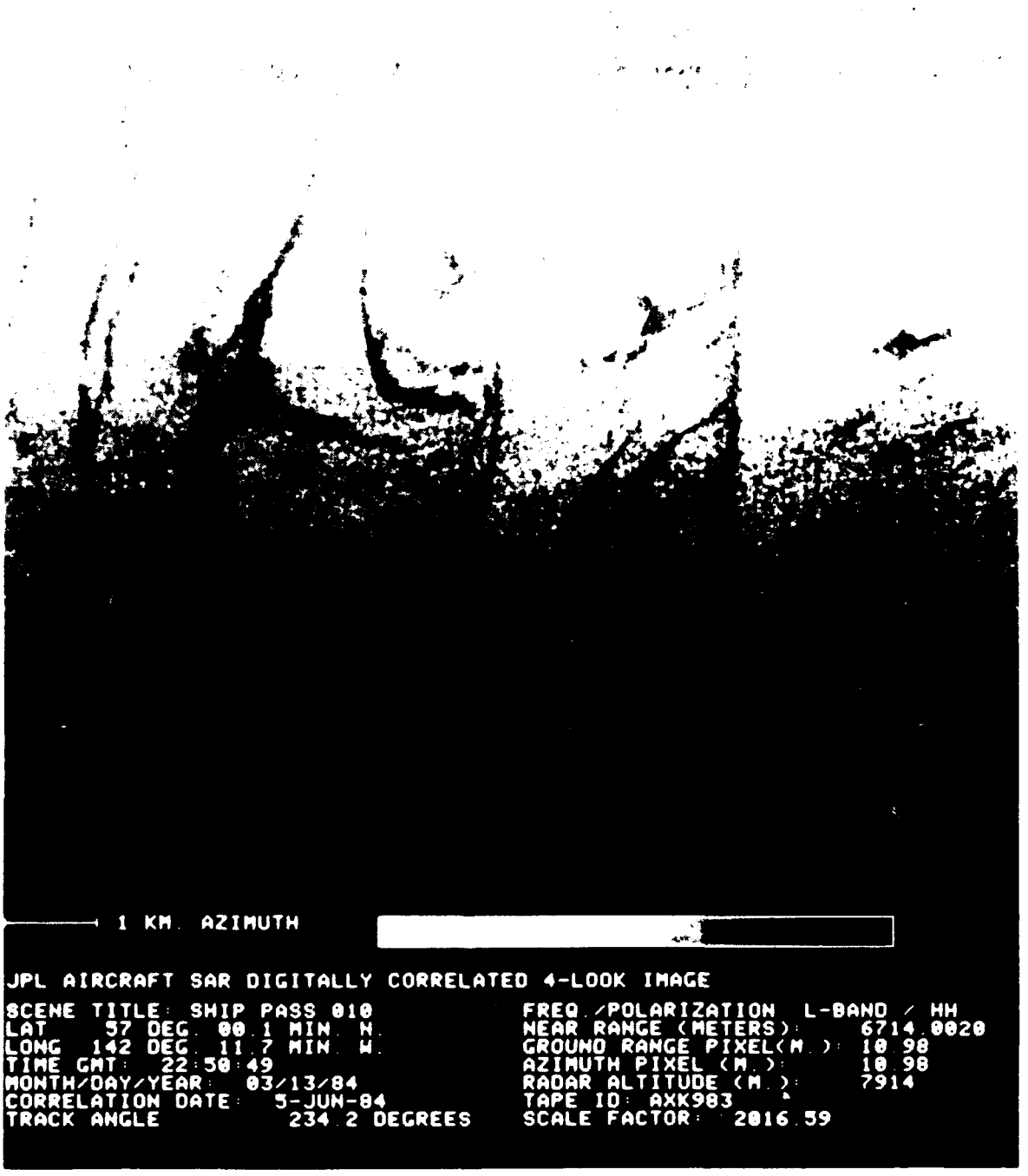

Figure 18. Same as Figure 14 Except Ship is Traveling in Range Direction.

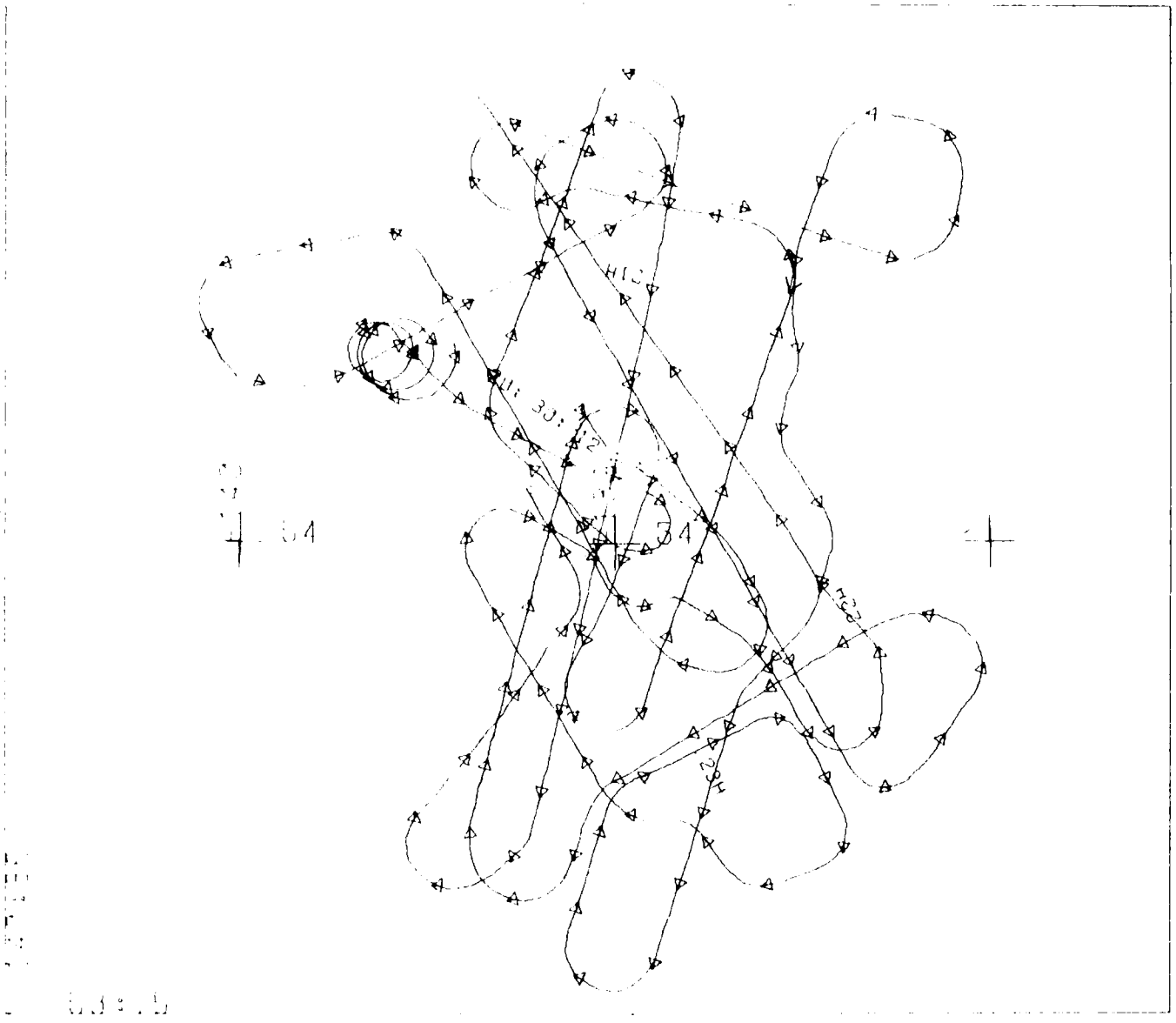

Figure 19. SAR Flight Pattern Over San Sinena II on 11 March 1984, Sea State 2
Time Tics Every One Min, Anchorage Local Time.

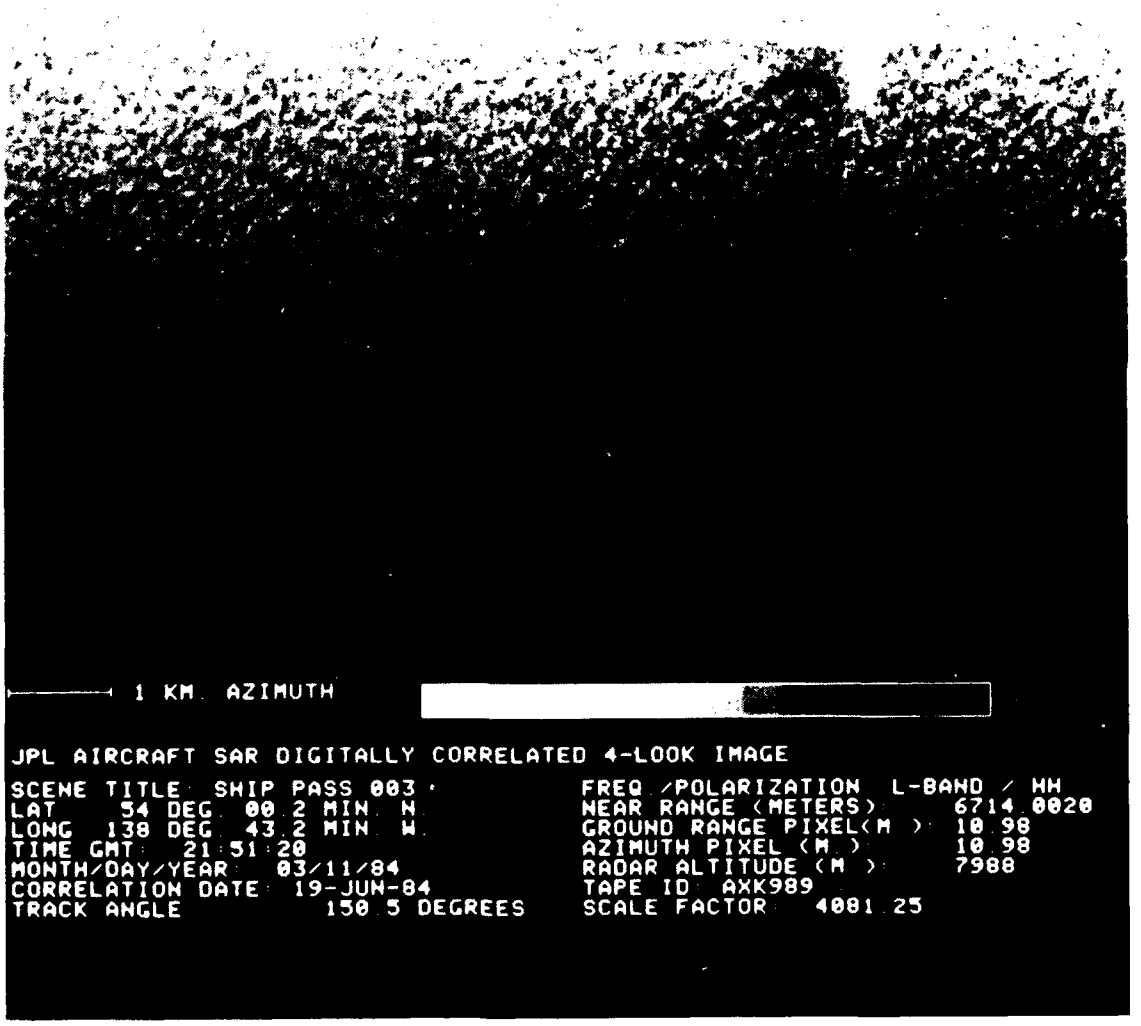

Figure 20. SAR Image of San Sinena-II on 11 March 1984, Sea State 2. Ship is Traveling in the Same Direction as Aircraft and Located in SAR Image at 44° Incidence Angle.

region can both be detected to 4.0km aft of the ship. Here, sea state has an important influence in determining the area aft of the ship over which the wake can be detected. More detailed analysis of ship wake lengths are given in Chapter IV. The optical images of the ship passes are shown in Appendix B.

3. SAR Flight over Unidentified Ship in Sea State 3

The CV-990 mission on 14 March 1984 was executed over Test Area II. A "horse race-track" pattern over an unidentified ship is shown in Figure 21. An image of the ship traveling in the same direction as aircraft is shown in Figure 22. The ship incidence angle is 46 deg. In this figure, only the turbulent wake appears to be visible aft of the ship to a distance of 3.5km. Another image of the same ship traveling in the opposite direction as the aircraft is shown in Figure 23. Here, only the turbulent wake appears to be visible, to a distance of 3.5km aft of the ship. As expected, the sea state influence is to reduce the detectability of ship wakes. More detailed analysis follows in Chapter IV. The optical images of the ship passes are given in Appendix B.

4. SAR Flight over "San Sinena II" in Sea State 3

The same ship that was encountered on 11 March 1984 heading towards Valdez, Alsaka, was encountered on its return voyage to California on 15 March 1984. The oil tanker was empty during the 11 March encounter. It was laden during the 15 March encounter. An image of the ship wake on 15 March is shown in Figure 24. Here, the ship is traveling in the same direction as aircraft, and is located at an incidence angle of 24°. In this image the bright arms of the V-wake are visible to 4.3km aft of the ship. The dark band between the bright arms (corresponding to the turbulent wake) can be detected to 5.5km aft of the ship. In comparing Figure 20 with Figure 24, both ship images show wakes that are at

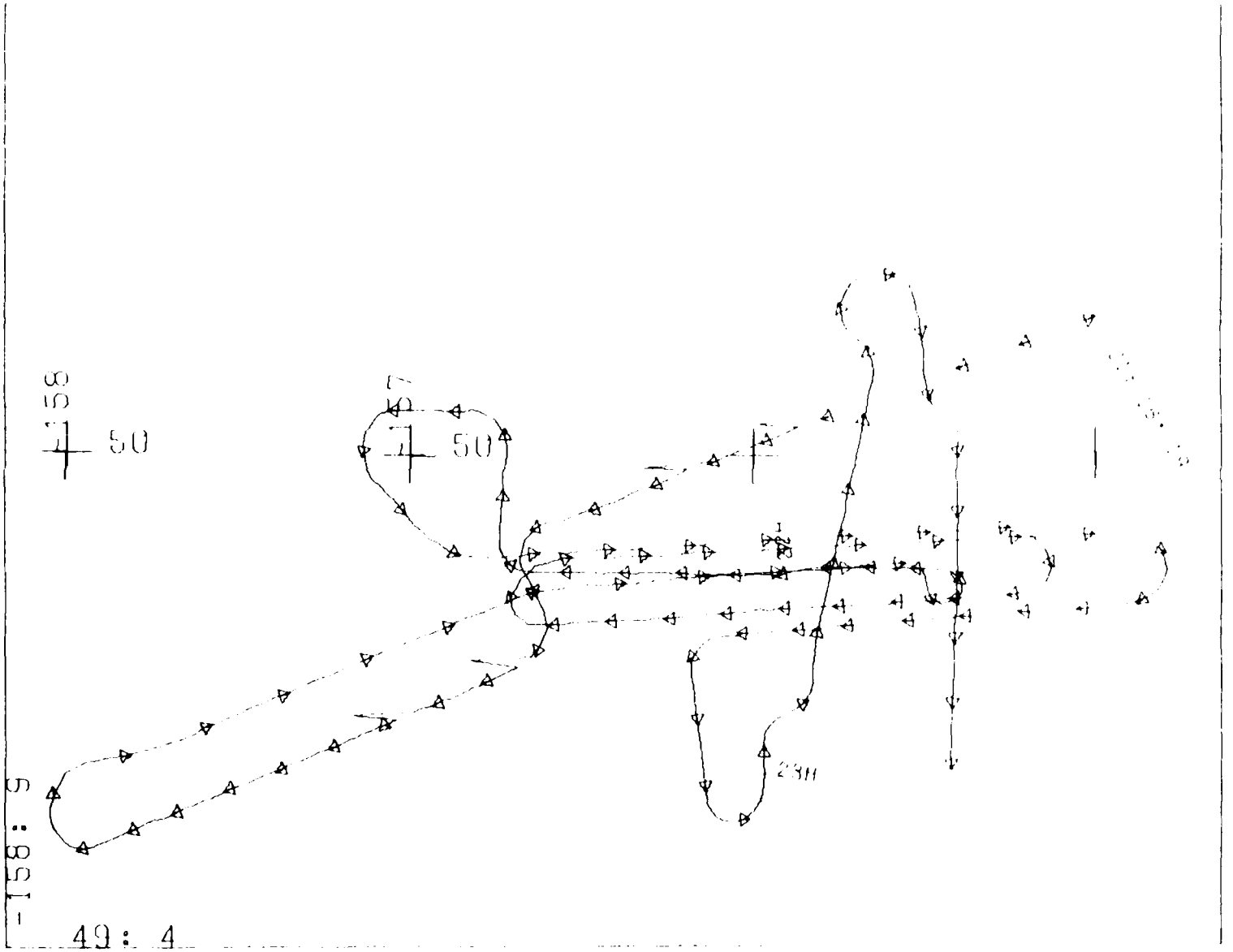

Figure 21. SAR Flight Pattern Over Unidentified Ship on 14 March 1984, Sea State 3. Time Ticks Every One Minute, Anchorage Local Time.

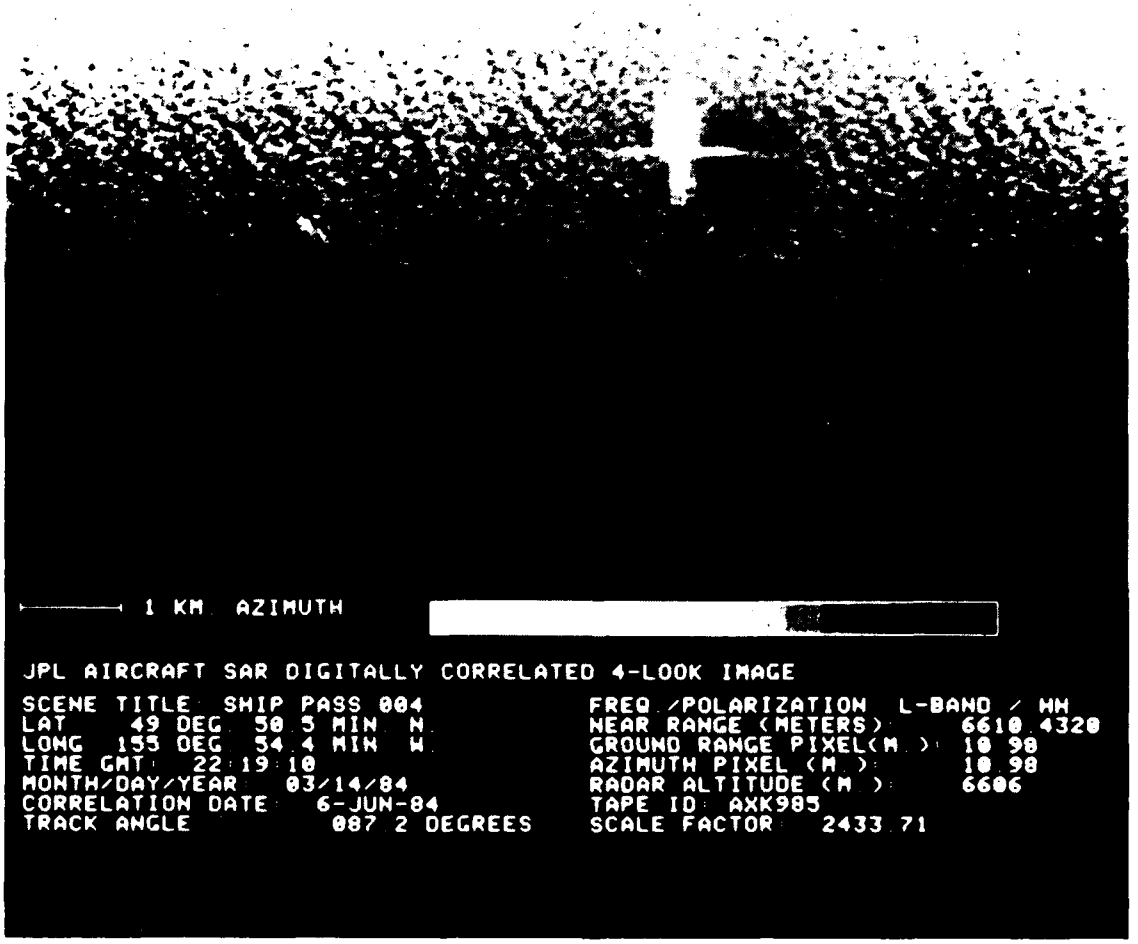

Figure 22. SAR Image of Unidentified Ship on 14 March 1984 in Sea State 3. Ship is Traveling in Same Direction as Aircraft and is Located in SAR Image at 46° Incidence Angle.

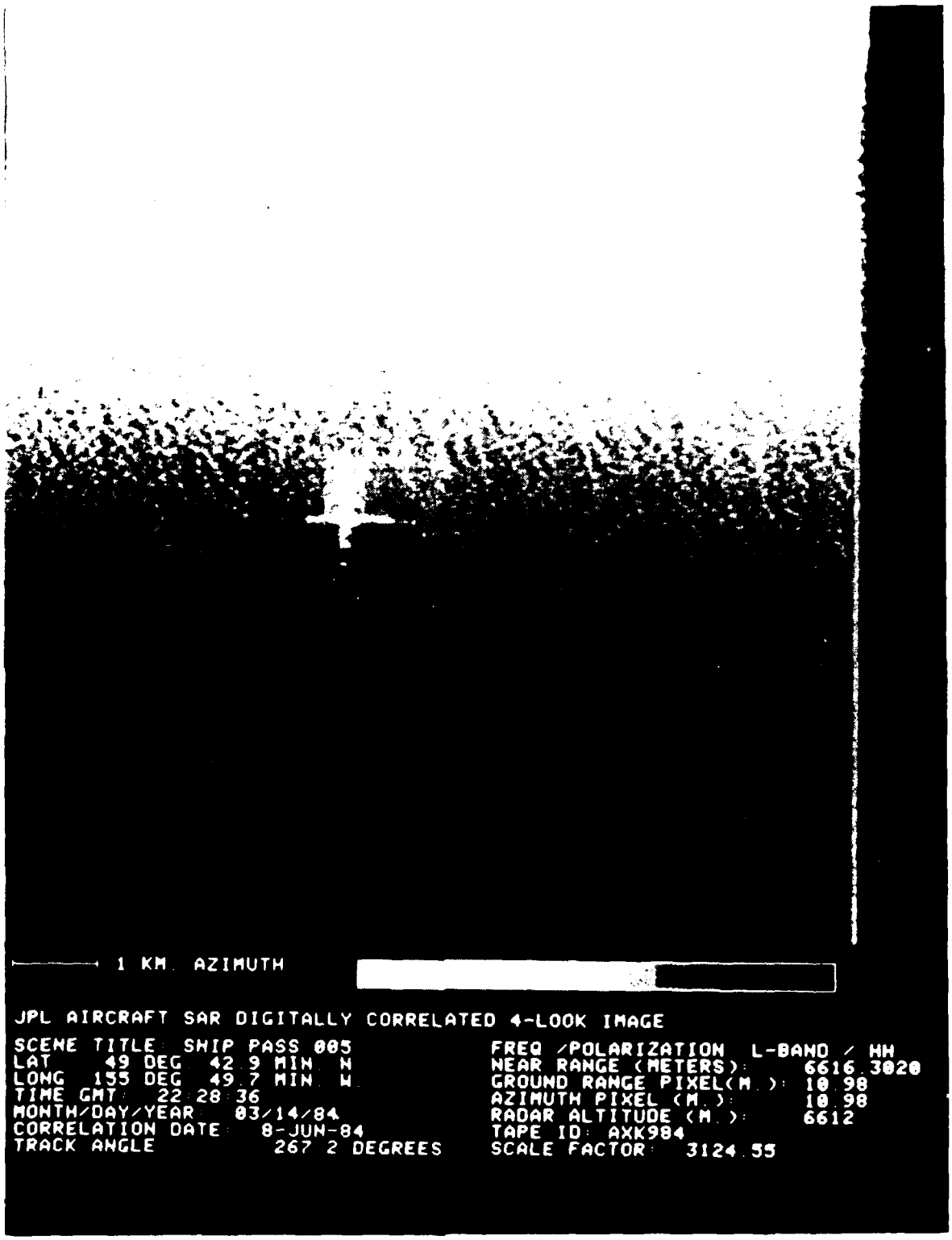

Figure 23. Same as Figure 22, Except Ship is Traveling in Opposite Direction to Aircraft and is Located in SAR Image at 43° Incidence Angle.

Figure 24. SAR Image of San Sinena II on 15 March 1984, Sea State 3. Ship is Traveling in the Same Direction as Aircraft and is Located in SAR Image at 24° Incidence Angle.

least 3.5km long. The higher sea state in Figure 24 appears to be offset by a smaller incidence angle and a laden ship in impacting the length of detectable wake aft of the ship. Detailed analysis of wake lengths is presented in Chapter IV. Also, optical images of all ship passes on 15 March are shown in Appendix B.

IV. EXPERIMENTAL RESULTS AND MODELING

The SAR data set acquired in the Gulf of Alaska provides a useful data base for addressing critical issues related to SAR imaging of ship wakes. In addition, unique information is provided on wake lengths and narrow-V angles in Sea States 1-4. Both digital and optical images are used in the analysis. The digital images are processed to include transformation from slant range to ground range. The pixel spacings are selected based on a carefully studied procedure that insures high geometrical fidelity between an image and a corresponding ocean surface. The measured wake half-angles are determined strictly from the digitally processed images. The optical images, shown in Appendix B, are used to determine the lengths of narrow-V or turbulent wakes. In general, wakes that are visible in the optical images are equally visible in the digital images. An optical image provides an uninterrupted view of the entire wake length, while the digital image provides only a portion of a long wake but with high geometrical fidelity. The wake lengths in the digital images are determined by the points at which the wake return becomes less than 1.0 dB relative to the background return. At such points the wakes disappear visually into the background. The optical and digital images give consistent results on wake lengths.

To facilitate discussion, the experimental results are discussed under the following sub-topics:

A. Narrow-V Wake Half-Angles

The measured ship wake half-angles are shown in Figure 25 as a function of the radar incidence angle. The data points scatter about a line based on the first-order Bragg theory, specified by Equations (1-4). For comparison the second order Bragg theory, based on Equation (5), is also shown. The experimental results do not substantiate the second order Bragg theory. The error

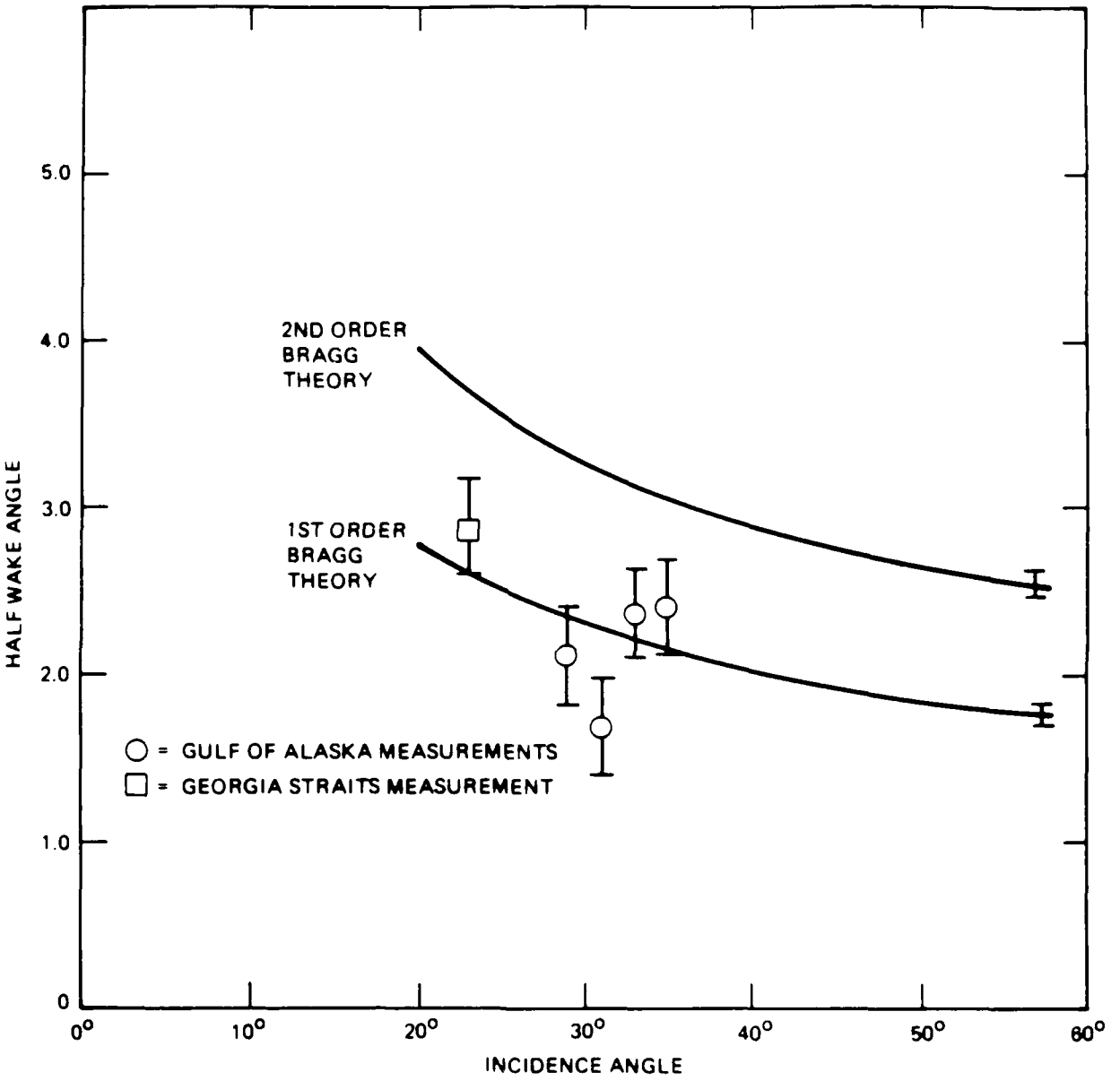

Figure 25. Narrow-V Wake Half Angle vs. Radar Incidence Angle. The Solid Lines are Based on First and Second Order Bragg Theory for a Ship Speed 7.7 m/s ± .25 m/s (The Solid Lines Error Bands are Based on Ship Speed Uncertainty). The Error Bands of Measurements are Based on Seperate Measurement Attempts. Only One Measurement from the Georgia Straits Experiment was Available, at Ship Speed 7.7 m/s.

bands of the experimental points are based on scatter from independent attempts at measuring the half angles.

The method of measuring the narrow-V half-angle is based on coordinate transformation from polar coordinates (in the real image) to Cartesian coordinates, as shown in Figure 26. The transformation angle is selected such that the two bright arms of the narrow-V wake become parallel in the transformed Cartesian coordinates. The distance between the two parallel arms gives an accurate measure of the total wake angle. The half-angle is obtained by dividing the total angle by two. Minor variations about the transformed angle produces lines that are not parallel in the transformed plane. Also, the position of the vertex must be properly selected to obtain the parallel arms in the transformed coordinates. The described method allows determination of the half-angles with errors less than ±0.3 degrees.

In all the measured wake angles, shown in Figure 25, the vertex was consistently found to be located one ship length ahead of the ship. The position of the vertex supports the hypothesis that the scatterers in the wake bright arms are generated by hydrodynamic processes along the ship's hull vs. the ship stern. The bright arms of the narrow-V wake appear to be tangents at the ship's hull, shown schematically below:

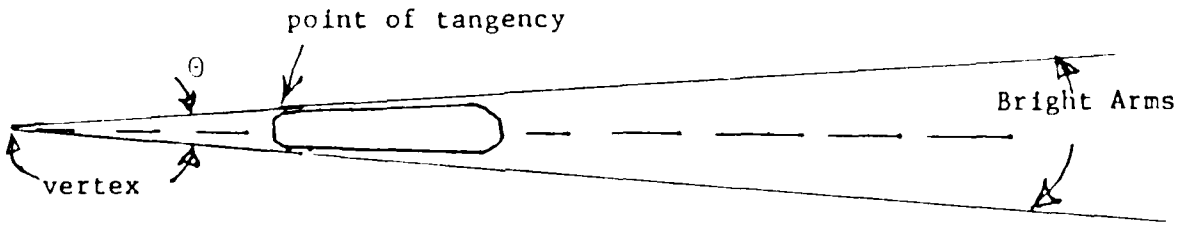

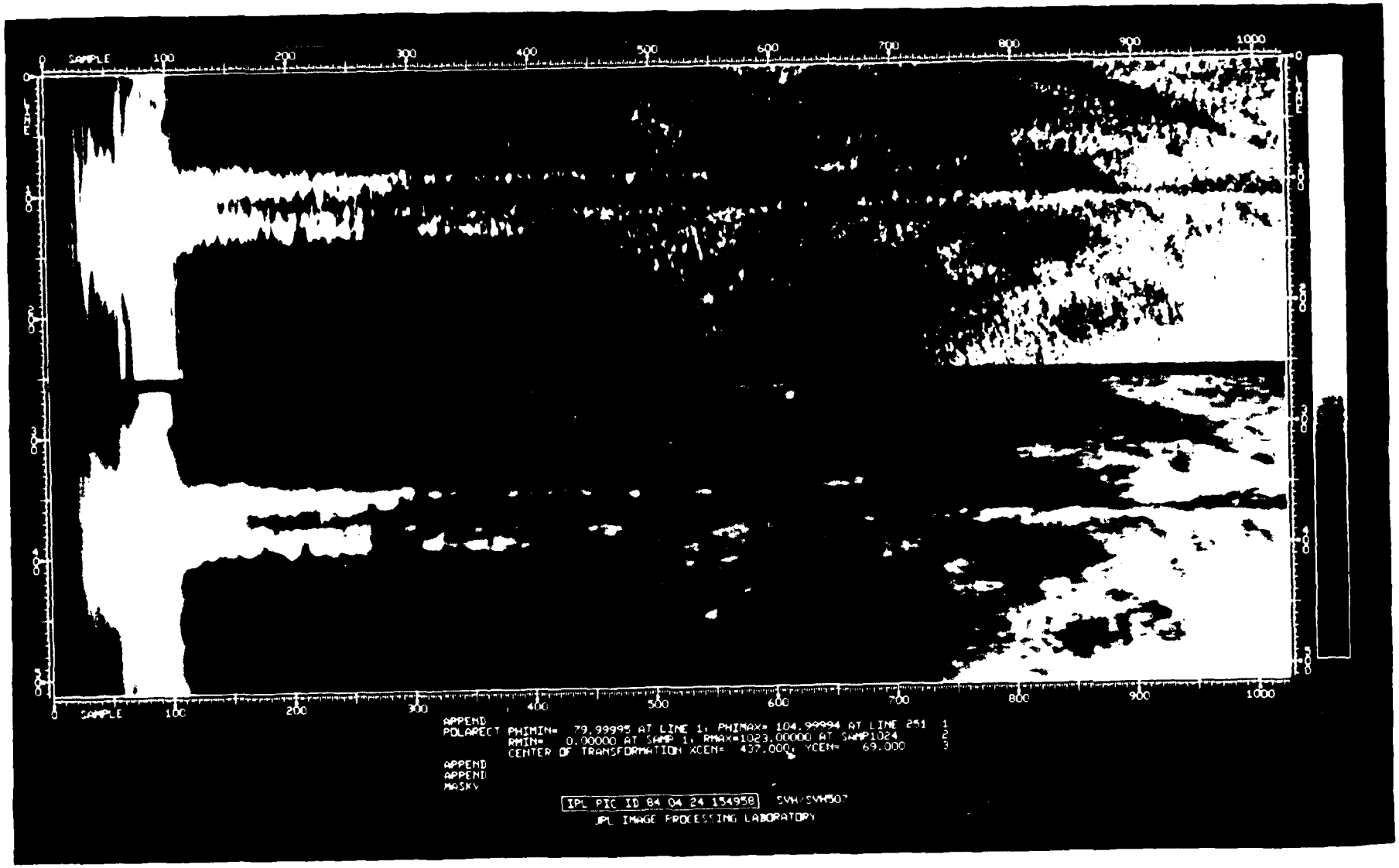

Figure 26. Coordinate Transformation of Ship Wake in Figure 15 from Polar to Cartesian Coordinates. The Distance between the Two Parallel Bright Arms of the Wake Gives the Ship Wake Angle, 2θ. The Top View has 11m Resolution Along the Wake Axis. The Bottom View has 143m Resolution Along the Wake Axis.

Another implication of the hull generation hypothesis relates to the radius of curvature of the scattering centers. The latter determines the radiative decay rate of the scatterers, which will be discussed below in (C) in relation to decay of the scatterers along the bright arms.

B. Backscatter Intensity Levels Along the Bright Arms and Turbulent Wake

The Bay Ridge encounter on 13 March 1984 (Sea State 1) is shown in Figure 15. This image gave the highest backscatter levels in the bright arms compared to ambient backscatter. Photographic views of this wake are shown in Figure 27. A raster scan of wake crossings is shown in Figure 28. Each crossing represents an average over a strip 143m wide. The scans show the backscatter increase in the bright arms above the background level. The narrow-V wake can be discerned easily in Figure 28. The bright arms eventually fade into the background at the upper edge of the figure.

The strength of the signal in the bright arms, normalized relative to the ambient backscatter, is shown in Figure 29 for three cuts located at 858m, 2,145m and 4,290m aft of the ship. The vertical scale in this figure is the ratio of wake signal to background in dB. The 858m cut shows a 13 dB rise above the background. This magnitude is similar to that noted by Hammond et al (1984) for SAR Pass 8-2 obtained in the Georgia Strait experiment. The difference in SAR resolution between the ERIM SAR system (3.0m) used in Georgia Strait experiment and the JPL system (11.0m) used here appears to be offset by the magnitude of the scatterers generated by the large ships in the Gulf of Alaska. The signal rise above the background diminishes with distance aft of the ship, as expected. The signal approaches 8-9 dB at 4,290m aft of the ship. The decay rate along the bright arms is given in (C) below.

Figure 29 also shows the radar backscatter level in the region between

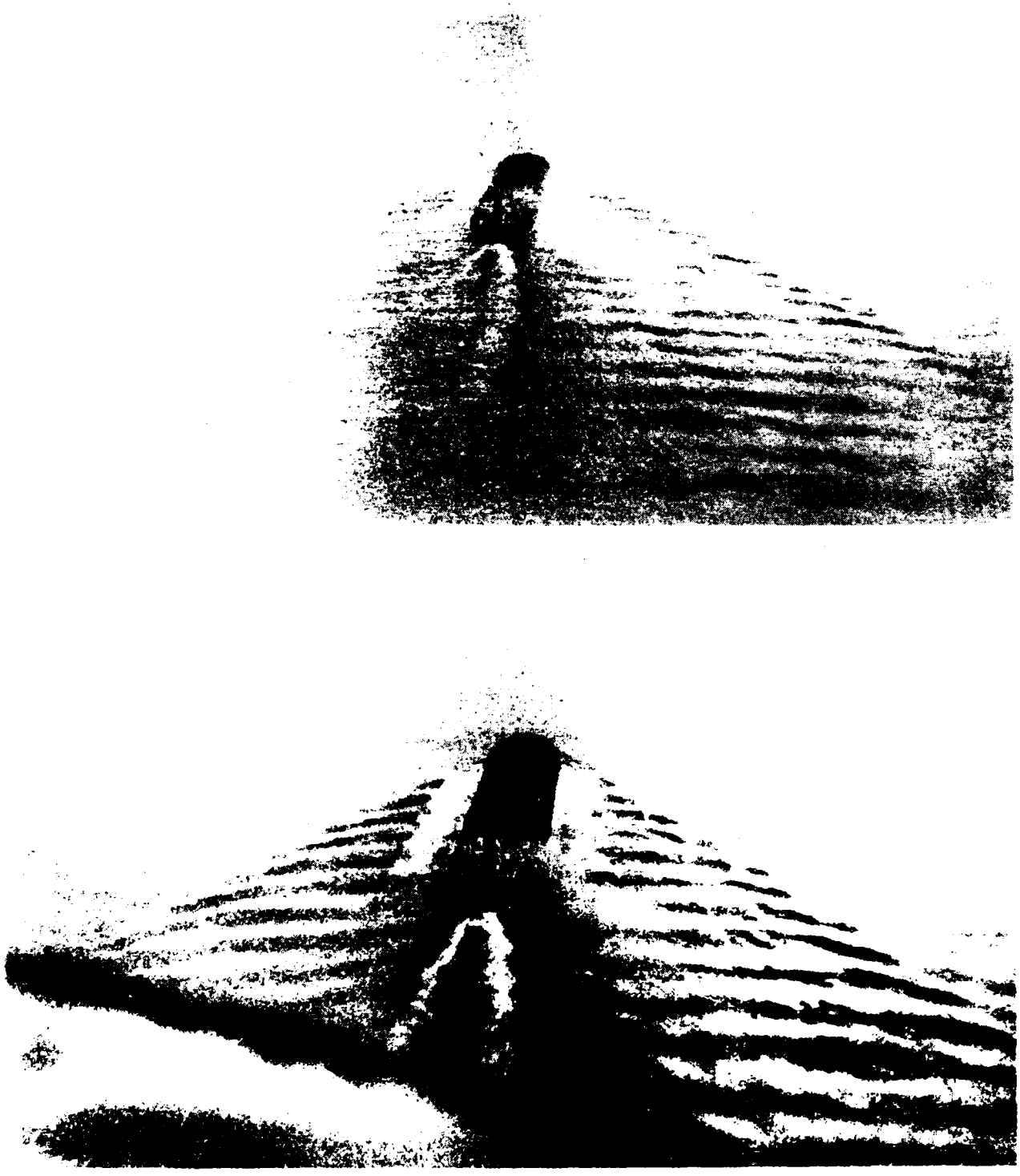

Figure 27. Bay Ridge on 13 March 1984, Sea State 1.

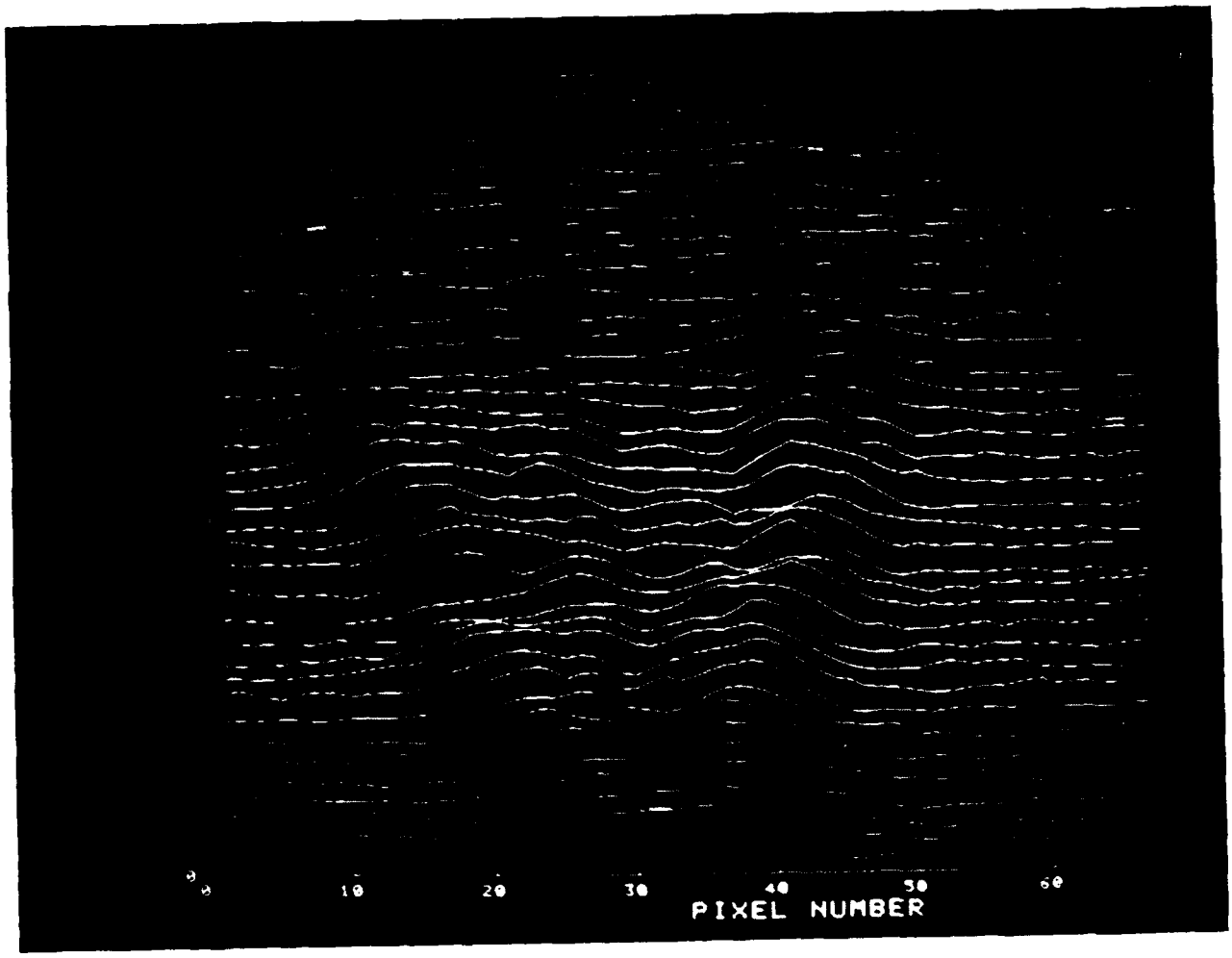

Figure 28. Raster of Cross-Wake Cuts for the Bay Ridge Displaced 143m Apart. The Bottom Cut is Located 143 m Aft of the Bay Ridge. The Top Cut is Located 5,291 m Aft of the Ship. The Bay Ridge Image is Shown in Figure 15.

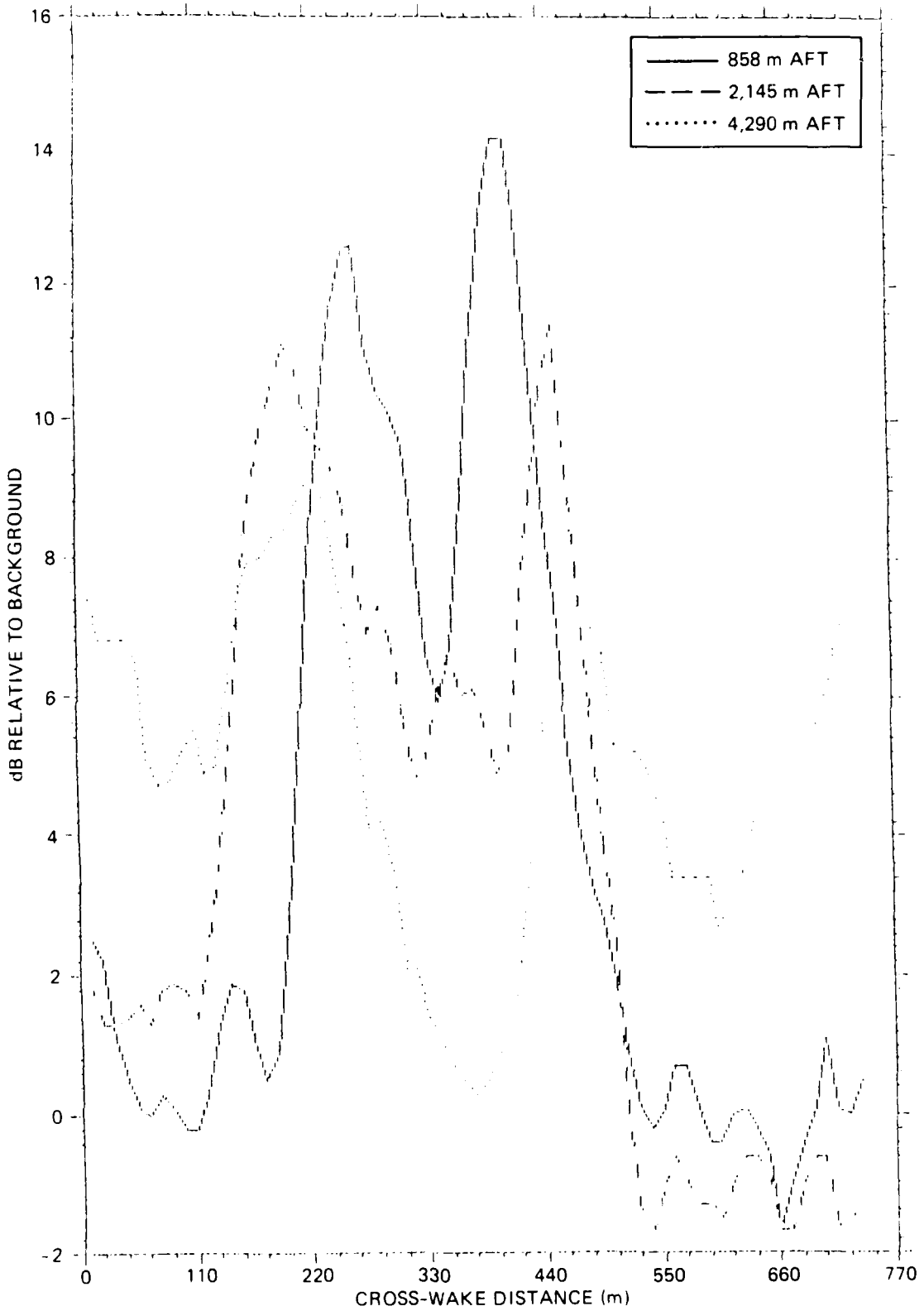

Figure 29. Cross-Wake Cuts for Bay Ridge, shown in Figure 15. Locations of Cuts are Noted in Insert.

the two bright arms of the narrow-V wake to be above the background level. The rise is 6 dB immediately aft of the ship, and drops to the background level at 4,290m aft of the ship. This description will be contrasted below to turbulent wakes imaged in higher sea states.

As expected, sea state has considerable influence on detectability of narrow-V wakes. This is demonstrated in Figure 30 where three cuts are shown across the ship San Sinena II, encountered in Sea State 2. The signal strength in the arms is noticeably lower compared to that in Figure 29 (Sea State 1). The rise in the bright arms is barely 2.0 dB above the background. The signal rise subsides into the background at 4,290m aft of the ship. Of interest in Figure 30 is the drop in signal strength in the turbulent wake region between the two bright arms to below background level. In all three cuts the signals in the turbulent wake remain approximately 3 dB below background. This result explains the detectability of dark turbulent bands in higher sea states, even when the arms of narrow-V wakes are barely visible.

In Sea State 3, Figure 31 shows a behavior similar to that in Figure 30 for Sea State 2. In this figure the bright arms in the three different cuts are displaced laterally relative to each other because the ship wake axis is not precisely parallel with the aircraft flight direction. The drop in backscatter below the ambient level is again seen at large distances aft of the ship in the turbulent wake region.

Figure 32 shows wake cuts in Sea State 4. Here, only the cut 858m aft of the ship shows a rise in the bright arms backscatter above the background, and a drop in the turbulent wake region below the ambient. The cut at 1716m aft of the ship shows backscatter levels in both the bright arms and turbulent wake to be near the ambient level. Beyond 1716m, no trace of any type wake can be discerned in this image.

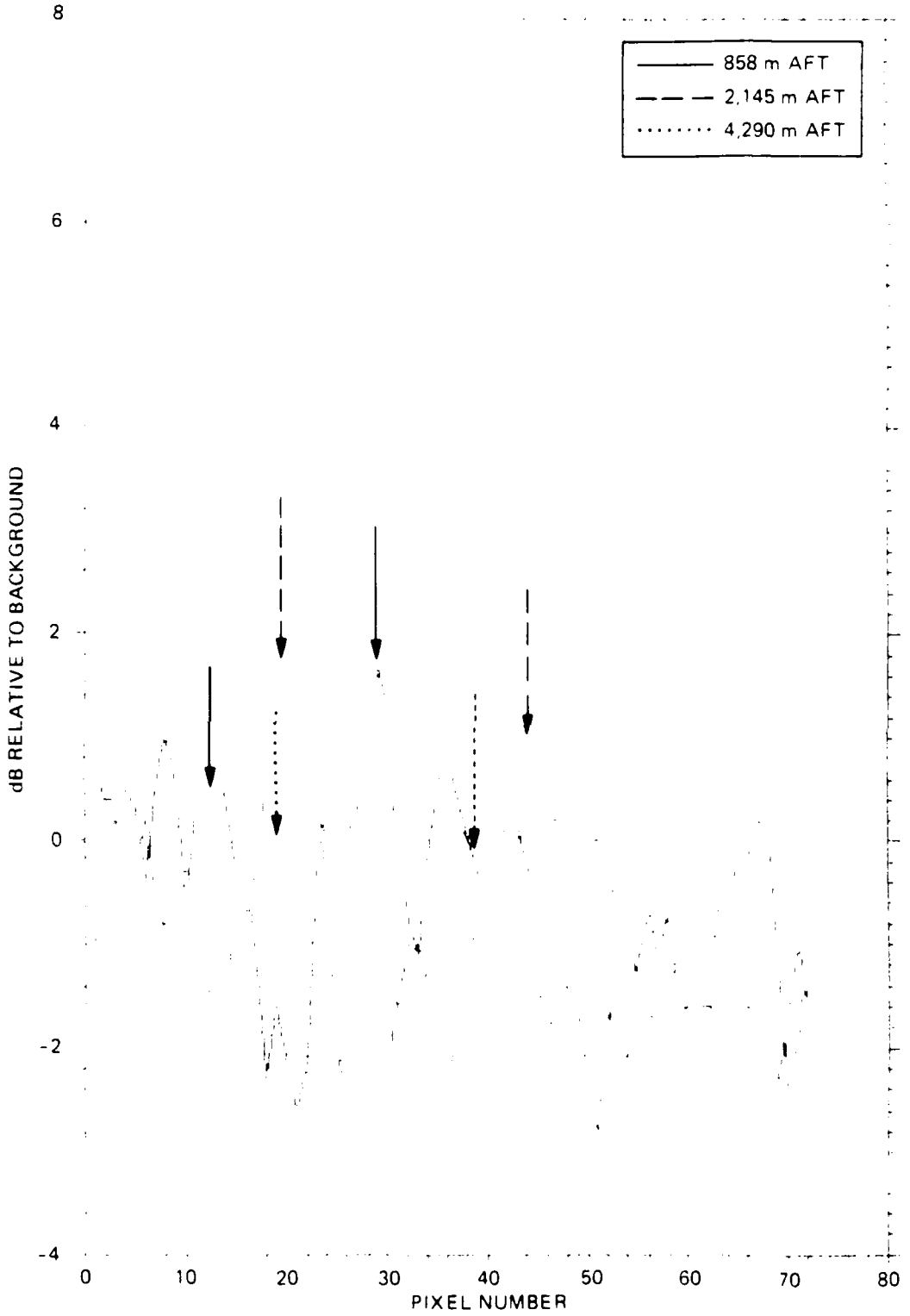

Figure 30. Cross-Wake Cuts for San Sinena II, shown in Figure 20, Sea State 2. Arrows Locate Positions of the Bright Arms for Each Cut. Locations of Cuts are Shown in Insert.

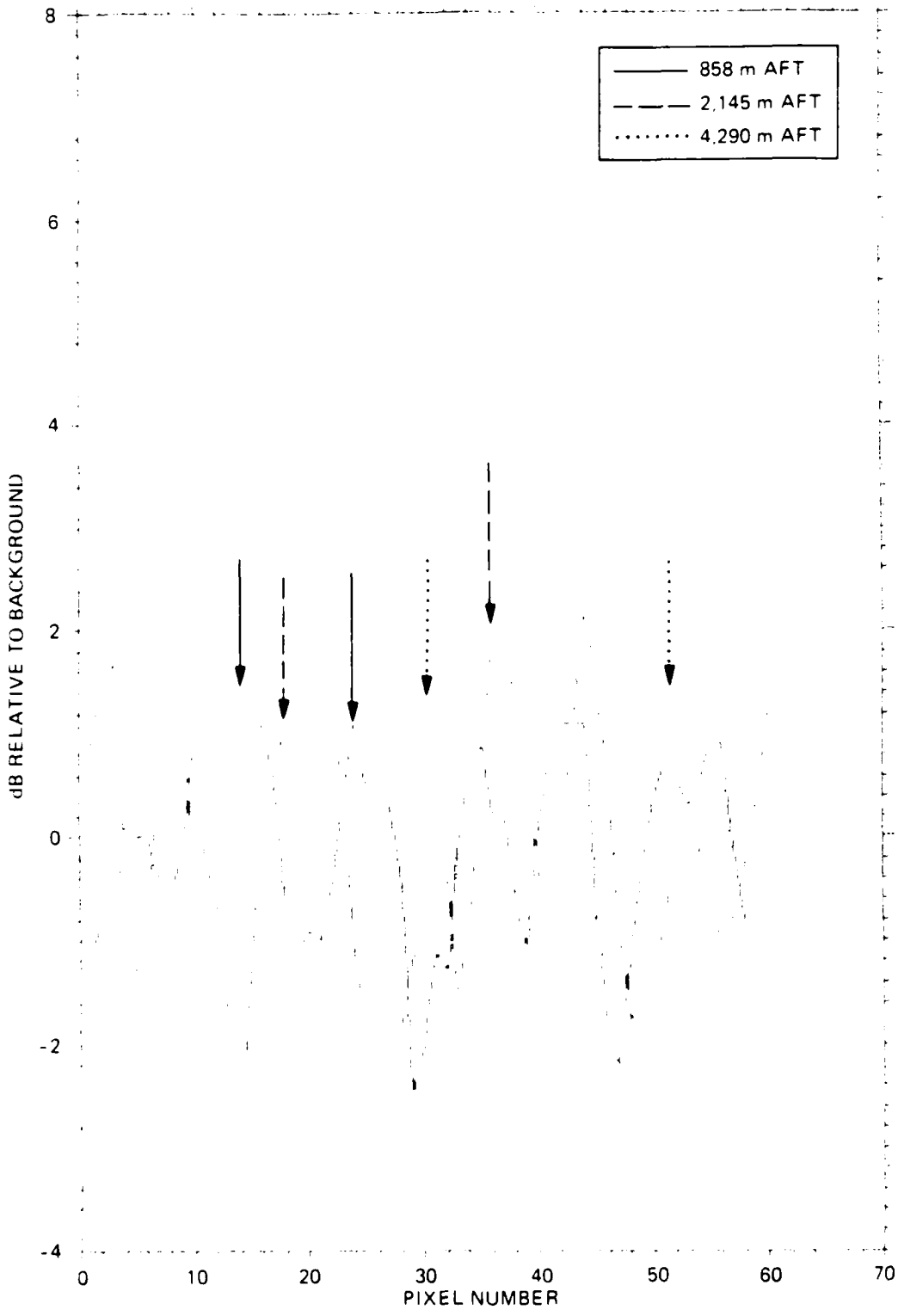

Figure 31. Cross-Wake Cuts for San Sinena II, Shown in Figure 24, Sea State 3. Arrows Locate Positions of Bright Arms for Each Cut. Locations of Cuts are Shown in Insert.

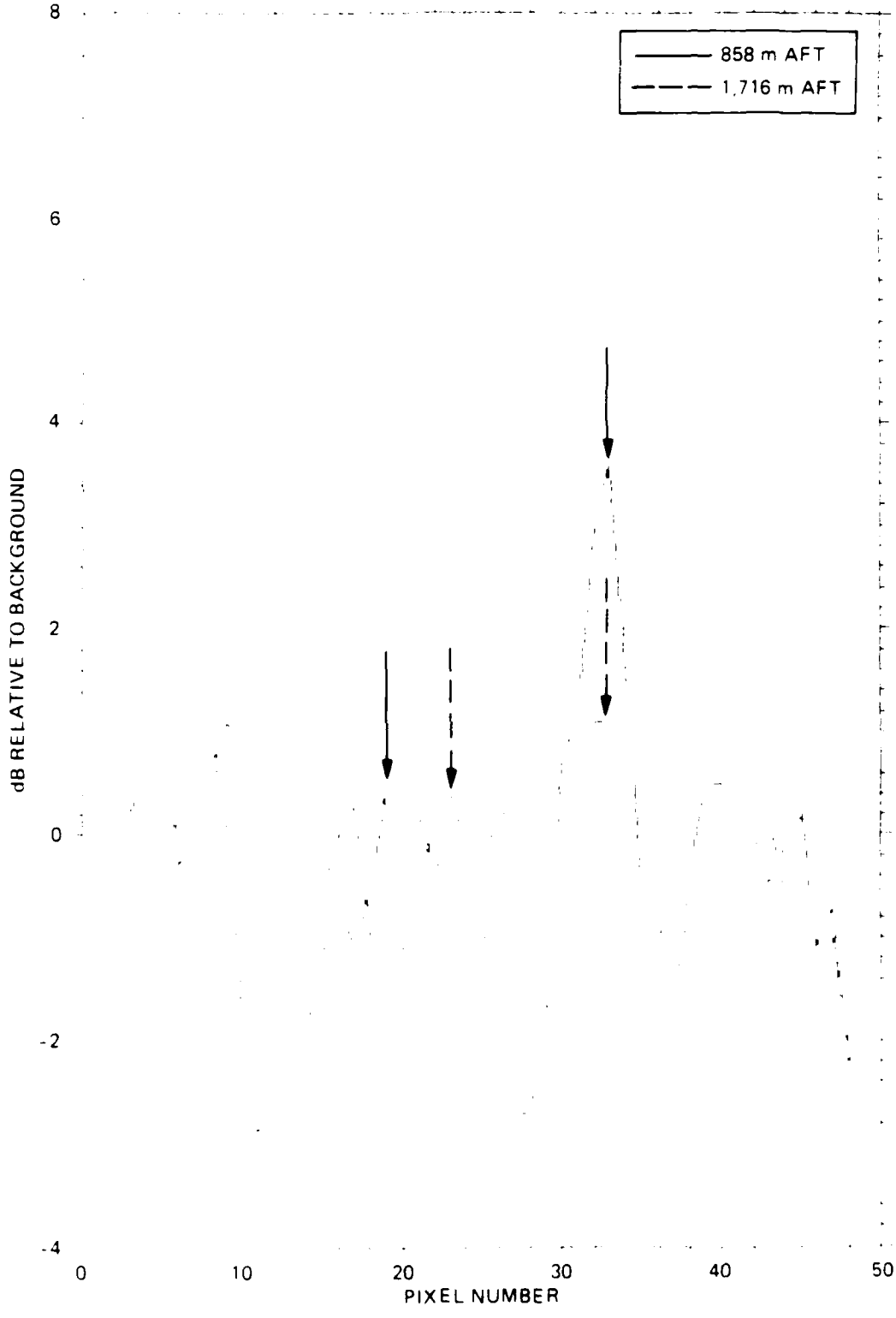

Figure 32. Cross-Wake Cuts for Arco Sag River, Sea State 4. Arrows Locate Positions of Bright Arms. Locations of Cuts are Shown in Insert.

The dramatic influence of sea state is highlighted in Figure 33, where the cross-wake cuts at 858m aft of the ships are compared for Sea States 1, 2 and 3. This figure shows maximum wake detectability in Sea State 1 to be in the bright arms of the narrow-V wake. In sea states 2 or greater, maximum wake detectability appears to be in the turbulent region between the two bright arms.

C. Decay Rate of Scatterers

It is essential that a clear understanding of the mechanisms responsible for generating the scatterers in the narrow-V wake arms be established in order to arrive at estimates of the scatterer decay rate along the bright arms. The results presented in (A) suggest that the scatterers in the bright arms are generated by the turbulent boundary layer along the ship's hull. Assuming that a highly turbulent boundary layer can generate surface displacements that include length scales in the Bragg region (see Witting and Vaglio-Lauren, 1985 for an analytical treatment), it is reasonable to expect that these surface displacements will propagate, outward from the ship's axis as surface waves. A clear indication that this may be occurring is shown in Figures 34 and 35. The aft view of the ship shows regions of white water propagating outward from the starboard and port sides of the hull.

In determining the decay rate of waves it is important to consider the radiation effect of scatterers propagating outward, in addition to decay rates due to dynamical processes such as viscous dissipation and wave-wave interactions. Assuming that the scatterers eminate in scattering centers near the ship's hull and radiate outward, the radii of curvature at points along the bright arms can be calculated in relation to the distance outward from the ship's axis. A careful examination of the photographs, shown in Figure 36 and 37, indicate that such scattering centers exist not only along the ship's hull

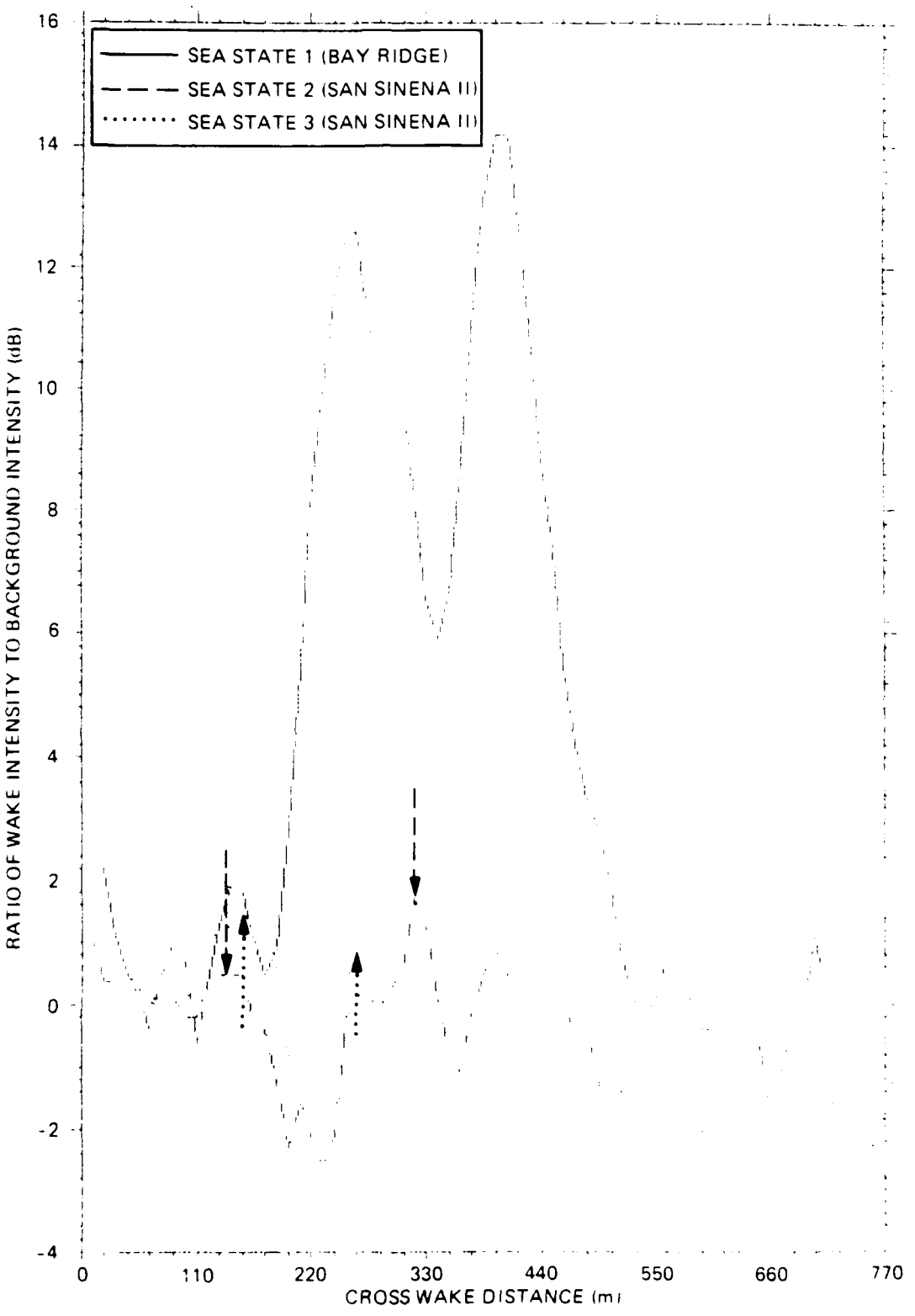

Figure 33. Cross-Wake Cuts at 858 m Aft of Ships. Arrows Locate Positions of Bright Arms in Sea States 1 and 2.

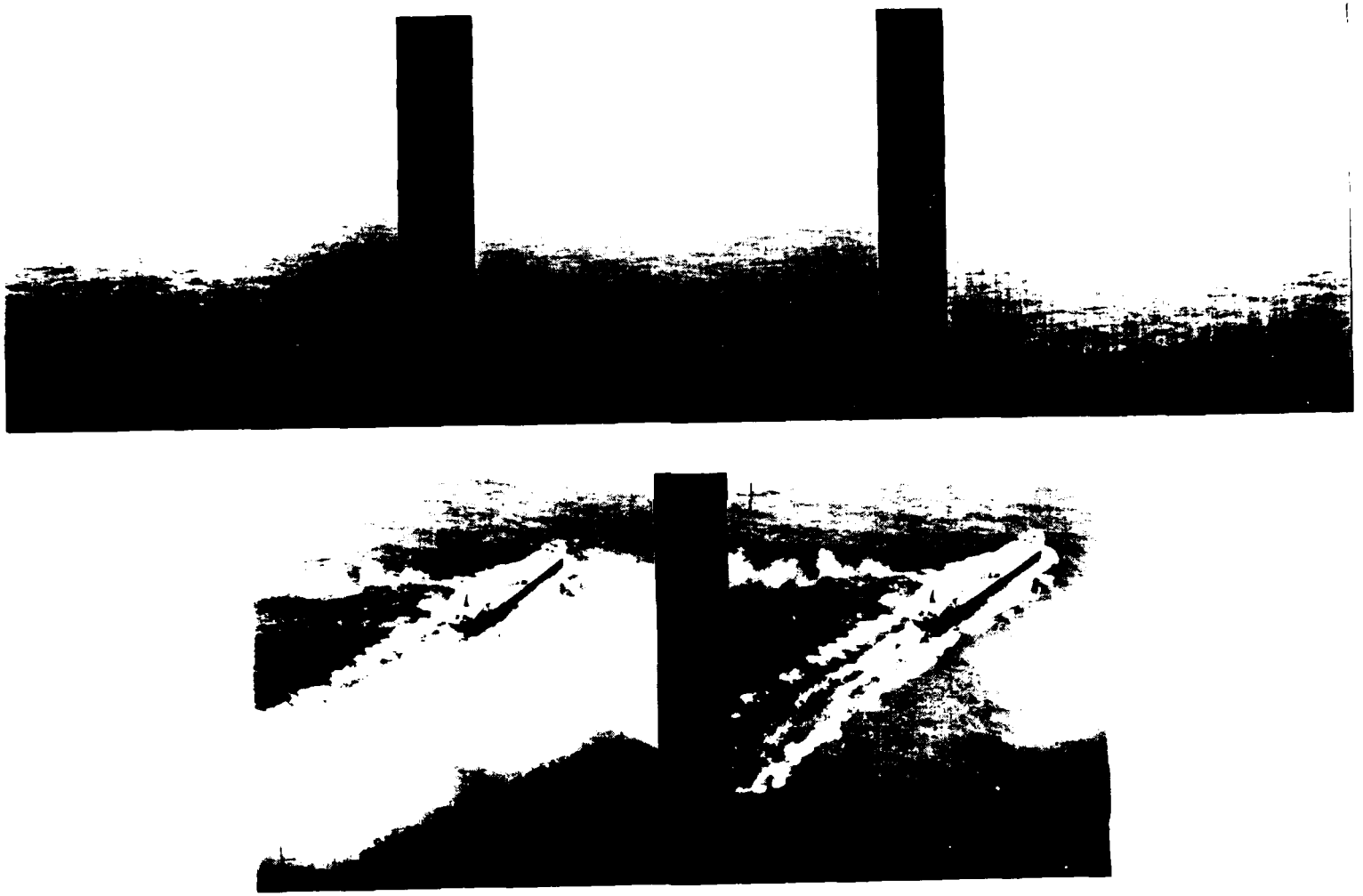

Figure 34. San Sinena II (Empty) on 11 March 1984, Sea State 2.

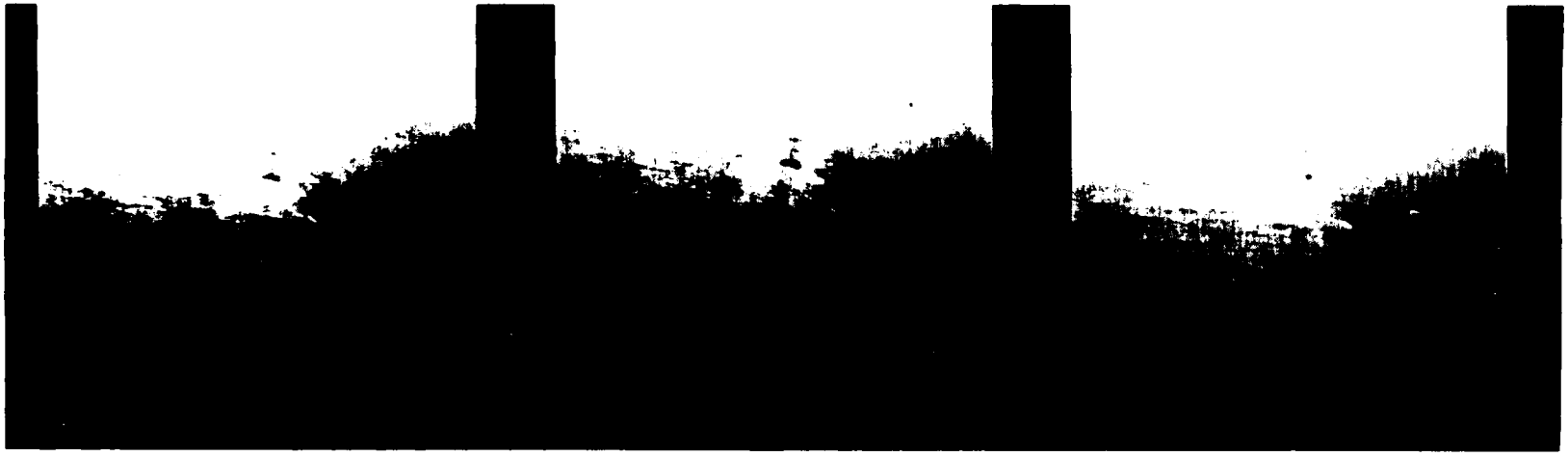

Figure 35. San Sinena II (Laden) on 15 March 1984, Sea State 3, Stern View.

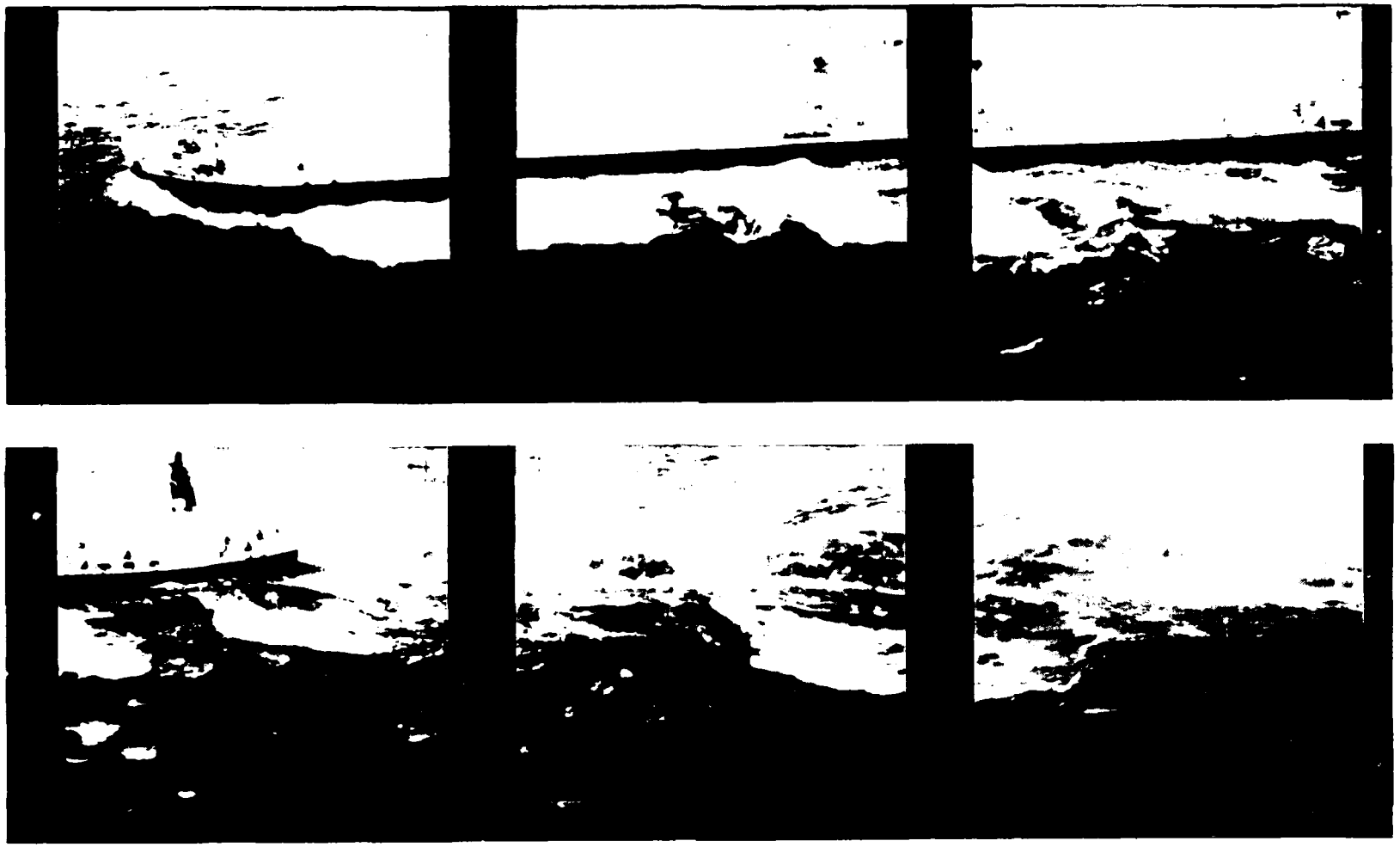

Figure 20. [illegible] on 15 March 1966, Sea State 4, Side View.

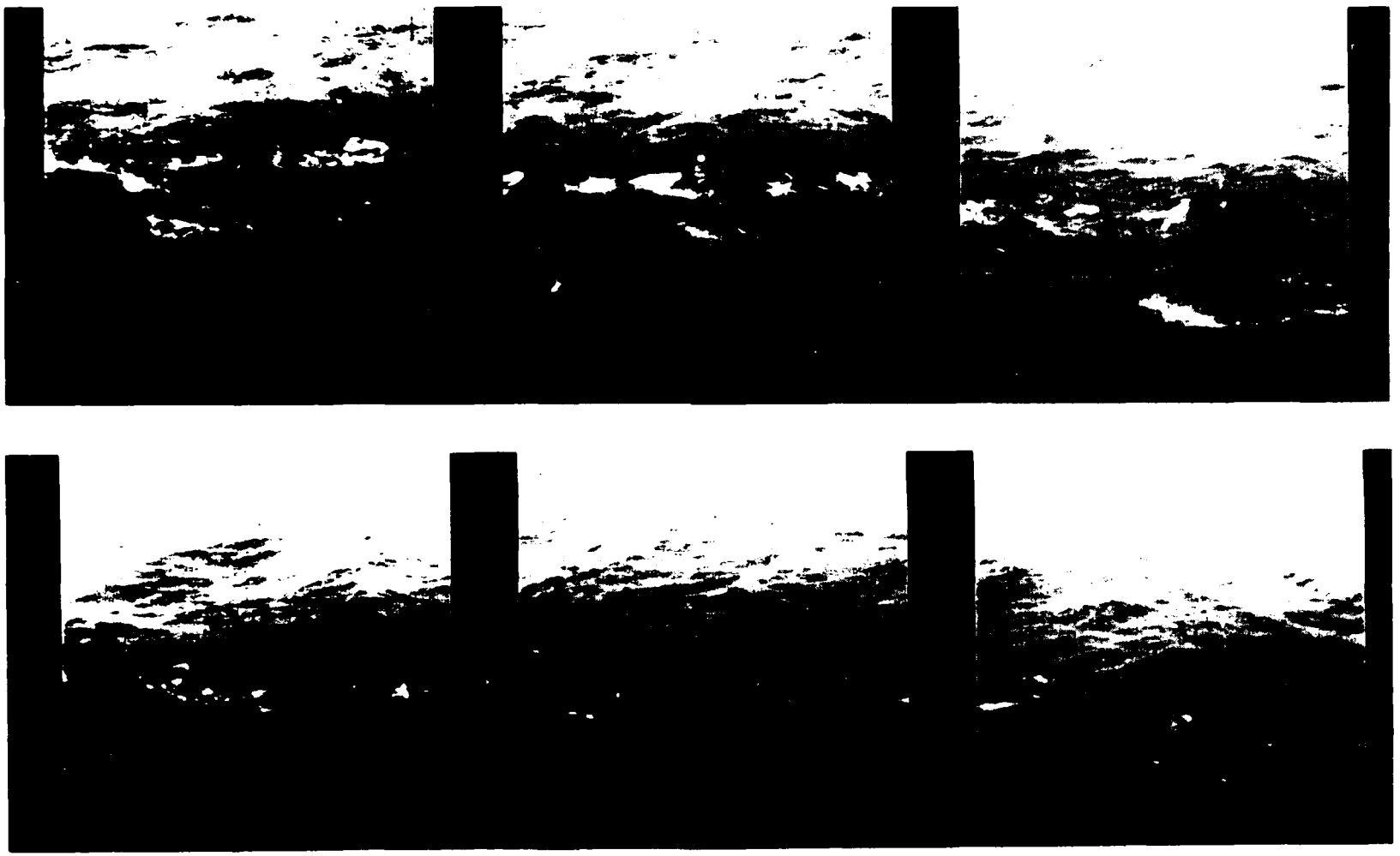

Figure 22. Tan Cheem II (Laden) on 15 March 1984, Sea State 3, Side View (Cont'd).

but also in the wake region aft of the ship. Using the ship length for a scale, the radii of the scattering centers are measured and found to remain constant along the hull length and beyond to a distance approximately one half of a ship length (see Appendix C for more details). The radii of curvature then begin to increase linearly with distance aft of that point. These observations point to a rational procedure for calculating the magnitude of the initial radius of curvature of the scattering center and its increase with distance aft of the ship. Given that the vertex of the bright arms is approximately one ship length ahead of the bow, the narrow-V wake half-angle can be used to calculate the outward distance to the bright arm at a point one half of a ship length aft of the ship. Using the measured half-angle for the narrow-V wake, the initial radius of curvature is estimated to be 28m for the Bay Ridge in Sea State 1. The radii of curvature of scattering centers further aft of the ship are then calculated in proportion to their outward distance from the ship's axis.

Using the above procedure, the radiative decay rate is calculated for the Bay Ridge, in Sea State 1, as shown in Figure 38. The equation for computing radiative decay rate is given in Appendix C. Also shown in this figure, is the decay rate associated with viscous dissipation. The equation for computing viscous decay is well known, and is also included in Appendix C for completeness. The combined decay rate is then compared with the measured decay rate along the starboard arm of the narrow V wake. The comparison is considered favorable suggesting that in Sea State 1 the scatterers in the bright arm are indeed surface waves propagating outward along radial lines and decaying in time due to viscous action. It is noted that the starboard arm of the wake, imaged on 13 March, provided the cleanest signal compared to all other data. In other measurements, the signals in the bright arms are contaminated by ambient backscatter.

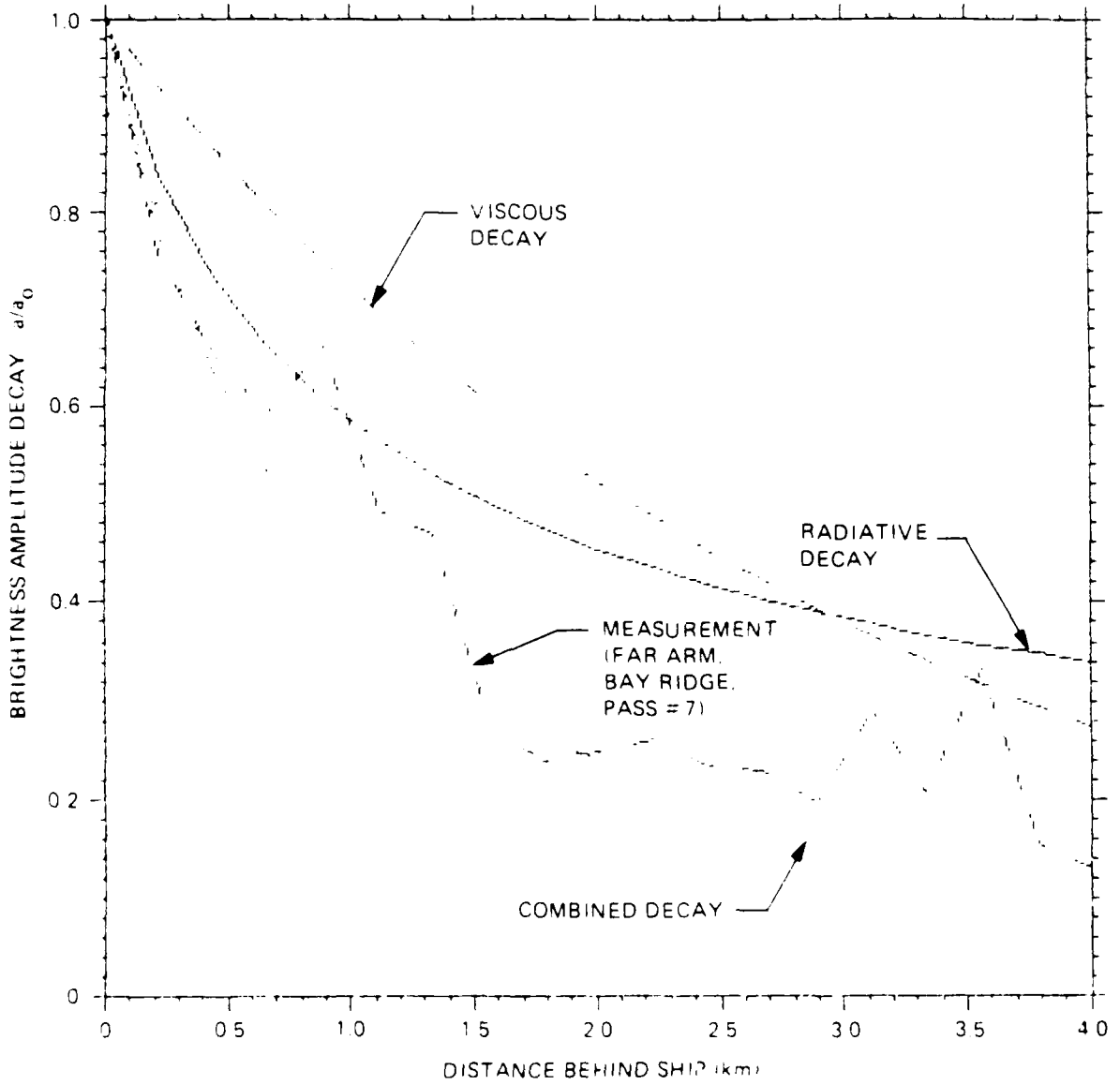

Figure 34. Brightness Amplitude Decay Along Bright Arm with Distance Aft of Ship (Bay Ridge, $\emptyset = 31°$, Sea State 1).

In Sea States 2-4, no discernable decay can be measured along the bright arms, suggesting that the ambient wind-generated ocean waves have a substantial impact on the ship-generated scattering centers. One possible explanation for this is suggested by Case et al. (1984). They introduce the possibility that the coherent structure of the ship-generated waves may be destroyed (hence made incoherent) by the random wind-generated waves. Another possible explanation, discussed in E, is the degradation of SAR resolution in higher sea states, attributed to the long wave orbital motion.

D. Dependence of Ambient Backscatter on Wind Speed

The dependence of ambient backscatter on wind speed and incidence angle is determined from range scans of the digitally-processed images in the various sea states encountered (1-4). Using sufficiently wide scans (30 pixels in the azimuthal direction) in regions far removed from the ships and their wakes, the results of such scans are shown in Figure 39. The range scans for sea states 1-3 all converge at the noise threshold level, which is at 50° incidence angle. The scan corresponding to Sea State 4 approaches a noise floor at 40° incidence angle. This is due to flight altitude, which was 12,660 m on this day compared to 7,930 m for the flights in Sea State 1-3. Hence, it is expected that the scan corresponding to Sea State 4 would approach the common intersection of the other scans, at incidence angle of 50°, if the noise floor is lowered to that of the other three. The range scans shown in Figure 39 are used to develop a model for predicting the lengths of bright arms in the wake.

E. SAR Noise and Degradation of Resolution

Noise in the SAR system can be either due to thermal noise or to quantization errors. The combined noise level can be determined by examining

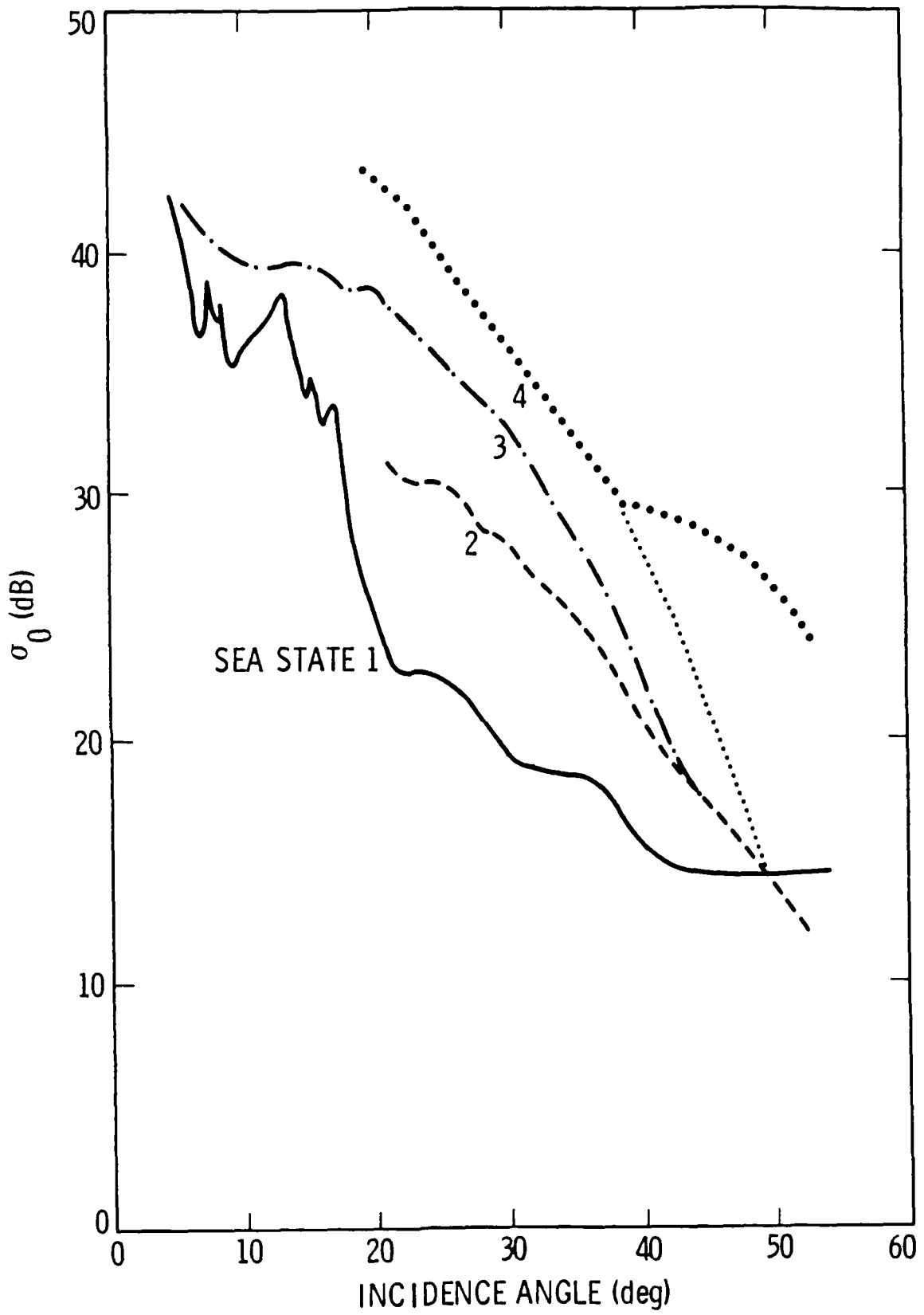

Figure 39. Radar Cross Section, σ_o, L-Band, HH, vs. Wind Speed and Incidence Angle.

the decrease in pixel intensity with incidence angle in a SAR image. Areas in the SAR image away from the ship or wake area must be considered for this determination. Comparing such variability to known σ_o variation with incidence angle, the noise floor level in an image can be determined. The decrease in pixel intensity with incidence angle in the Gulf of Alaska images indicates that the noise floor is reached when the incidence angle exceeds 50 degrees, for the images obtained on 11-15 March (Sea States 1-3), and 40 degrees for the images obtained on 9 March (Sea State 4), as shown in Figure 39.

It will be shown in (F) than no ship wakes are detected at incidence angles greater than 43 deg. The noise analysis suggests that the absence of ship wakes at large incidence angles is partially due to the SAR system noise level, whcih becomes larger than the ambient radar backscatter at those incidence angles. In principle, a signal that rises above the noise floor can be detected, as indeed the ship is clearly visible at 53 deg incidence angle. However, the bright arms of the narrow-V wake are not detectable in Figure 17 at 53 deg incidence angle, indicating that the signal in the bright arms has descended below the noise floor level.

A calculation based on the radar equation using the same scatterers in the bright arms indicates that the backscatter from the bright arms at 31 deg incidence angle is 16.9 dB greater than that at 53 deg incidence angle. This, however, still places the backscatter in the bright arms at 53 deg incidence angle above the noise floor. A further calculation that includes the k^{-4} effect of surface waves places the radar backscatter below the noise floor at the 53 deg incidence angle. A summary of these calculations is given below:

Incidence Angle	31 deg.	53 deg (Radar Equation Without k^{-4} Effect)	53 deg (With k^{-4} Effect Included)
Signal Strength	109.7×10^{-3}	2.2×10^{-3}	0.4×10^{-3}
Ambient Background	5.5×10^{-3}	0.5×10^{-3}	0.5×10^{-3}
Noise Floor	1.3×10^{-3}	1.3×10^{-3}	1.3×10^{-3}

The above calculations do not invoke the need for a coherent specular hypothesis, as suggested by Case et al. (1984).

Degradation of SAR resolution due to sea state is known to be substantial (Shemdin et al., 1986). The estimates suggested by different theoretical approaches differ by as much as one order of magnitude. More recently, and because of progress made in the TOWARD experiment, the differences are better understood. It is now considered reasonable for a SAR image, with a nominal land resolution of 4.6m, to have degraded resolutions in Sea States 1, 2 and 3 that correspond to 20m, 60m and 80m, respectively. These estimates are consistent with the TOWARD experimental results. Adopting these calculations, it is seen that a signal strength 13 dB above background, as noted in Figure 33 for Sea State 1, can become degraded to 3.5 dB in Sea State 2 and 1.0 dB in Sea State 3. These estimates are not in conflict with the measurements shown in Figure 33. The effect of resolution degradation on reduced backscatter in the bright arms in Sea States 2 and 3, compared to Sea State 1, obviates the need for a coherent specular theory to explain the observation. What is required is that the ship-generated surface waves in the scattering centers be sufficient in numbers and intensity to produce a 13 dB rise above the ambient clutter, in Sea State 1.

F. Wake Lengths vs. Sea State and Radar Incidence Angles

A compilation of measured lengths of narrow-V wakes is made from all the available digitally and optically processed images. The results are shown graphically in Figure 40 in relation to sea states and incidence angles. The longest narrow-V wakes correspond to Sea State 1 at 31 incidence angle. The wake lengths decrease rapidly with increasing incidence angles, and are not observed (in any sea state) at incident angles greater than 44 degrees. The narrow-V wake lengths also decrease rapidly with sea state, as shown in Figure 41. The observed decrease in wake lengths is attributed to noise, degradation

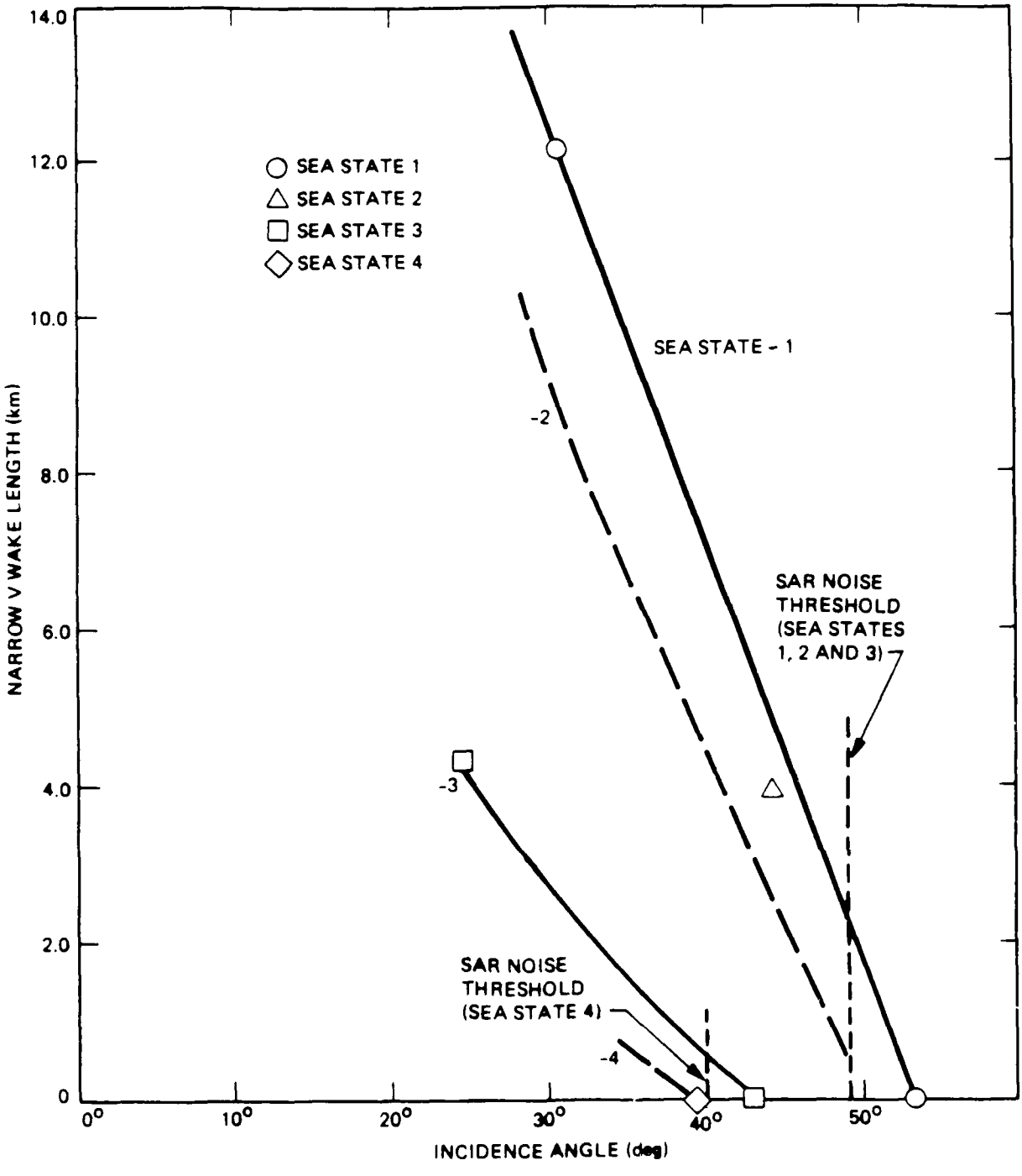

Figure 40. Narrow-V Wake Length vs. Incidence Angle for Sea States 1-4. Solid Lines are Best Fits to the Data Points.

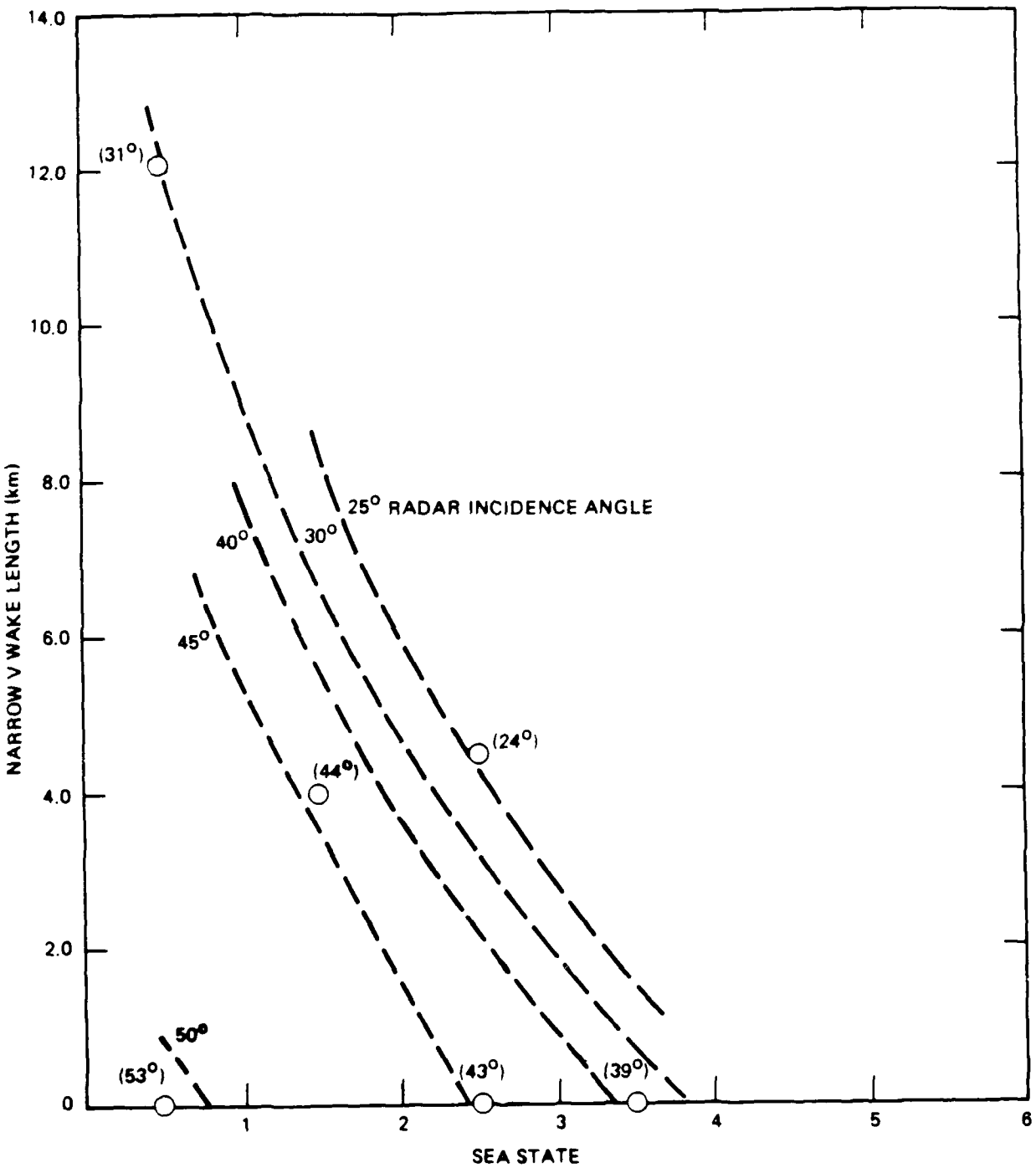

Figure 41. Narrow-V Wake Length vs. Sea State for Incidence Angles 30-55 Degrees. Solid and Dashed Lines are Expected Fits to Data.

of resolution, decrease in intensity of scatterers with increasing incidence angle and decrease in σ_o with increasing incidence angles. Our present level of understanding of these parameters, based on the Gulf of Alaska measurements, is sufficient to formulate a model for predicting the wake lengths observed in Figures 40 and 41. A scatter plot of the predicted and measured wake lengths is shown in Figure 42. A detailed description of this model is given in Appendix C.

The turbulent wake, identified as the dark band between the bright arms, is found to be more detectable in higher sea states compared to the narrow-V wakes. A summary of all observed lengths of the turbulent wake is given in Table 7 for various sea states and incidence angles. The turbulent wake is shown in this table to be up to 41 km long in Sea State 1, 4.5 km in Sea State 2, and 5.5km in Sea State 3. Wakes are not observed at incidence angles greater than 44 deg. The visibility of the turbulent wakes at Sea States 1-3 is not clearly understood at present. It may be attributed to the destruction of the ambient wind-generated waves by the current field within the wake. This possibility is suggested by the drop in backscatter level in the turbulent wake to below the ambient level, as shown in Figures 30-32. The development of an adequate theory to predict these observations is an important follow-on objective to pursue.

Ship-Generated Internal Waves

A simulation of ship-generated internal waves for the Gulf of Alaska experiment was executed by Dynamic Technology, Inc. The results are presented here for completeness. The simulation procedure is described by Liu et al (1984). Briefly, the B-V profile determined for the Gulf of Alaska, shown in Figure 43, is used to compute the dispersion curves for internal waves, which are shown in Figure 44 for several modes. The computed surface velocities and strains are shown in Figure 45. The maximum surface velocity is shown to be 6.0 cm/s and the maximum surface strain is shown to be 10^{-5} s^{-1}. Based on these

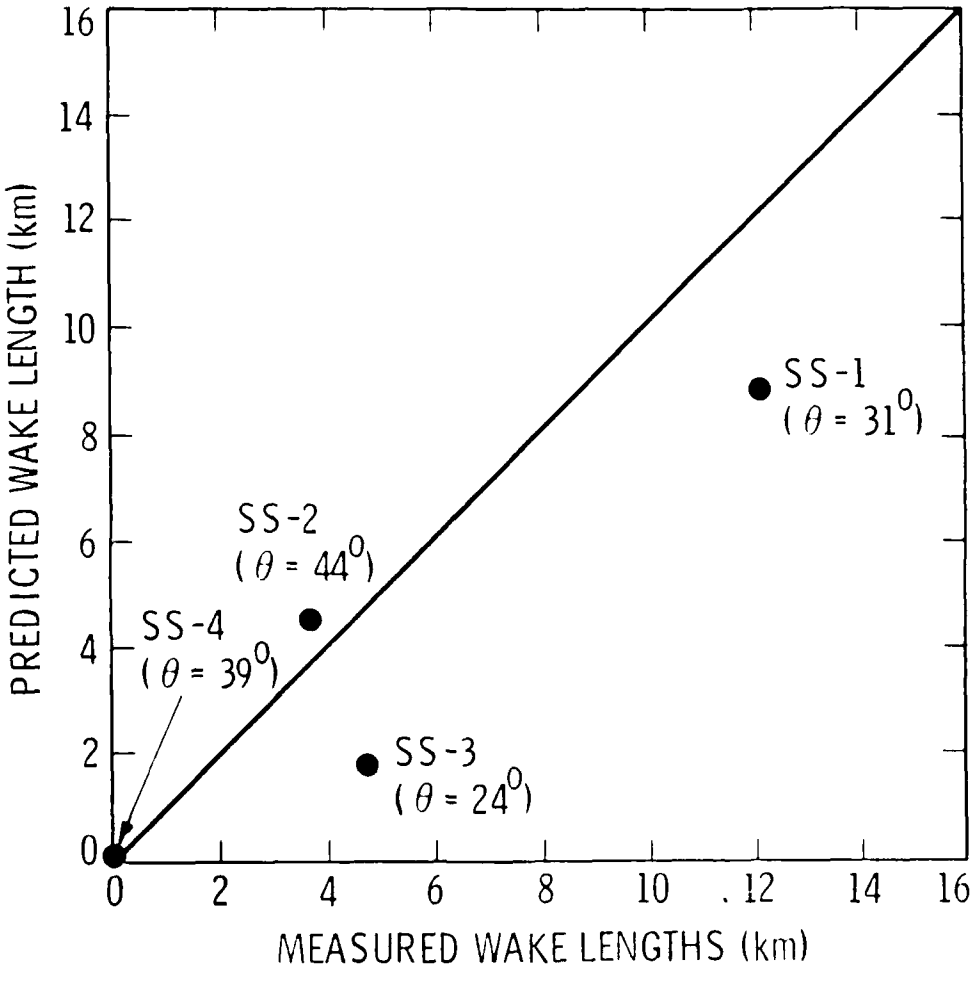

Figure 42. Comparison Between Predicted and Measured Wake Lengths.

Table 7. Summary of Turbulent Wake Lengths Measured for All the Ships Encountered in the Gulf of Alaska.

RADAR INCIDENCE ANGLE (deg)	LENGTHS (km) IN SEA STATE		
	1	2	3
24			5.5
31	32		
33	19		
35		4.5	
37	41		
38	35		
43			3.5
46	NOT VISIBLE		
48	34[1]		
49			2.0[1], 2.1[1], 4.4[1]
50			2.1[1]
51			NOT VISIBLE
53	2.4[1]		
54			NOT VISIBLE
56	2.1[1]		

[1] MARGINALLY VISIBLE

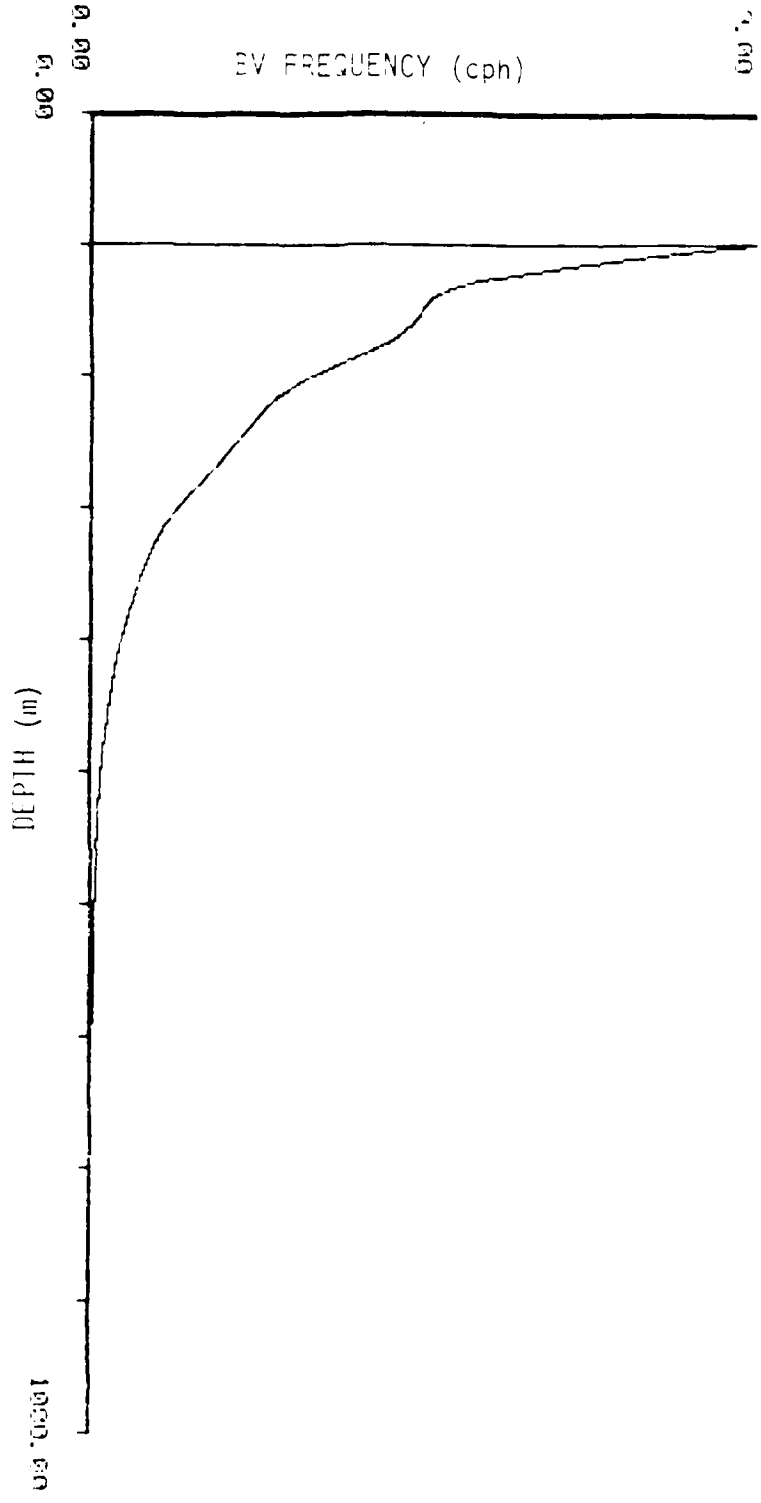

Figure 43. B-V Profile Used by Dynamic Technology (See Figure 12) to Compute Ship-Generated Internal Wave Modulations.

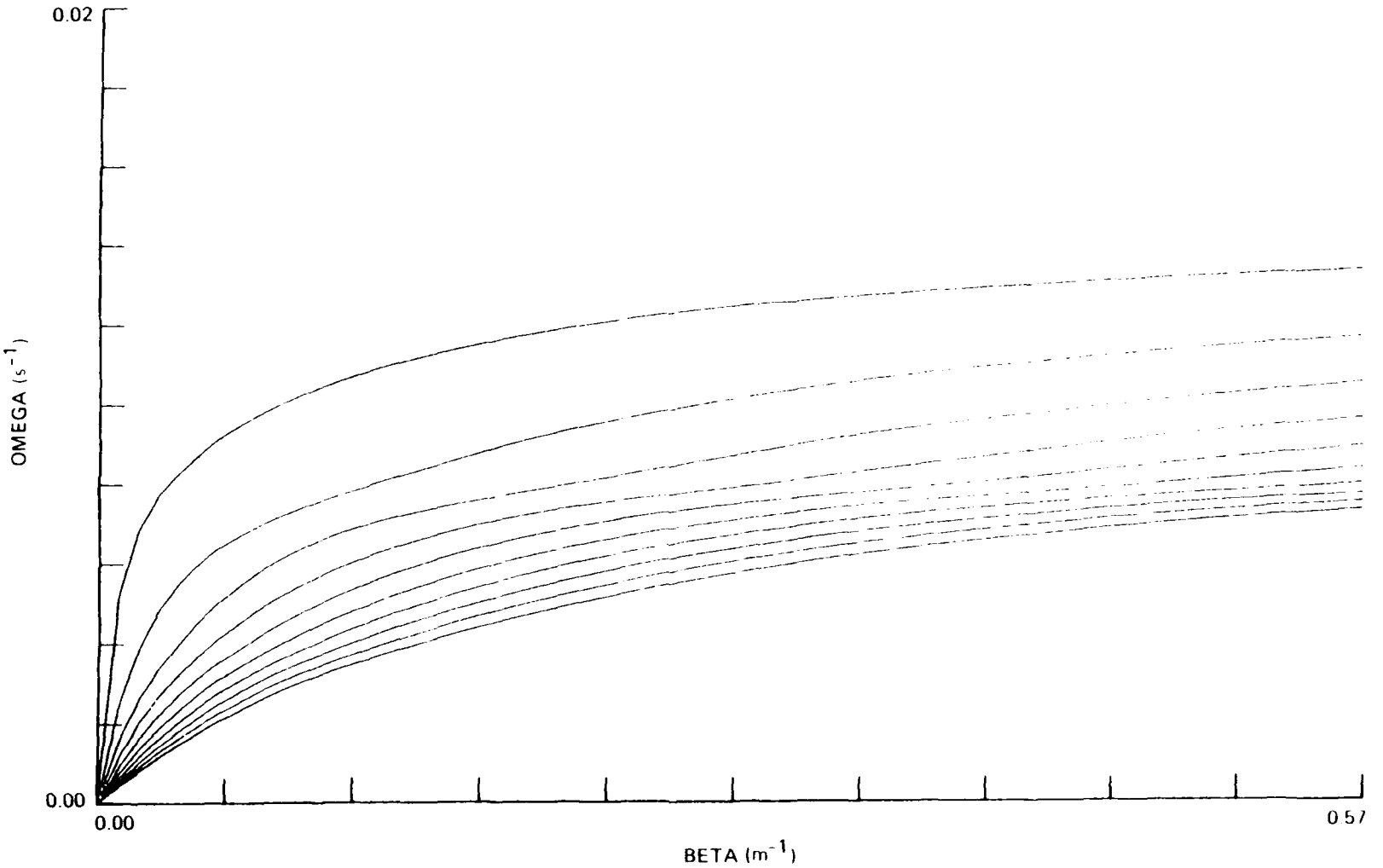

Figure 44. Dispersion Curves for Gulf of Alaska Stratified Layer in the Proximity of Bay Ridge on 13 March 1984.

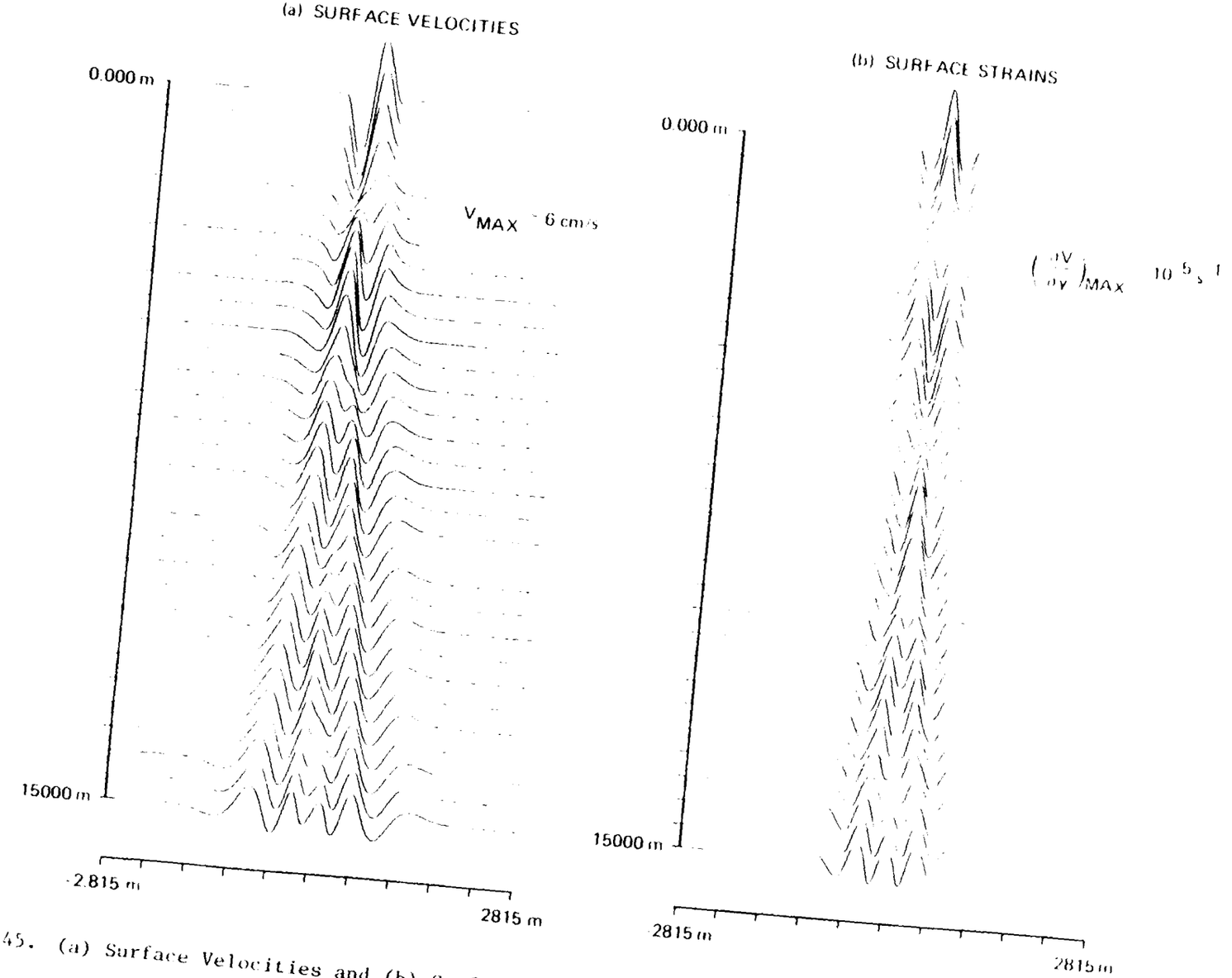

Figure 45. (a) Surface Velocities and (b) Surface Strains Computed by Dynamic Technology for Bay Ridge on 13 March 1984.

simulated surface strains and currents, an estimate of radar backscatter modulation is shown in Figure 46. The maximum modulation is found to be 0.5% of the ambient. The ship, radar and environmental parameters used in the simulation are also shown in Figure 46. The simulation shows, within the assumptions used, that radar backscatter modulation associated with ship-generated internal waves are negligible compared to those generated by ship-induced surface waves. This conclusion is valid for mixed layer depths of order 100m, as encountered in the Gulf of Alaska experiment. It confirms the validity of choosing the Gulf of Alaska for a site to emphasize the effect of surface waves (that are generated by the ship hull) on narrow-V wakes imaged by SAR.

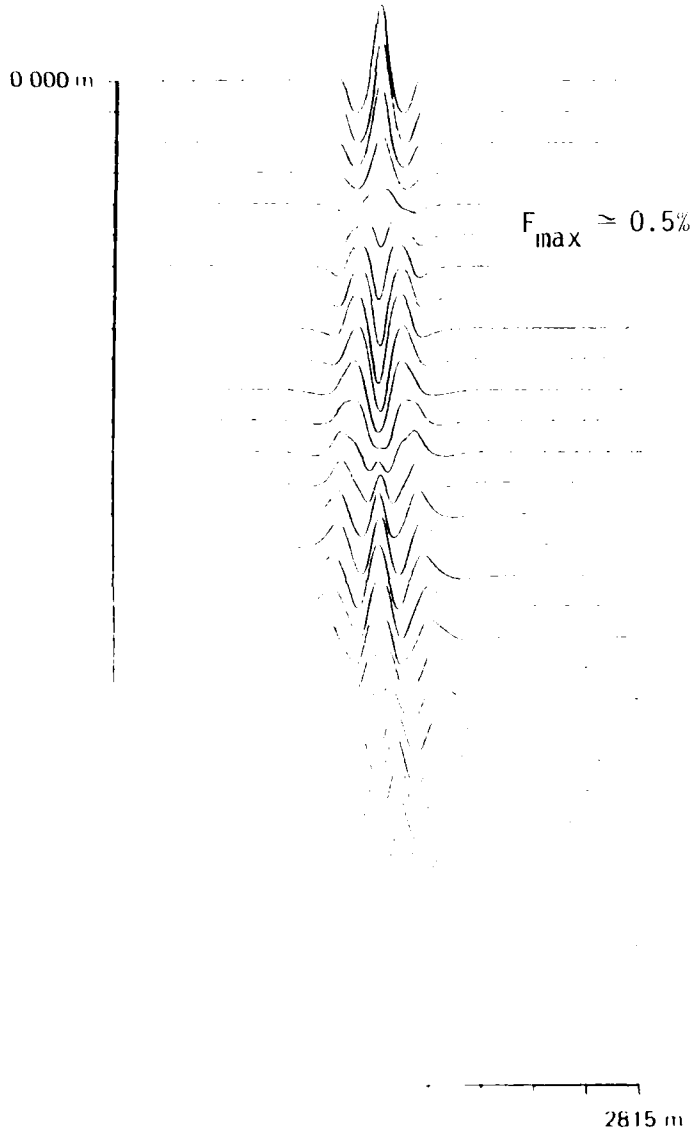

- SHIP PARAMETERS
  - 240 M LENGTH
  - 103,812 TON
  - 15 KNOTS
  - 145^0 (FROM NORTH)
- WIND CONDITION
  - 5 KNOTS
  - 110^0 (FROM NORTH)
- RADAR OPERATION
  - L-BAND
  - 30^0 INCIDENCE ANGLE
  - CROSS-TRACK LOOK

... by Ship-Generated Internal Waves that Would Correspond

V. SUMMARY AND CONCLUSION

Important progress has been achieved toward improving our understanding of ship-generated narrow-V wakes. The Gulf of Alaska experiment has produced a definitive data set, in Sea States 1-4, to resolve outstanding questions on the mechanisms responsible for generating narrow-V wakes. Also, the acquired images provide valuable insights on lengths of narrow-V wakes and on the turbulent wake in Sea States 1-4. The following specific conclusions are derived:

1. The half-angles associated with narrow-V wakes are consistent with first-order Bragg surface wave theory described by Case et al (1984).
2. The decay rate along the bright arms of the narrow-V wake is consistent with a combined viscous and radiation decay of short surface waves with first-order Bragg wave lengths.
3. Narrow-V wakes are observed in Sea States 1-3 at incidence angles less than or equal to 44 degrees. The limitation is due to the noise threshold of the SAR system used.
4. The longest narrow-V wakes bright-arm observed is 12.0 km (31 degree incidence angle) in Sea State 1, 3.9 km (44 degree incidence angle) in Sea State 2 and 4.3 km (24 degree incidence angle) in Sea State 3. In Sea State 4 no narrow-V wakes could be observed.
5. The turbulent wake (dark band between bright arms) is observed in Sea States 1-3 at incidence angles less than 53 degrees. The limitation is due to the noise threshold in the SAR system used.
6. The longest turbulent wake length observed is 41 km (37 degree incidence angle) in Sea State 1, 4.5 km (35 degree incidence angle) in Sea State 2 and 5.5 km (24 degree incidence angle) in Sea State 3. No turbulent wake is observed in Sea State 4.

7. Continued follow-on effort is recommended to formulate and test models for predicting lengths of narrow-V and turbulent wakes. More specifically, the following tasks require additional effort: (a) establish decay rates of surface waves in Sea States greater than 1, (b) verify the clutter levels in Sea States 1-4, (c) determine the interaction of surface waves with current in the turbulent wake region, and (d) incorporate the influence of sea state on degradation of SAR resolution in producing reduced signals in the bright arms.

REFERENCES

Case, K., C. Callan, R. Daschen, R. Davis, W. Munk, J. Vesecky, K. Watson, F. Zachariasen (1984). SEASAT III and IV, MITRE Corp. Report No. JSR-84-203, McLean, VA, 150 pp.

Durden, S. L. (1986). Microwave Scattering from the Ocean Surface, Stanford Electronics Laboratory Scientific Report No. D901 - 1986 - 1, 177 pp.

Fu, L. and B. Holt (1982). "SEASAT Views Oceans and Sea Ice with Synthetic Aperture Radar," JPL Publication 81-120, 200 pp.

Gasparovic, R., et al. (1986). The DARPA SAR Program: Interim Report on the Georgia Strait Experiment, SAR Technology and Processing Investigations - Volume I, Applied Physics Laboratory Report, John Hopkins Univ. Laurel, MD, 284 pp.

Gasparovic, R. and the SARSEX Experiment Team (1985). SARSEX Interim Report, Applied Physics Laboratory Report, John Hopkins University, Laurel, MD, 115 pp.

Guinard, W. N., J. R. Ransone, Jr., and J. C. Daley (1971). J. Geophys. Res., 76, No. 6, pp. 1525-1538.

Hammond, R. R., R. R. Buntzen and E. E. Floren (1984). "Use of Ship Wake Patterns in the Evaluation of SAR Ocean Wave Imaging Mechanisms," Interim Report, Naval Ocean Systems Center, San Diego, CA, 52 pp.

Held, D., C. Werner and S. Wall (1983). The Absolute Amplitude Calibration of the SEASAT Synthetic Aperture Radar: An Intercomparison with Other L-Band Radar Systems, Digest of the 1983 Int'l Geoscience and Remote Sensing Symposium, San Francisco, CA.

Kwoh, D. and B. Lake (1983). "Microwave Backscattering from Short Gravity Waves: A Deterministic, Coherent, and Dual-Polarized Lab. Study," TRW Report No. 37564-6001-UT-00, Redondo Beach, CA.

Liu, A. K., D. A. Berge and S. R. Borchardt (1984). Surface Signatures of Ship-Generated Internal Wave, Dynamic Tech. Inc. Report No. DT-8311-01, Torrance, CA, 42 pp.

Lyden, J. D. (1985). Analysis of SEASAT Revolution 407 Ship Wake Data, ERIM Report No. 155900-32-T, Ann Arbor, MI, 17 pp.

Lyden, J. D., D. R. Lyzenga, R. A. Shuchman and E. S. Kasischke (1985). Analysis of Narrow Ship Wakes in Georgia Strait SAR Data, ERIM Topic Report No. 155900-20-T, Ann Arbor, MI, 118 pp.

Schmitt, K. F., E. D. Brown, D. C. Wyatt, R. E. Hall and S. B. Buchsbaum (1987). The Nonlinear Wake Experiment (NOWEX), SAIC Report No. SAI-87/1555, San Diego, CA, 51 pp.

Shemdin, O. H. (1985). SAR Imaging of Ship Wakes in the Gulf of Alaska: Flights During 9-15 March (Progress Report), Ocean Research and Engineering, La Canada, CA. 30 pp.

Shemdin, O. H. and The TOWARD Experiment Team (1986). TOWARD Field Experiment Interim Report, Jet Propulsion Laboratory Report, Pasadena, CA, 300 pp.

Stark, V. L. and C. H. Sinex (1983). (U) "Strategic Area Note Book: Mixed-Layer Depths - North East Pacific Ocean," STDR 90, JHU-APL Report, Confidential Report.

Thompson, T. W. (1986). NASA/JPL Aircraft SAR Operations for 1984 and 1985, JPL Publication 86-20, Pasadena, CA, 66 pp.

Valenzuela, G. R. (1978). Theories for the Interaction of Electromagnetic and Ocean Waves - Review, Bound. Layer Meteo., 13, 61-85.

Swanson, C. V. (1984). Radar Observability of Ship Wakes, Private Communication.

Witting, J. M. and R. Vaglio-Laurin (1985). Mechanisms and Models of Narrow-V Wakes, ORI Report No. 2529, 75 pp.

APPENDICES

A. B-V Profiles for 1984 Gulf of Alaska Survey

B. CV-990 Aircraft Data and Optical Images from the Gulf of Alaska Experiment

C. Model for Determining Lengths of Bright Arms in Narrow-V Wakes.

APPENDIX A

B-V Profiles for 1984 Gulf of Alaska Survey

by

C. Sinex, APL/JHU

Introduction

During March 1984, three AXBTs were dropped in the Gulf of Alaska. The resulting depth-temperature profiles for these three AXBTs, labeled #14, 15 and 16, are shown in Figure 1. Since salinity is a critical factor to stratification in this region, these AXBTs are not by themselves adequate for calculating B-V profiles. Some estimate of the salinity structure is also required. This note provides such an estimate and makes the required B-V calculations. The first part of the note discusses stratification in the halocline region, around 100 m and deeper, while the second part of the note discusses stratification in the "mixed layer" extending from the surface down to the top of the halocline.

Stratification in the Halocline

Figure 2 shows the locations of the three AXBT profiles, marked with a circle, and the locations of all historical profiles with salinity data for the months of February and March contained in the MOODS data base. There are ten such profiles, six from February and four from March, marked with a triangle.

The depth-salinity profiles for these ten historical profiles are shown overplotted in Figure 3. With the exception of one profile, "mixed layer" depths appear to fall in the range of 75 to 100 meters. Below the base of this "mixed layer," a strong halocline extends down to about 200 meters, with the salinity increasing by about 1½ parts per thousand. It is within this halocline region that salinity has a dominant effect on stratification.

Unfortunately, there are difficulties in matching historical temperature-salinity data to temperature-only data (such as provided by AXBTs) in the Gulf of Alaska. In particular, there is no unique relationship between temperature and salinity through the halocline that can be used to adjust historical salinity to temperature profiles. As will be seen later, some temperature profiles are nearly isothermal through the halocline, other temperature profiles have a temperature inversion at the top of the halocline while still other profiles have a normal, but weak, thermocline at the top of the halocline.

The approach used in this note takes advantage of the fact that the shape of the halocline in Figure 3 appears more or less constant, regardless of the location of the top of the halocline. An approximate fit to this shape as a function of distance below the top of the halocline was then obtained from Figure 3 and is reproduced in Table 1 below.

Table 1

Approximate Halocline Shape

Distance Below Halocline Top (meters)	Salinity (ppz)
0	32.5
25	33.16
50	33.45
75	33.62
100	33.72
125	33.77
150	33.80
175	33.82
200	33.85
225	33.87
250	33.90

The location of the top of the halocline for each of the three AXBTs in Figure 1 was then estimated based on a comparison of these profile shapes and all available historical data (shown later in Figures 10-29). For AXBT profiles 14 and 15, this halocline top was estimated to be at about 100 meters and at about 125 meters for profile 16.

Figures 4, 6 and 8 show these AXBT temperature profiles together with the best estimate of the salinity profile. Salinity is taken as a constant 32.5 ppt in the "mixed layer". Figures 5, 7 and 9 show the corresponding

B-V profiles in units of cycles/hour. Peak B-V values are typically about 10 cph in the halocline. Above the halocline in the "mixed layer," the weak temperature gradients occasionally produce B-V values between 1 and 2 cph. The temperature inversions are usually salinity-compensated as will be seen in the next section; B-V is taken as zero where such temperature inversions occur.

Stratification in the "Mixed Layer"

The temperature-salinity profiles and B-V profiles for each of the ten historical MOODS profiles are shown in Figures 10 through 29. In general, the stratification in the halocline peaks between 5 and 10 cph, consistent with the earlier estimates for the three AXBT drops. Above the top of this halocline, however, the "mixed layer" generally shows considerable variability with weak thermal and salinity gradients occurring frequently. Typically B-V values in this "mixed layer" are around 1 to 2 cph, with occasionally larger values occurring. None of the ten historical profiles showed a completely mixed "mixed layer" down to the halocline top. In fact, weak stratification, up to about 2 cph, appeared to be a more common occurrence than complete mixing. It is assumed that such conditions are also typical of the three AXBT profiles shown in Figure 1. Consequently, the stratification estimates for the mixed layers in Figures 5, 7 and 9 are considered lower limits at best. However, the actual stratification levels in these "mixed layers" are not generally expected to exceed much more than about two cycles/hour based on available

historical data. Out of the ten historical profiles shown here, only one, profile #29346 in Figures 20 and 21, shows B-V values in the "mixed layer" above 5 cph. This historical profile also shows considerable temperature finestructure associated with these high B-V sections; such temperature finestructure is not present in the three AXBT profiles in Figure 1.

C. H. Sinex

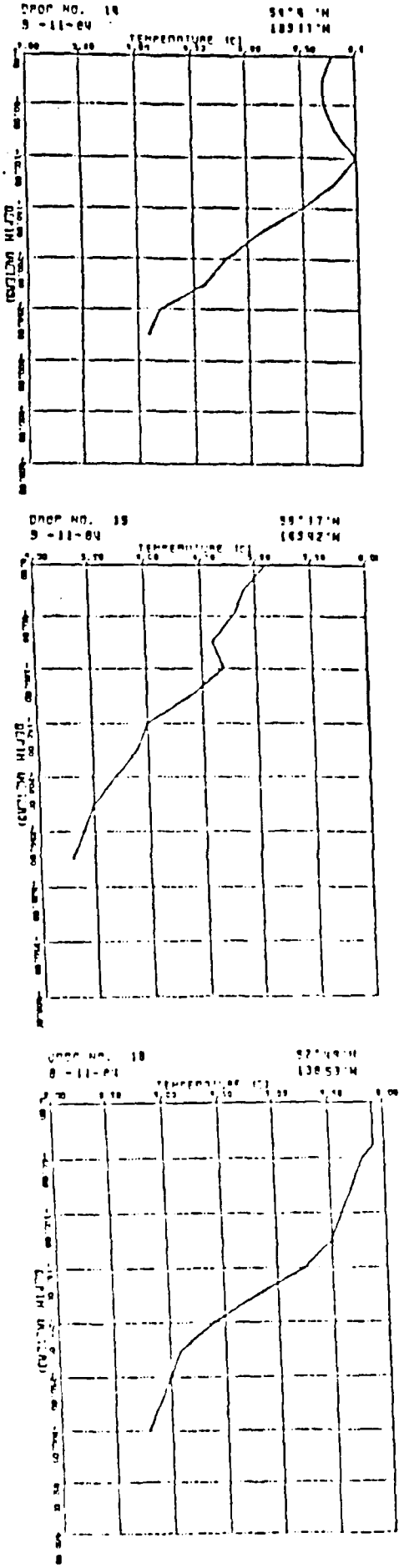

Figure A-1 1984 AXBT Depth-Temperature Profiles

Figure A-2 Locations of 1984 and Historical Profiles.

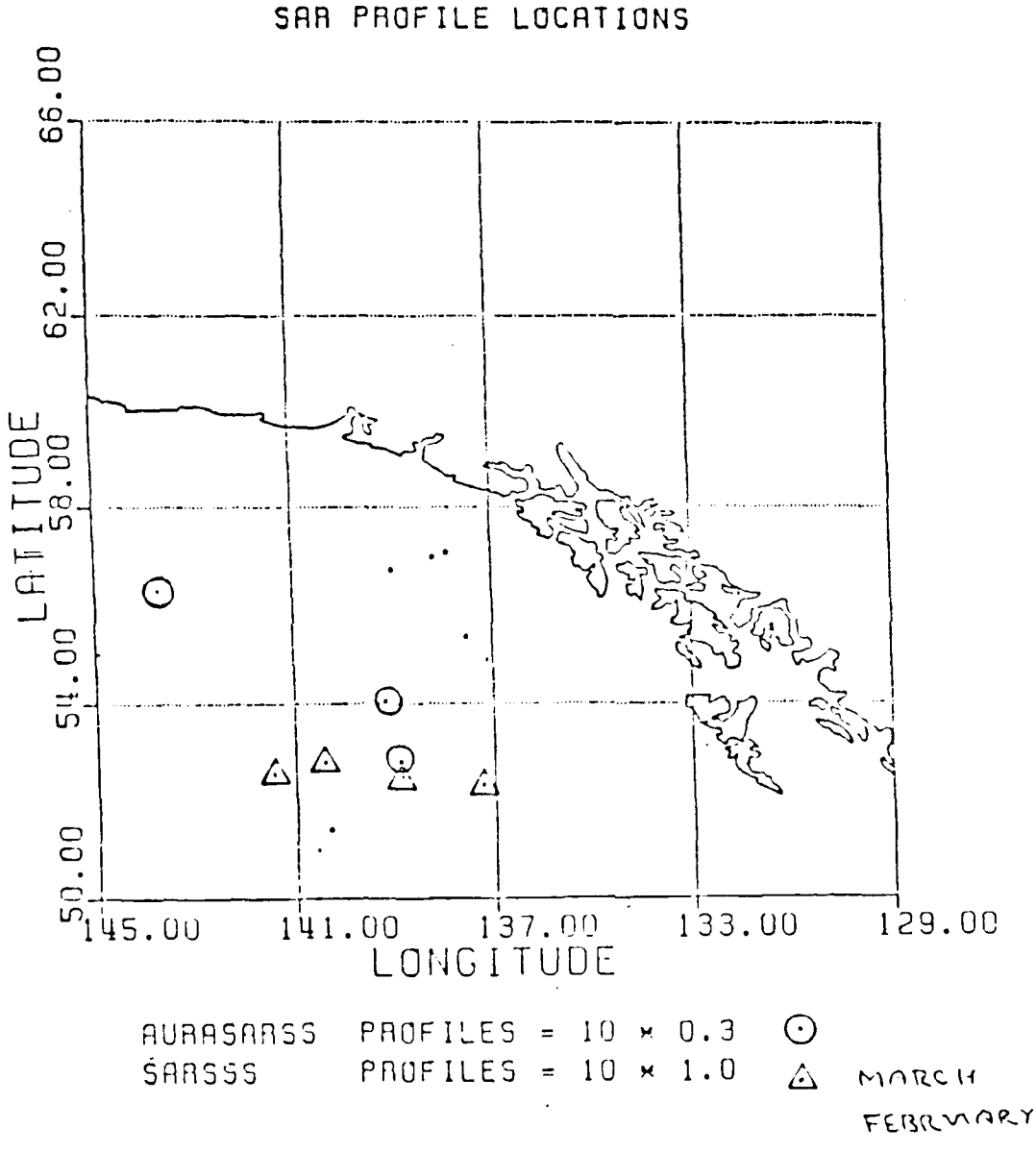

Figure A-3
Historical Depth-Salinity Profiles.

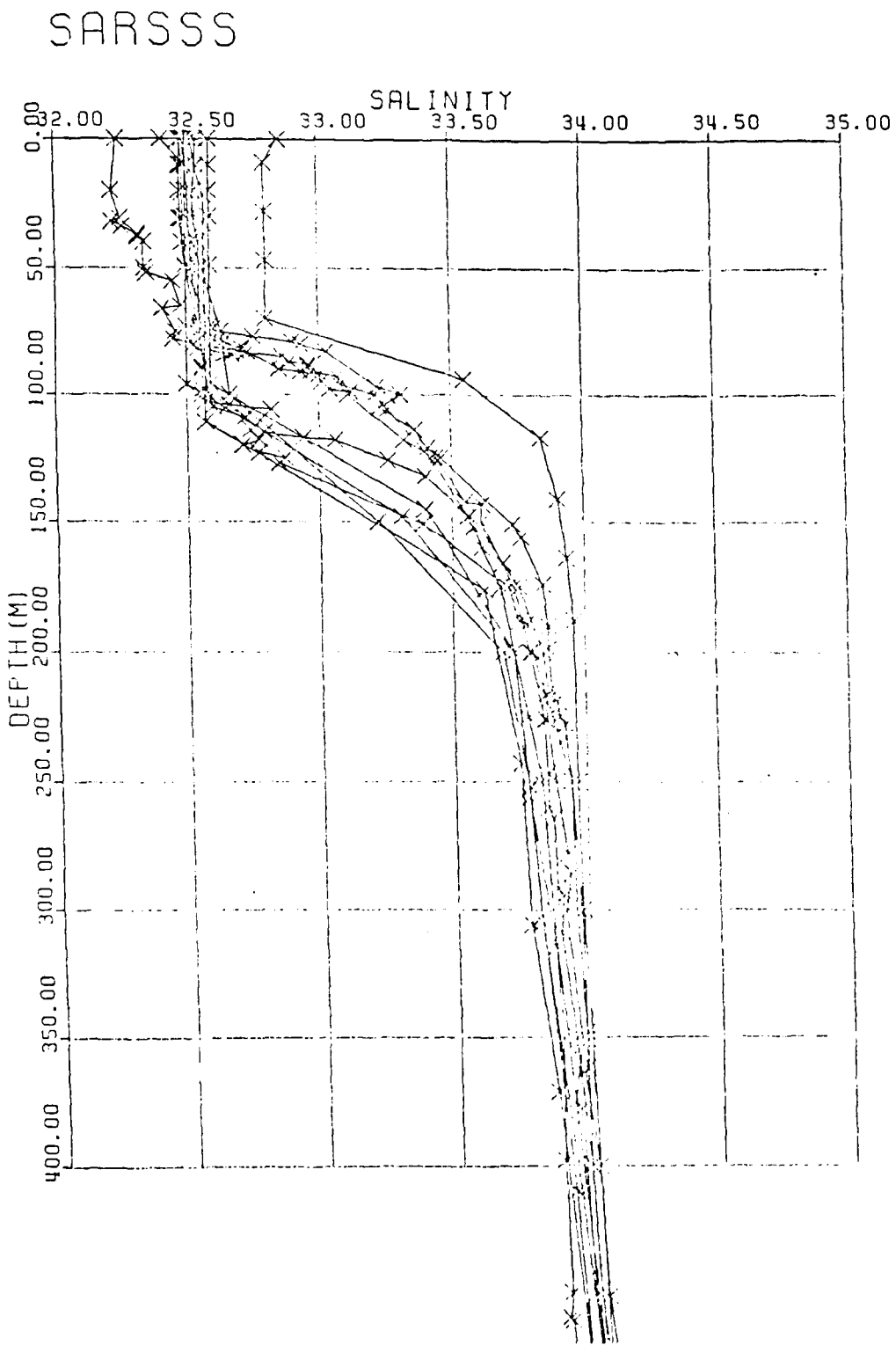

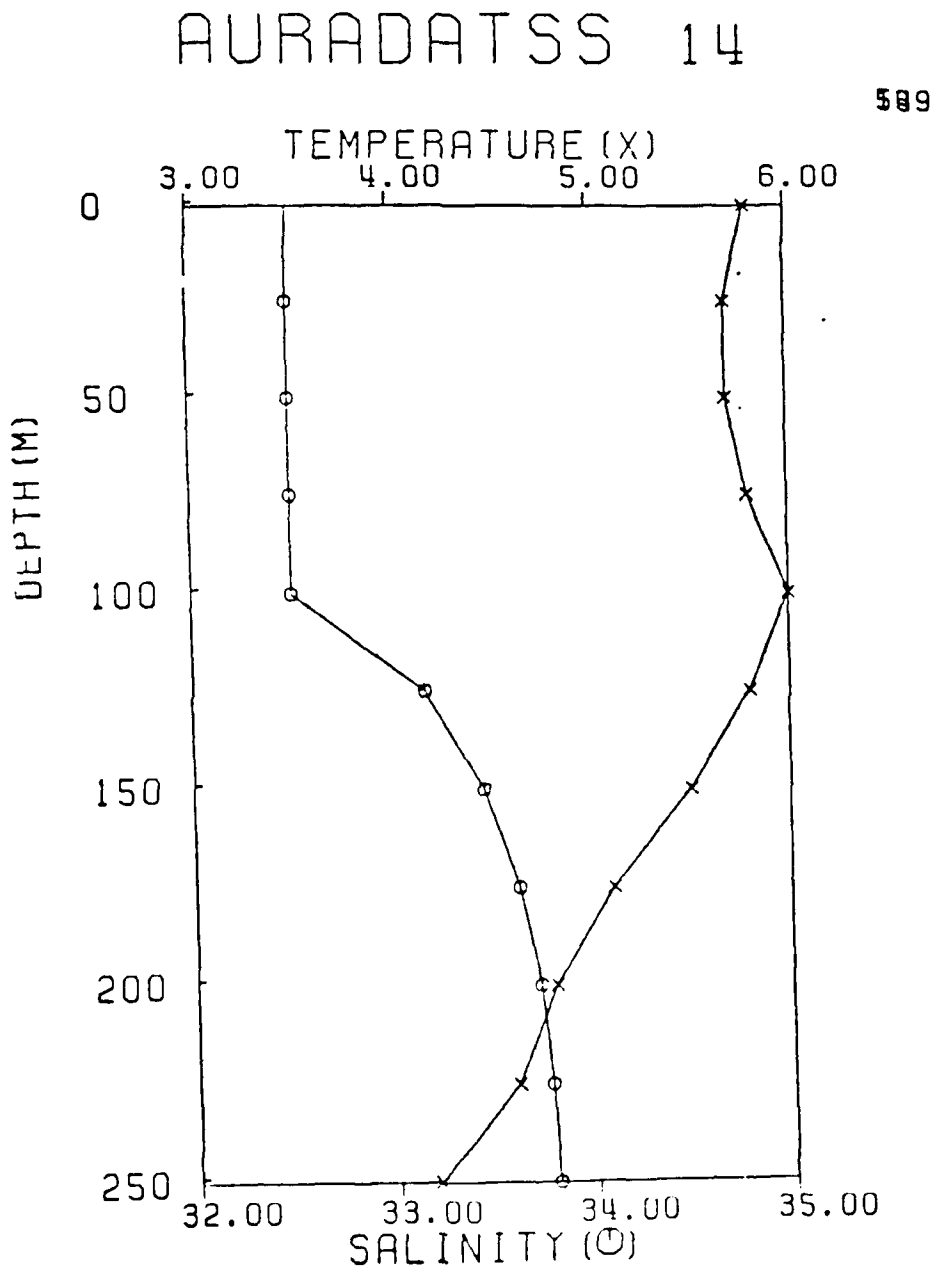

Figure A-4 Temperature and Best Estimated Salinity Profiles for Drop 14.

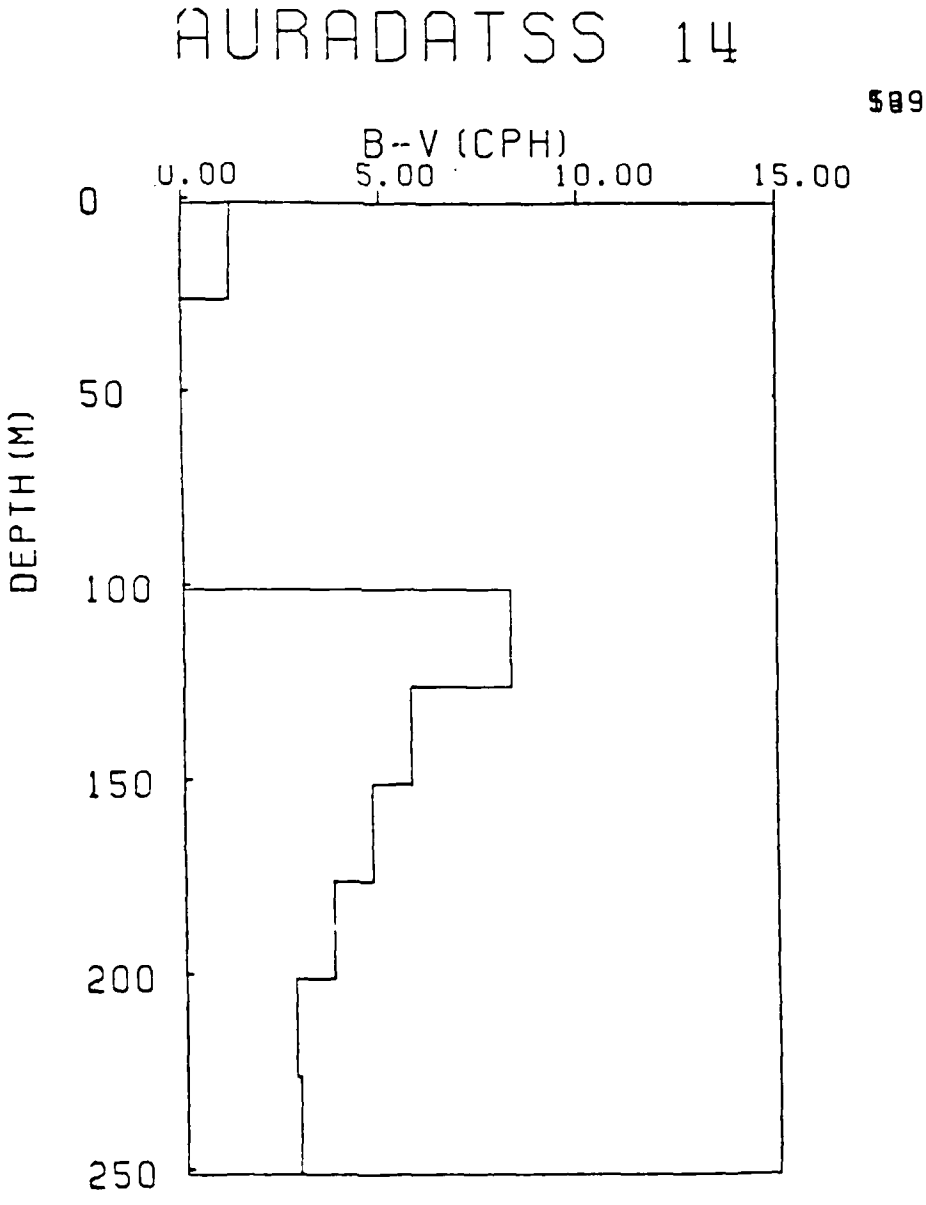

Figure A-5 B-V Profile for Drop 14.

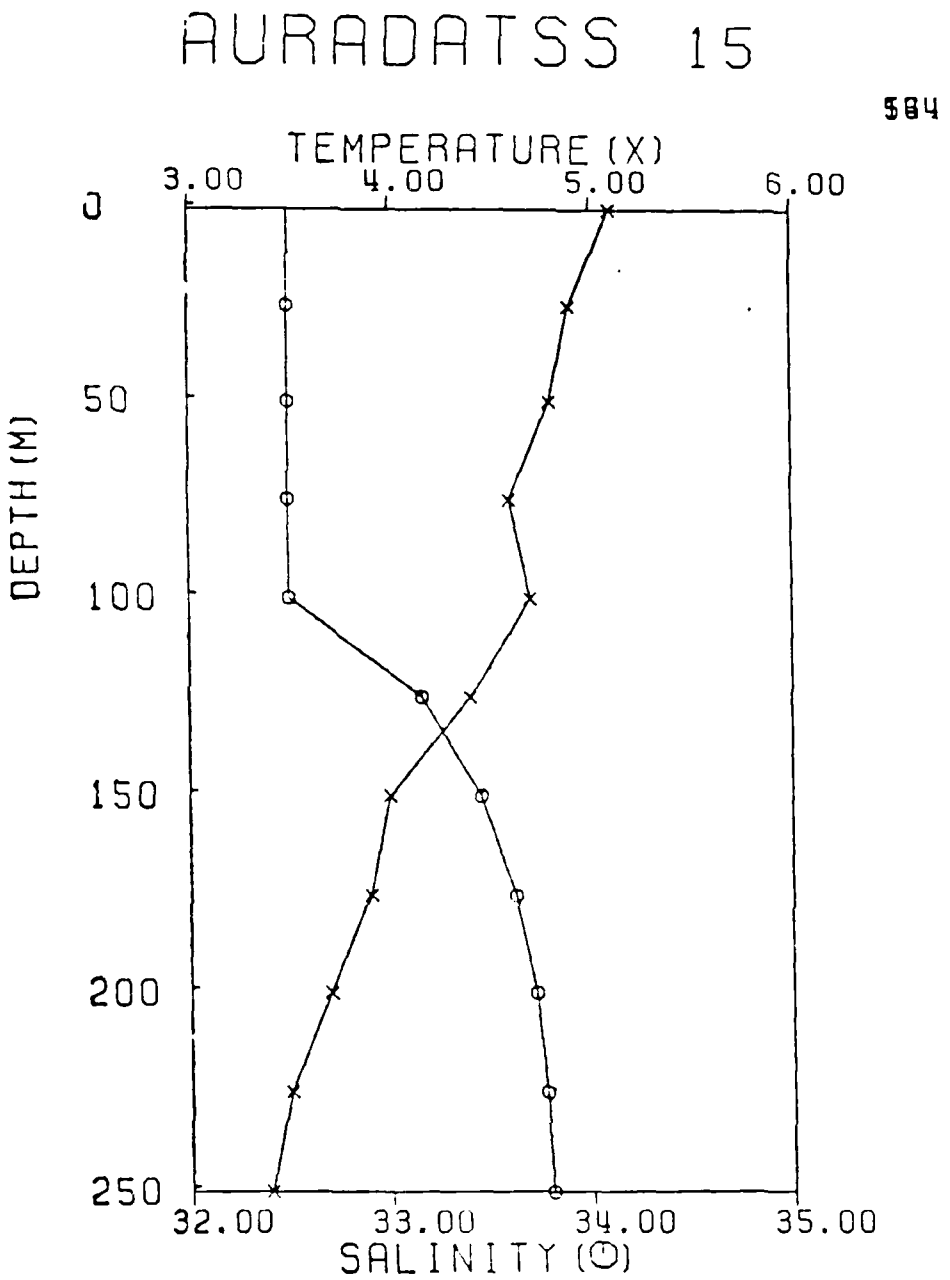

Figure A-6 Temperature and Best Estimated Salinity Profiles for Drop 15.

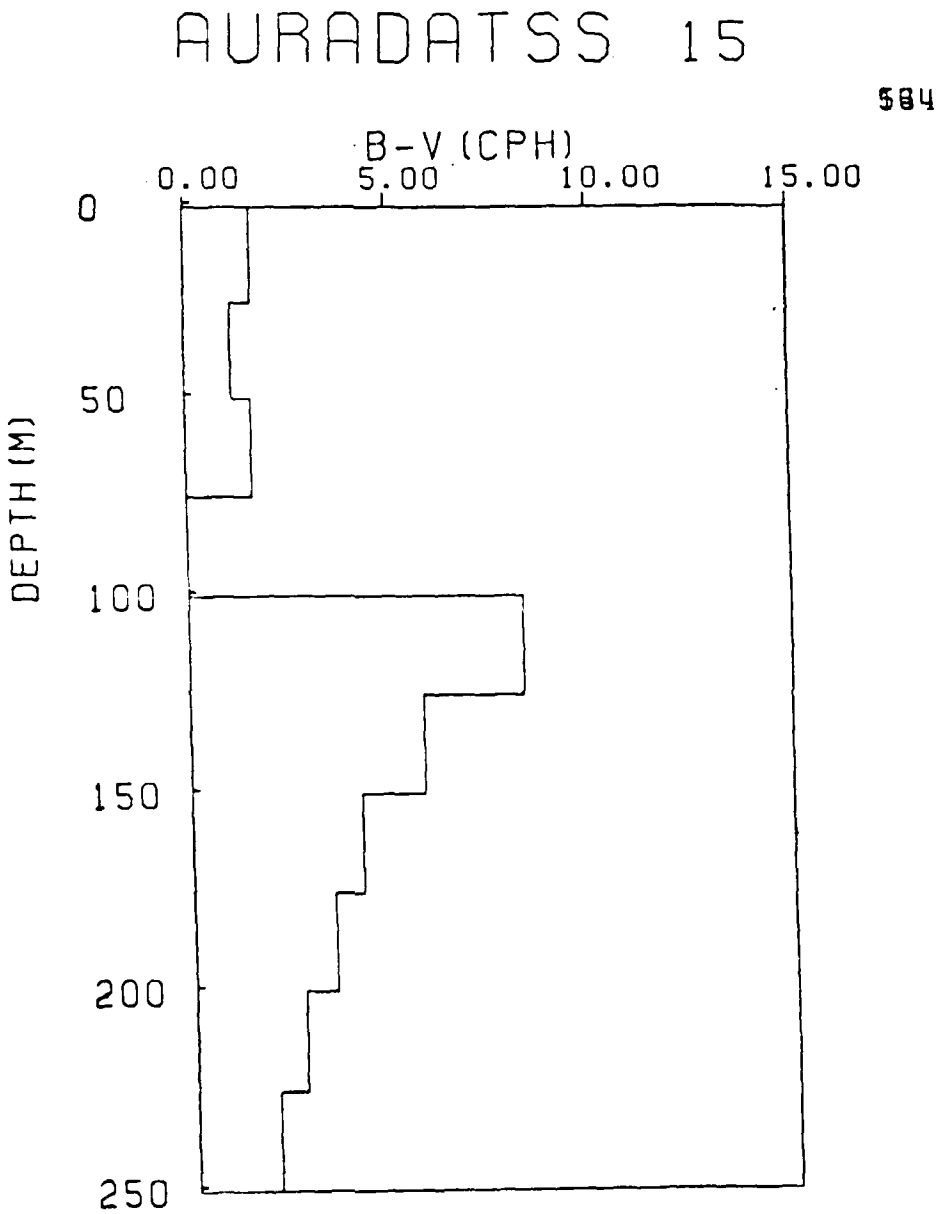

Figure A-7 B-V Profile for Drop 15.

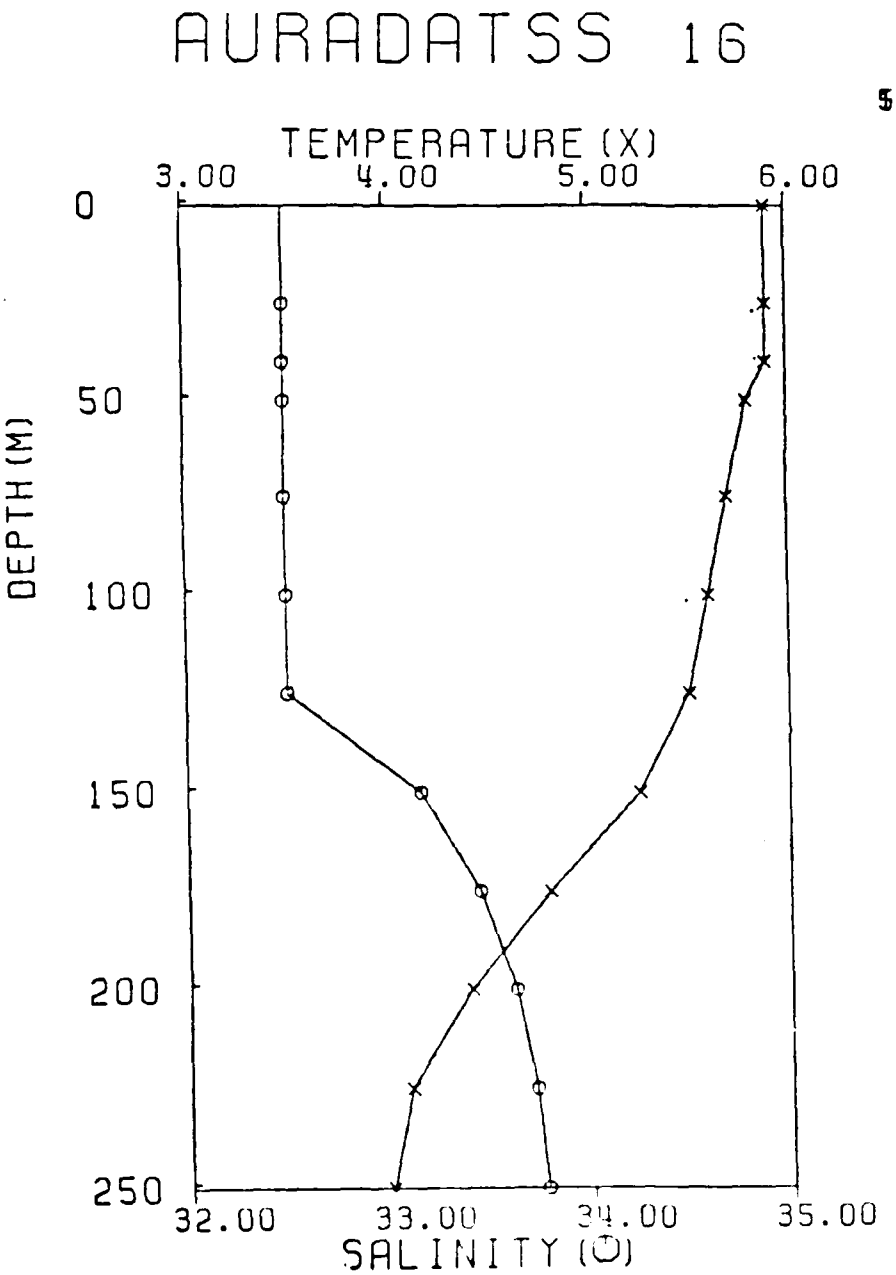

Figure A-8 Temperature and Best Estimated Salinity Profiles for Drop 16.

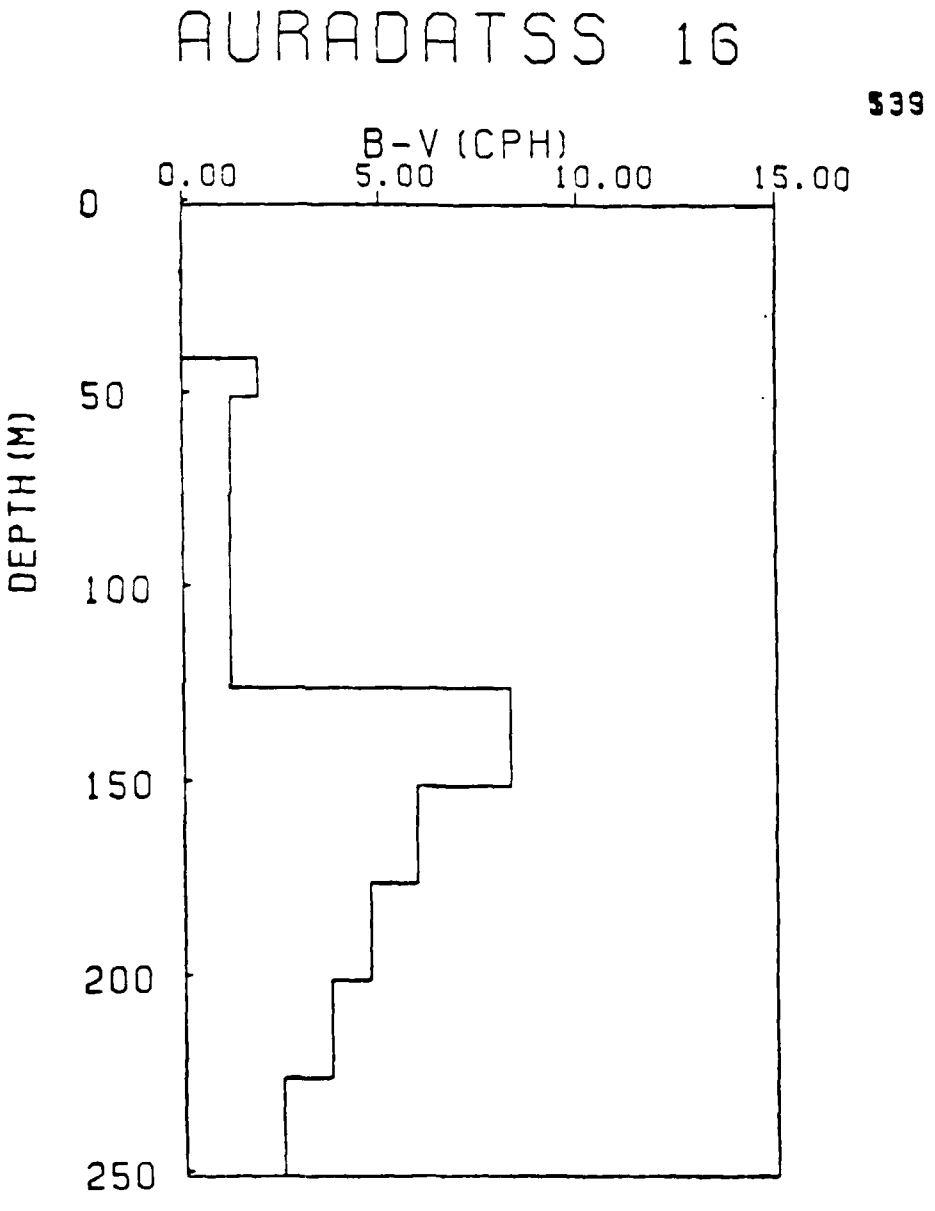

Figure A-9 B-V Profile for Drop 16.

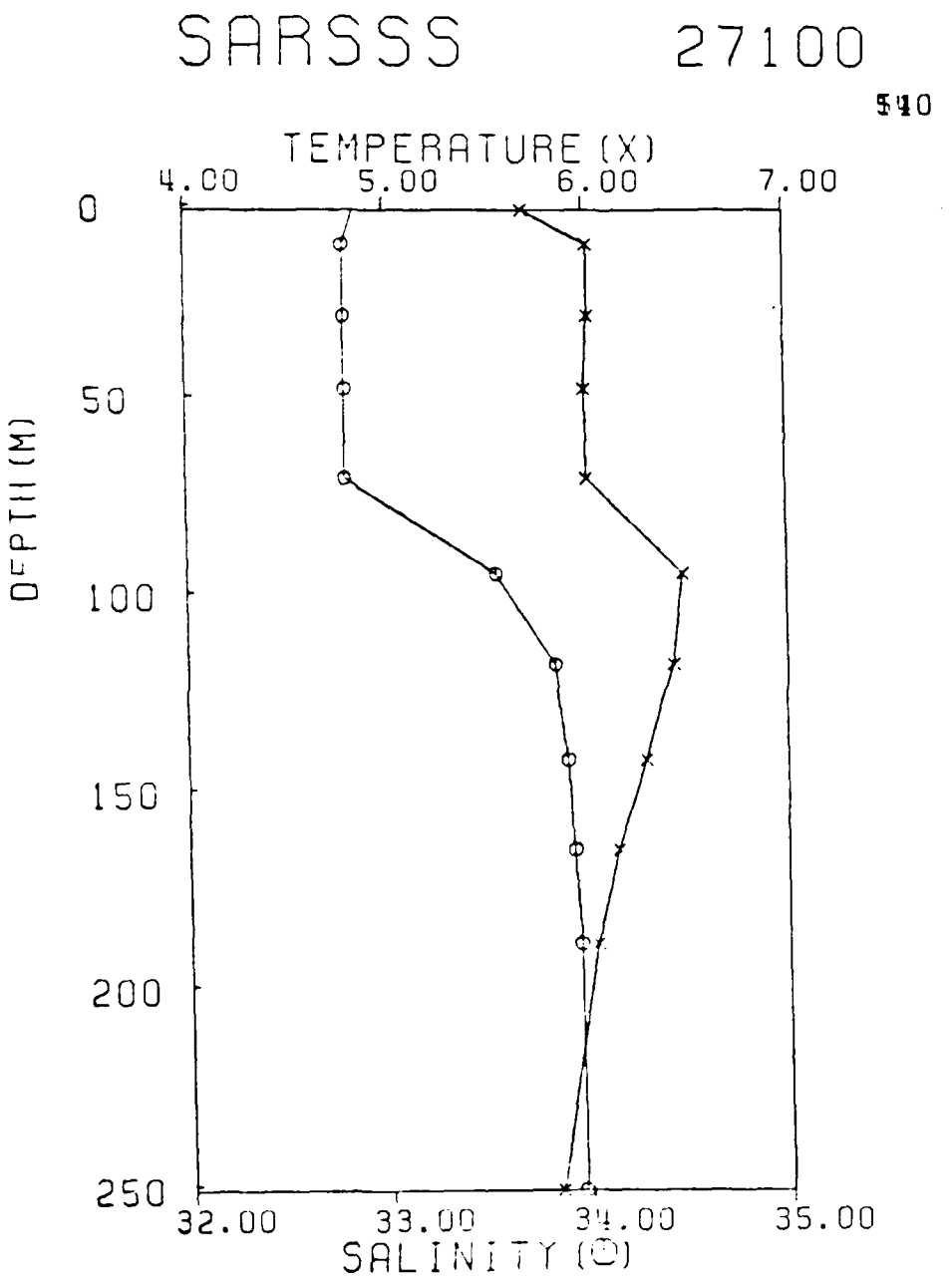

Figure A-10 Historical Profile #27100.....1961 Day 41

51°26'N 140°19'W.

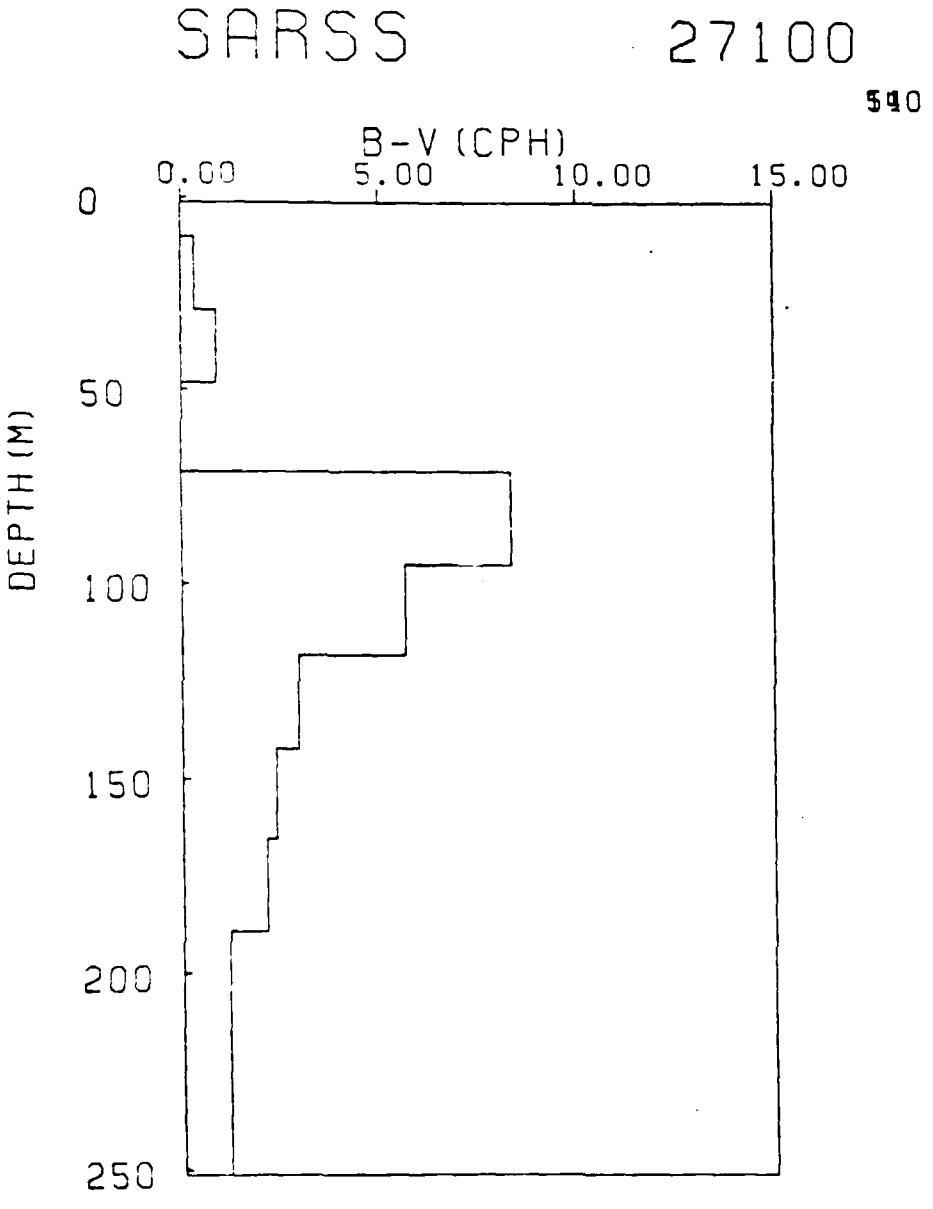

Figure A-11 B-V Profile for Figure A-10.

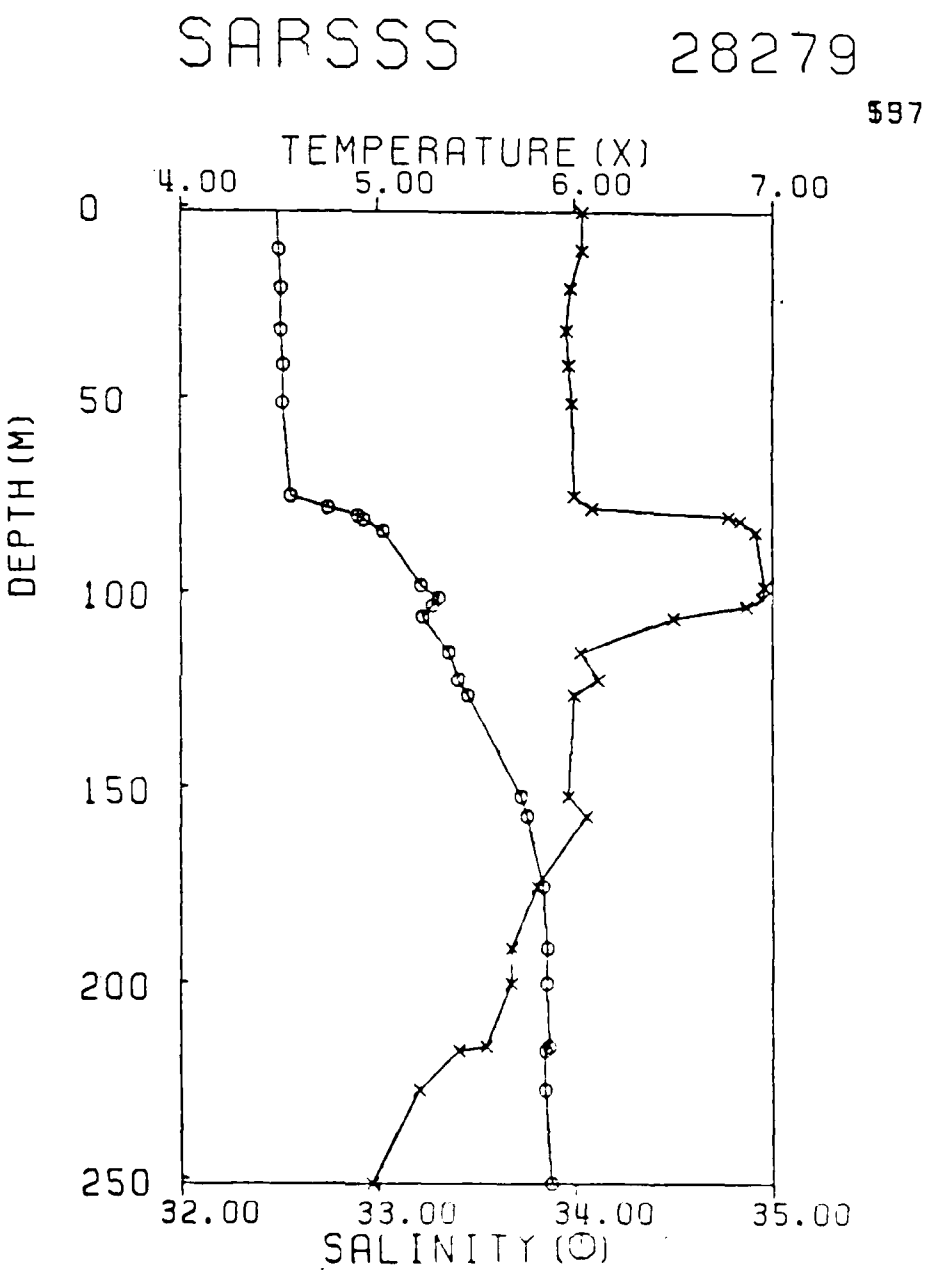

Figure A-12 Historical Profile #28279....1978 Day 39.

54°51'N 137°6'W

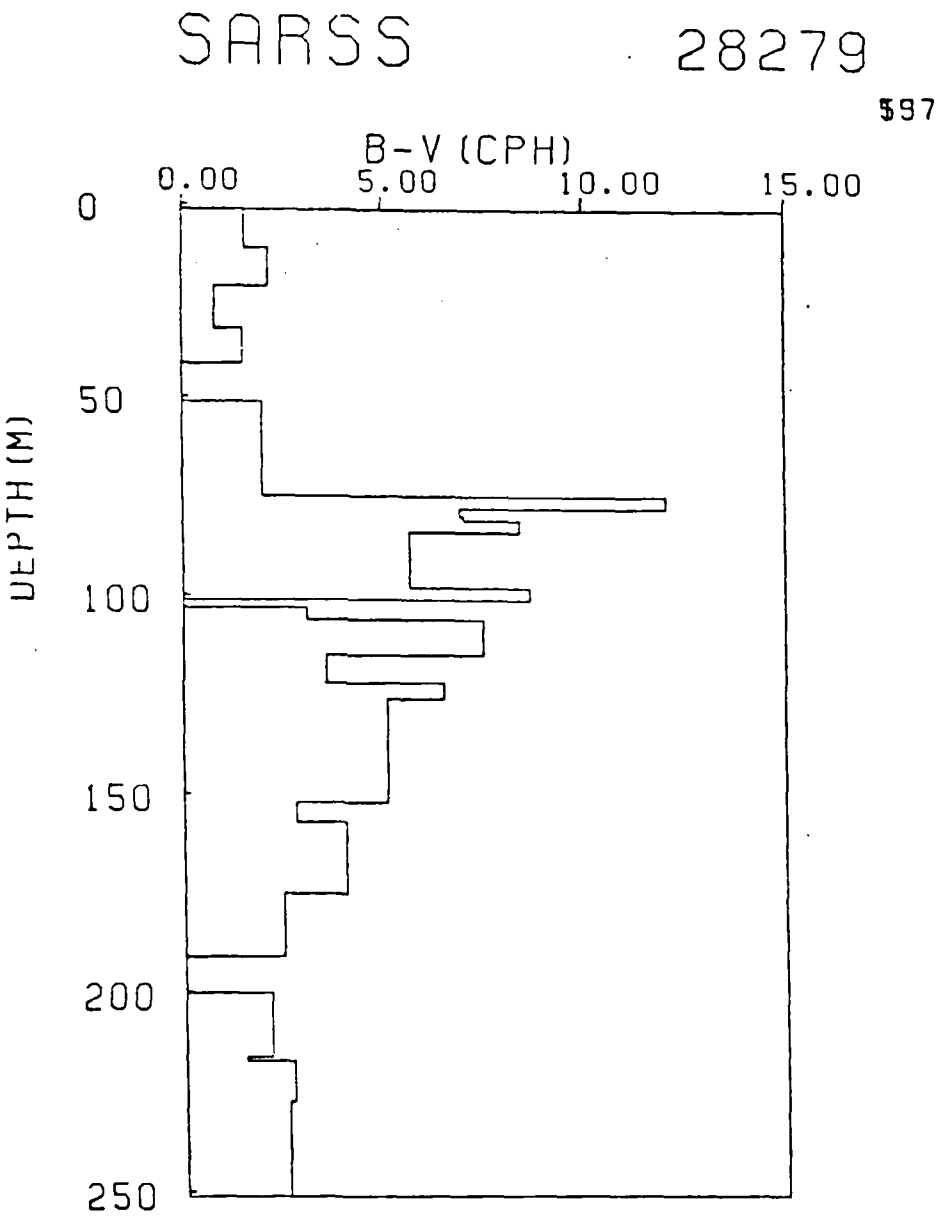

Figure A-13 B-V Profile for Figure A-12.

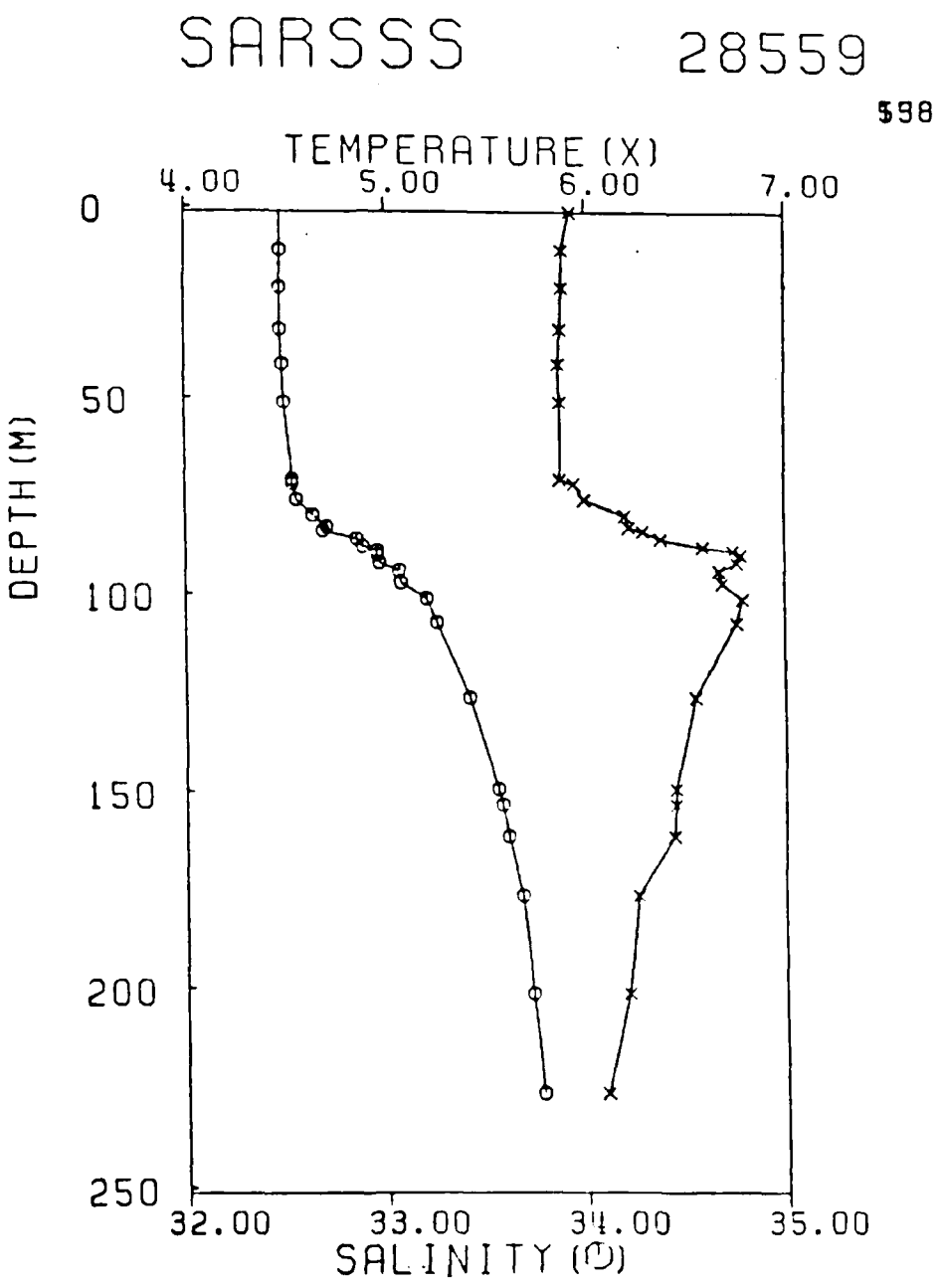

Figure A-14 Historical Profile #28559....1978 Day 34

55°19'N 137°30'W

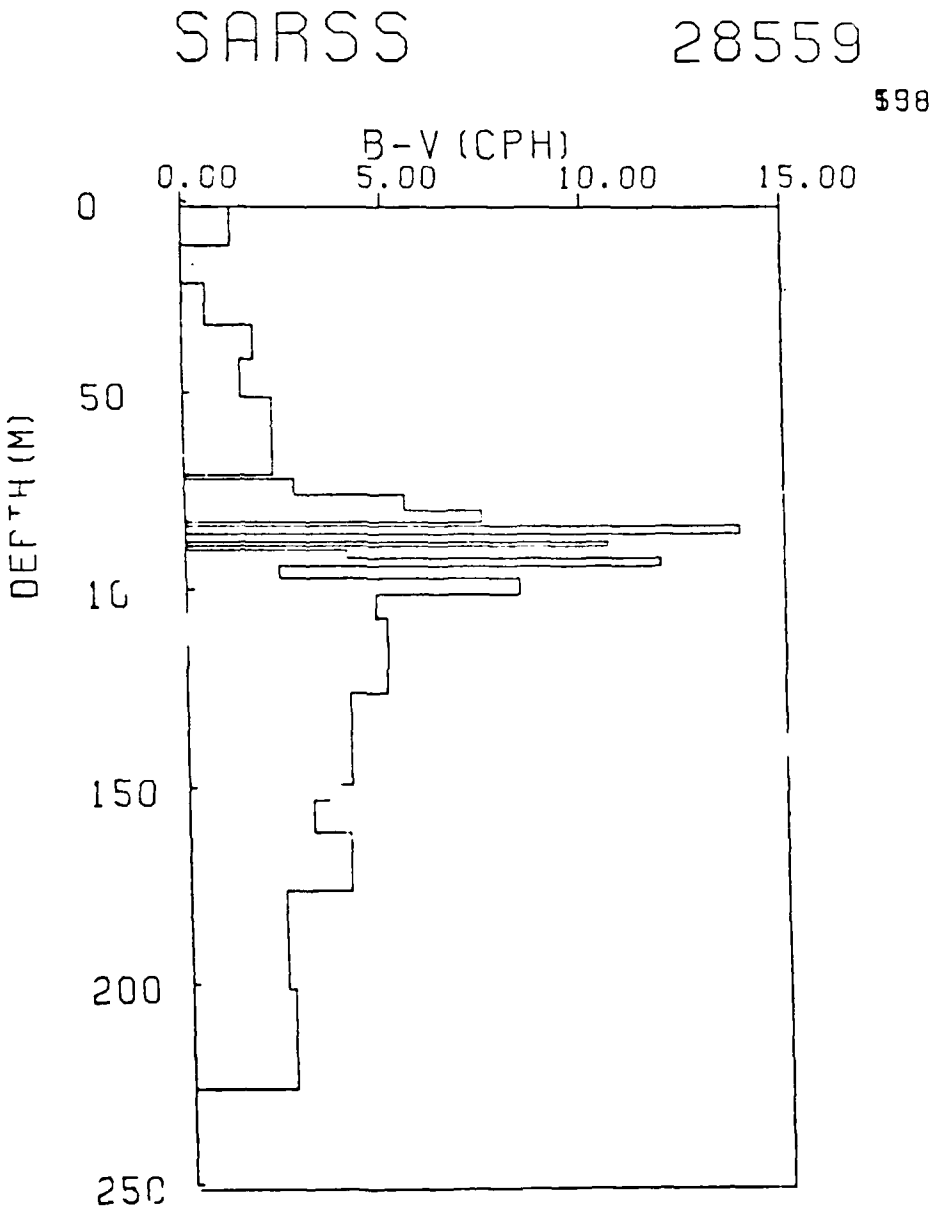

Figure A-15 B-V Profile for Figure A-1

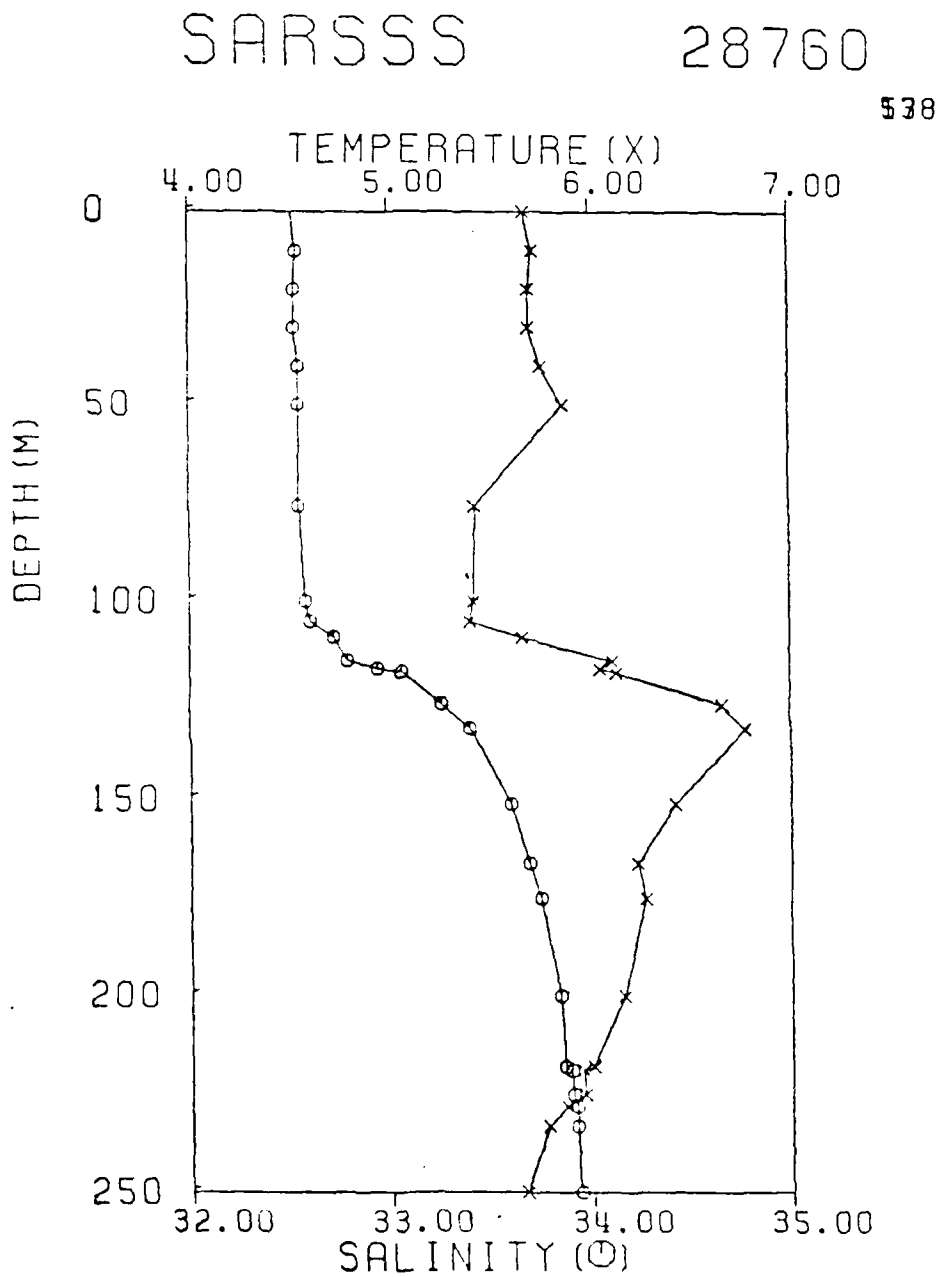

Figure A-16 Historical Profile #28760....1978 Day 32

56°59'N 138°10'W.

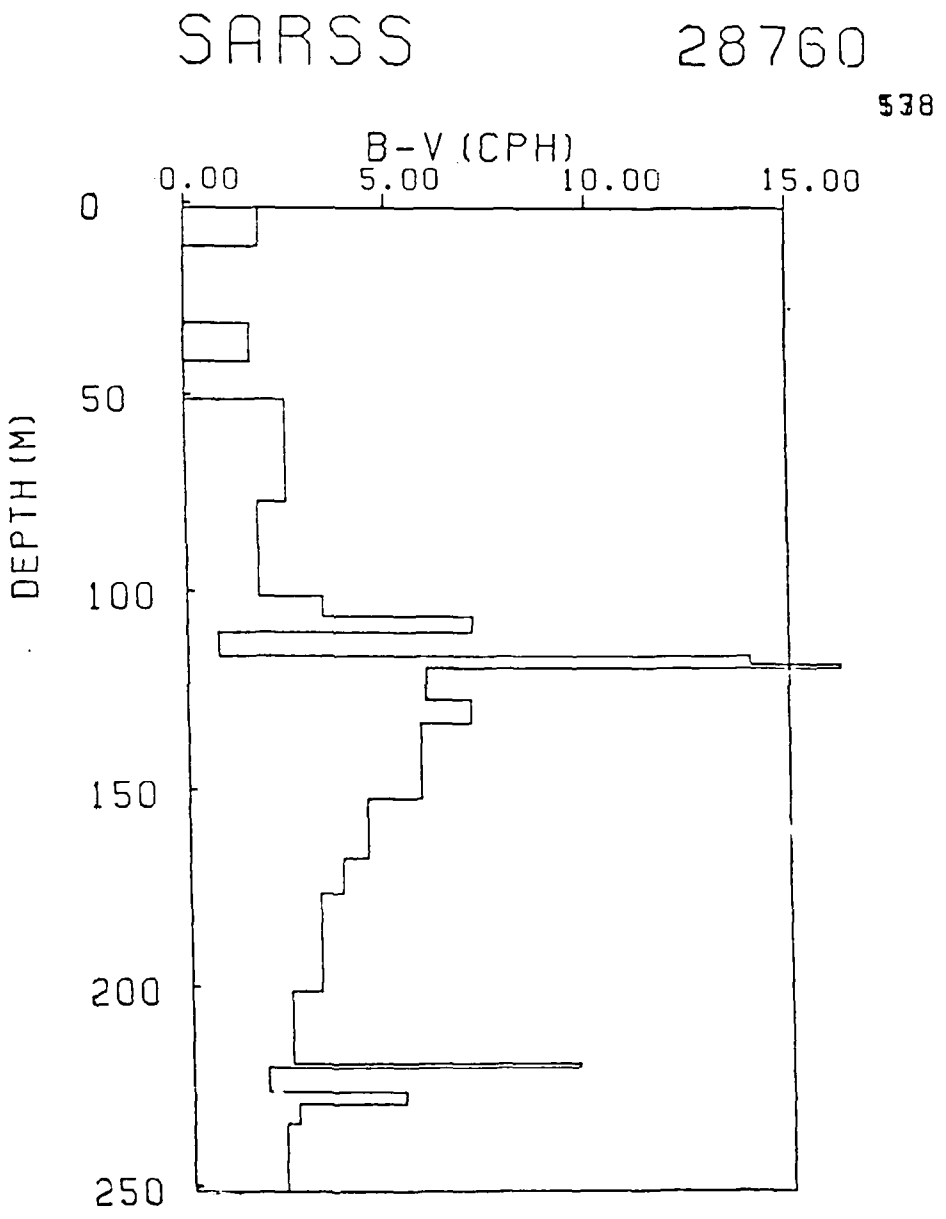

Figure A-17 B-V Profile for Figure A-16.

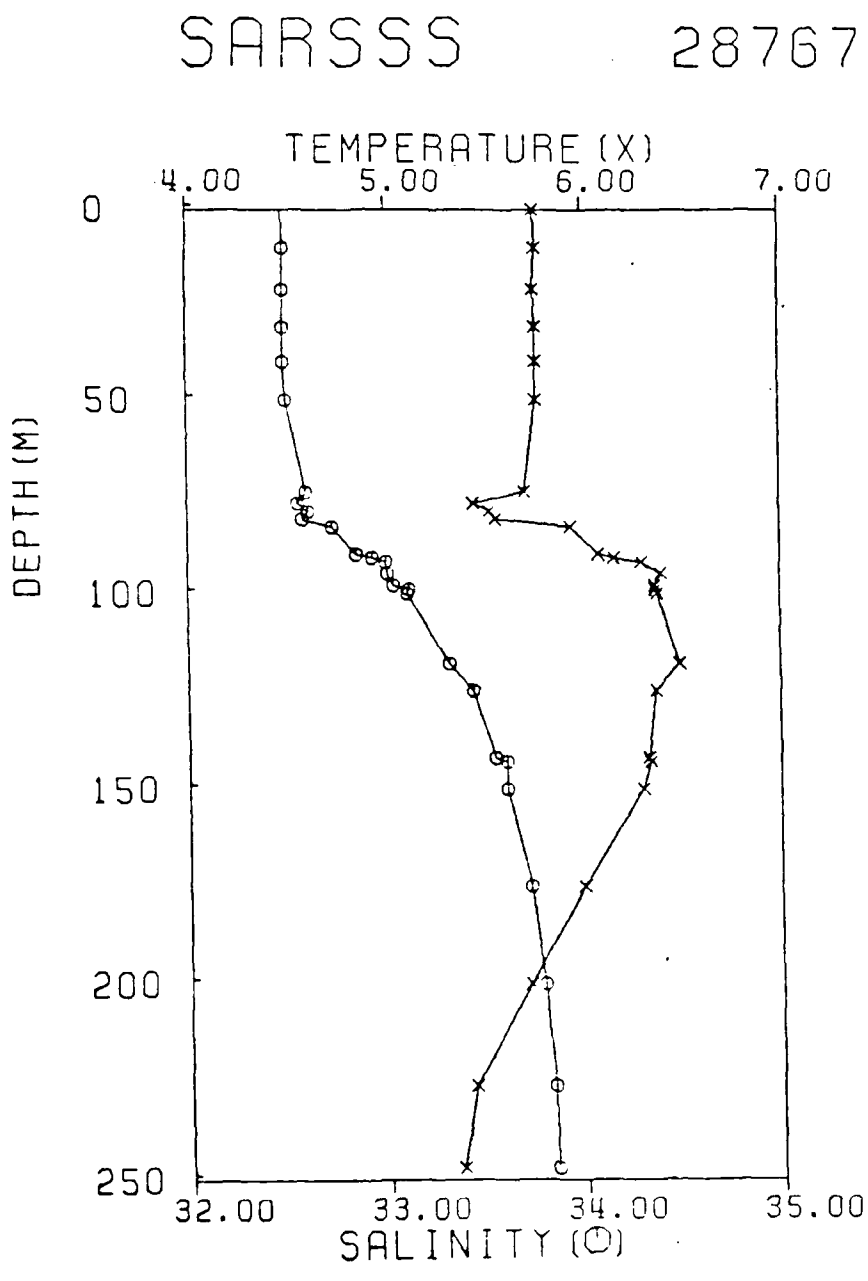

Figure A-18 Historical Profile #28767....1978 Day 32.

56°43'N 139°00'W

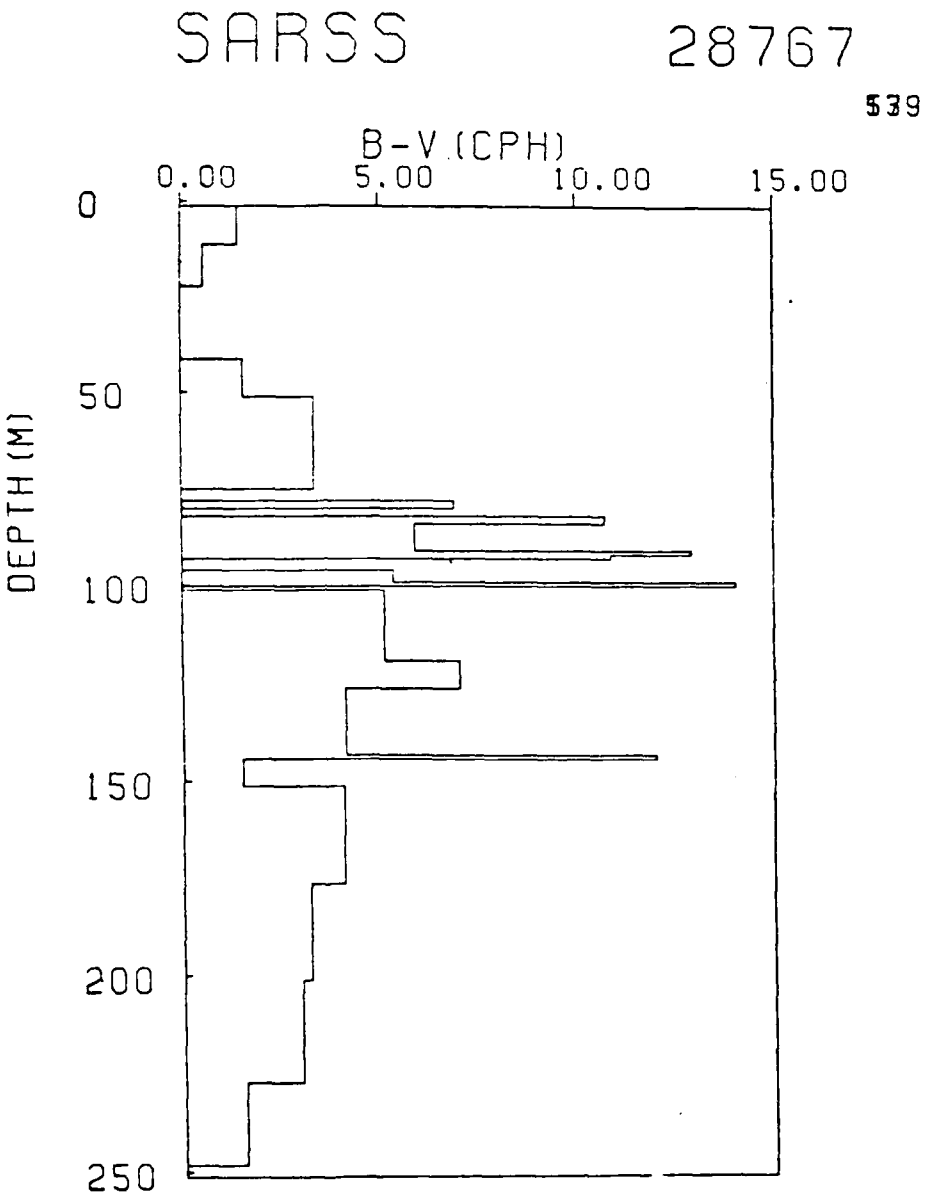

Figure A-19 B-V Profile for Figure A-18.

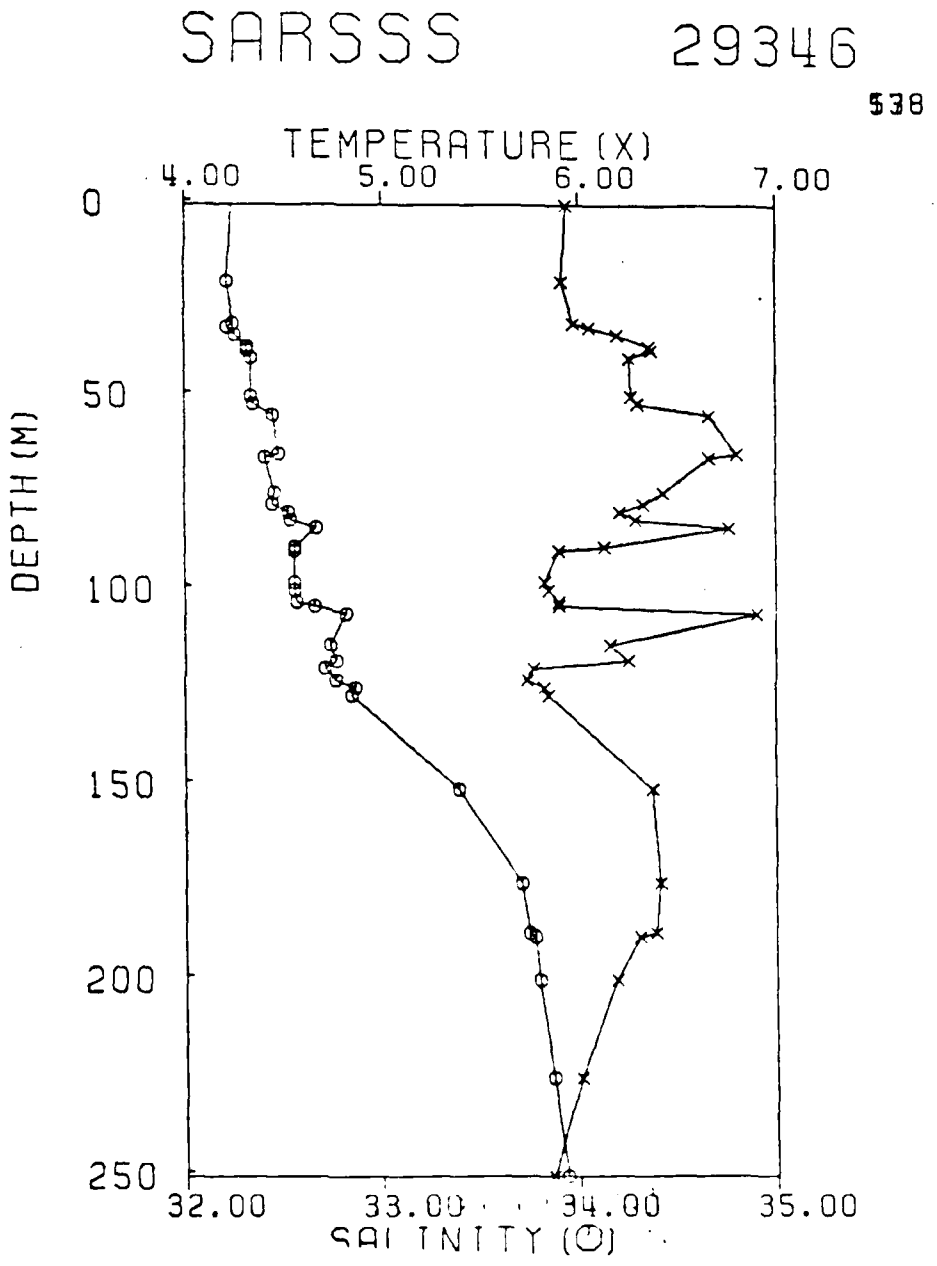

Figure A-20 Historical Profile #29346....1978 Day 32

57 4'N 137 53'W.

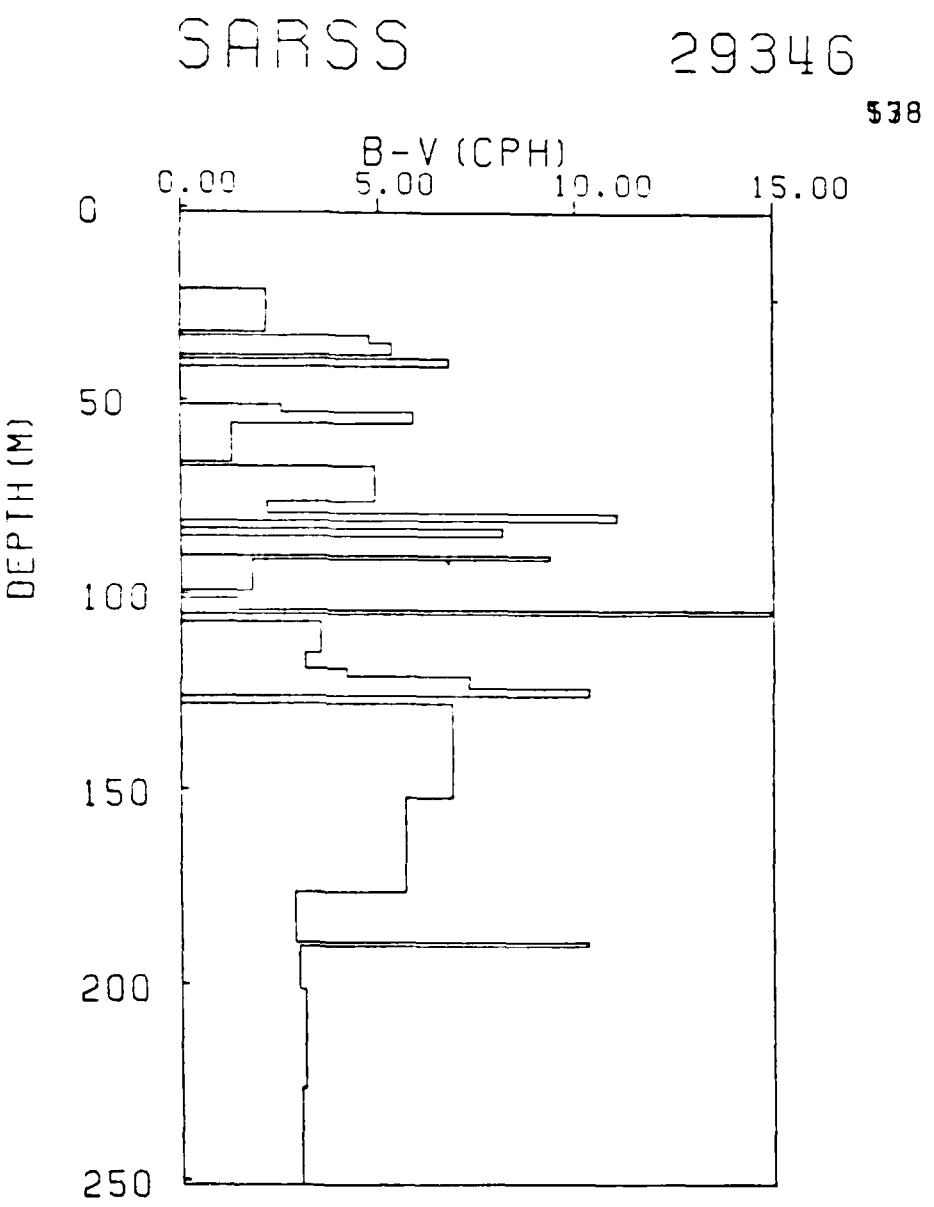

Figure A-21 B-V Profile for Figure A-20.

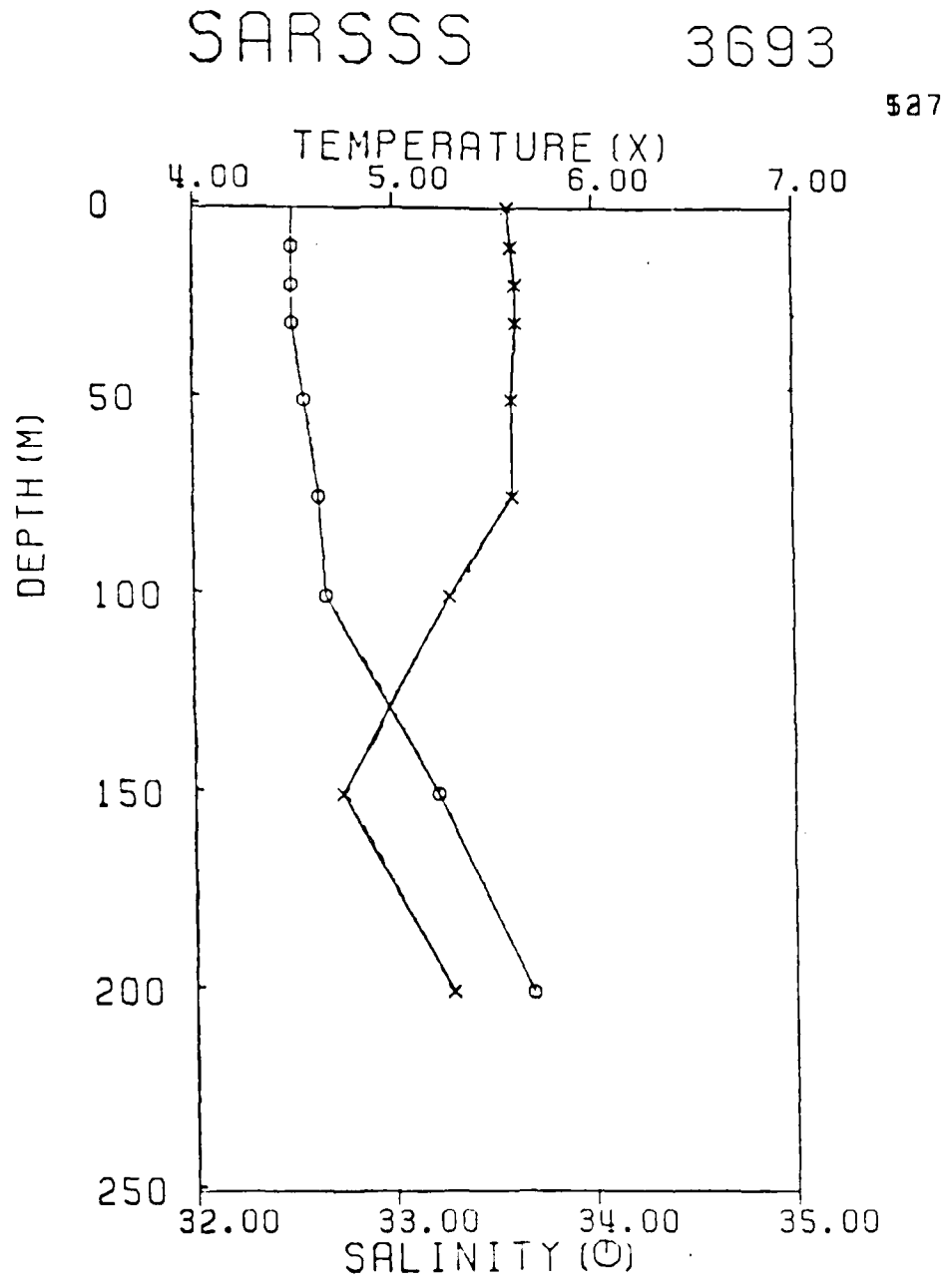

Figure A-22 Historical Profile #3693.....1973 Day 75

52°19'N 137°14'W.

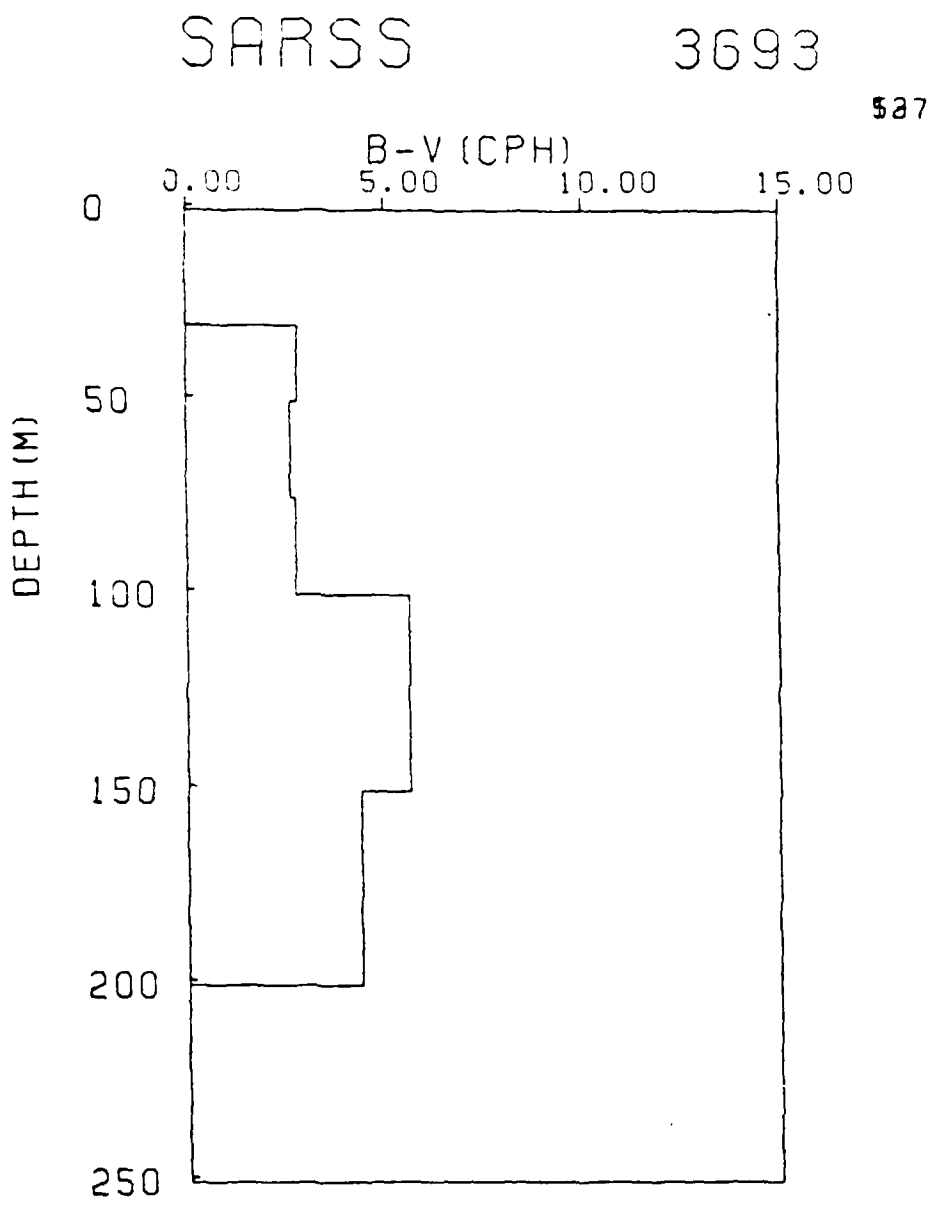

Figure A-23 B-V Profile for Figure A-22.

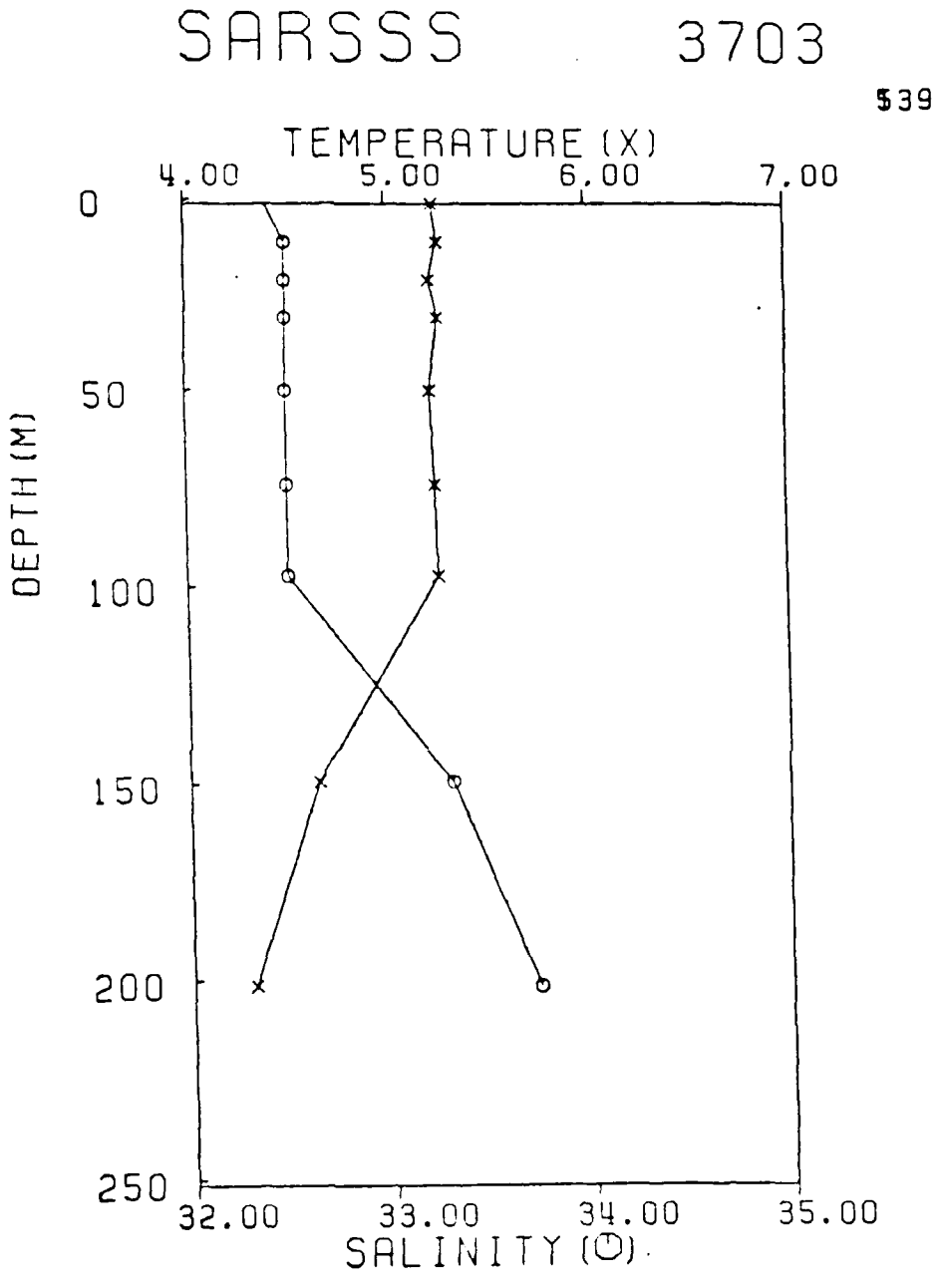

Figure A-24 Historical Profile #3703....1973 Day 75

52°30'N 138°52'W.

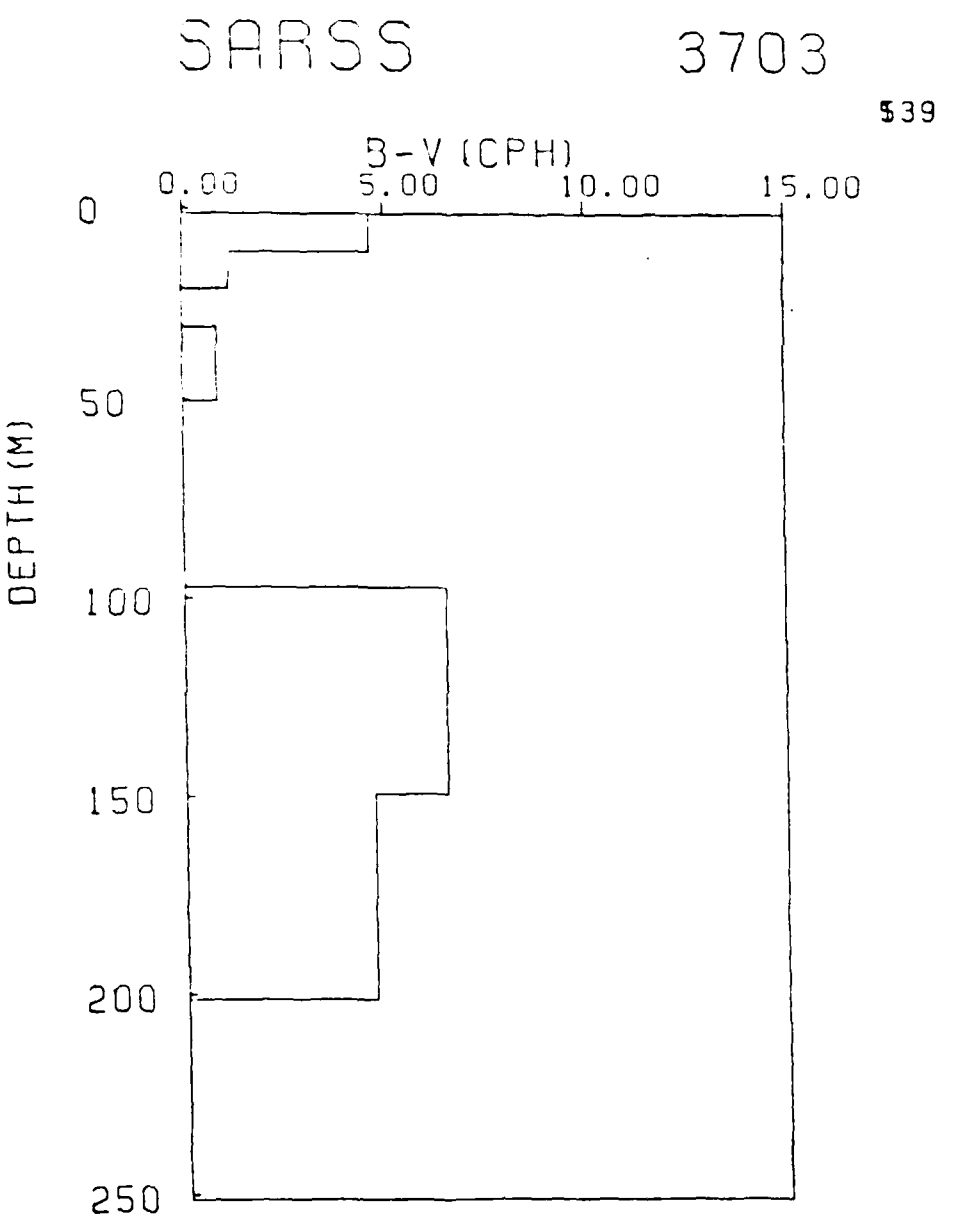

Figure A-25 B-V Profile for Figure A-24 .

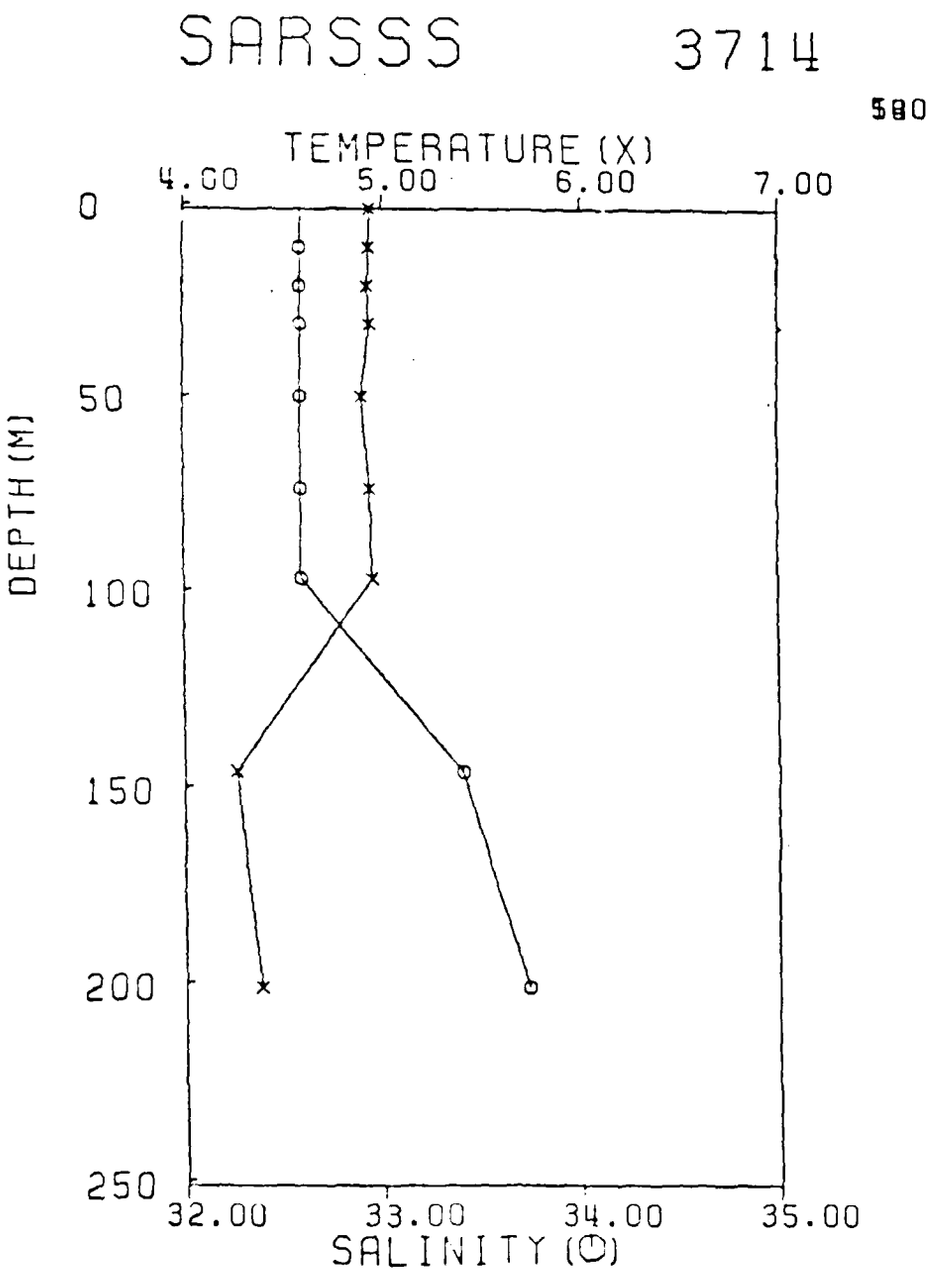

Figure A-26 Historical Profile #3714.....1973 Day 74

52°47'N 140°25'W.

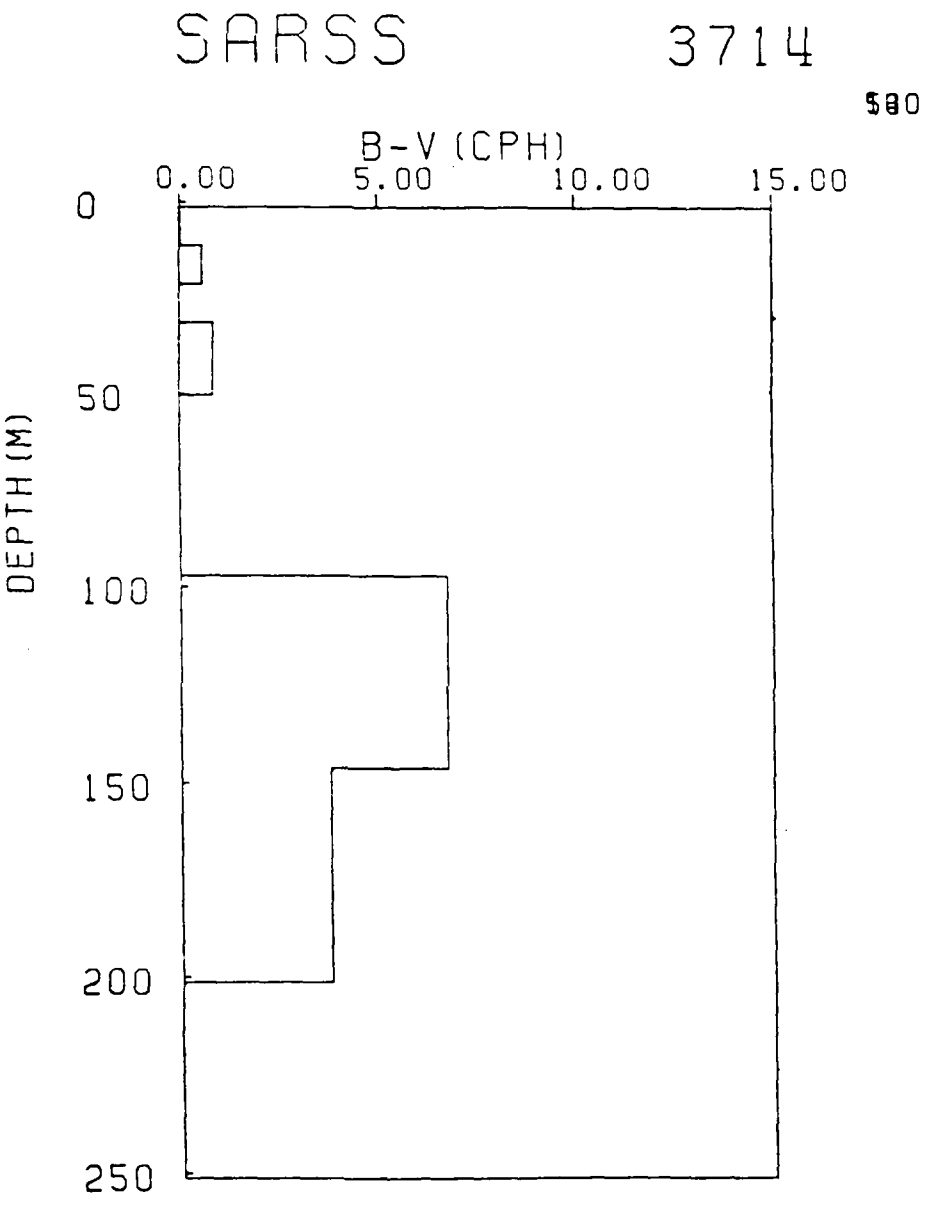

Figure A-27 B-V Profile for Figure A-26.

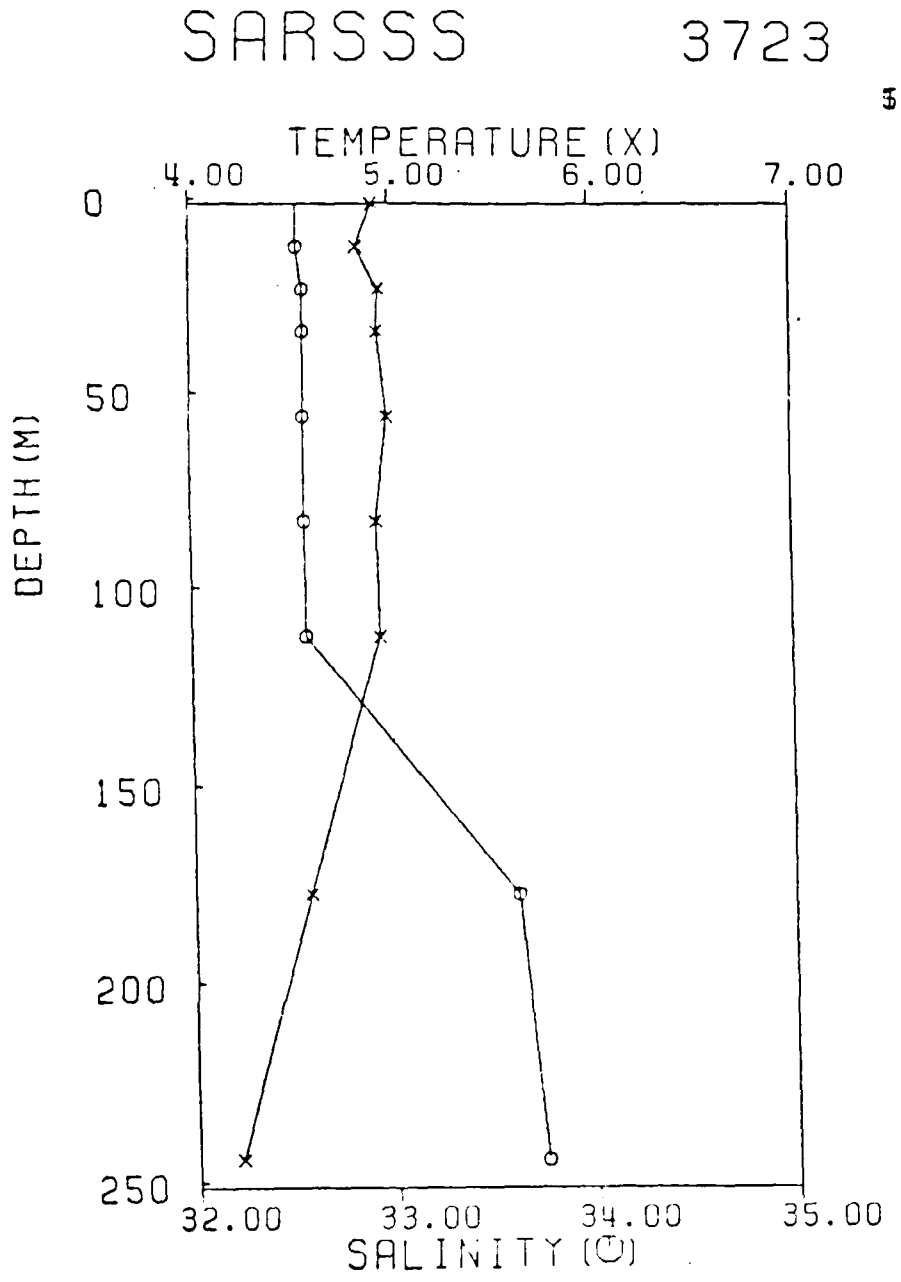

Figure A-28 Historical Profile #3723.....1973 Day 74

52°34'N 141°26'W.

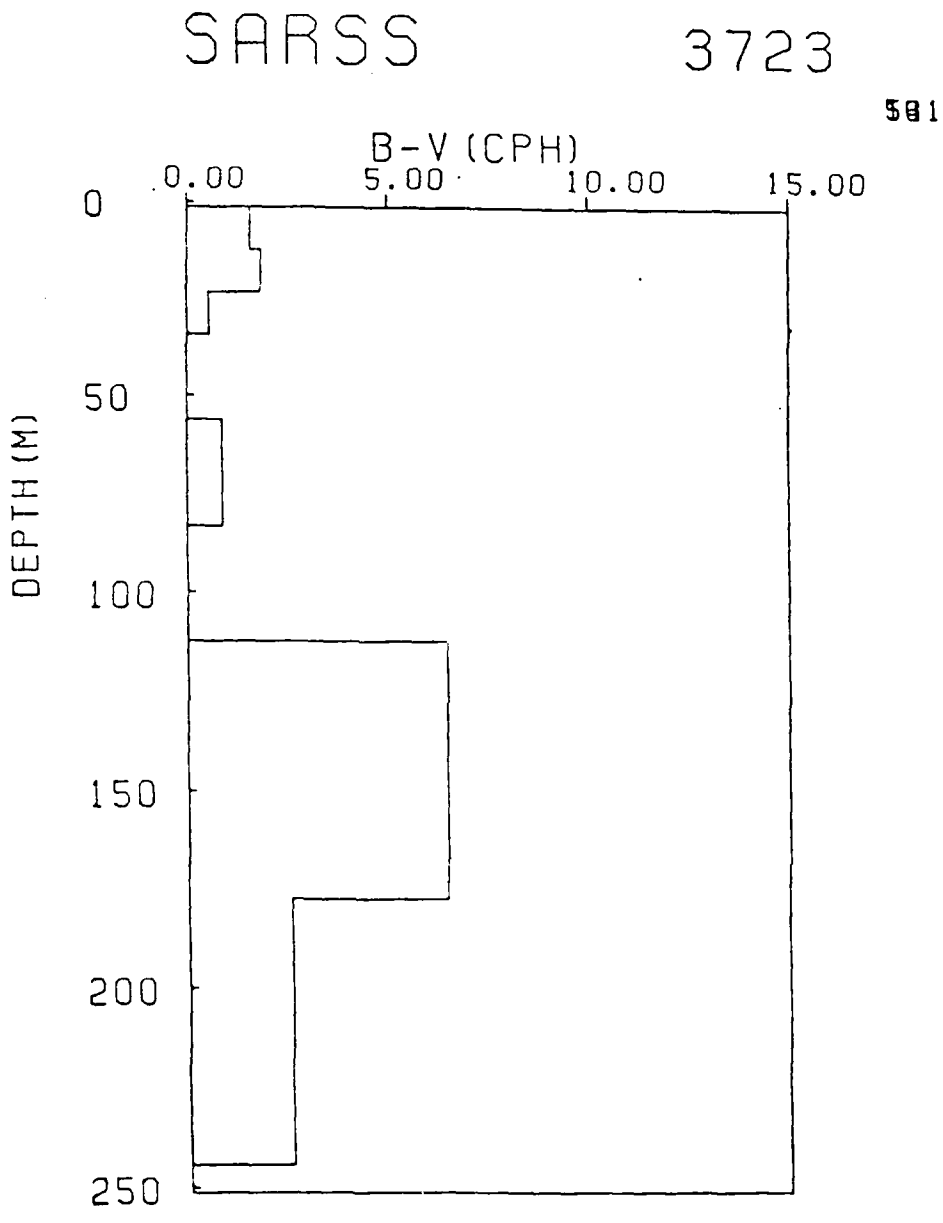

Figure A-29 B-V Profile for Figure A-28.

This package contains 6 representative profiles from the Gulf of Alaska for the month of March. Three different regions were selected, and two profiles from each region were extracted from the MOODS data base, one from the beginning of the month and one from near the middle or end of the month.

Region 1 - Ocean Weather Station "PAPA"

Profile Number	2324	2396
Latitude	50°N	50°N
Longitude	145°W	145°W
Year	1971	1971
Day	63	81

Region 2 - SW Portion of the Gulf of Alaska

Profile Number	3041	3035
Latitude	50°N	50°49'N
Longitude	157°W	155°W
Year	1975	1967
Day	60	72

Region 3 - Near Coastal Region 5 of Kodiak Island

Profile Number	4500	4966
Latitude	54°19'N	55°N
Longitude	152°W	155°W
Year	1970	1962
Day	65	78

For each profile, 3 pieces of information are provided. The first is a plot of the temperature and salinity profiles over the upper 250 meters. The second is a plot of Brunt-Vaisala frequency in cycles/hour over the upper 250 meters, calculated using first differences. The third item is a listing of the B-V values calculated over the upper 250 meters. Because of the large vertical spacing between data points (typically 20 to 25 meters), the peak B-V values are underestimated from these historical data. Sensitivity analyses have indicated actual peak B-V values are about 50% larger than the peak values shown here.

Regions 1 and 2 are both well-mixed down to around 100 m, and the peak stratification is caused by the halocline with B-V values in the 7-10 cph range. The peak B-V also tends to occur just below the mixed layer. In contrast, the near-coastal region 3 shows mixing only down to about 70 m, and the peak B-V appears to be lower than in the other regions further off shore.

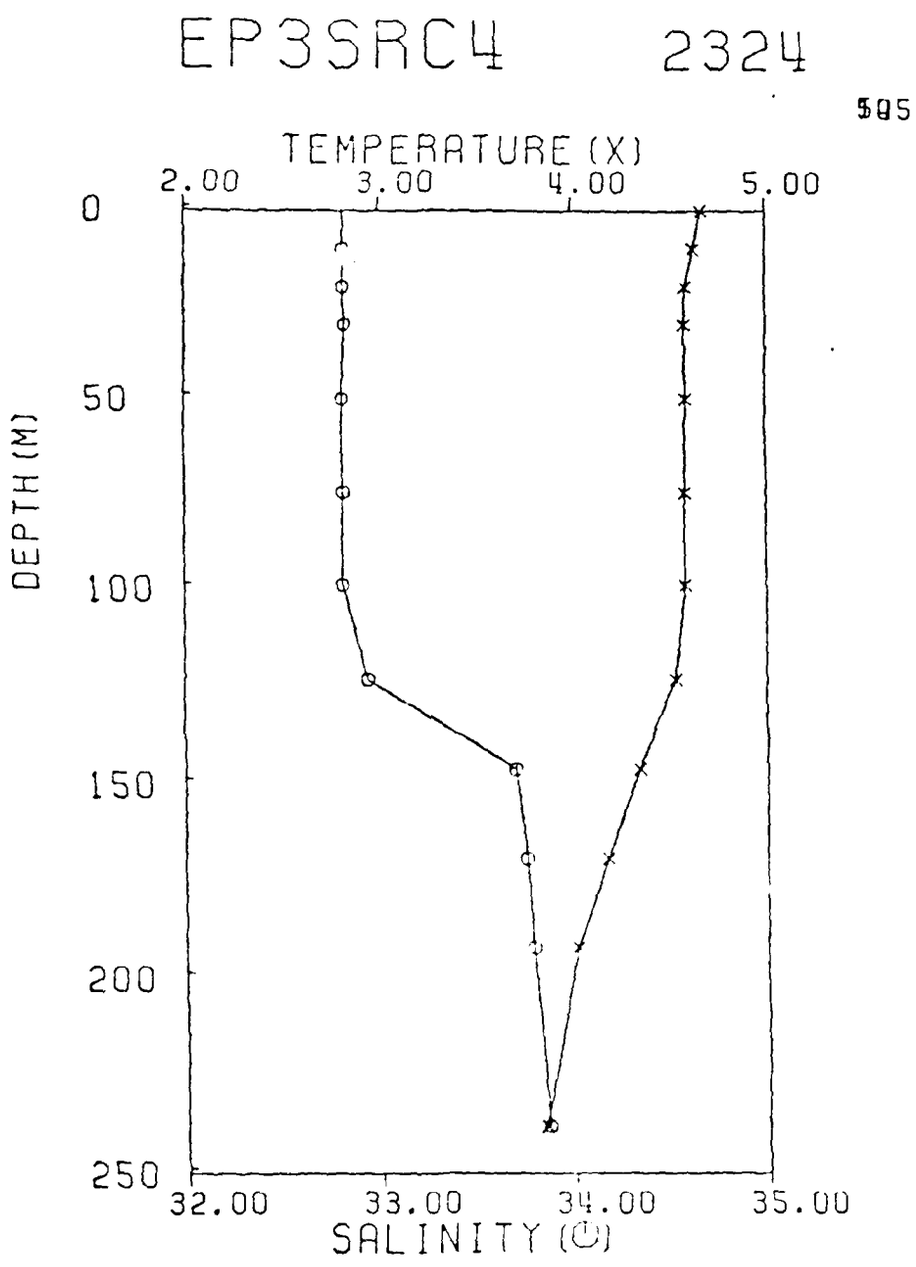
EP3SRC4 2324
595
TEMPERATURE (X)
2.00
3.00
4.00
5.00
0
50
100
150
200
250
DEPTH (M)
32.00
33.00
34.00
35.00
SALINITY (‰)

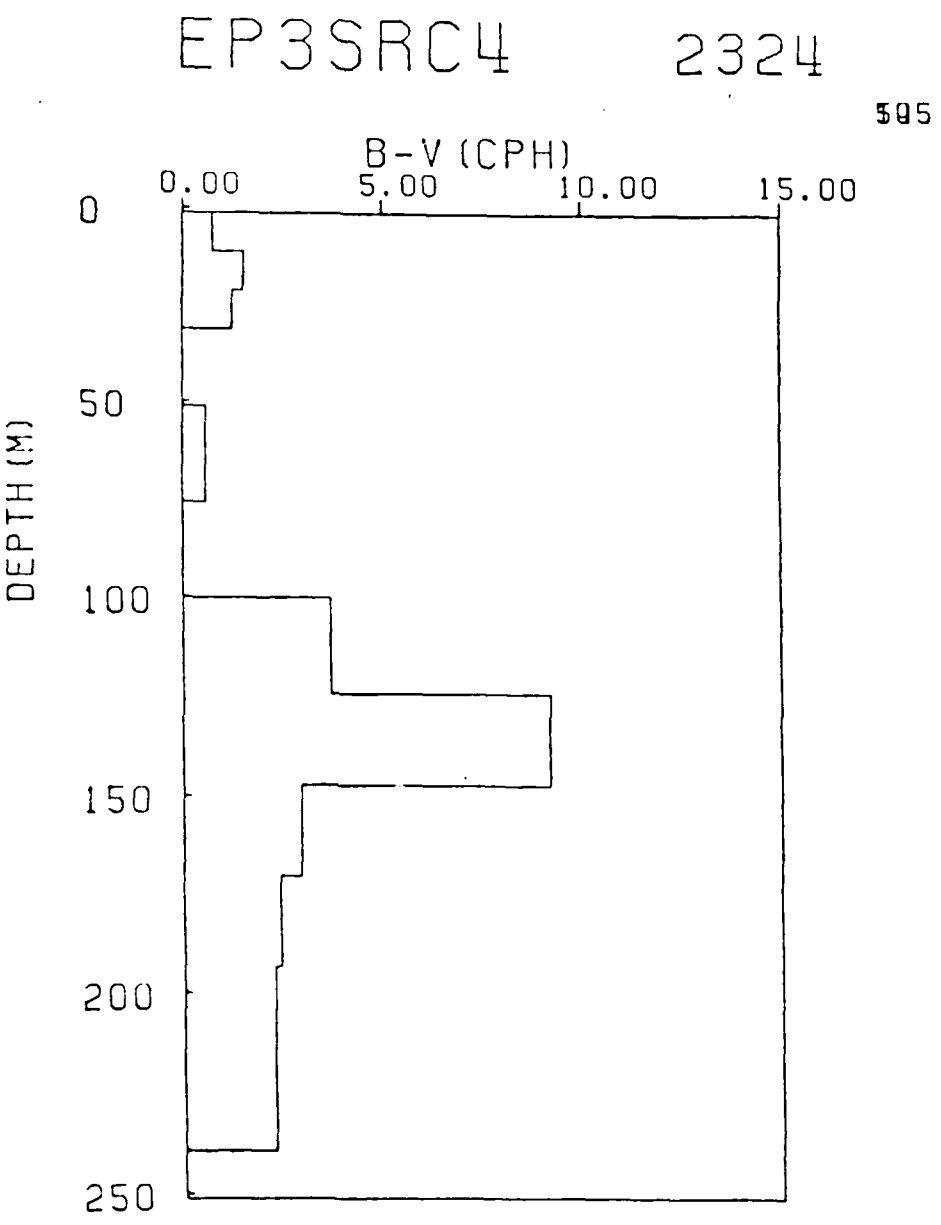
EP3SRC4 2324
505
B-V (CPH)
0.00
5.00
10.00
15.00
DEPTH (M)
0
50
100
150
200
250

BV VALUES IN CPH FOR PROFILE.. 2324

Region 1

DEPTH	BV
0.00	0.76
10.00	0.76
20.00	1.52
30.00	1.25
50.00	0.00
75.00	0.57
99.00	0.00
123.00	3.70
146.00	9.21
169.00	2.95
192.00	2.42
238.00	2.27
284.00	0.00
376.00	0.00
474.00	0.00
579.00	0.00
779.00	0.00
977.00	0.00
1176.00	0.00
1476.00	0.00
1979.00	0.00
2484.00	0.00
2991.00	0.00
3497.00	0.00
4001.00	0.00

Region 1

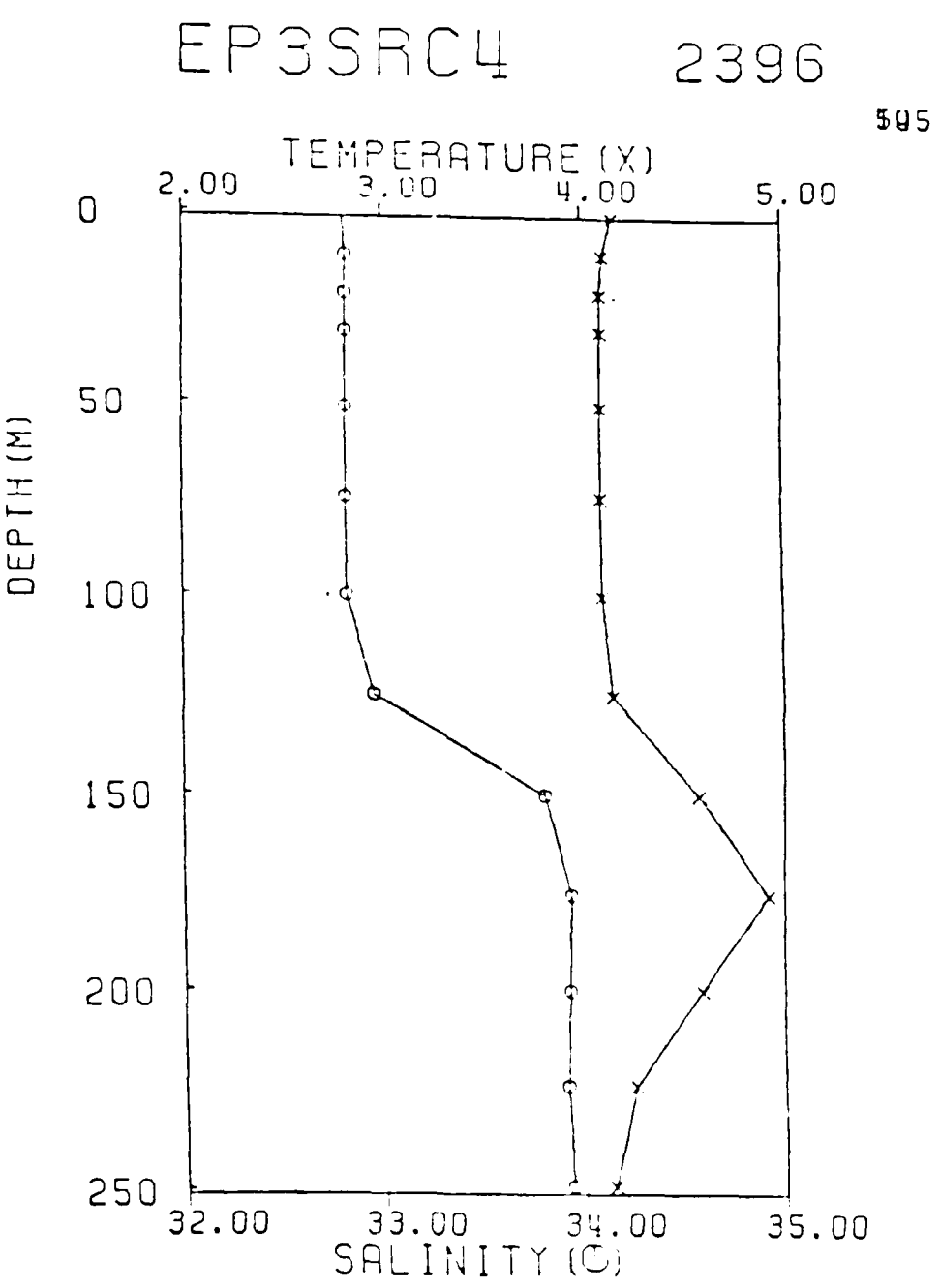
EP3SRC4 2396
595
TEMPERATURE (X)
2.00
3.00
4.00
5.00
0
50
100
150
200
250
DEPTH (M)
32.00
33.00
34.00
35.00
SALINITY (C)

Region 1

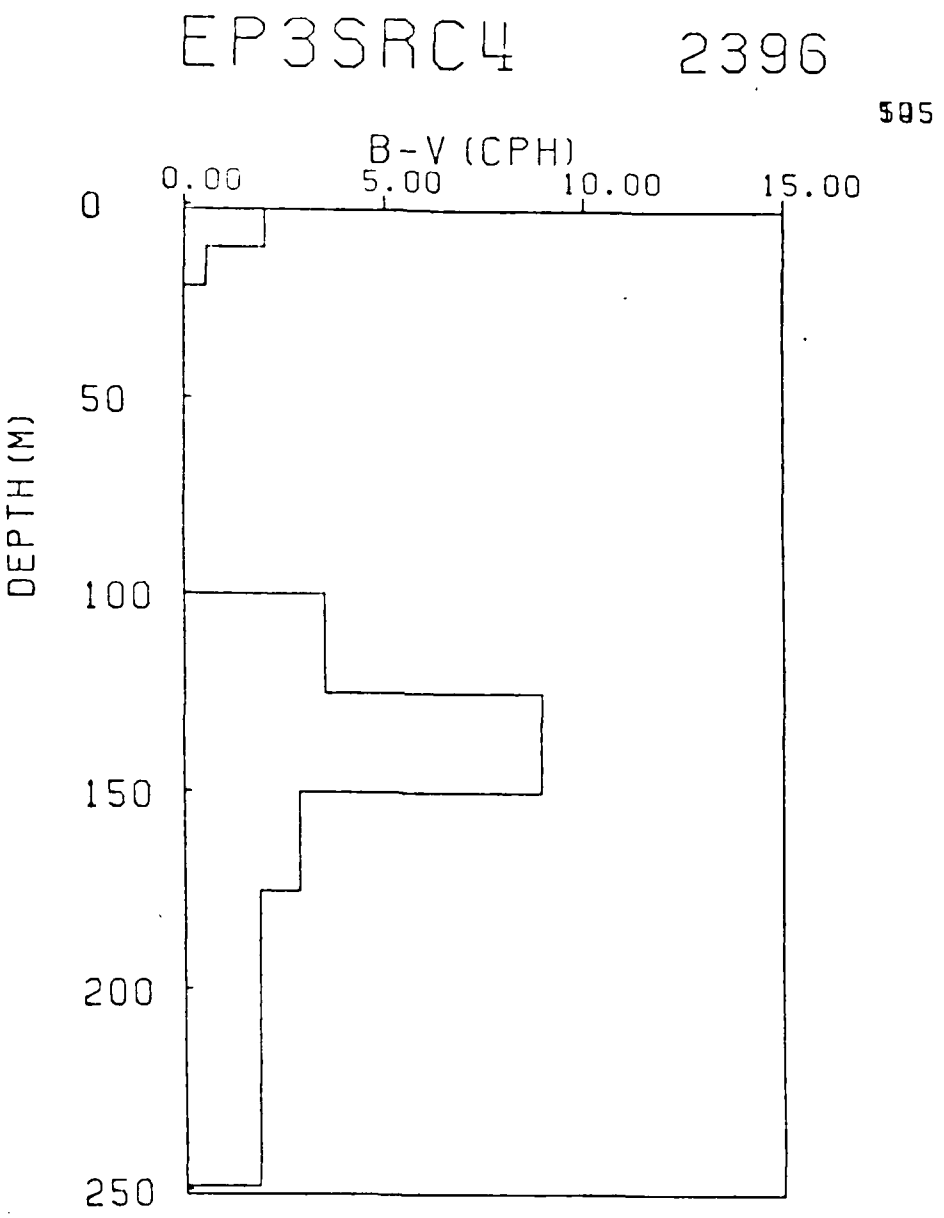
EP3SRC4 2396
595
B-V (CPH)
0.00
5.00
10.00
15.00
0
50
100
150
200
250
DEPTH (M)

BV VALUES IN CPH FOR PROFILE.. 2396

Region 1

DEPTH	BV
Ø.ØØ	2.Ø1
1Ø.ØØ	2.Ø1
2Ø.ØØ	Ø.56
3Ø.ØØ	Ø.ØØ
5Ø.ØØ	Ø.ØØ
74.ØØ	Ø.ØØ
99.ØØ	Ø.ØØ
124.ØØ	3.51
149.ØØ	8.94
174.ØØ	2.87
199.ØØ	1.88
223.ØØ	1.87
248.ØØ	1.85
298.ØØ	Ø.ØØ
397.ØØ	Ø.ØØ
496.ØØ	Ø.ØØ
595.ØØ	Ø.ØØ
793.ØØ	Ø.ØØ
99Ø.ØØ	Ø.ØØ
1188.ØØ	Ø.ØØ
1483.ØØ	Ø.ØØ

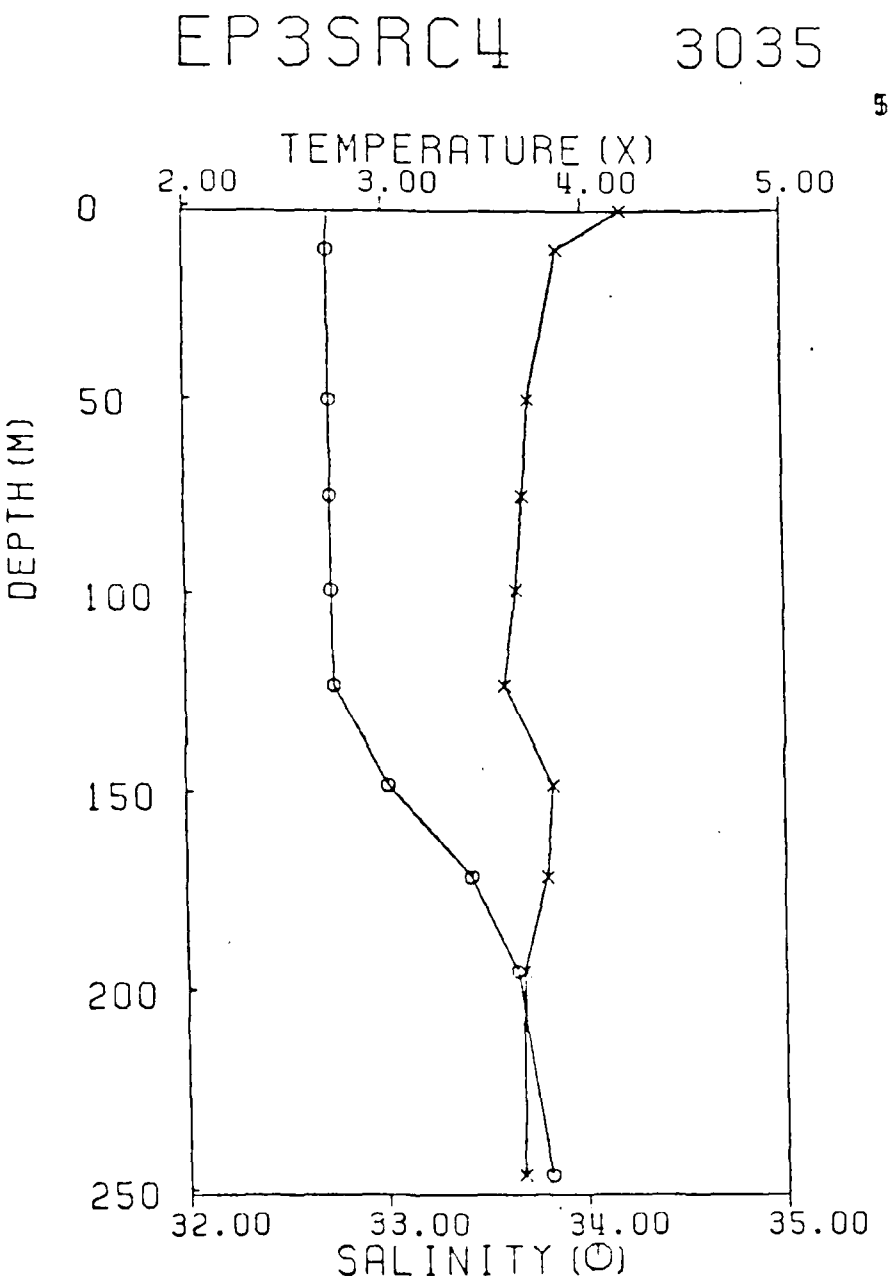
EP3SRC4 3035
555
TEMPERATURE (X)
2.00
3.00
4.00
5.00
0
50
100
150
200
250
DEPTH (M)
32.00
33.00
34.00
35.00
SALINITY (‰)

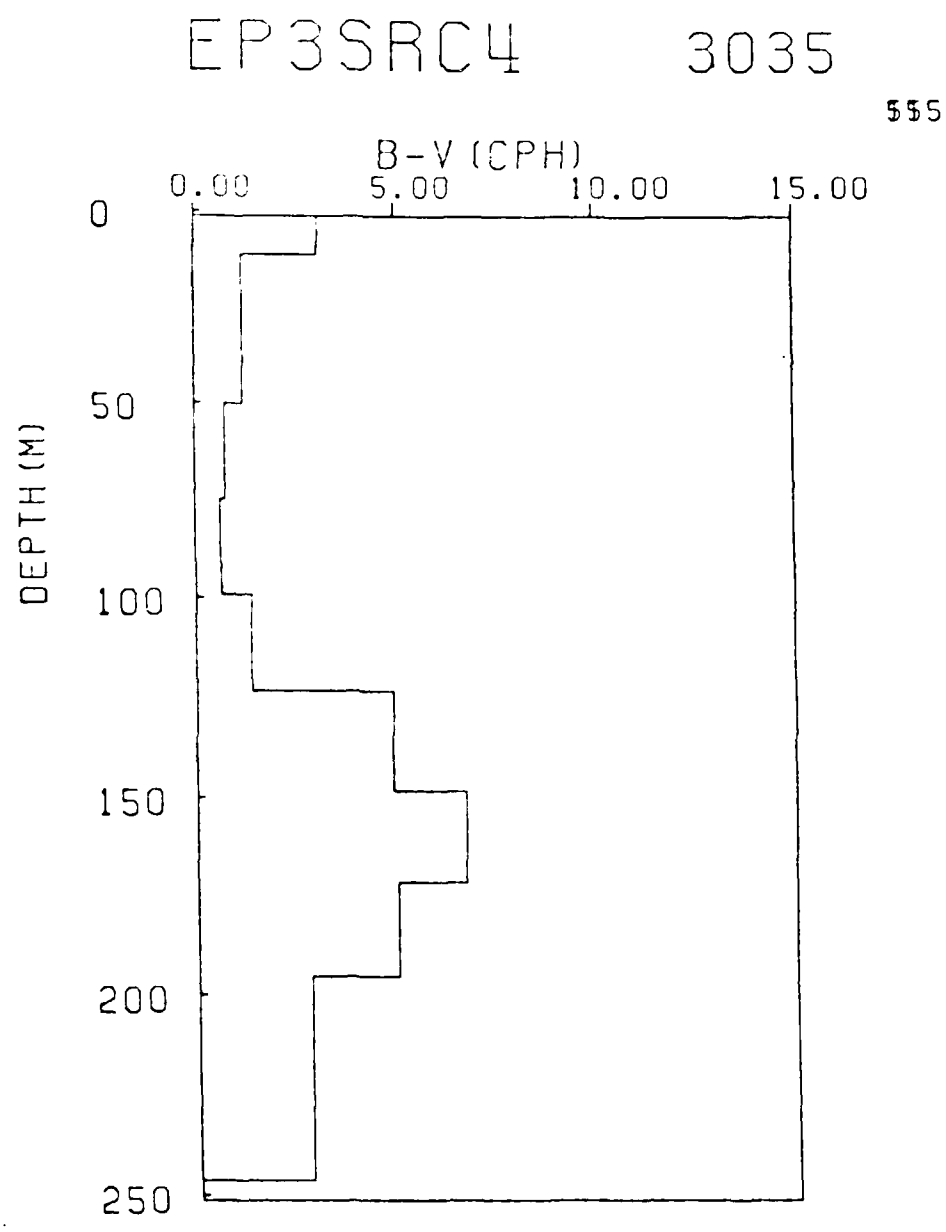
EP3SRC4 3035
$$5
B-V (CPH)
0.00
5.00
10.00
15.00
0
50
100
150
200
250
DEPTH (M)

BV VALUES IN CPM FOR PROFILE.. 3035

Region 2

DEPTH	BV
0.00	3.09
10.00	3.09
49.00	1.21
74.00	0.74
98.00	0.62
122.00	1.37
147.32	4.90
170.00	6.73
194.00	5.01
245.00	2.82
294.00	0.00
392.00	0.00
492.00	0.00

Region 2

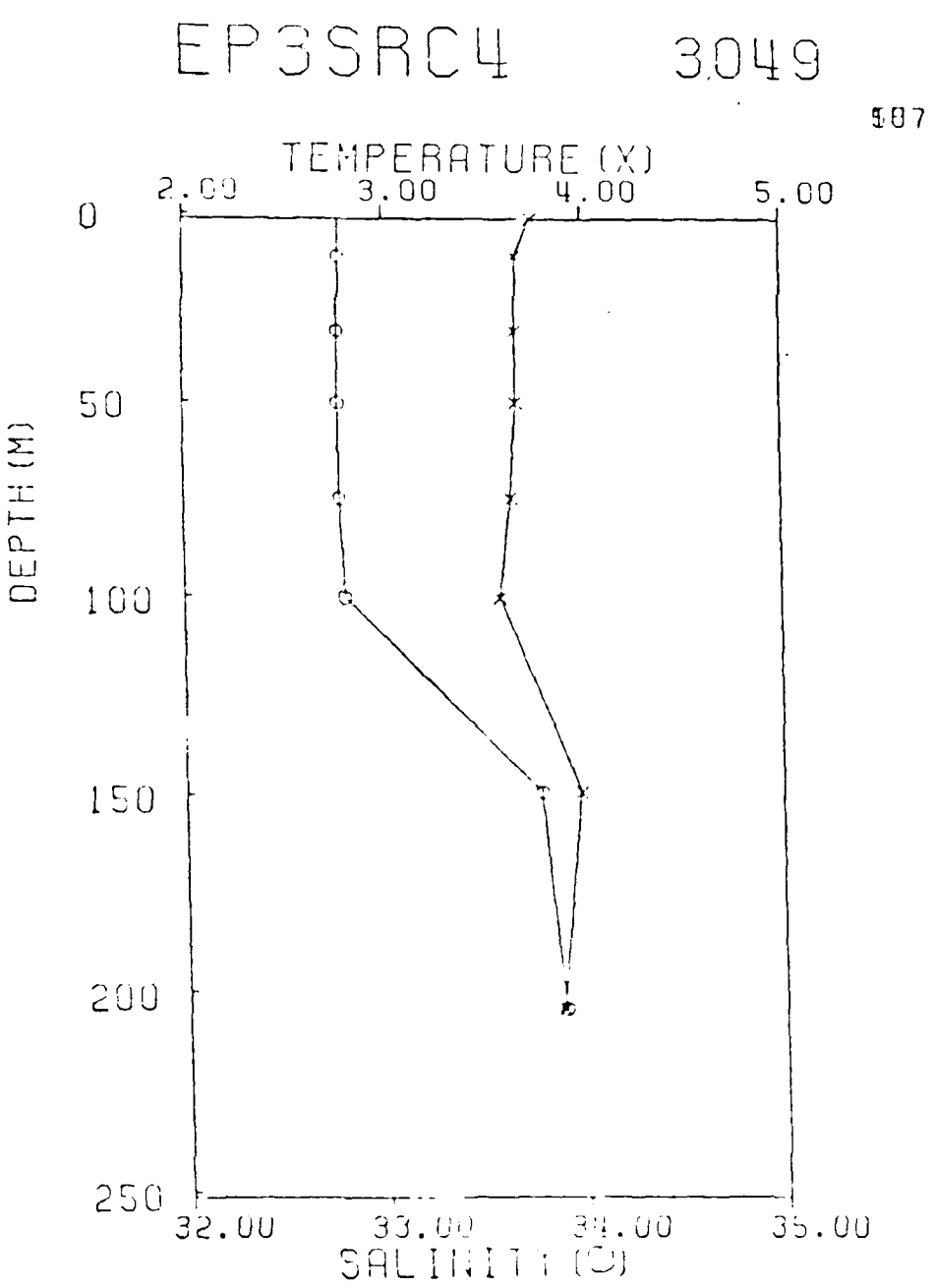
EP3SRC4 3049
TEMPERATURE (X)
2.00
3.00
4.00
5.00
0
50
100
150
200
250
DEPTH (M)
32.00
33.00
34.00
35.00
SALINITY (O/

Region 2

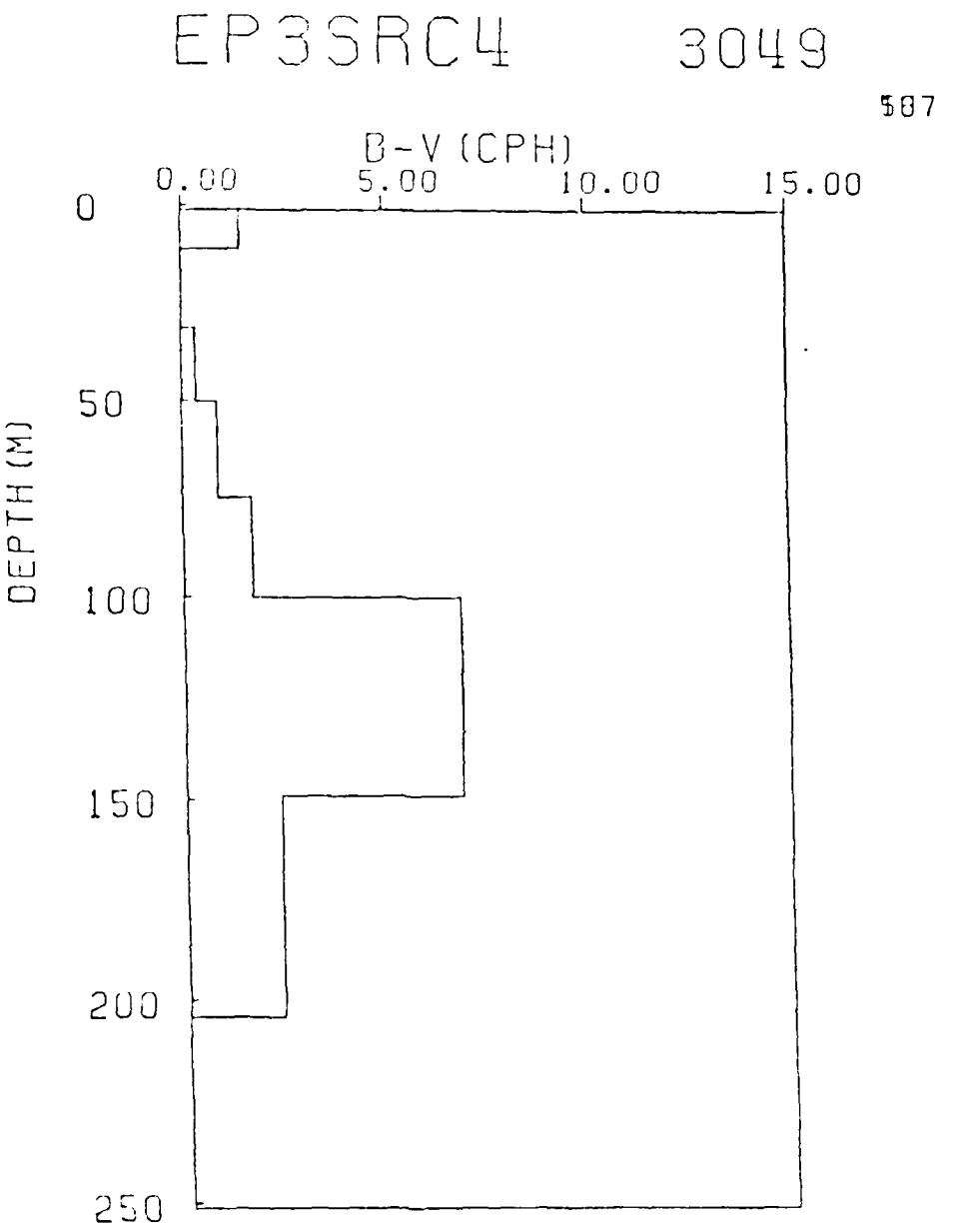
EP3SRC4 3049
$87
B-V (CPH)
0.00
5.00
10.00
15.00
0
50
100
150
200
250
DEPTH (M)

BV VALUES IN CPH FOR PROFILE.. 3049

Region 2

DEPTH	BV
0.00	1.45
10.00	1.45
30.00	0.00
49.00	0.36
74.00	0.86
99.00	1.70
148.00	6.87
200.00	2.35
300.00	0.00
400.00	0.00
500.00	0.00
600.00	0.00
1000.00	0.00
1512.00	0.00

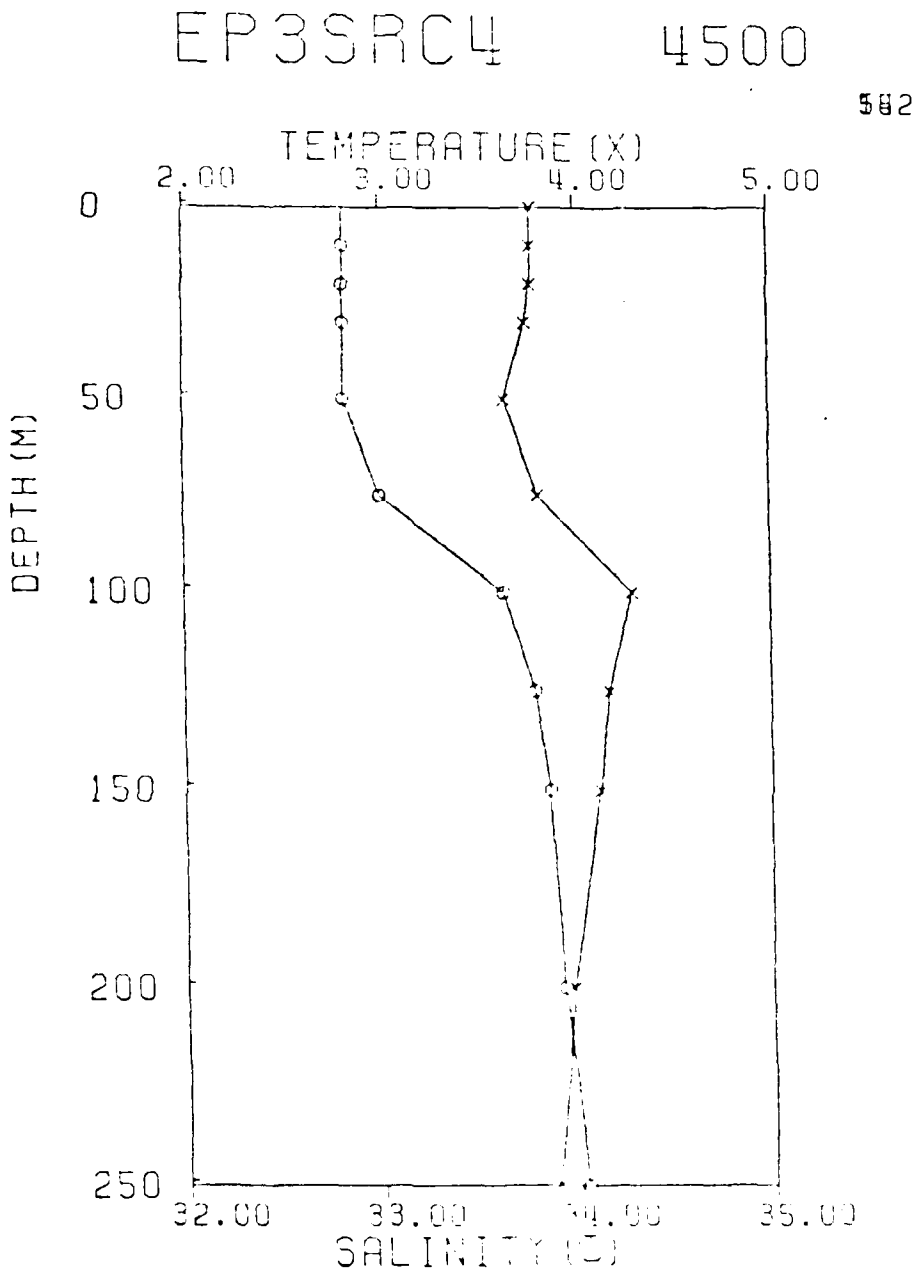
EP3SRC4 4500
TEMPERATURE (X)
2.00
3.00
4.00
5.00
0
50
100
150
200
250
DEPTH (M)
32.00
33.00
35.00
SALINITY (S)

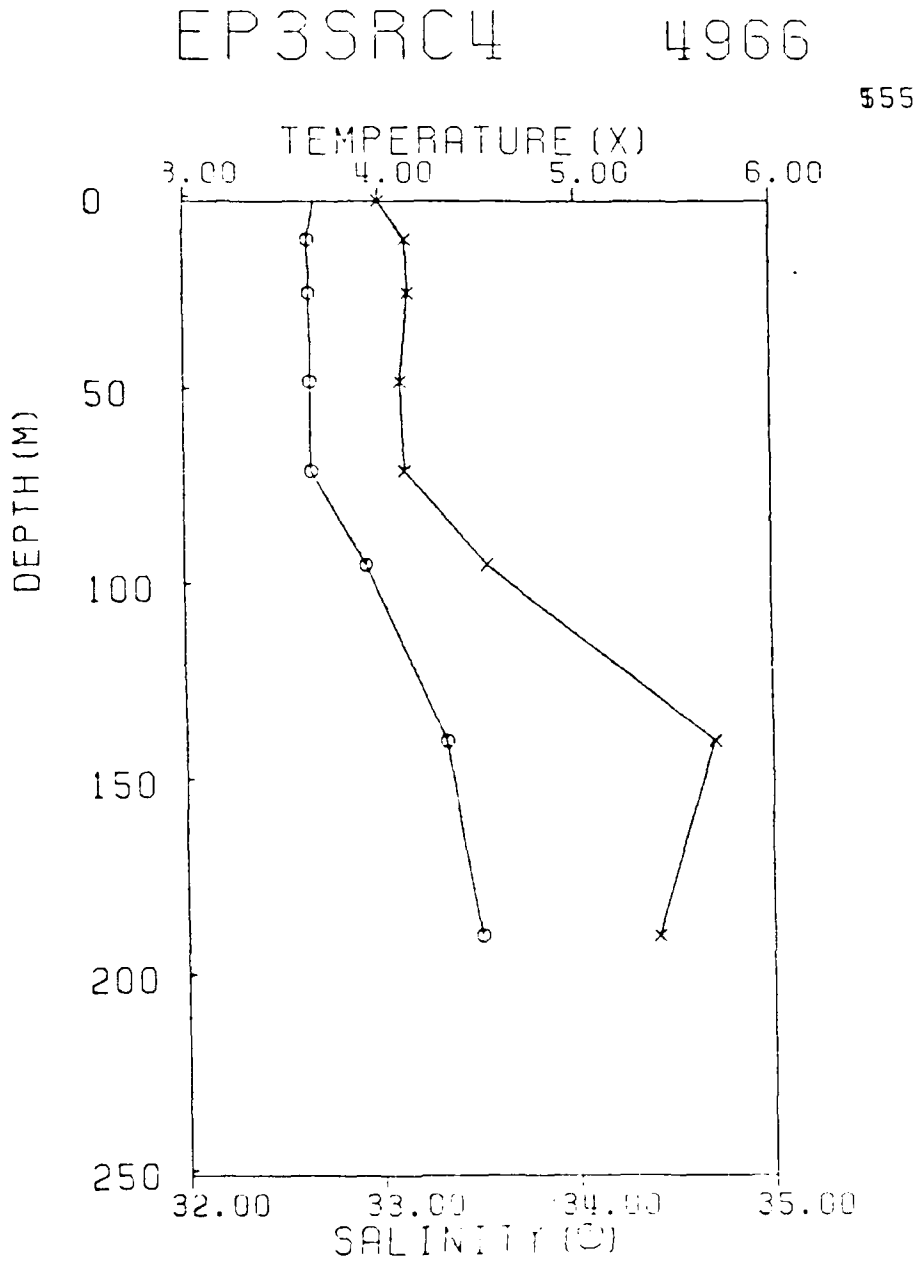
EP3SRC4 4966
$55
TEMPERATURE (X)
3.00
4.00
5.00
6.00
0
50
100
150
200
250
DEPTH (M)
32.00
33.00
34.00
35.00
SALINITY (‰)

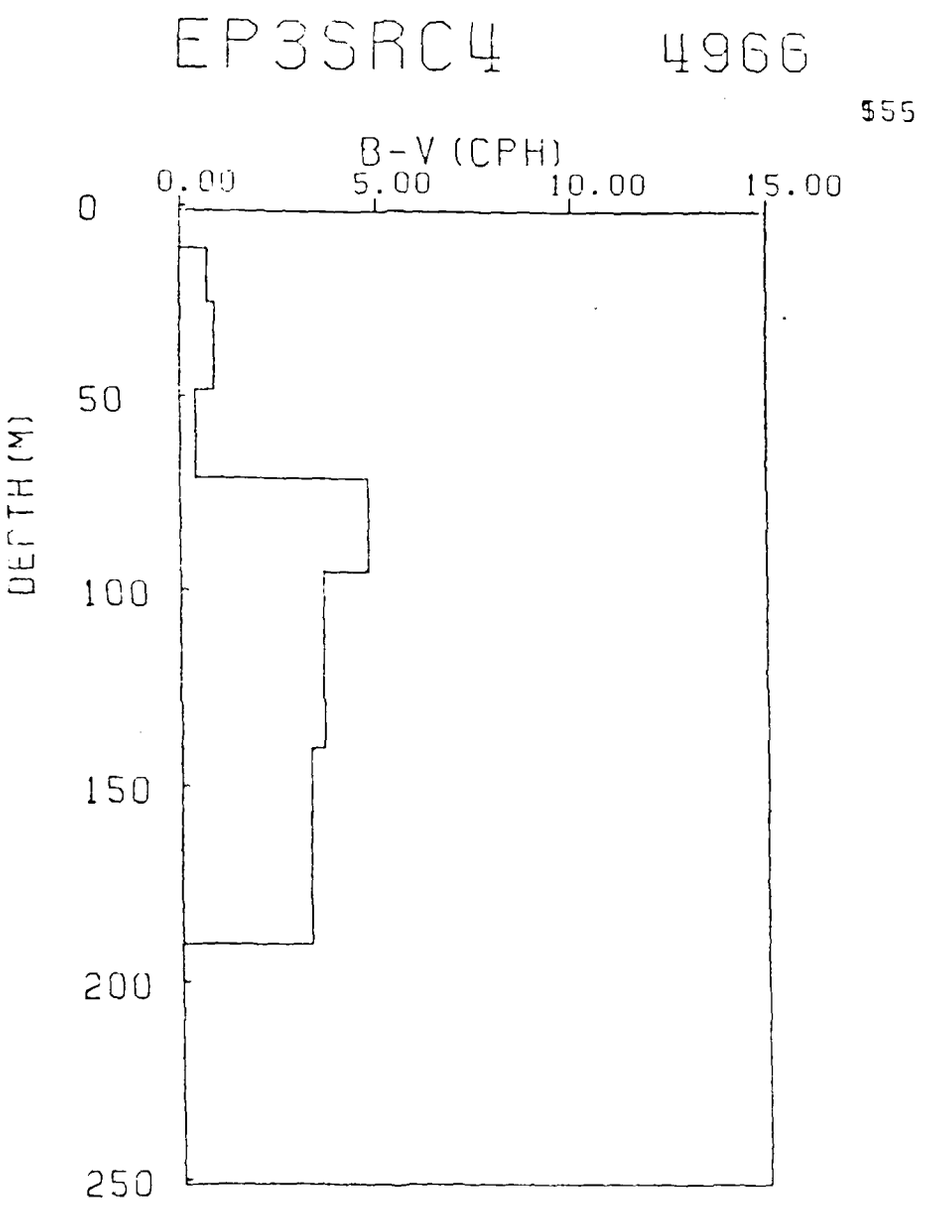
EP3SRC4 4966
$55
B-V (CPH)
0.00
5.00
10.00
15.00
0
50
100
150
200
250
DEPTH (M)

BV VALUES IN CPH FOR PROFILE.. 4966

Region 3

DEPTH	BV
0.00	0.00
10.00	0.00
24.00	0.70
47.00	0.87
70.00	0.41
94.00	4.81
139.00	3.64
189.00	3.29
284.00	0.00
378.00	0.00
473.00	0.00
568.00	0.00
756.00	0.00
1043.00	0.00

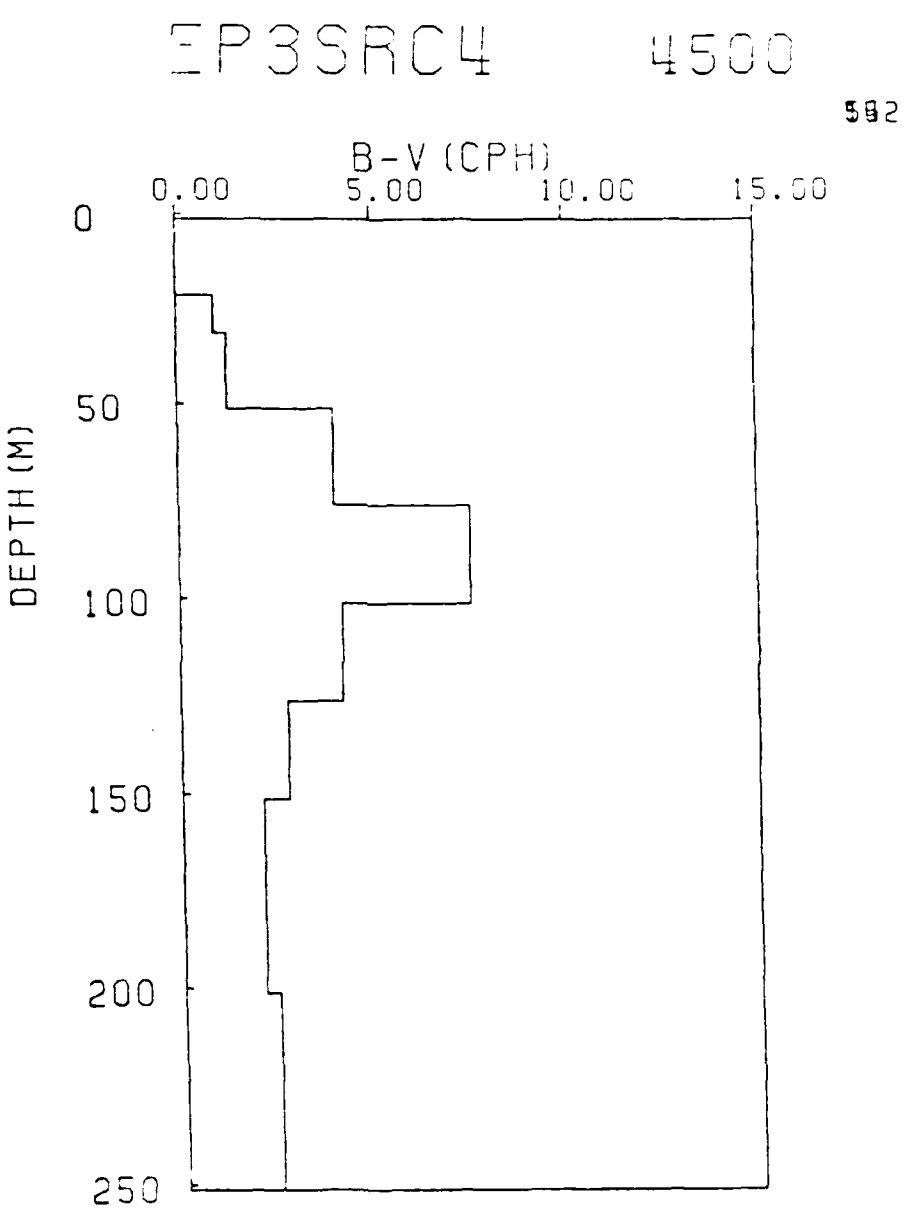
EP3SRC4 4500
582
B-V (CPH)
0.00
5.00
10.00
15.00
0
50
100
150
200
250
DEPTH (M)

BV VALUES IN CPH FOR PROFILE.. 4500

Region 3

DEPTH	BV
0.00	0.00
10.00	0.00
20.00	0.00
30.00	0.94
50.00	1.27
75.00	3.99
100.00	7.53
125.00	4.18
150.00	2.76
200.00	2.09
250.00	2.46
300.00	0.00
400.00	0.00
500.00	0.00
600.00	0.00
700.00	0.00
800.00	0.00
1000.00	0.00
1200.00	0.00
1500.00	0.00

APPENDIX B

NASA: CV-990 Aircraft Data and Optical Images from the Gulf of Alaska Experiment

The NASA: CV-990 executed five missions in support of the Gulf of Alaska experiment, as indicated in Table 6. In this note, detailed flight patterns and aircraft data from three typical missions are presented in order of increasing sea states. Also optically processed images obtained from all five flights are presented. The optical images have been reduced in scale to fit this report. They are included for completeness to give the reader the full scope of available images They are not intended for use in following analyses. For the latter, contact prints of the actual images will be made available by the author upon request. All digitally processed images are presented in Chapter III.

1. Sea State 1: 13 March 1984

The flight track for the mission executed on 13 March 1984 is shown in Figure B-1. The aircraft data recorded continuously during the flight are indicated below:

1. Pressure altitude in feet
2. Radar altitude in feet
3. True aircraft air speed in knots
4. True aircraft heading
5. Aircraft roll in degrees
6. Aircraft ground speed in knots
7. Wind speed at altitude in knots
8. Wind direction at altitude in °T
9. IR surface temperature in °C
10. Static air temperature in °C
11. Dew point temperature in °C

The above data are shown in Figure B2 for the flight on 13 March 1984.

The optical SAR images for all ship passes recorded during this mission are shown in Figure B3.

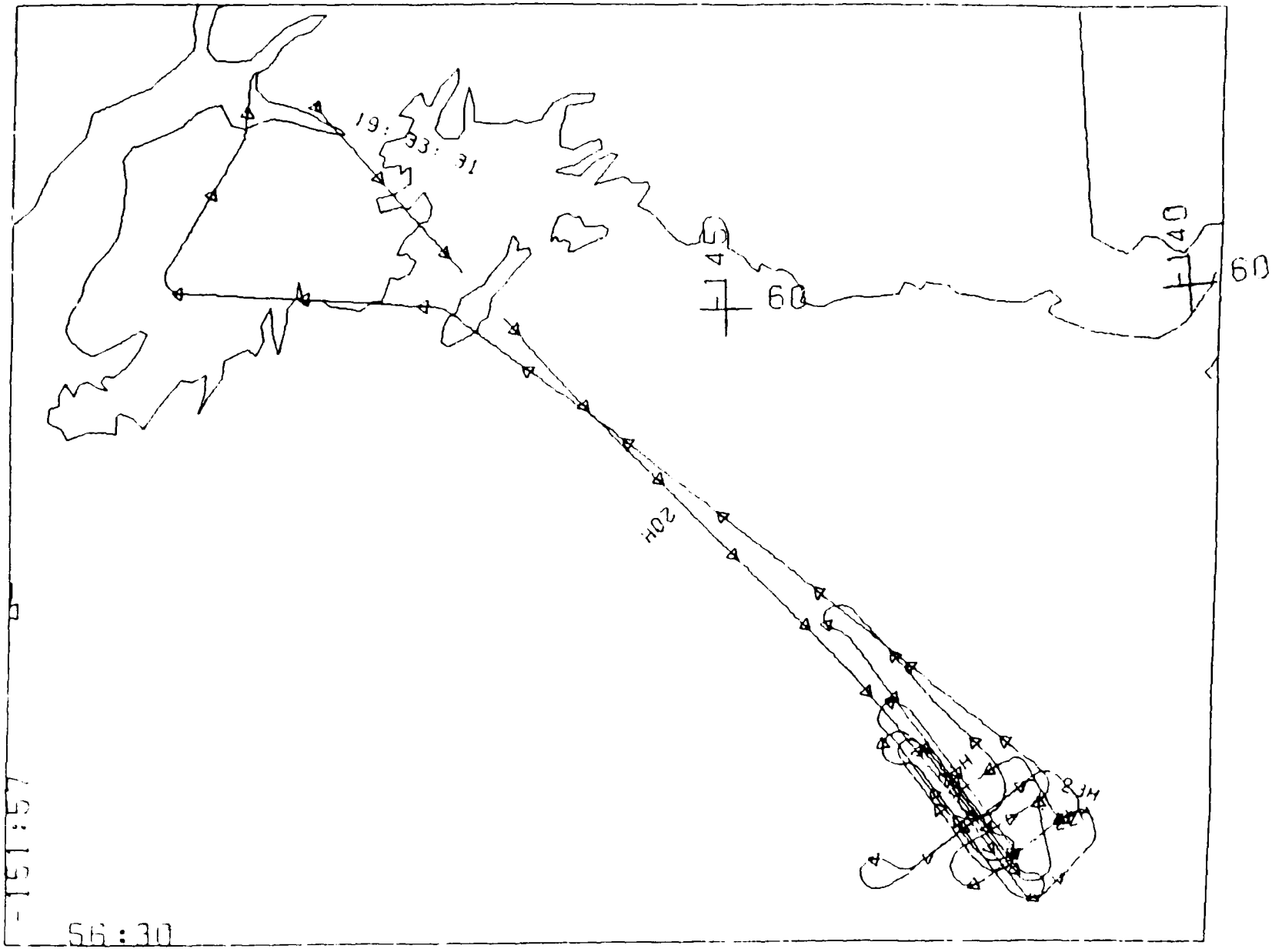

Figure B1. CV-990 Flight Track on 13 March 1984 Including Pattern Over Bay Ridge, Sea State 1. Time Tics Every 5 Min. Anchorage Local Time.

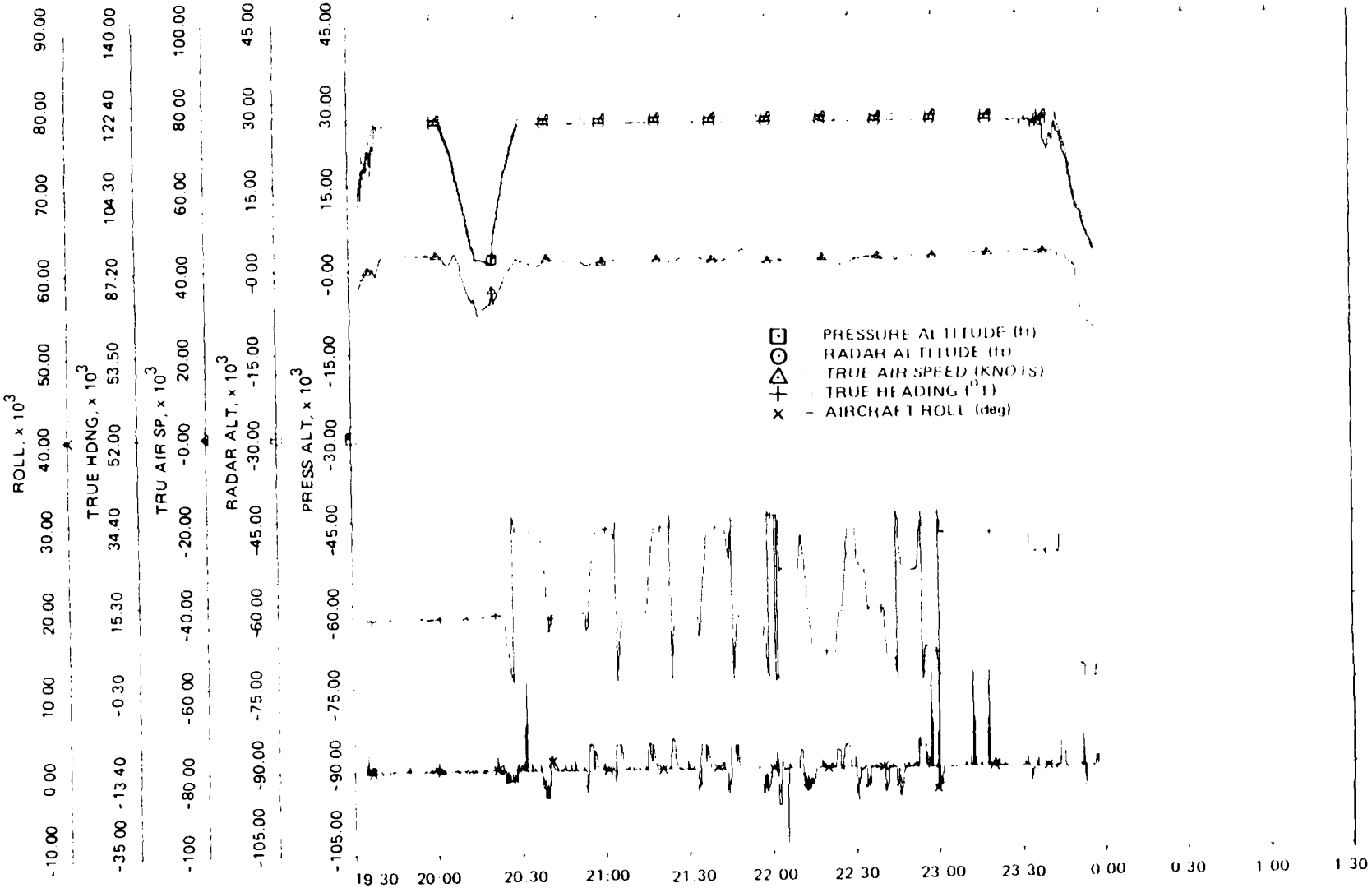

Figure B2. CV-990 Aircraft Data During Flight on 13 March 1984 Over Bay Ridge, Sea State 1.

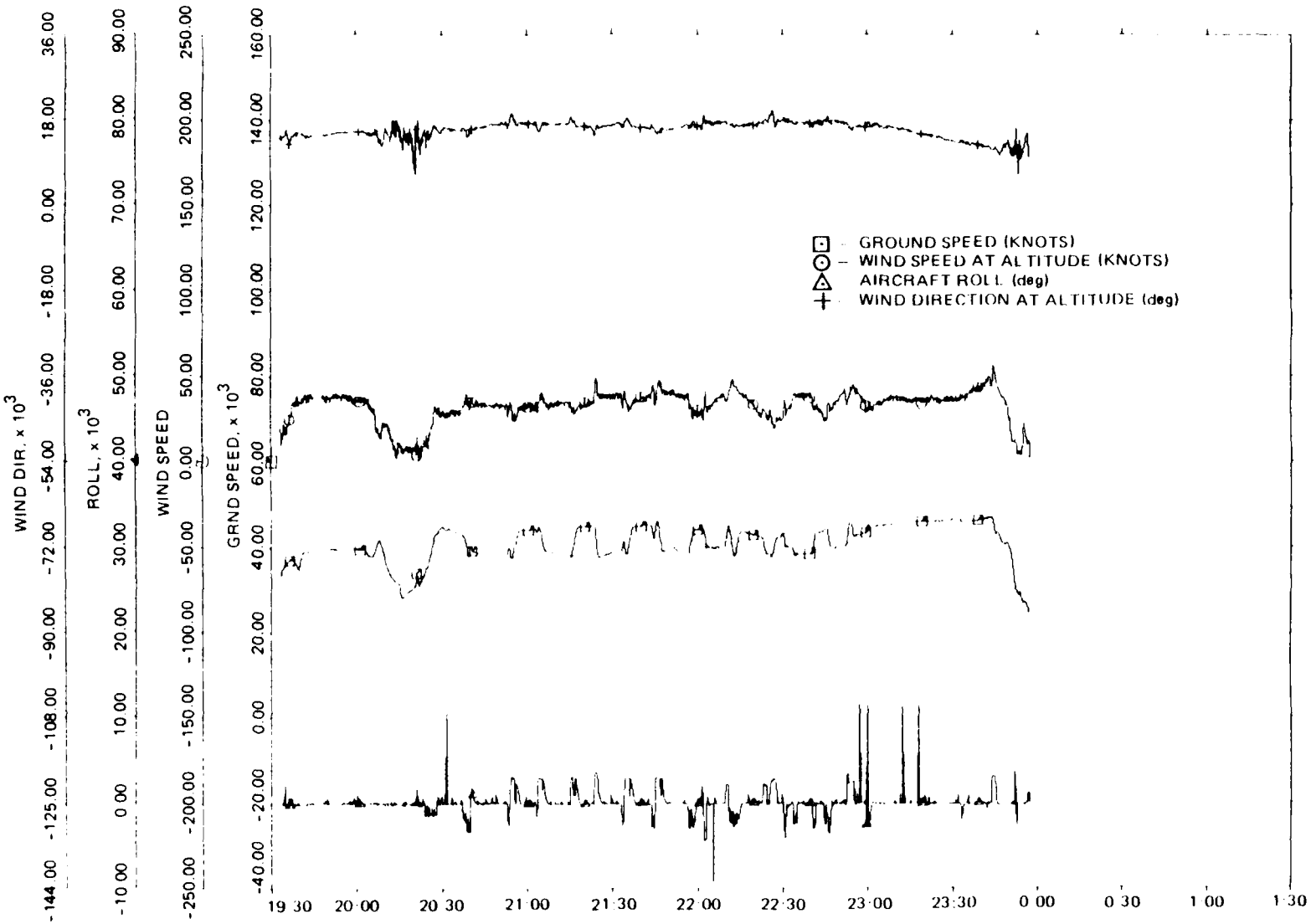

Figure B2(cont'd). C-130 Aircraft Data During Flight on 13 March 1985 Over Bay Ridge, Sea State 1 (Cont'd).

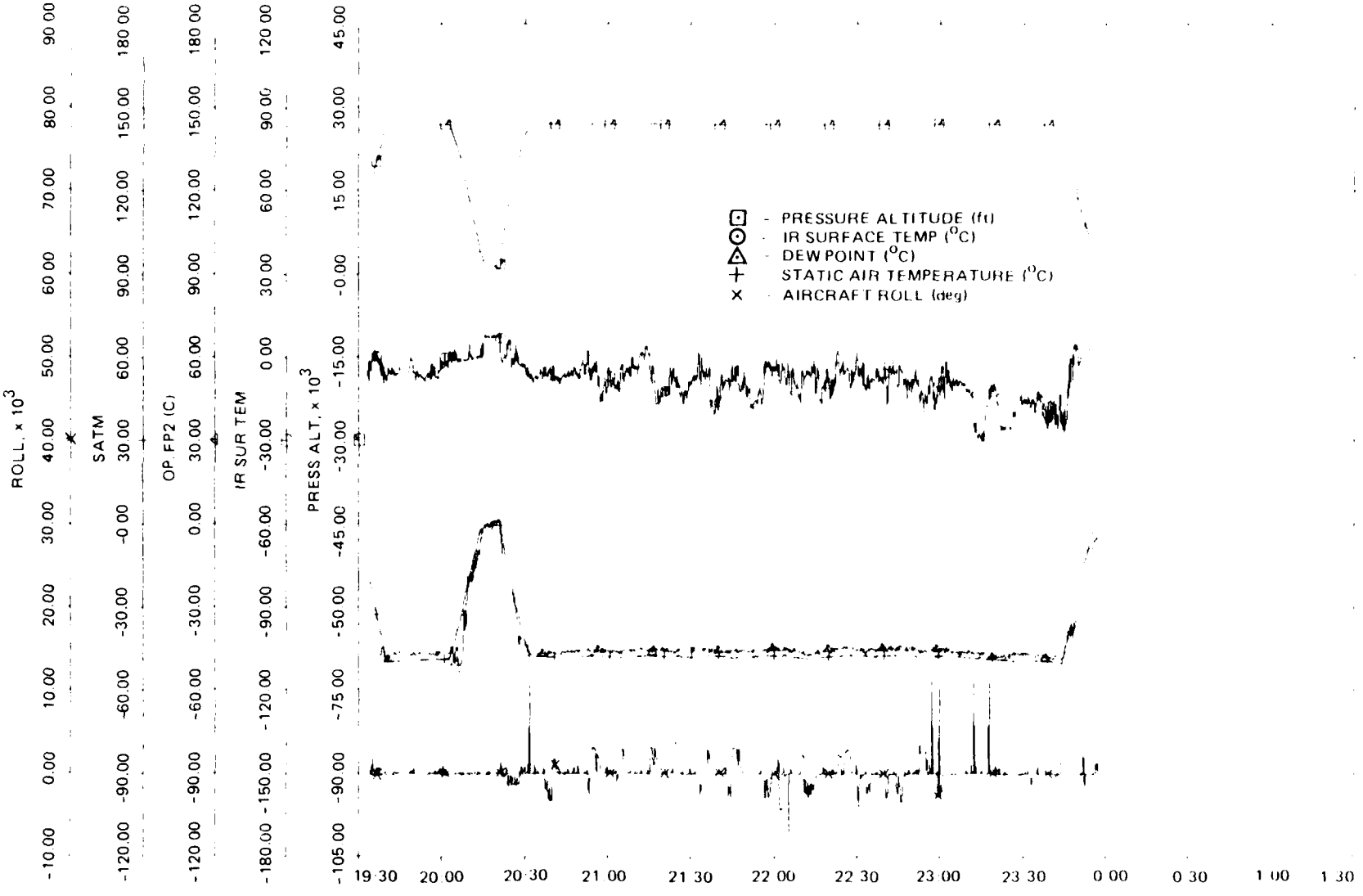

Figure B.2(b). CV-990 Aircraft Data During Flight on 13 March 1985 Over Bar Ridge, Sea State 1 (Cont'd).

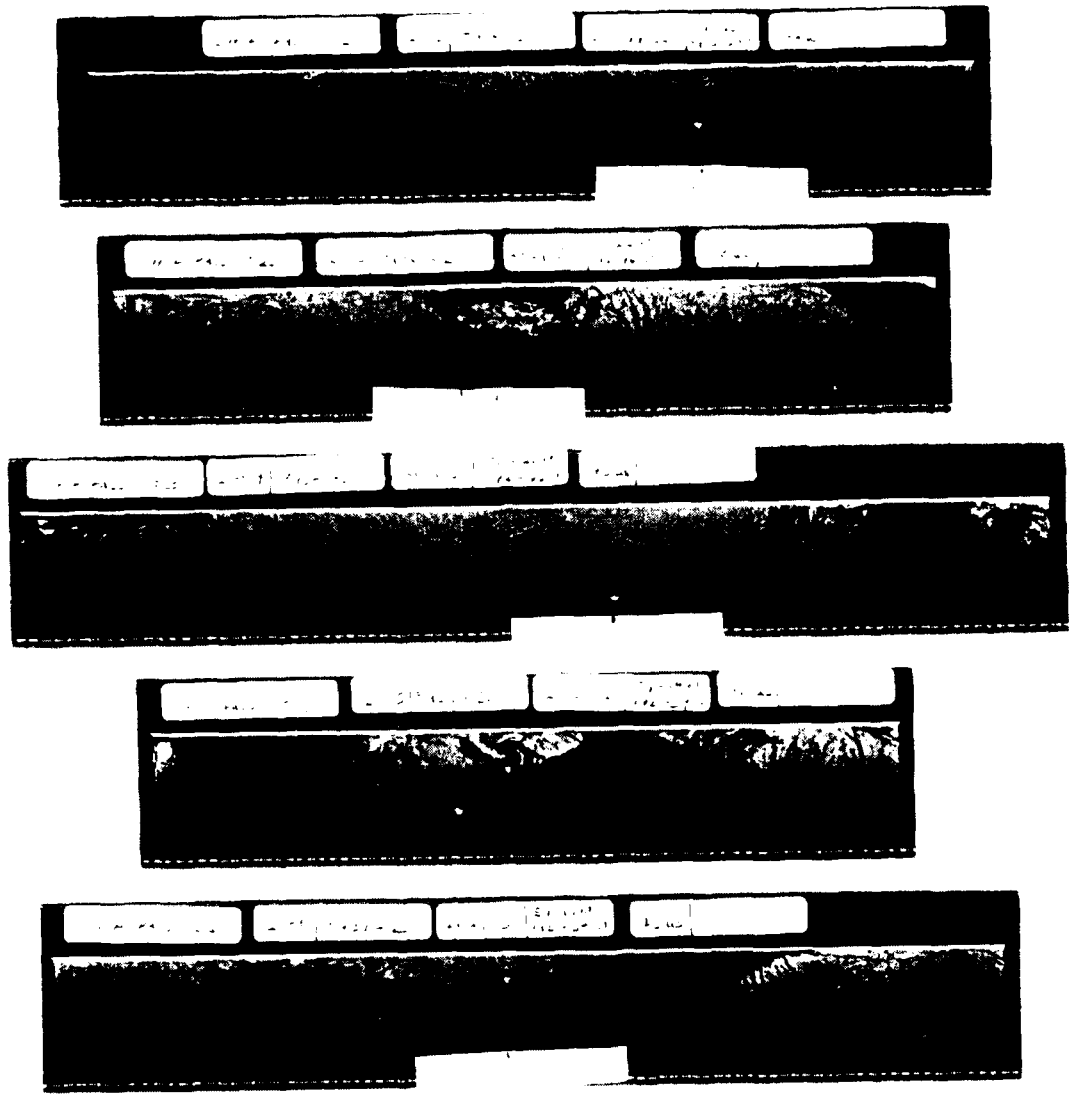

Figure B3. Optical SAR Images of All Ship Passes Recorded During Mission of 13 March 1984 (Sea State 1).

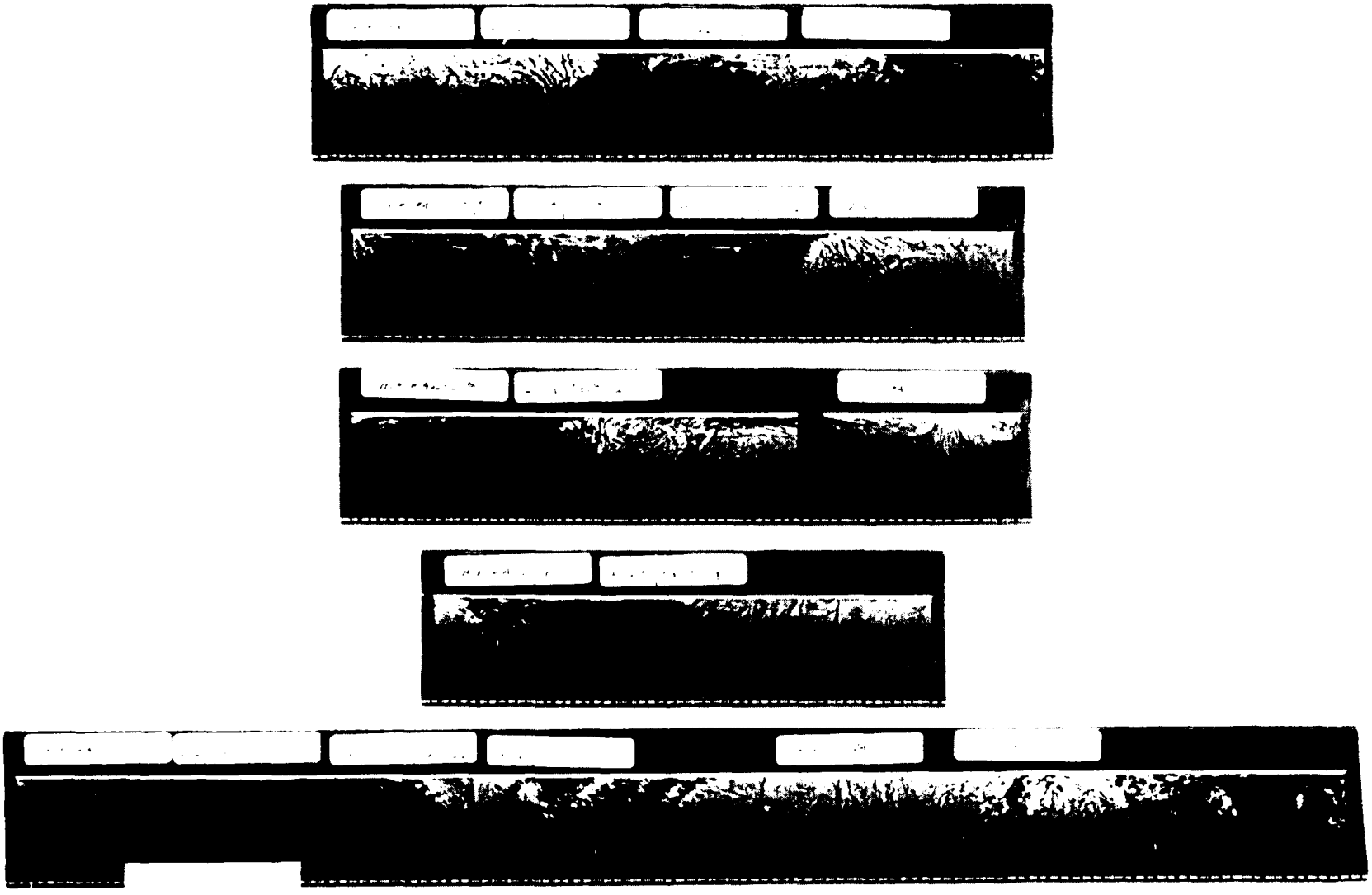

Figure B3. Optical SAR Images of All Ship Passes Recorded During Mission of 13 March 1985 (Scale to (Cont'd)

2. Sea State 2: 11 March 1984

The flight track for the mission executed on 14 March 1984 is shown in Figure B4. The aircraft data for this flight are shown in Figure B5. Optical images of all ship passes recorded during this mission are shown in Figure B6.

3. Sea State 3: 14 March 1984

The flight track for the mission executed on 14 March 1984 is shown in Figure B7. The aircraft data are shown in Figure B8. Optical images of all ship passes encountered in this mission are shown in Figure B9.

The mission executed on 15 March 1984 encountered the ship San Sinena II in Sea State 3. The flight track and detailed aircraft data are not available in graphical formats for this mission. They can be retrieved from digital tapes, however. The optical images of all ship passes recorded are shown in Figure B-10.

4. Sea State 4: 9 March 1984

The first mission, on 9 March 1983, encountered ships in Sea State 4. The flight track and aircraft data are not available in graphical format for this mission. They can be retrieved from the digital tapes, however. The optical images for all ship encounters on this mission are included in Figure B-11.

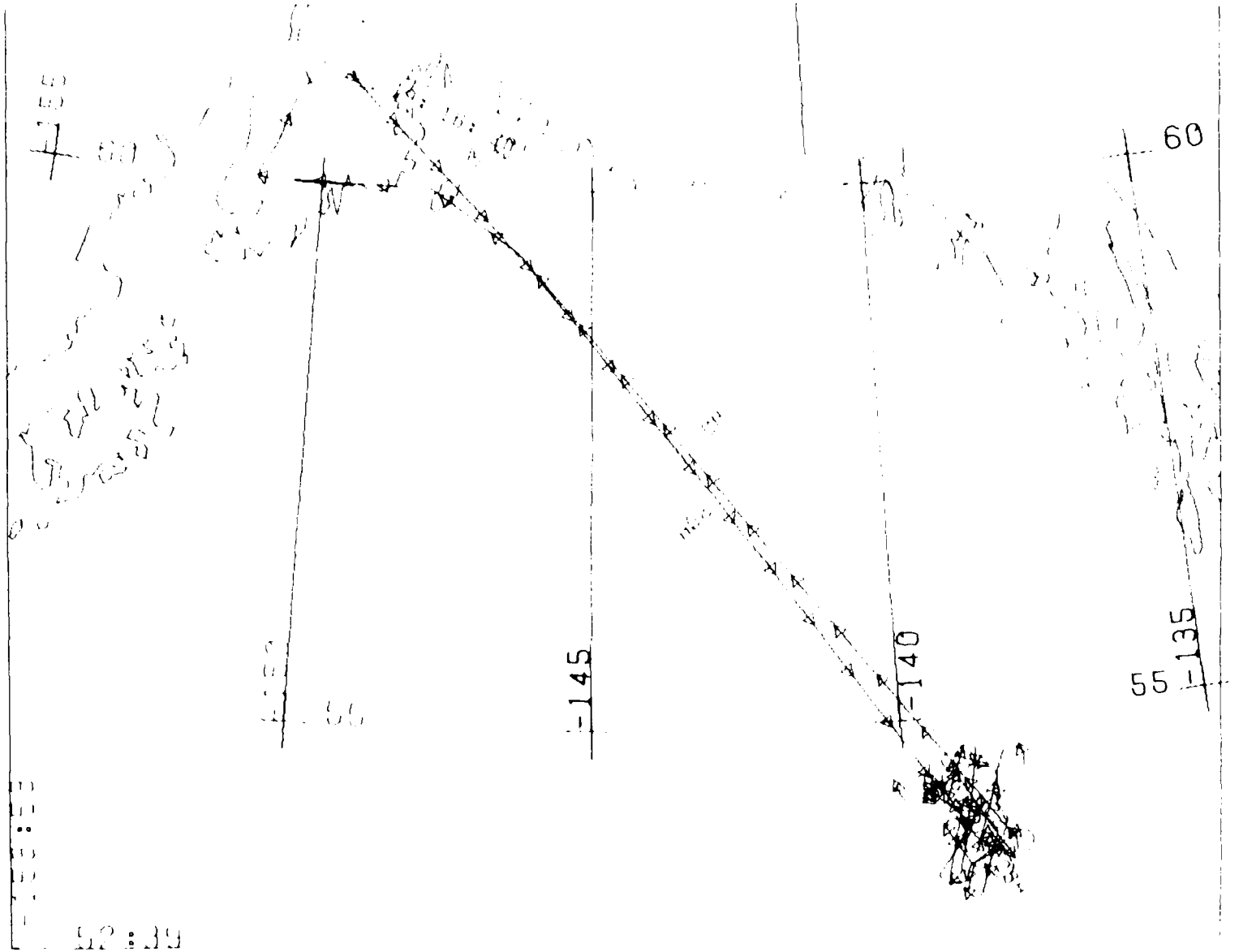

Figure B-... CV-990 Flight Track on 11 March 1987, Including Pattern Over ... Illinois, ... State 2, Time Tick ... Min, Approximate Local Time.

Figure B-5. (CV-990) Aircraft Data Parameters Flight on 11 March 1983, Over Ship San Simeon II, San Salvador.

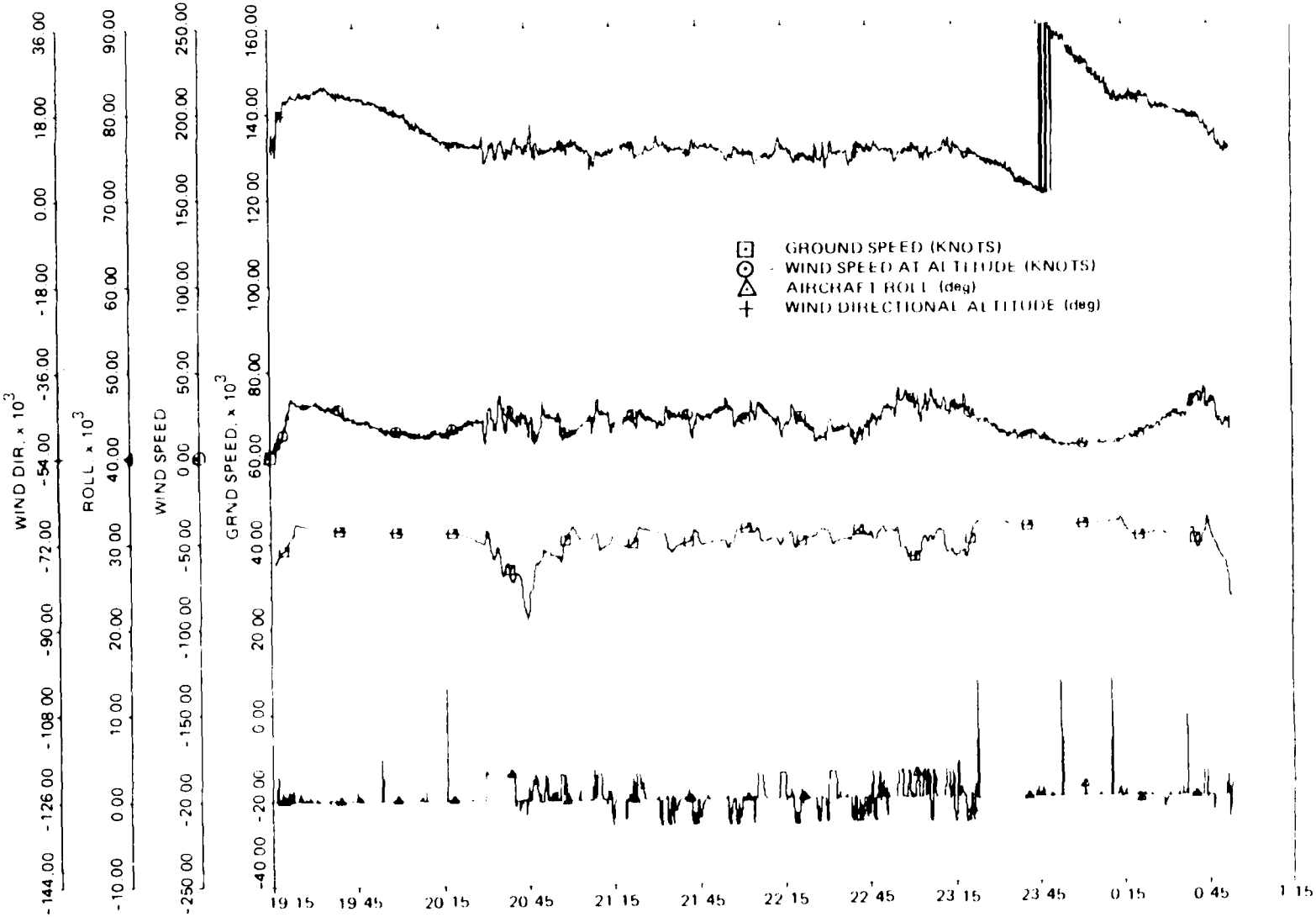

Figure B-6. CV-990 Aircraft Data During Flight on 11 March 1985, Over Ship San Simeon II, Sea State 2 (Cont'd).

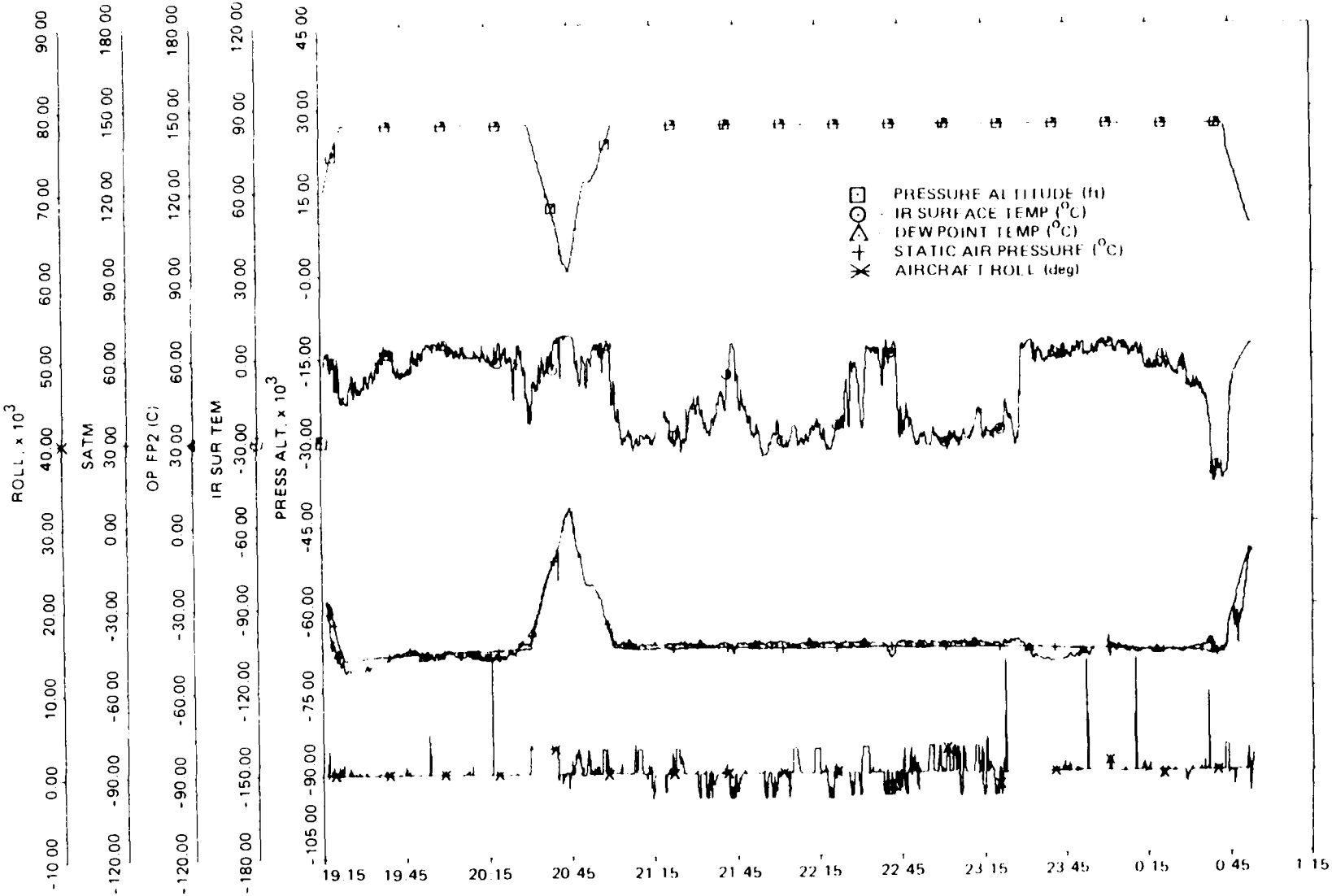

Figure B-6(b). CV-990 Aircraft Data During Flight on 11 March 1984 Over Ship San Simeon II, Sea State 2 (Cont'd).

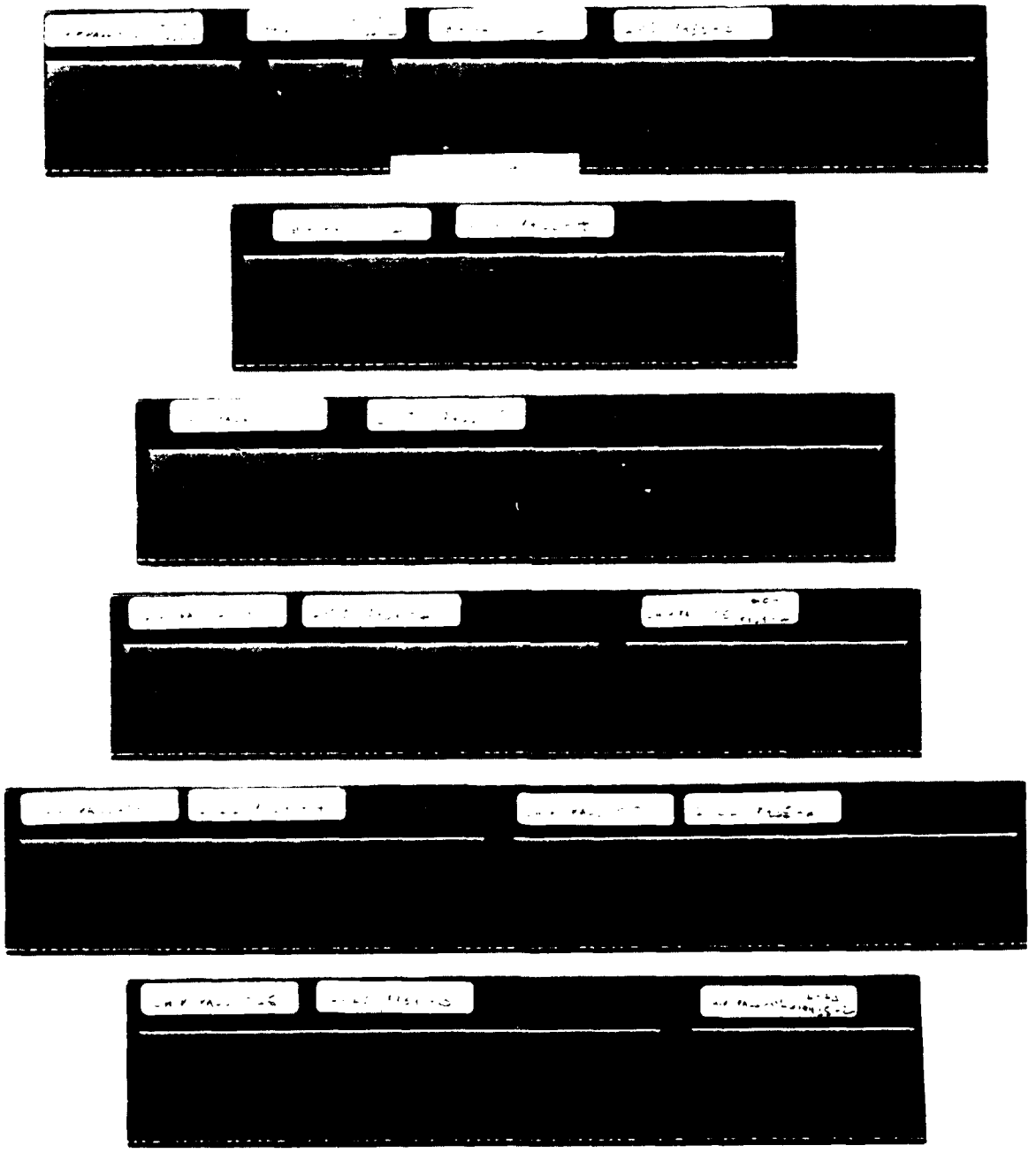

Figure B6. Optical SAR Images of All Ship Passes Recorded During Mission of 11 March 1984 (Sea State 2).

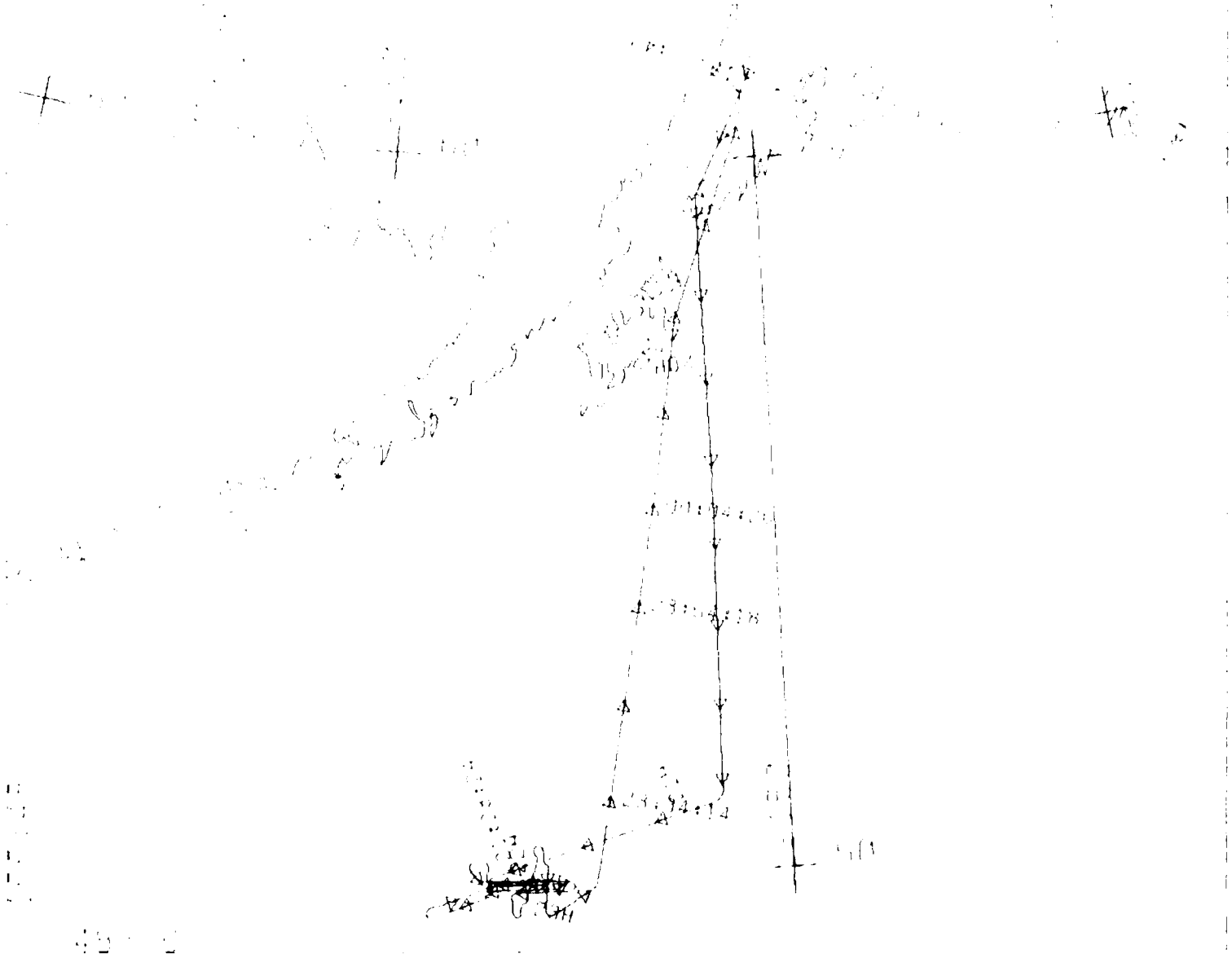

Figure B7. CV-990 Flight Track on 15 March 1984 Including Pattern Over Unidentified Ship, Sea State 3. Time Ticks Every 10 Min, Anchorage Local Time.

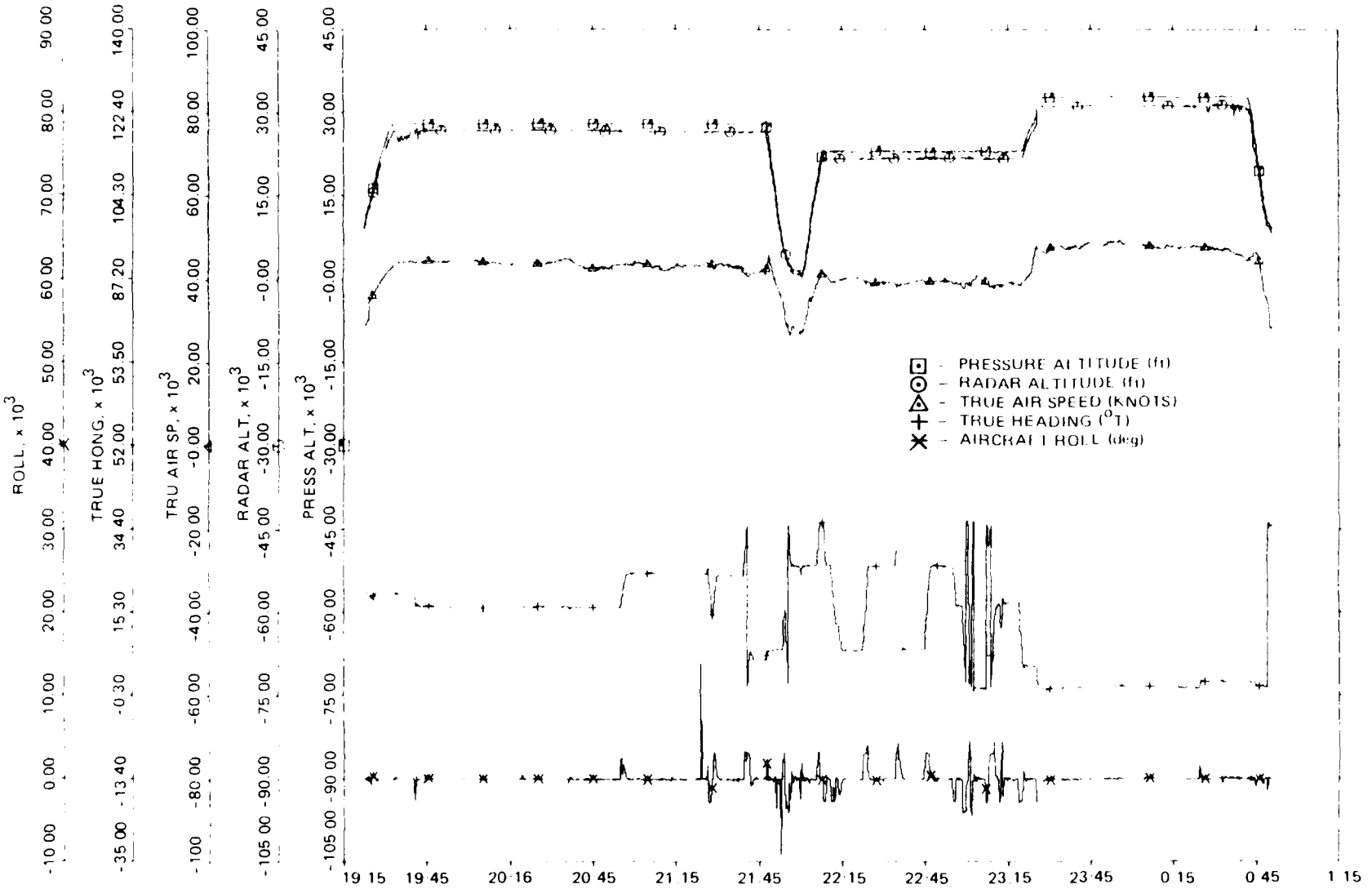

Figure 68. CV-990 Aircraft Data During Flight on 14 March 1985 Over Unidentified Ship, see State 3.

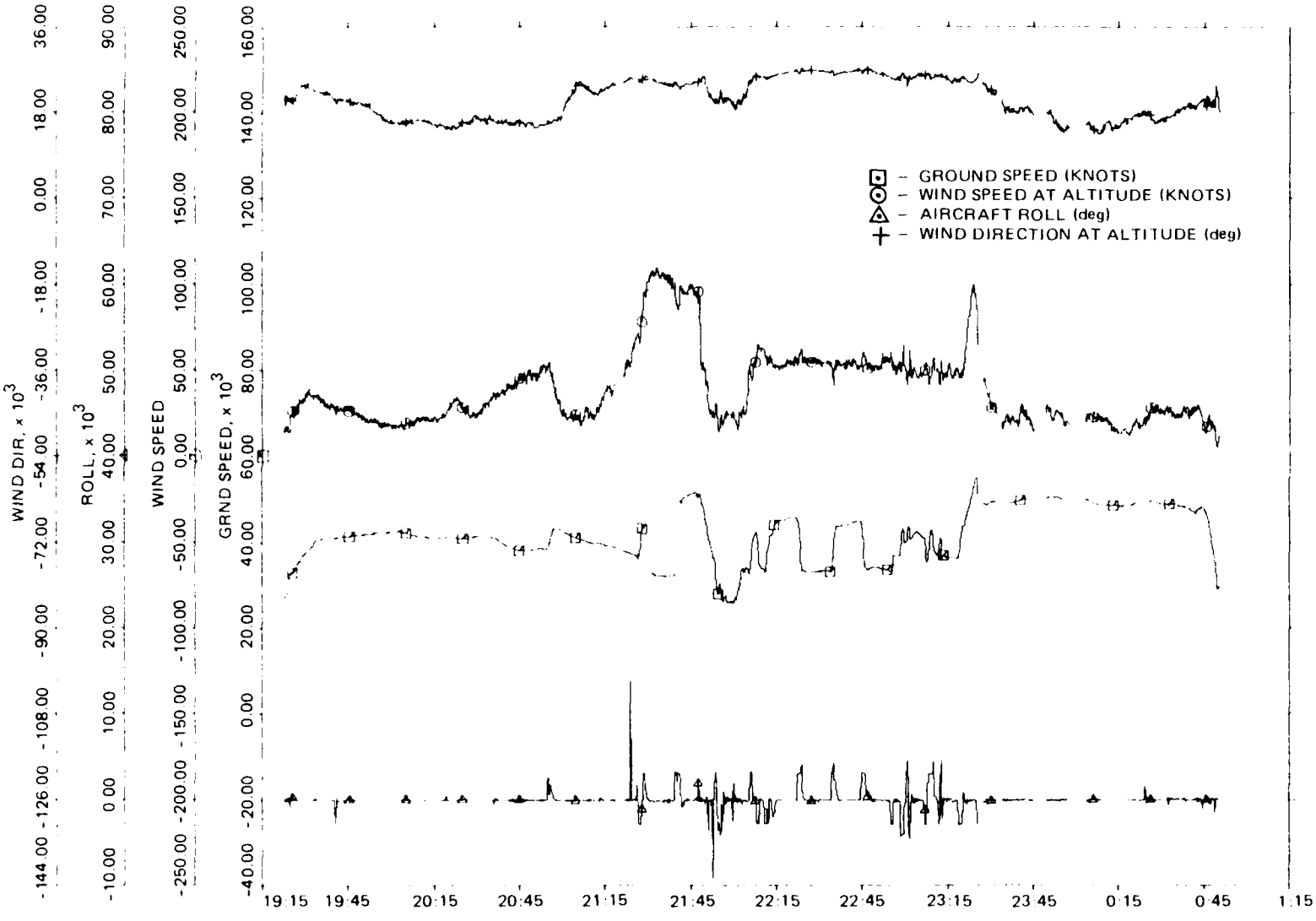

Figure B8(a). CV-990 Aircraft Data During Flight on 14 March 1984 Over Unidentified Ship, Sea State 3 (Cont'd).

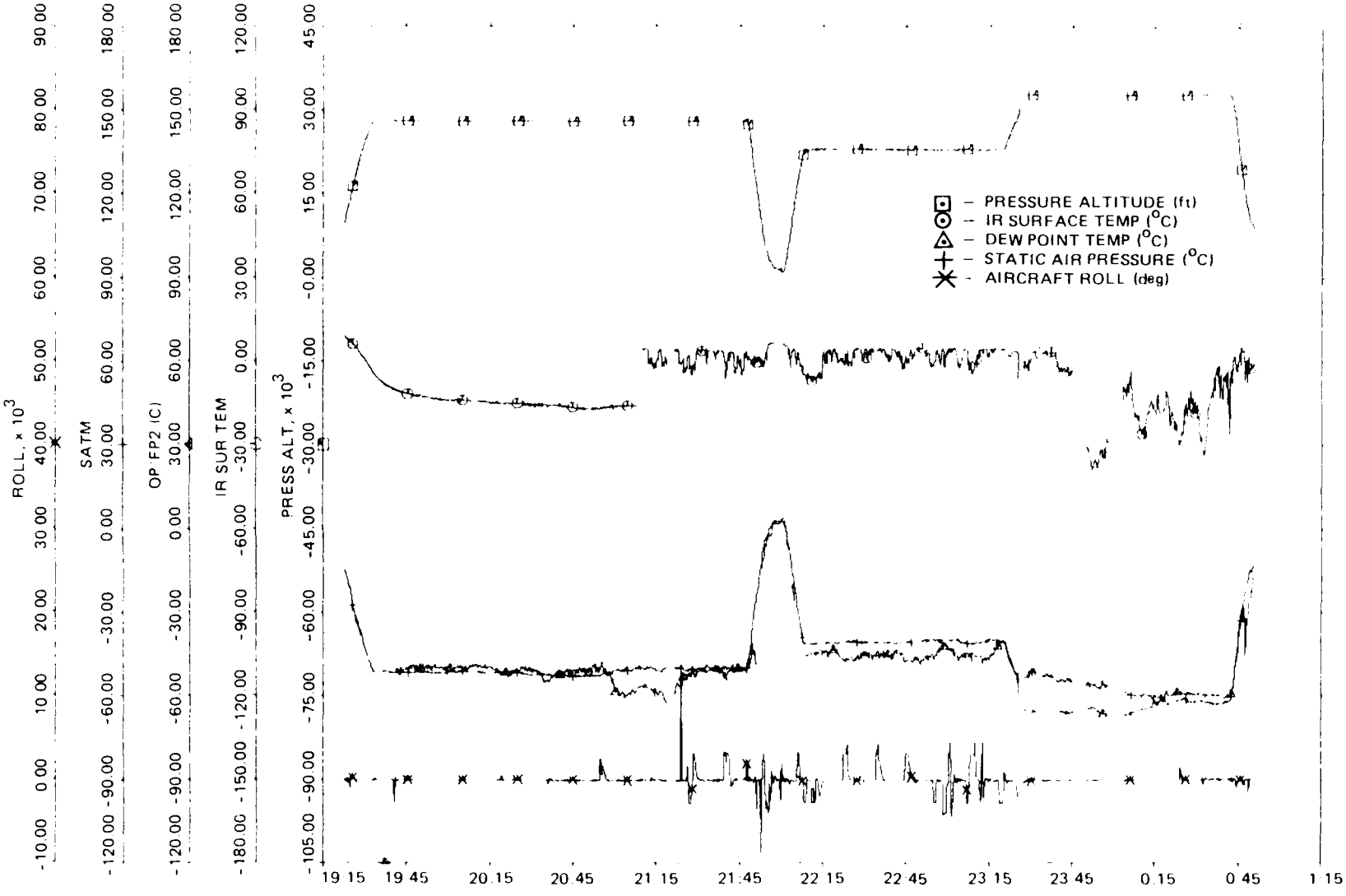

Figure B8(b). CV-990 Aircraft Data During Flight on 14 March 1985 Over Unidentified Ship, Sea State 3 (Cont'd).

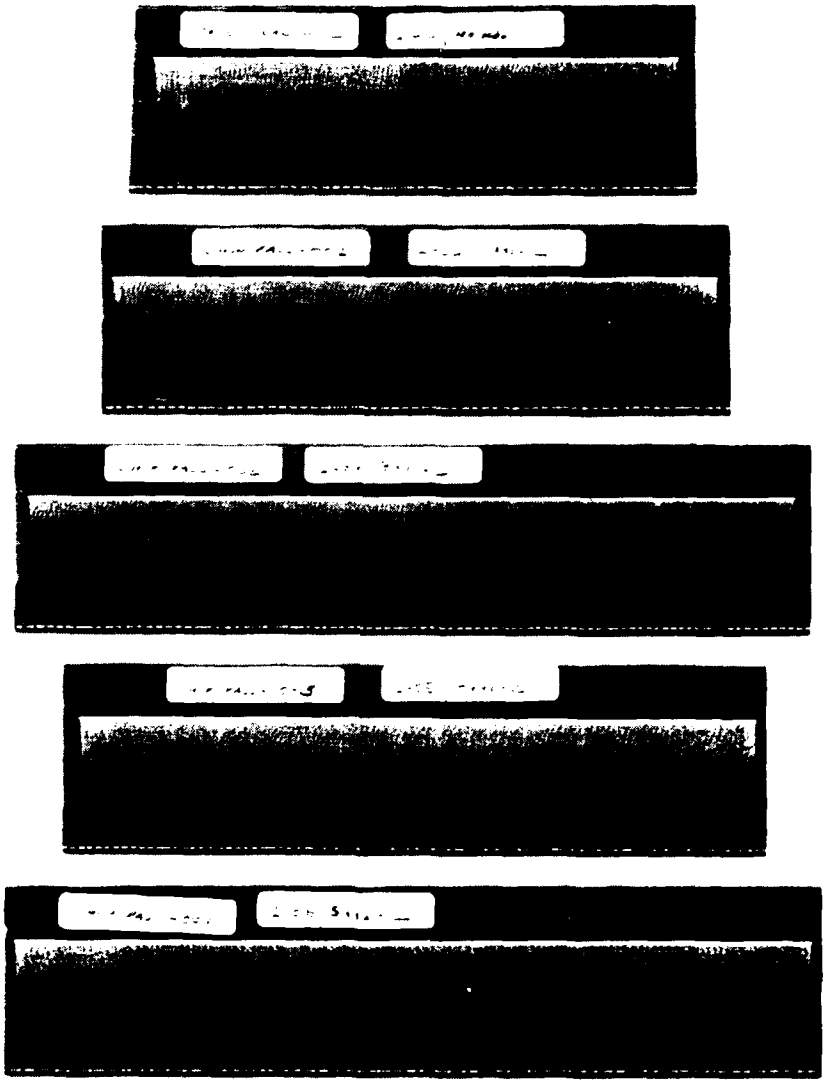

Figure B9. Optical SAR Images of All Ship Passes Recorded During Mission of 14 March 1984 (Sea State 3).

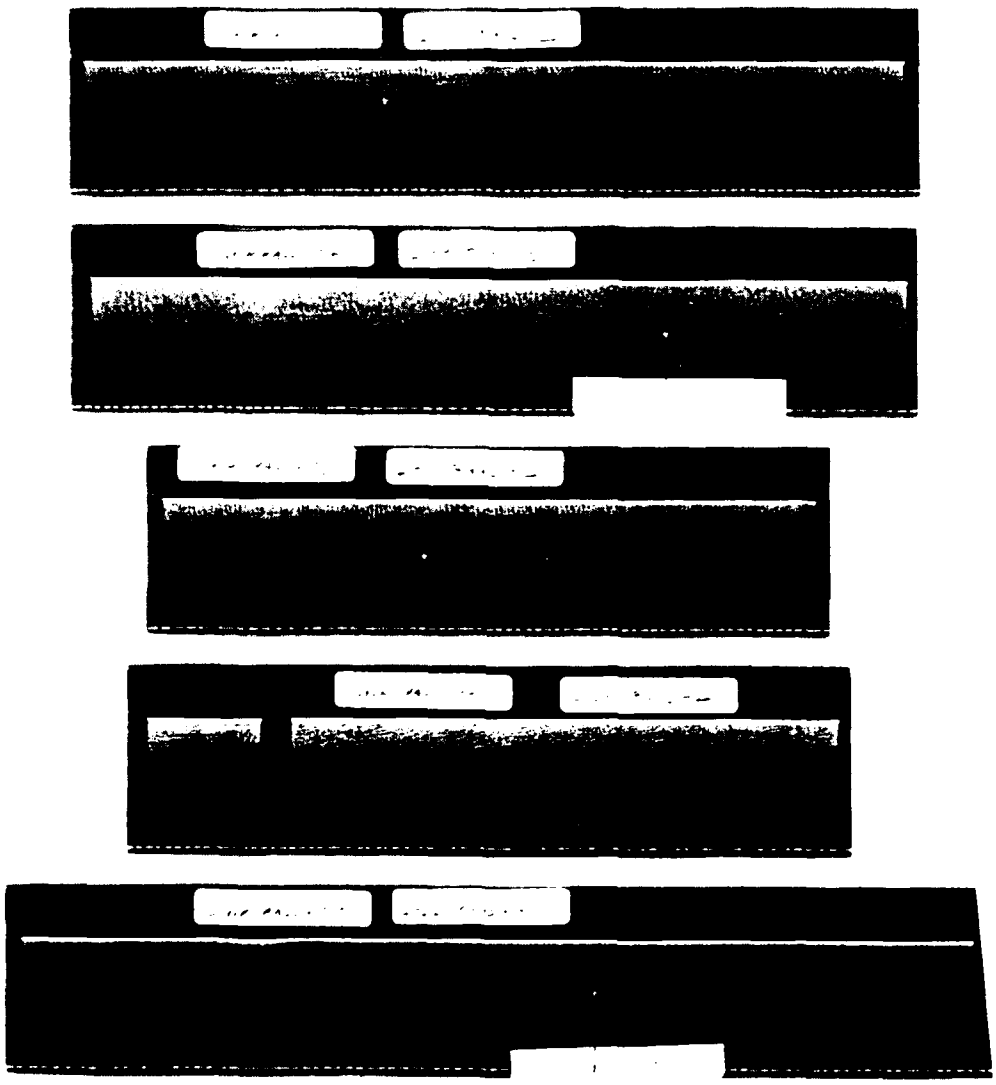

Figure B-7. Optical SAR Images of All Ship Passes Recorded During Mission 01 14 March 1984 (Sea State 3) (Cont'd).

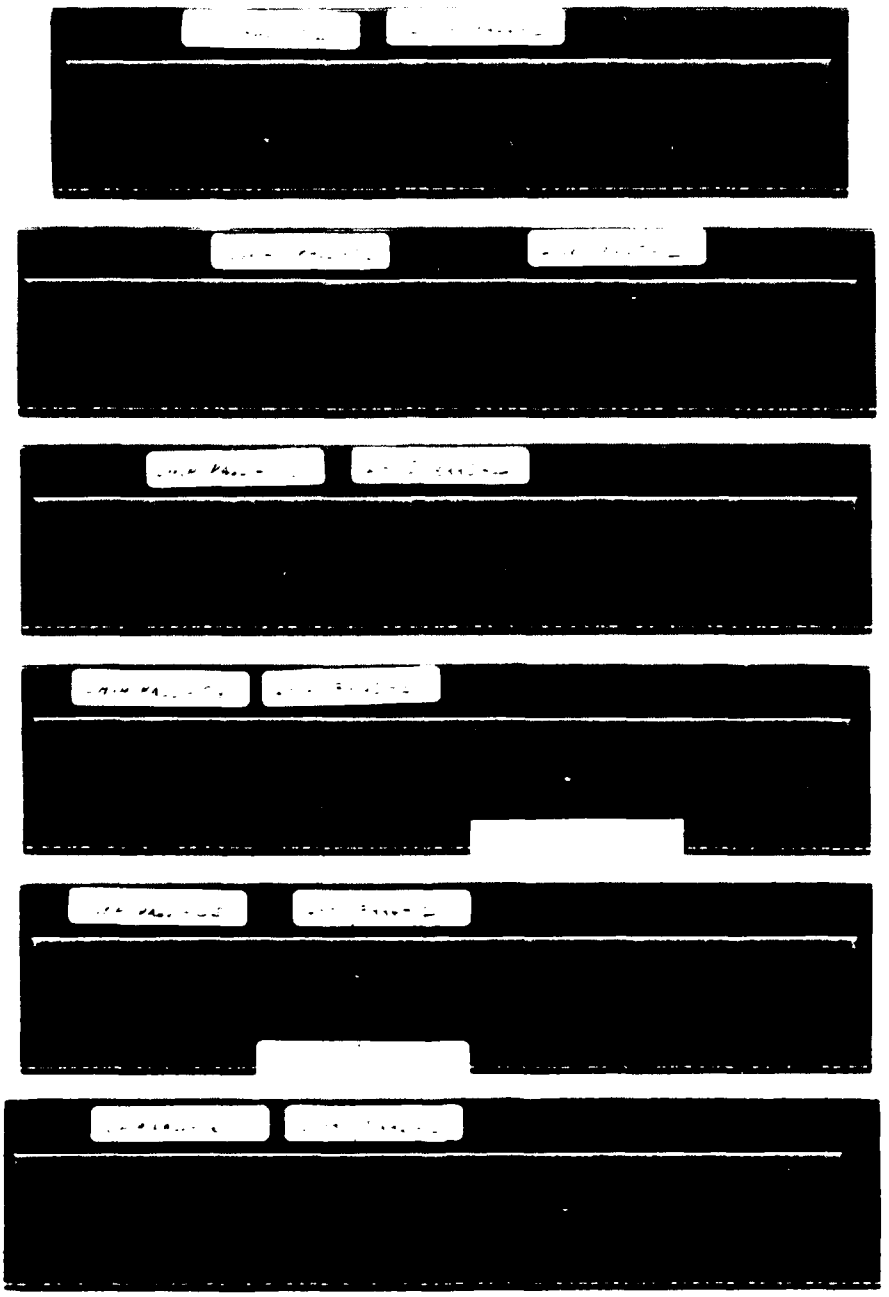

Figure B10. Optical SAR Images of All Ship Passes Recorded During Mission of 15 March 1984 (Sea State 3).

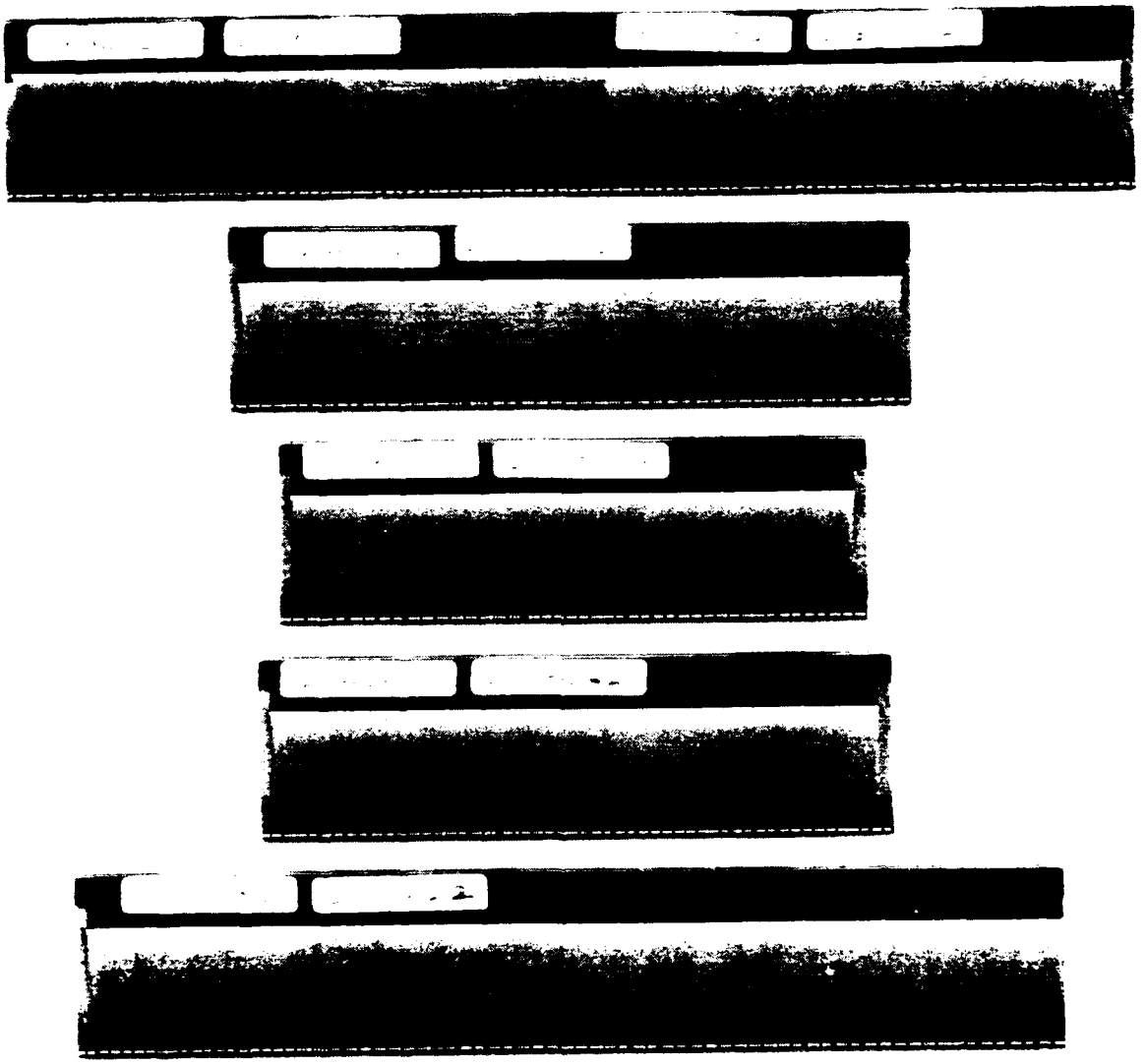

Figure B11. Optical SAR Images of All Ship Passes Recorded During Mission of 9 March 1984 (Sea State 4).

APPENDIX C

Model for Determining Lengths of Bright Arms in Narrow-V Wakes

In this Appendix the available information, derived from the Gulf of Alaska experiment, is reviewed and reformatted for the purpose of developing a predictive model for the length of the bright arms in the narrow-V wakes. The available measurements, related to the latter, are given in Figures 40 and 41 of the main text of the report. The bright arms in the SAR images are measured (at one end) from the point at which the two bright arms become distinct from each other, aft of the ship, to the point where they disappear into the image background at the far end aft.

For the purpose of developing a predictive model it is important that the zone along the ship's hull and the turbulent region ahead of the bow be considered. The best fit narrow-V's, matched to the Gulf of Alaska SAR images, indicated consistently that the vertex is ahead of the bow; with the distance being approximately one ship length. A schematic diagram of such a narrow-V wake is shown in Figure C-1. Of central importance for a predictive model is the determination of radar backscatter intensity in the bright arms (also referred to as source strength) as a function of radar incidence angle and distance aft of the ship. The model proposed here establishes the length of a bright arm by

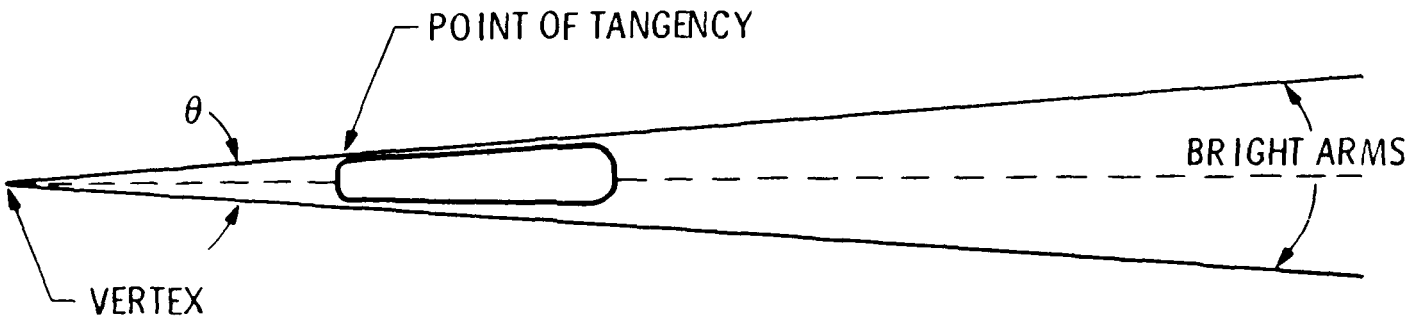

Figure C-1. Schematic Diagram of Narrow-V Wakes Showing the Vertex Ahead of the Bow.

the point at which the decreasing source intensity intersects the ambient radar backscatter intensity, for a particular sea state and incidence angle. Figure 39 of the main report shows the ambient backscatter levels in the sea states encountered in the Gulf of Alaska experiment.

Source Backscatter Intensity

It is hypothesized here, based on the observations made in this experiment, that the ocean surface scatterers in the bright arms are generated by the ship's bow and by the turbulent boundary layer along the ship's hull. The short surface waves generated by these interactions propagate outward from the ship's axis of motion with speeds that are proportional to their group velocities. At radar incidence angles greater than 20 deg, it is assumed that the scatterers with lengths that are resonant with the radar frequency contribute most of the backscatter intensity. The lengths of these resonant surface waves vary with radar incidence angle according to Equation (C-1). For a given ocean wave height spectrum, the radar resonates with different components of the wave height spectrum according to

$$\lambda_s^{(1)} = \frac{\lambda_r}{2 \sin \phi} , \qquad \text{(C-1)}$$

where the variables are specified in the main text of this report. In the proposed model, the k^{-4} distribution, where

$k = 2\pi / \lambda_s$, is adopted to specify the energy density in short waves.

The dependence of radar backscatter intensity on incidence angle is given by the radar equation

$$P_r = P_t \frac{\lambda_r^2 \, c \, \tau \, \beta \, G^2 \, \sigma_0(\phi)}{(4\pi)^3 \sin\phi \, R^3} , \quad (C\text{-}2)$$

where P_t and P_r are the transmitted and received powers, c is the speed of light, τ is radar pulse width, G is maximum antenna gain, β is antenna beam width, ϕ is radar incidence angle, R is range to surface, λ_r is radar wave length and σ_0 is normalized radar cross-section. Noting that $R = h / \cos\phi$, where h is aircraft altitude, and grouping the terms that have ϕ dependence in Equation (C-2) yields

$$P_r = \frac{P_t \, \lambda_r^2 \, c \, \tau \, \beta \, G^2}{(4\pi)^3 \, h^3} \left[\frac{\cos^3\phi \, \sigma_0(\phi)}{\sin\phi} \right] . \quad (C\text{-}3)$$

Note that only the terms inside the parenthesis on the right hand side of Equation (C-3) have ϕ dependence. The others are constants determined by the radar system. Assuming that in the region $20° \leq \phi \leq 70°$ Bragg scattering holds, so that

$$\sigma_0 \sim E(k) , \quad (C\text{-}5)$$

where E(k) is the wave height of the ocean surface. Using the familiar k^{-4} distribution for the wave height spectrum, it is stipulated for the Bragg resonance domain that

$$\sigma_0 \sim k^{-4} . \quad (C\text{-}6)$$

Substituting Equation (C-6) into Equation (C-3) and noting that

$$k = 2\, k_r \sin \phi, \qquad \text{(C-7)}$$

where k_r is the radar wave number, it follows

$$P_r \sim \frac{P_t\, \lambda_r^2\, c\, \tau\, \beta\, G^2}{(4\pi)^3\, h^3\, (2k_r)^4} \left[\frac{\cos^3 \phi}{\sin^5 \phi} \right] . \qquad \text{(C-8)}$$

The dependence of radar return on incidence angle is given by the terms in the parenthesis on the right hand side of Equation (C-8). The terms outside the parenthesis are determined by the radar system parameters and the operating geometry of the SAR platform.

The decay rate of scatterers with distance aft of the ship is determined by viscosity, radiation decay and wave-wave interaction. In the presence of oil slicks, faster decay rates can be expected because of surface elasticity effects. In low sea states, and in the absence of oil slicks, only viscous and radiative effects are assumed to be present. This is corroborated by the results shown in Figure 38 of the main text of the report. The equation for viscous decay is given by

$$E(k) = E_0(k) \exp [-4\, \gamma\, k^2\, t\,] , \qquad \text{(C-9)}$$

where γ is kinematic viscosity of water, E_0 is reference energy, and t is time which is related to distance aft of ship by the velocity of ship, V,

$$X = Vt \quad . \qquad \text{(C-10)}$$

The equation of radiative decay is given by the conservation of radial energy

$$E(k) = \frac{E_0(k)}{r} , \qquad \text{(C-11)}$$

where r is the radius of the radially propagating waves. Equation (C-11) may be written as

$$E(k) = C \frac{r_0}{r} , \qquad \text{(C-12)}$$

where C is constant and r_0 is an initial radius of radiative decay. It is important to know r_0 if the radiative decay aft of the ship is to computed with acceptable accuracy.

By careful examination of photographs, such as shown in Figures 36 and 37 of the report, areas of scattering centers are identified where the waves propagate outward along radial lines. Futhermore, it is found that the radii of these scattering centers remain constant along the ship's hull and beyond to approximately half a ship length aft of the ship. Thereafter, the radii increase linearly with distance. A graph of the normalized radii of scattering centers vs. distance aft of ship is shown in Figure C-2. The radius used for normalization is 10 m. Figure C-2 clearly indicates that the initial radii of the scattering centers are finite in size, are larger in magnitude compared to the ship's half beam width, and beyond half a ship length increase linearly in magnitude with distance aft of ship.

The above observations point to a rational method for computing the initial radii of the scattering centers. Given

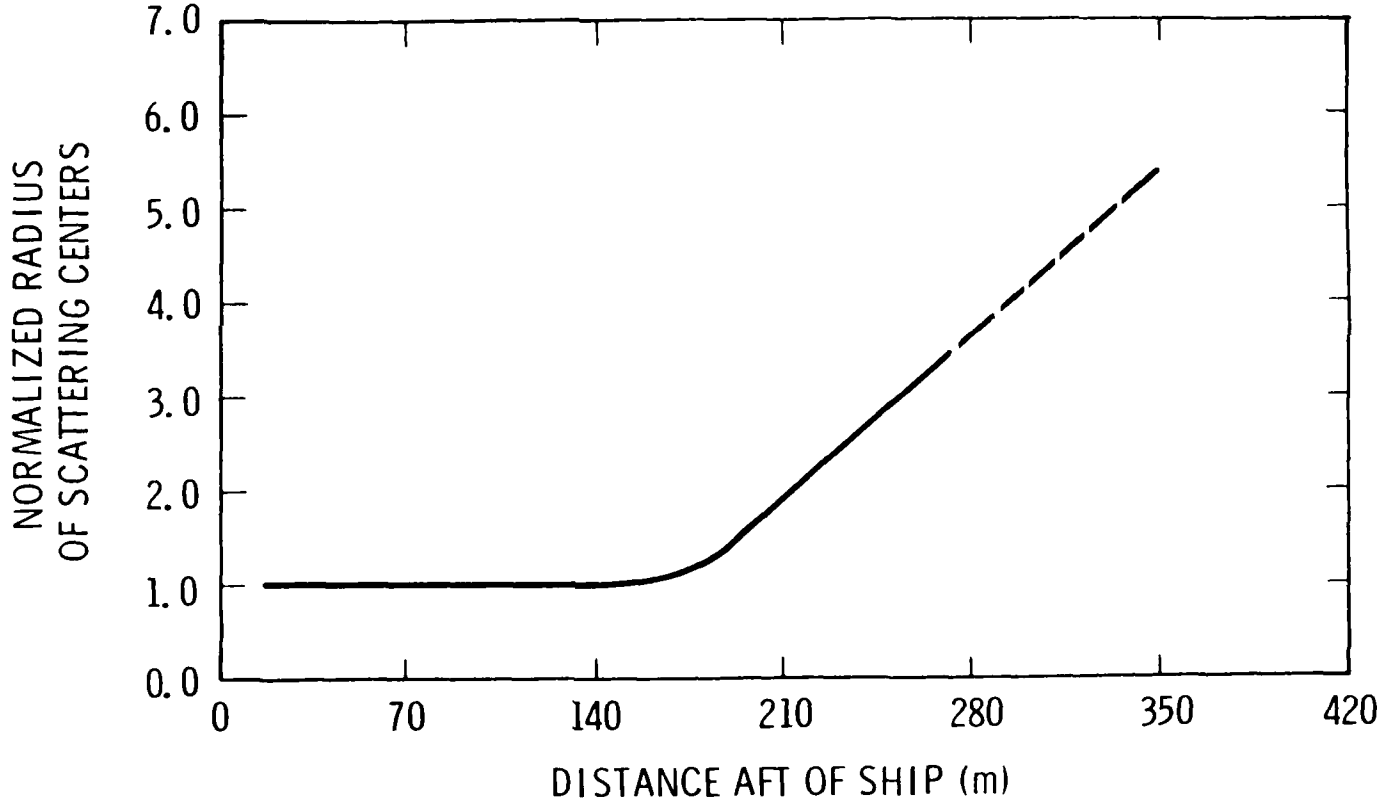

Figure C-2. Relative Change in Radii of Scattering Centers with Distance Aft of Ship, from Photographs of *San Sinena II* on 15 March 1984.

that the vertex of the bright arms is approximately one ship length ahead of the bow, the narrow-V wake half-angle can be used to calculate the initial radius as the outward distance to the bright arms at a point equal to half a ship length aft of the ship. For the Bay Ridge, in Sea State 1, the estimated initial radius is 28 m. This value is used to calculate the radiative decay rate shown in Figure 38, which in combination with the viscous decay rate gives results that are in reasonable agreement with observations.

In sea states greater than 1, it is anticipated that the combined decay rate will be influenced by wave-wave interactions and wind, such as discussed in Appendix C of Case *et al* (1984). The interaction between wind-generated waves and ship generated waves is not presently understood. In the spirit of arriving at a simple model first, these influences are not included in present estimates of the decay rate of ship generated waves aft of the ship.

Using Equation (C-8), the radar backscatter level at different incident angles is computed first. Then, using Equations (C-7), (C-9) and (C-12) the decrease in radar return with distance aft of the ship is computed. The results are shown graphically in Figure C-3. The final step in constructing the present model is to relate the magnitude of these backscatter results to the levels associated with the ambient backscatter in various sea states.

The variation in ambient backscatter as a function of wind speed and incidence angle is shown in Figure 39 of the

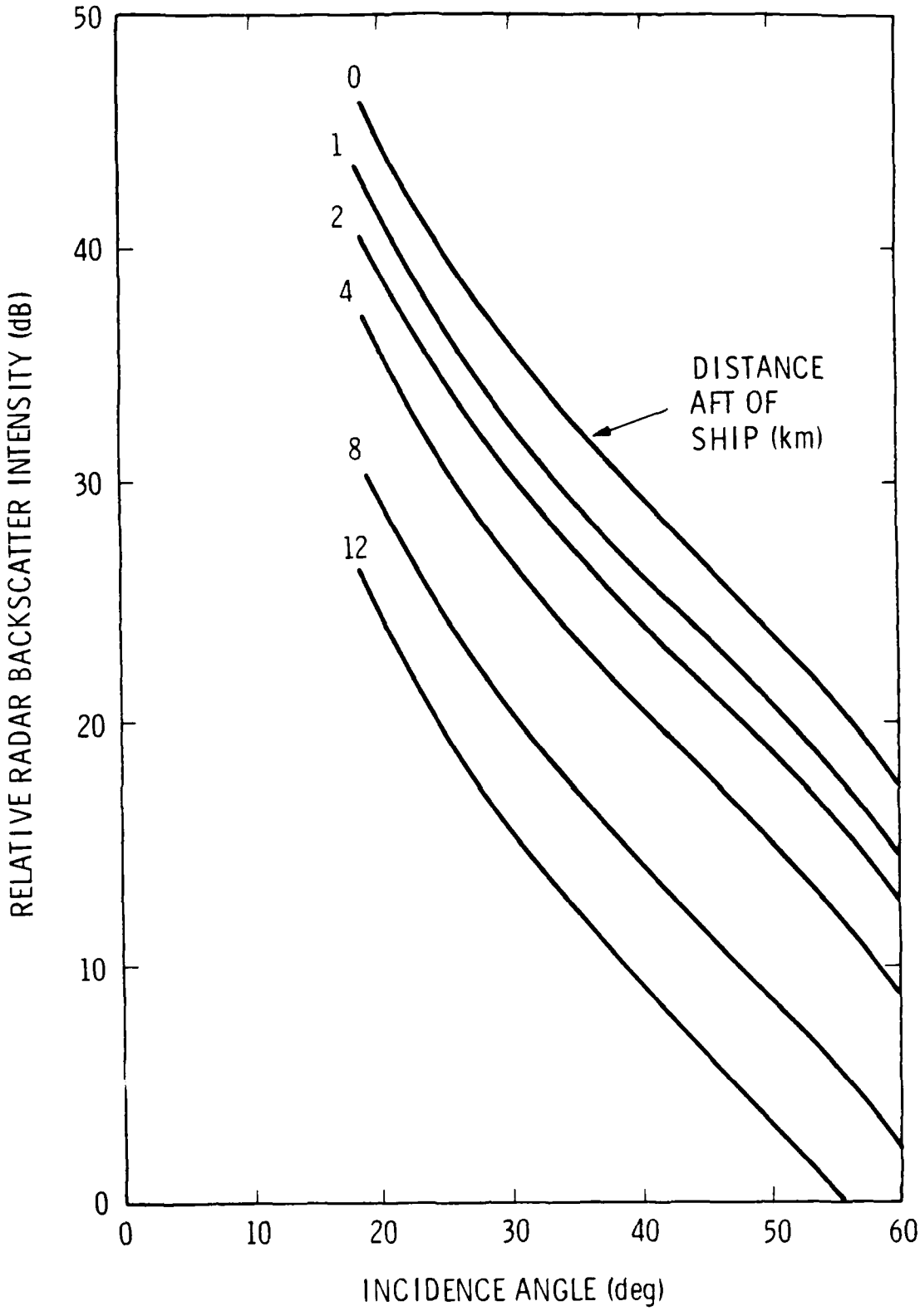

Figure C-3. Computed Radar Backscatter Intensity vs. Incidence Angle Using Radar Equation. The Curves Aft of Ship are Based on Radiation and Viscous Decay Shown Graphically in Figure 38.

main text of the report. In Figure C-4 these ambient backscatter measurements are compared with the computed radar backscatter curves shown in Figure C-3. The observations in Figures 40 and 41 indicate that no narrow-V wakes were observed in Sea State 4. It is of interest to note in Figure C-4 that the computed radar backscatter curve denoted by 0 km aft of ship, has the same slope as the ambient backscatter curve for Sea State 4. By adjusting the vertical scales so that these two curves match, the observation that no narrow-V wakes were observed in sea state 4 is satisfied. From this match the lengths of narrow-V wakes in all other sea states can be predicted, by comparing the ambient backscatter for each incident angle and sea state with the distance required for the source backscatter level to intersect the ambient level. A scatter diagram of predicted vs. measured narrow wake lengths is given in Figure 42 of the report.

In principle, the backscatter variations discussed in Figure C-4 can be computed exactly if the radar system is carefully calibrated, the radar backscattering mechanisms from the ocean surface are precisely understood and the intensity of scatterers can be predicted, both based on ship parameters and on wind sped. Unfortunately, our present level of knowledge is somewhat short of this need. Hence, the present model is proposed to provide early predictions. The scatter plot in Figure 42 shows reasonable correlations between measured and predicted narrow-V wake lengths.

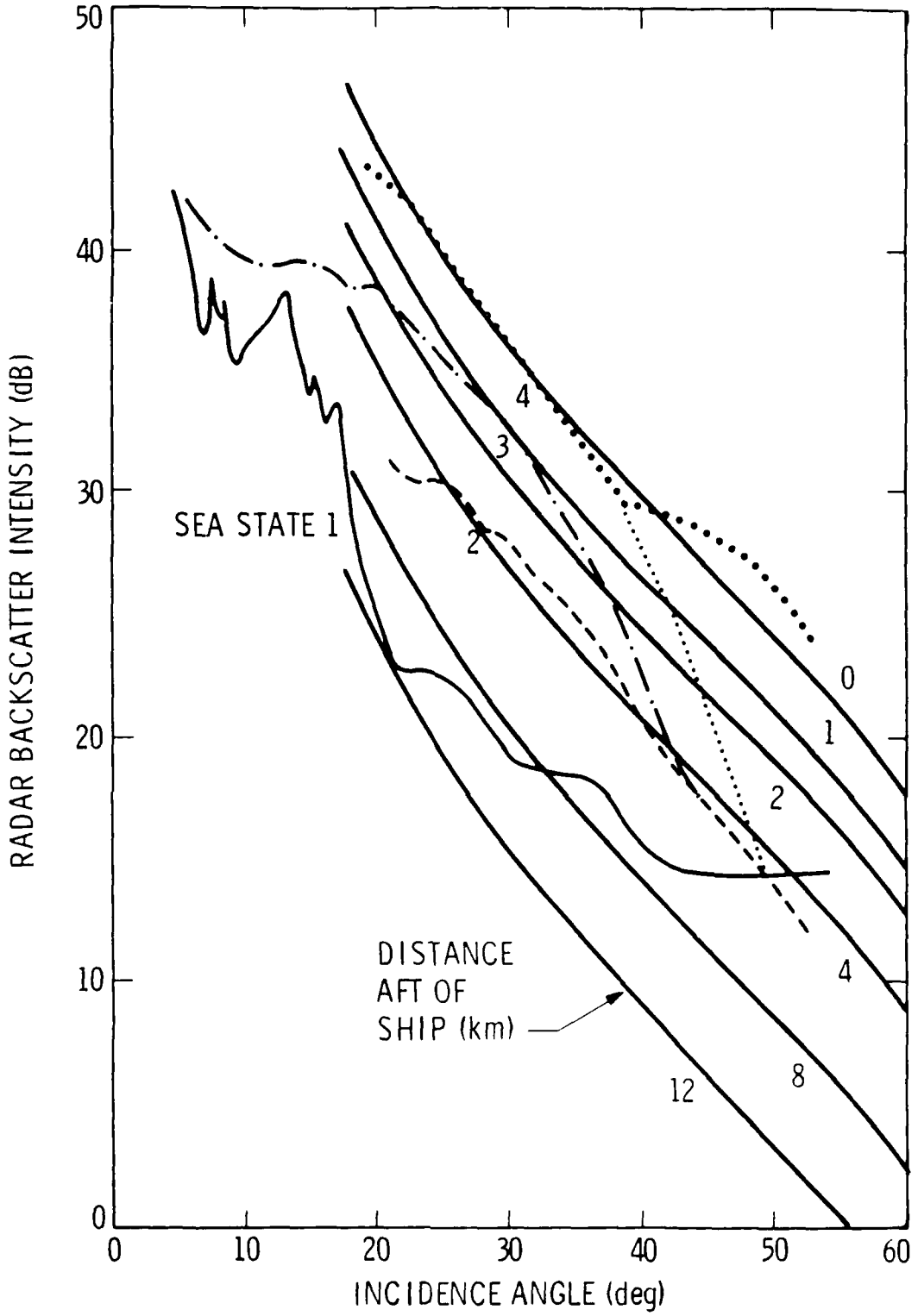

Figure C-4. Comparison of Predicted Radar Backscatter Intensity in the Bright Arms of the Narrrow-V Wake with Measured Ambient Radar Backscatter, in Different Sea States. The Point of Intersection at a Given Incident Angle and Sea State is Used to Determine the Predicted Lengths of the Bright Arms.